

**RODENT MODELS OF ALZHEIMER'S DISEASE:
INTRACEREBROVENTRICULAR ADMINISTRATION OF
 β -AMYLOID 1-42 OLIGOMERS INTO WILD TYPE RATS
AND TESTING LA1011 DRUG CANDIDATE ON APP/PS1
TRANSGENIC MICE**

Theoretical Medicine Doctoral School
Department of Medical Chemistry
Faculty of Medicine
University of Szeged

Ph.D. Thesis

Ágnes Kasza

Supervisor:
Prof. Botond Penke Ph.D, D.Sc
Department of Medical Chemistry
University of Szeged

**Szeged
2018**

1. LIST OF PUBLICATION

1.1. Full papers, patents directly related to the subject of the thesis

- I. **Studies for improving rat model of Alzheimer`s disease: icv administration of well-characterized β -amyloid 1-42 oligomers induce dysfunction in spatial memory**

Á. Kasza, B. Penke, Z. Frank, Z. Bozsó, V. Szegedi, Á. Hunya, K. Németh, G. Kozma, L. Fülöp (2017) *Molecules* **22**, 2007 (IF: 2.861)

- II. **Dihydropyridine derivatives modulate heat shock responses and have a neuroprotective effect in a transgenic mouse model of Alzheimer`s disease**

Á. Kasza, Á. Hunya, Z. Frank, F. Fülöp, Z. Török, G. Balogh, M. Sántha, Á. Bálint, S. Bernáth, K. L.I.M. Blundell, C. Prodromou, I. Horváth, HJ Zeiler, P.L. Hooper, L. Vigh, B. Penke (2016) *Journal of Alzheimer`s Disease* **53**: 557–571. (IF: 3.731)

- III. **Controlled in situ preparation of A β (1–42) oligomers from the isopeptide “iso-A β (1–42)”, physicochemical and biological characterization**

Z. Bozsó, B. Penke, D. Simon, I. Laczkó, G. Juhász, V. Szegedi, Á. Kasza, K. Soós, A. Hetényi, E. Wéber, H. Tóháti, M. Csete, M. Zarándi, L. Fülöp (2010) *Peptides* **31**: 248-56. (IF: 2.654)

1.2. Full papers not related to the subject of the thesis

- IV. **Small peptide inhibitors of β -amyloid toxicity**

L. Fülöp, B. Penke, M. Zarándi, Zs. Bozsó, D. Virók, T. Janáky, Y. Verdier, Zs. Datki, V. Szegedi, R. Busa-Fekete, K. Soós, Á. Kasza, A. Kocsor, E. Borbély (2013) *Hungarian Patent Notification*, Reg. **P1300317**. 2013. 05. 17; PCT: Reg. P 1 400 042, 2014.05.08.

- V. **Intranasal delivery of human β -amyloid peptide in rats: effective brain targeting**

E. Sipos, A. Kurunczi, A. Fehér, Z. Penke, L. Fülöp, Á. Kasza, J. Horvát, S. Horvat, Sz. Veszélka, G. Balogh, L. Kürti, I. Erős, P. Szabó-Révész, Á. Párducz, B. Penke, M. A. Deli (2010) *Cell Mol Neurobiol* **30**: 405-13. (IF:2.423)

- VI. **β -Amyloid pathology in the entorhinal cortex in rats contributes to the memory deficits associated with Alzheimer's disease**

E. Sipos, A. Kurunczi, Á. Kasza, J. Horváth, K. Felszeghy, S. Laroche, J. Toldi, Á. Párducz, B. Penke, Zs. Penke (2007) *Neuroscience* **147**: 28-36. (IF:3.352)

1.3. Posters, Abstracts

- **Amyloid plaques confer neuroprotection against exogenous A β**

H. Tanila, I. Gureviciene, E. Mugansteva, Á. Kasza, Z. Frank, K. Gurevicius, P. Asberg, J. Horváth, B. Penke, L. Khirug, *The 11th international Conference on Alzheimer's & Parkinson's Diseases, Florence, Italy, 2013*

- **Intracerebroventricular administration of the syntethic AB1-42 to the rat brain. Connection of spatial memory and spine density**

E. Borbély, J. Horváth, Á. Kasza, Zs. Frank, S. Furdan, G. Főr, T. Szögi, K. Németh, L. Fülöp, Z. Bozsó, Z. Penke, B. Penke, *75th Anniversary of Albert Szent-Györgyi's Nobel Prize Award, Szeged, Hungary, 2012*

- **Amyloid plaques confer neuroprotection against exogenous A β**

I. Gureviciene, Á. Kasza, Z. Frank, E. Mugantseva, Z. Datki, E. Borbély, J. Horváth, L. Khirug, B. Penke, H. Tanila, *SfN Annual Meeting, New Orleans, LA, 2012*

- **Szintetikus A β 1-42 bevitele patkányagyba: az intracerebroventrikuláris és a hippocampális injekció hatása a térbeli memóriára**

E. Borbély, Á. Kasza, *XVIII. Szent-Györgyi Napok, Szeged, Hungary, 2011*

- **Amyloid β -peptide induces dysfunctions in hippocampal area: an ICV injected rat model for Alzheimer's disease**

Á. Kasza, V. Szegedi, G. Juhász, Z. Frank, E. Sipos, D. Simon, Z. Datki, Z. Penke, B. Penke, *IBRO International Workshop Pécs, Hungary, 2010*

- **icv injected A β -peptide induces dysfunctions in hippocampus and in spatial memory: model for Alzheimer's disease**

Á. Kasza, V. Szegedi, G. Juhász, Z. Frank, Z. Penke, B. Penke, *The 5th Central European Conference – Chemistry towards Biology, Primosten, Croatia, 2010*

- **Histological changes in entorhinal cortex induced by beta-amyloid in a rat model**

J. Horváth, E. Sipos, A. Kurunczi, Zs. Penke, Á. Kasza, B. Penke, *X. Hungarian Alzheimer Congress, Szeged, Hungary, 2006*

- **A potential in vivo rat model of the Alzheimer's disease**

E. Sipos-Bodó, A. Kurunczi, Á. Kasza, J. Horváth, K. Felszeghy, Zs. Penke, Á. Párducz, J. Toldi, B. Penke, *FENS Wien, Austria, 2006*

- **Evaluation of memory deficit induced by beta-amyloid in rat model**

E. Sipos-Bodó, A. Kurunczi, Á. Kasza, J. Horváth, K. Felszeghy, Zs. Penke, Á. Párducz, J. Toldi, B. Penke, *IBRO International Workshop, Budapest, Hungary, 2006*

- **Evaluation of memory deficit induced by beta-amyloid in rat model**

E. Sipos-Bodó, A. Kurunczi, Á. Kasza, J. Horváth, K. Felszeghy, Zs. Penke, Á. Párducz, J. Toldi, B. Penke, *The 4th Kuopio Alzheimer Symposium, Microtekia, Kuopio, Finland, 2006*

- **Evaluation of memory deficit induced by beta-amyloid in rat model**

E. Sipos-Bodó, A. Kurunczi, Á. Kasza, J. Horváth, K. Felszeghy, Zs. Penke, Á. Párducz, J. Toldi, B. Penke, *IX. Hungarian Alzheimer Congress, Kecskemét, Hungary, 2005*

2. CONTENTS

1.	LIST OF PUBLICATION.....	2
1.1.	Full papers, patents directly related to the subject of the thesis	2
1.2.	Full papers not related to the subject of the thesis	2
1.3.	Posters, Abstracts.....	3
2.	CONTENTS	5
3.	ABBREVIATIONS.....	7
4.	INTRODUCTION	8
4.1.	General consideration about the Alzheimer's disease.....	8
4.2.	The main hypotheses of the cellular mechanisms of AD.....	9
4.3.	Genetic background of AD	12
4.4.	Key proteins and events in AD development	14
4.4.1.	Physiological roles of the β -amyloid and tau protein.....	14
4.4.2.	The amyloid precursor protein: sorting, trafficking and processing	15
4.5.	AD as a protein folding and protein homeostasis disorder.....	17
4.5.1.	$A\beta$ conformational changes and aggregation. Extracellular and intracellular $A\beta$	17
4.5.2.	The prionoid character of $A\beta$	18
4.5.3.	Tau-based neurofibrillary tangles in the Braak stages	18
4.5.4.	Central role of ER in protein homeostasis and the role of chaperone proteins	19
4.6.	Drug targets for treatment AD: a new era in drug research.....	20
4.6.1.	Heat shock protein coinducers as putative AD drugs.....	22
4.7.	Modeling Alzheimer's disease	23
4.8.	Aims.....	26
5.	MATERIALS AND METHODS	27
5.1.	Preparation of used chemical compounds.....	27
5.1.1.	Preparation of different $A\beta$ 1-42 oligomeric assemblies.....	27
5.1.2.	Atomic force microscopy studies (AFM) of o $A\beta$ 1-42 assemblies	27
5.2.	Experimental animals and housing.....	27
5.2.1.	Wild-type rats.....	28
5.2.2.	Transgenic and wild-type mice	28
5.3.	Treatments.....	28
5.3.1.	Experiments with rats.....	28
5.3.1.1.	Surgery and icv administration of o $A\beta$ 1-42.....	28
5.3.1.2.	Fluorescent microscopy for the pilot study	28
5.3.1.3.	Studies of two different icv administered o $A\beta$ 1-42	29
5.3.1.4.	Systematic studies for finding the most toxic form among six different o $A\beta$ 1-42 samples	29
5.3.1.5.	Validation of the toxic form of the $A\beta$ 1-42oligomers with MWM task	29
5.3.2.	Experiment with mice	29
5.3.2.1.	Experiment with drug candidate LA1011 in APP/PS1 tg line	29
5.4.	Behavioural testing.....	30
5.5.	Histology	30
5.5.1.	Cresyl-violet (Nissl) staining	30
5.5.2.	TAU- and $A\beta$ -immunohistology	31
5.6.	Quantification of dendritic spine density using Golgi-Cox impregnation.....	31

5.7. Ex vivo electrophysiological studies.....	32
5.7.1. Stimulation protocols	32
5.7.2. Multi-electrode array recordings	33
5.8. Statistical analysis	33
6. RESULTS	35
6.1. Application of an AD model using icv microinjections of oAβ1-42 in rat	35
6.1.1. Pilot experiment with icv administration of AMCA-labeled A β 1-42 samples	35
6.1.2. Studies on the neurotoxic effect of two different, icv administered oA β 1-42 aggregates.....	36
6.1.2.1. Histology	36
6.1.2.2. Studying the change of dendritic spine density using Golgi-Cox impregnation	37
6.1.2.3. Electrophysiological studies.....	37
6.1.3. Systematic studies for finding the most toxic form of the A β 1-42oligomers.....	38
6.1.3.1. AFM studies of the concentration and the aggregation time of A β 1-42oligomers	38
6.1.3.2. Spatial navigation in Morris water maze.....	39
6.1.3.3. Histology	40
6.1.3.4. Ex vivo electrophysiological recordings with multi-electrode array (MEA)	42
6.1.4. Validation of the most toxic form of the A β 1-42oligomers	43
6.1.4.1. Spatial navigation in Morris water maze.....	43
6.1.4.2. Studying the change of dendritic spine density using Golgi-Cox impregnation	43
6.2. Experiment with LA1011 drug candidate on APP/PS1 transgenic mice	44
6.2.1. Experiment with LA1011 treatment on APP/PS1 mice	44
6.2.1.1. Spatial navigation in Morris water maze.....	44
6.2.1.2. Histology	45
7. DISCUSSION	47
8. SUMMARY	51
9. ACKNOWLEDGMENTS	52
10. REFERENCES.....	53
11. APPENDIX.....	71

3. ABBREVIATIONS

ACE	angiotensin converting enzyme	iA β	intracellular β -amyloid
ACSF	artificial cerebrospinal fluid	icv	intracerebroventricular
AD	Alzheimer's disease	IgG	immunoglobulin G
AICD	the APP intracellular domain	ihc	intrahippocampal
ALS	amyotrophic lateral sclerosis	ip	intraperitoneal
AMCA	7-amino-4-methylcoumarin-3-acetic acid	LTP	long-term potentiation
ApoE ϵ 4	apolipoprotein E epsilon4	MAMs	mitochondria-associated ER-membranes
APP	amyloid precursor protein	MCI	mild cognitive impairment
APP CTF	APP C-terminal fragment	MEA	multi-electrode array
A β	β -amyloid peptide	MTT	3-(4,5-dimethylthiazol-2-yl)-2,5 - diphenyltetrazole
BBB	blood-brain barrier	MWM	Morris water maze
CA1	cornu ammonis 1	NFTs	neurofibrillary tangles
CAT	choline acetyltransferase	NMDA	<i>N</i> -methyl D-aspartate
CATCH	cerebral hypoperfusion	NTs	neuropil threads
CNS	central nervous system	oA β	A β oligomer
DG	gyrus dentatus	PBS	theta-burst stimulation
DHP	dihydropyridine	PD	Parkinson's disease
eA β	extracellular β -amyloid	PS1, PS2	presenilin-1 and -2
ER	endoplasmic reticulum	pTau	phosphorylated tau protein
ERAD	ER-assisted protein degradation	PTM	post-translational modifications
fA β	fibrillar β -amyloid	SAD	sporadic Alzheimer's disease
fEPSP	postsynaptic potential	tg	transgenic
GWAS	genome-wide association studies	UPR	unfolded protein response
HC	hippocampus	wt	wild type
HCBS	hydrocarbonated saline buffer	α 7-nAChR	α 7-nicotinic acetylcholine receptor
HPSs	heat shock proteins		

4. INTRODUCTION

4.1. General consideration about the Alzheimer's disease

AD is a neurodegenerative disease and the most common form of progressive dementia (Esteban 2004, Dodart 2005, Avraamides 2008, Kolarova 2012, Reinvang 2012, Song 2012, Cavanaugh 2014, Sasaguri 2017). Neurodegenerative diseases are characterized by disturbed protein homeostasis (proteostasis) and the ubiquitous presence of misfolded proteins that form aggregates. In the pathogenesis of AD, the misfolding and aggregation of β -amyloid and tau peptides play a central role, which give rise to amyloid plaques and neurofibrillary tangles (NFTs) (Braak 1991, 1995, Esteban 2004, Duyckaerts 2009, Yerbury 2015, Goloubinoff 2016, Ciechanover 2015), and neuronal death, in selective brain regions including the hippocampus and cortex (Rhein 2009, Kishimoto 2017). The precise signaling pathways leading to the disease have not been elucidated (Cakala 2007). NFTs and neuropil threads (NTs), collectively called the neurofibrillary changes, are pathological hallmarks of AD, which exhibit a stereotypical pattern of hierarchical progression initiated around the hippocampus (HC) (Uematsu, 2018). AD is clinically characterized by the progressive loss of cognitive abilities, particularly the retention of recently learned information (Dodart 2005, Spowart-Manning 2005, Takeda 2009, Kolarova 2012, Stöhr 2012, Nussbaum 2013, Kishimoto 2017). The most significant risk factor for neurodegenerative diseases is aging (Yerbury 2015) and it is becoming more prevalent in aging populations worldwide (Mucke 2009, Prince 2016).

A β pathology is initiated at least two decades before cortical tau pathology and the onset of clinical symptoms. After disease onset, it is increasingly difficult to treat symptoms (Sasaguri 2017, Ciechanover 2015). The degenerative brain is characterized by the presence of extracellular fibrillar β -amyloid (fA β) in diffuse and neuritic plaques and the accumulation of intracellular neurofibrillary tangles (NFTs) of hyperphosphorylated tau (pTau) (Braak and Braak 1991, Manzón-Mayor 2000, Hetényi 2002, Datki 2004, Esteban 2004, Lansbury 2006, Rowan 2007, Hu 2008, Hung 2008, Ikonomic 2008, Rezai-Zadeh 2008, Duyckaerts 2009, Bossers 2010, Oikawa 2010, Crespo-Biel 2012, Reitz 2012, Spuch 2012, Nussbaum 2013).

Oxidative stress is also one of the earliest changes and plays an important role in the pathological process in AD (Spuch 2012).

Based on findings from *in vitro* and *in vivo* studies, it has been proposed that A β plays a significant role by initiating synaptic dysfunction and cognitive decline in AD patients (Hardy 1991, 2002, 2009; Spuch 2012). The loss of dendritic spines have been reported in the AD-affected human brain (Baloyannis 2009). Deficits of episodic memory are the cognitive hallmarks of this disease

(Dodart 2005, Doran 2012, Reinvang 2012). The executive problems appear after memory disorders in time (Reinvang 2012) and is the usual complaint in mild cognitive impairment (MCI) (Morris 1989, Reinvang 2012, Song 2012) that is considered as a transition state between normal and aging AD, but it is not a distinct entity (Morris 1989). The MCI may take several forms, and the amnesic MCI has been recognised as an early stage of AD (Duyckaerts 2009, Reinvang 2012). The early symptom of the disease is a slow and insidious destruction of memory and cognitive skills (Alkadhi 2010).

There are two main forms of AD: the familial (it starts in the age of forties-fifties) and the more complex sporadic form, which begins in the age of sixties, although the two forms represent the same disease (Proctor and Gray 2012). Less than 1% of the AD cases are the early onset familial and hereditary; the sporadic, late onset AD is evident in the vast majority of the cases (Alkadhi 2011). Additionally, an increasing number of cases of sporadic AD in young people (early-onset sporadic AD) have also been described. A large amount of knowledge has been gained in the past decade on the etiopathology of the disease mainly thanks to genetic studies of familial AD and to the increasing use of animal models (Balducci 2010, Cavanaugh 2014, Onos 2016, Orta-Salazar 2016, Esquerda-Canalas 2017).

In association with the global trend of prolonging human life and increasing number of elderly in the human population, AD becomes one of the most important health and socioeconomic problems (Jacobsen 2005, Kolarova 2012, Cavanaugh 2014, Esquerda-Canals 2017, Sasaguri 2017), nowadays affects more than 40 million people worldwide and it is predicted to exponentially increase in the coming decades (Cavanaugh 2014, Esquerda-Canals 2017). AD is responsible for approximately 60-70% of all dementia cases (Reinvang 2012, Spuch 2012) and its prevalence increases exponentially with age (Bossers 2010). In light of this frightening prospect, new and effective methods for preventing, detecting, and treating AD are desperately needed (Cavanaugh 2014).

4.2. The main hypotheses of the cellular mechanisms of AD

Despite more than 100 years of extensive research, the cause of AD is still not perfectly known and no curative treatments are available (Onos 2016). A large part of the research on the etiology of AD has been focused around six main hypotheses: the cholinergic, the amyloid, the tau, the vascular, the immune-inflammatory and the proteostasis imbalance hypothesis.

1. The cholinergic hypothesis was put forward in the mid-1970s when it was found that the activity of choline acetyltransferase (CAT), an enzyme that parallels the distribution of cholinergic neurons, was reduced in the cerebral cortex and the hippocampus in post-mortem AD brains (Bowen 1976).

In AD a marked selective loss of cholinergic neurons is observed in the nucleus basalis of Meynert (Whitehouse 1981). The first generation of AD drugs aim at increasing cholinergic levels to restore cognitive deficits in AD patients. However, the benefits of these cholinesterase inhibitors in treating AD are marginal and short-lasting, due to the progressive degeneration of cholinergic neurons throughout the course of AD (Doody 2003).

2. In the early nineties, *the amyloid cascade hypothesis* was proposed (Hardy 1991). This hypothesis states that the accumulation of the A β peptide (a heterogeneous mixture of 39, 40, 42 and 43 amino acid peptides) is the primary influence driving AD pathogenesis. The A β peptide is derived through the proteolytic cleavage of the amyloid- β precursor protein (APP) by the enzymes β - and γ -secretase, and it accumulates in the brain as neuritic plaques. However, only 1% of all AD cases worldwide can be linked to genetic mutations directly involved in APP processing (familial AD).

The amyloid cascade hypothesis has been radically changed several times during the past decade. The A β hypothesis has been modified to include soluble oligomers and protofibrils as the cause of AD (Walsh 2002), since these A β species were shown to be toxic *in vitro* and in transgenic animal models. Immunization against A β has been suggested as a possible preventive or therapeutic treatment for AD, but so far clinical trials based on the original amyloid hypothesis have failed to show efficacy (Aisen 2009). Despite the negative results of AD treatment with A β antibodies, the amyloid hypothesis reached a firm research consensus.

3. *The tau hypothesis* offers the idea that tau protein abnormality (hyperphosphorylation) within the neurons initiates the AD cascade by disrupting microtubule function, thereby impairing axonal transport and triggering abnormal synaptic transmission (Trojanowsky 1995). Although it has been suggested that inhibition of abnormal hyperphosphorylation of tau offers a promising therapeutic target for AD (Gong 2010), no successful clinical studies have been carried out so far. The most recent results demonstrate the secondary role of tau in AD development: tau acts as mediator in AD-related synaptic deficits (Liao 2014).

4. *Vascular hypothesis of AD*

According to the cerebral hypoperfusion (CATCH) hypothesis, chronically disturbed capillary blood flow will impair normal delivery of essential nutrients to neuronal and glial cells, as well as impede catabolic outflow of central nervous system (CNS) waste products, leading oxidative stress and mitochondrial dysfunction (de la Torre 2000). Hypoperfusion results in increased A β production and reduced A β clearance, favoring the formation of neuritic plaques and cerebral amyloid angiopathy (van Groen 2005). In turn, A β peptides can further enhance hypoperfusion of

the brain. The synergistic negative effects of the amyloid and the vascular pathway on cerebral perfusion cause a vicious cycle, further enhancing the pathological cascade, which could ultimately result in development in progression of AD. The micron stroke hypothesis of AD and dementia emphasizes the role of recurrent insults in brain aging process and rapid aging in AD (Orehek 2012).

5. *Immune-inflammatory theory*

Several lines of evidence suggest that immune-inflammatory processes may also play important roles in certain neurodegenerative diseases like AD with selective initial injury of specific groups of neurons in the CNS. In amyotrophic lateral sclerosis (ALS) the upper and lower motor neurons, in Parkinson's disease (PD) the dopaminergic neurons of the substantia nigra, and in AD the cholinergic neurons in the basal forebrain and the dorsal raphe nucleus are damaged primarily. Site- and disease specific immune-inflammatory reaction was demonstrated in ALS (Engelhardt 1993), PD and AD tissue. T lymphocytes, macrophages and dendritic cells appeared in the lesion sites as a necessary (but not sufficient) proof of local antigen presentation (Henkel 2004). Recently, immunoglobulin G (IgG) Fc receptor was discovered in vulnerable cell population in AD and it was demonstrated that these receptors contribute to the development of hypercholesterolaemia-associated features (increased brain levels of IgG, upregulated Fc receptors in neurons susceptible to A β accumulation, Fernandez-Vizarra 2012). Using cells, AD-model mice and human AD tissue, Kam et al. found that the IgG Fc gamma receptor IIb mediates A β toxicity in neurons. Synthetic peptides targeting this interaction may treat A β pathology in AD (Kam 2013).

6. *Proteostasis and the neurodegenerative disorders*

Most recently AD and other protein conformational diseases are considered as protein misfolding and proteostasis imbalance diseases caused by cellular stress, protein folding problems and *malfunction of endoplasmic reticulum* resulting in unfolded protein response (details see in 5.5.4). The main cellular mechanisms effectively controlling protein homeostasis in youth and healthy adulthood are: the molecular chaperones, acting as aggregate unfolding and refolding enzymes, the chaperone-gated proteases, acting as aggregate unfolding and degrading enzymes, the aggresomes, acting as aggregate compacting machineries, and the autophagosomes, acting as aggregate degrading organelles (Yerbury 2015, Goloubinoff 2016, Ciechanover 2015). Misfolded proteins generated in various cellular compartments, including the cytoplasm, nucleus and endoplasmic reticulum (ER), are efficiently removed by quality control systems composed of the ubiquitin-proteasome system, chaperone mediated autophagy and macroautophagy. The first line of defense in degrading soluble misfolded proteins is the ubiquitin-proteasome system, a selective proteolytic

system in which substrates are tagged with ubiquitin, and cleaved into short peptides while passing through the narrow chamber of the proteasome (Goloubinoff 2016, Yerbury 2016, Ciechanover 2015). Dysfunction of neuronal autophagy causing an increase in the amount and size of endosomes at the cellular-level may be involved in the pathogenesis of AD (Sanabria-Castro 2017). In the last few years there have been significant advances in our understanding of how proteostasis collapse is associated with the pathogenesis of neurodegenerative diseases (Yerbury 2016), especially in aged neurons, toxic aggregates may accumulate, induce cell death and lead to tissue degeneration (Goloubinoff 2016, Yerbury 2016, Ciechanover 2015).

4.3. Genetic background of AD

Familial AD (FAD) has a clear genetic background: causative mutations in the APP gene or in presenilin-1 (PS1) and presenilin-2 (PS2) genes. In the pathomechanism of sporadic, late onset AD (LOAD), genome instability may play an important role. DNA damage and alterations in cellular DNA repair capacity are implicated in the aging associated neurodegenerative diseases (Hou 2017). Genome-wide association studies (GWAS) proved that AD is a multifactorial disease. Up to know 30-35 genes have been found that are involved in the development of sporadic AD (Harold 2009, Lambert 2009, Seshadri 2010, Hollingworth 2011, Naj 2011). The causative and risk variants of genes in AD are recently reviewed (Zhang 2017). The results of GWAS (Table I) support several hypotheses and confirm the results of the previous proteomic studies (Juhász 2011, Penke 2012, Földi 2013, Sasaguri 2017):

1. The amyloid pathway plays important role in AD. The importance of the apolipoprotein E epsilon4 (ApoE ϵ 4) allele has been well known for many years (Fullerton 2000) in increasing AD risk (two ApoE ϵ 4 alleles cause elevated risk for dementia), however, also other gene products participate in the trafficking and amyloidogenic processing of APP.
2. The immune–inflammatory hypothesis got a strong confirmation with the participation of big number of genes involved in immune reactions.
3. The role of genes and proteins in lipid transport and metabolism is verified.
4. Genes and gene products concerning synaptic cell functioning and endocytosis are also important. The role of endocytotic pathways of APP resulting intracellular A β is explained by the participation of these genes.
5. The role of tau pathology got also a confirmation with the genetic background.
6. The importance of cytoskeletal function and axonal transport in neurodegeneration process of AD has been verified.

7. Several genes in connection with hippocampal synaptic function, cell migration and myeloid cell functions are new in AD genetic background, more detailed studies are needed for understanding their roles.

Table I: Genes and pathways involved in the development of AD.

Pathway	Genes
Amyloid pathway	APOE, SORL1, CLU, CR1, PICALM, BIN1, ABCA7, CASS4, PLD3
Immune system inflammation	CLU, CR1, EPHA1, ABCA7, MS4A4A/MS4A6E, CD33, CD2AP, HLA-DRB5/CRBI, INPP5D, MEF2C, TREM2/TREML2
Lipid transport and metabolism	APOE, CLU, ABCA7, SORL1
Synaptic cell functioning/endocytosis	CLU, PICALM, BIN1, EPHA1, MS4A4A/MS4A6E, CD2AP, PTK2B, SORL1, SLC24A4/RIN3, MEF2C
Tau pathology	BIN1, CASS4, FERMT2,
Cell migration	PTK2B
Hippocampal synaptic function	MEF2C, PTK2B
Cytoskeletal function and axonal transport	CELF1, NME8, CASS4
Microglial and myeloid cell function	INPPD5

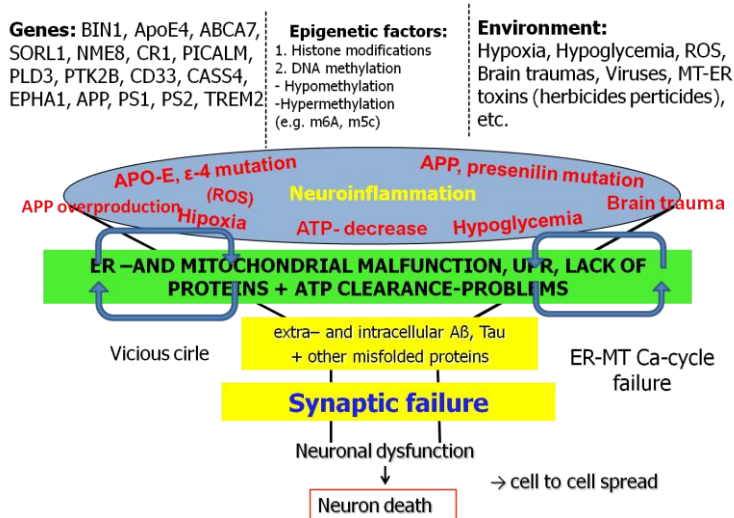


Fig. 1. Common AD mechanisms: in center the formation of Aβ peptides AD shows a heterogenic genetic background. (Penke 2017).

We think that the different AD hypotheses have common denominators: malfunction of the proteostasis pathways, formation of misfolded proteins, endoplasmic reticulum (ER) stress and unfolded protein response. The toxic effect of Aβ peptides is involved in starting and continuing the pathological process. Fig. 1 shows the central role of Aβ formation in the complex AD pathology.

4.4. Key proteins and events in AD development

4.4.1. Physiological roles of the β -amyloid and tau protein

Both A β peptide and tau protein are normal cellular constituents (Duyckaerts 2009, Doran 2012). Despite the fact that A β is present in the cerebrospinal fluid and plasma of healthy individuals throughout life (Esteban 2004), the deposition of A β is related to an imbalance between its production and clearance (Duyckaerts 2009). Since the first description of the neurotoxic properties of the A β peptide, an enormous number of studies have investigated the cellular and molecular pathology triggered by A β . Nevertheless it is still far from clear, how the accumulation of this peptide leads to the cognitive decline and more importantly, whether the A β has an important physiological role in the brain (Esteban 2004). This peptide has been found to act positively on synapses at picomolar concentrations (Fig. 2), but the interacting substance of A β has not been firmly identified yet (Duyckaerts 2009). Soluble oligomeric form of A β (oA β) in AD brains have been found to bind to neuronal surfaces, specifically to a subset of synapses where they colocalize with a postsynaptic density marker, suggesting that A β may regulate postsynaptic function directly (Wang 2012). Recent studies suggest that the α 7-nicotinic acetylcholine receptor (α 7-nAChR), a Ca²⁺-permeable homopentameric ion channel highly expressed in the HC and cerebral cortex, is another potential target of A β (Wang 2012).

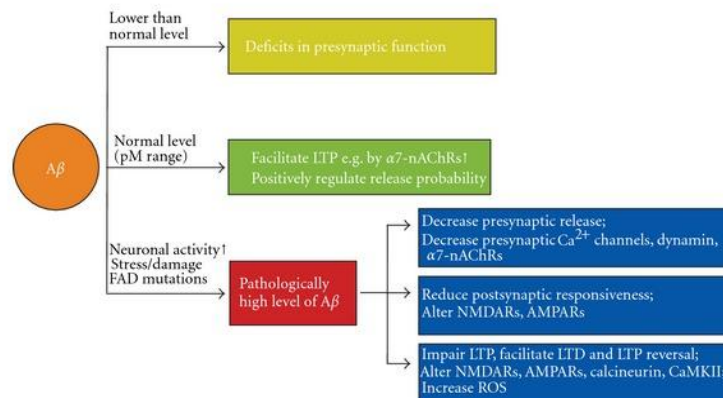


Fig. 2. Concentration-dependent effects of A β on synaptic function. At normal physiological levels (picomolar range), A β peptides have positive effects on synaptic function: they can positively regulate presynaptic release probability and facilitate α 7-nAChR (Wang 2012).

High affinity binding between oA β 1-42peptide and α 7-nAChRs either inhibits or activates α 7-nAChR signaling. It is possible that oA β 1-42peptide may facilitate α 7-nAChRs at low concentrations but may inhibit α 7-nAChRs when the burden of A β increases. This concentration dependent role of A β peptides is suggested from studies showing that at normal concentrations (picomolar range) A β peptides positively regulate presynaptic release at hippocampal synapses and

facilitate long-term potentiation (LTP) and learning by activating $\alpha 7$ -nAChRs. When the level of A β is too low or too high (nanomolar range), A β peptides cause either deficits in presynaptic function or abolish hippocampal LTP and learning via its interaction with $\alpha 7$ -nAChRs (Wang 2012, Fig. 2).

Neurons are polarized cells with two types of cell extensions, dendrites and axons, whose establishment depends on the microtubule cytoskeleton (Konzack 2007). Tau protein that belongs to a group of proteins referred to as microtubule-associated proteins (Konzack 2007, Götz 2011, Crespo-Biel 2012) is an axonal phosphoprotein in normal adult brain (Götz 1995) and also been localized to dendrites (Ittner 2010). Tau promotes tubulin assembly into microtubules, one of the major components of the neuronal cytoskeleton that defines the normal morphology and provides structural support to the neuron. Tubulin binding of tau is regulated by its phosphorylation state, which is regulated normally by coordinated action of kinases and phosphatases on tau molecule (Kolarova 2012, Fig. 3).

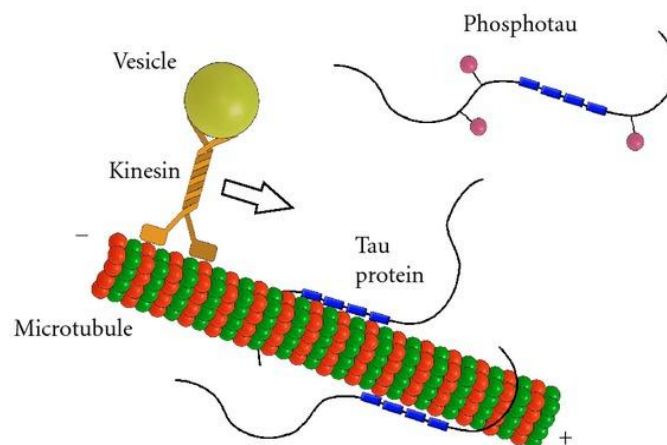


Fig. 3. Normal function of tau protein. Tau protein stabilizes microtubules through four tubulin binding domains (blue boxes) in case of the longest isoform. Binding of tau protein to the microtubules is maintained in equilibrium by coordinated actions of kinases (Kolarova 2012).

4.4.2. The amyloid precursor protein: sorting, trafficking and processing

To date, over 150 mutations in three autosomal dominant genes, APP, PS1 and PS2, are known to cause FAD (Jacobsen 2005). PS1 and PS2 play a critical role in γ -secretase-mediated cleavage of APP and the subsequent generation of β -amyloid peptides (Sasaguri 2017, Kishimoto 2017). A mutation in one of these 3 genes (APP, PS1, and PS2) accounts for approximately 1 to 5 percent of all AD, this subtype of AD is known as FAD (Sasaguri 2017, Kishimoto 2017).

Surprisingly, the physiological function of APP is not fully understood, although the protein is highly conserved throughout evolution and expressed widely in many different cell types (Jacobsen 2005). Very recent studies demonstrate the protective role of APP in acute neuronal insults (Hefter

2017): both APP and its soluble extracellular fragment (APPs α) can promote cell survival. APP mediates Ca²⁺-homeostasis via NMDA receptors, participates in synapse formation and function (Müller 2017). The intracellular domain of APP, the AICD peptide plays an important role in lipid homeostasis (Grimm 2017). Abnormal proteolysis of this membrane-bound protein triggers a pathologic cascade years, or decades before the overt clinical manifestations of the disorder (Crespo-Biel 2012, Sasaguri 2017). The neuronal dysfunction induced by A β can progress trans-synaptically from the neurons in the entorhinal cortex that selectively overexpress APP to the terminal end of the dentate gyrus (Nath 2012). APP processing occurs by two pathways: a β -secretase-based amyloidogenic and α -secretase-based nonamyloidogenic pathway (Claeysen 2012, Spuch 2012, Fig. 4). In the nonamyloidogenic pathway, cleavage occurs by α -secretase within the A β domain and generates the large soluble N-terminal fragment and a non-amyloidogenic C-terminal fragment of 83 amino acid residues. Further cleavage of this C-terminal fragment by γ -secretase generates the nonamyloidogenic peptide and APP intracellular domain (Spuch 2012, Fig. 4). The A β peptide was commonly considered as a dangerous, unfortunate byproduct of APP processing by β - and γ -secretases (Clippingdale 2001, Esteban 2004, Clifford 2007). In the amyloidogenic pathway APP cleavage occurs by β -secretase at the beginning of the A β domain, generating the soluble N-terminal fragment and the amyloidogenic C-terminal fragment of 99 residues. This C-terminal fragment is further cleaved by γ -secretase and generates A β (Spuch 2012, Fig. 4). Current studies support the idea that not only A β but other fragments from the processing of APP, such as C83 or AICD, contribute to the pathogenesis of AD (Simon 2010).

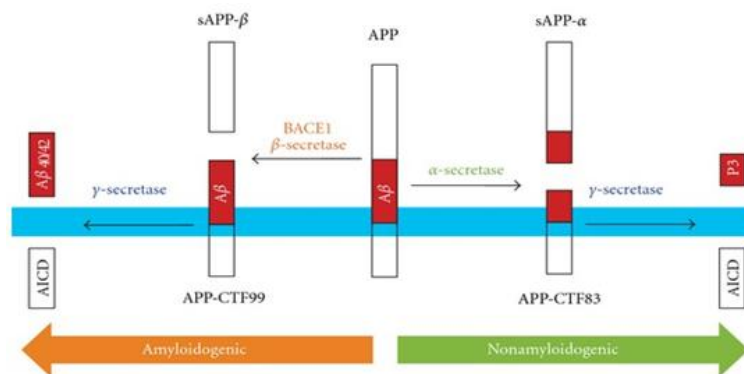


Fig. 4. APP processing pathways (membrane indicated in blue): α -secretase cleaves in the middle of the A β region (red) to release the soluble APP-fragment sAPP- α . The APP C-terminal fragment 83 (APP-CTF83) is then cleaved by γ -secretase to release the APP intracellular domain (AICD) and P3 fragment. β -secretase cleaves APP to produce the soluble fragment sAPP- β . APP-CTF99 is then cleaved by γ -secretase to produce A β 1-40, A β 1-42 and AICD (Wang 2012).

Recently Claeysen et al. (2012) reviewed the studies on APP trafficking: APP is biosynthesized in the ER and transported to the Golgi via the constitutive secretory pathway. The most frequent two splicing forms of APP (695 and 751 amino acids) show different behaviour. APP 751 is sorted

rather to the plasma membrane and processed to shorter peptides by non-amyloidogenic pathway. In the neurons the main form is APP 695, it is sorted mainly to the Golgi, and thus APP 695 undergoes rather the processing by amyloidogenic pathway resulting in A β . In the Golgi apparatus, APP undergoes various post-translational modifications (PTM) and transported to the plasma membrane. These PTMs enhance the non-amyloidogenic pathway and decrease A β -production. General consensus: impaired APP-transport along the constitutive secretory pathway is deleterious and leads to the increased A β -production (Claeysen 2012). Most recent results demonstrate that early endosomes are the most important places for APP processing to A β .

4.5. AD as a protein folding and protein homeostasis disorder

4.5.1. A β conformational changes and aggregation. Extracellular and intracellular A β

A β peptide is a natively unfolded peptide having high propensity to conformational change and aggregation into cross-A β amyloid fibrils (fA β) through a nucleation-dependent mechanism (Brännström 2011, Doran 2012). It has been postulated that toxic intermediates, such as small soluble oligomers are generated along the aggregation pathway (Lambert 1998, Wals 2002, Cleary 2005, Cooke 2006, Lansbury 2006, Lesné 2006, Rowan 2007, Hung 2008, Shankar 2008, Duyckaerts 2009). The A β -s, first of all A β 1-42 have a high, spontaneous tendency to oligomerize (Fülöp 2004, Duyckaerts 2009), which is the most toxic form (Takeuchi 2000, Hetényi 2002, Clifford 2007, Takeda 2009). Water soluble oA β s are the major neurotoxic congeners in the AD brain and are involved in degeneration of synapses (Cooke 2006) causing cognitive dysfunction in the early stages of AD (Tomiya 2010). oA β may disrupt synaptic plasticity mechanism via glutamate receptors (Rowan 2007, Hu 2008, Korczyn 2008, Duyckaerts 2009), rapidly inhibits LTP and reduce dendritic spine density (Duyckaerts 2009, Alkadhi 2010). Very recently, it has been demonstrated that the synaptotoxic effects of A β depend on expression of APP. The impairment of synaptic plasticity is associated with A β , localizing to synapses, and the binding of soluble A β aggregates (oligomers) to synapses requires APP (Wang 2017).

The toxic effect of A β assemblies can be measured by the simple colorimetric cell viability test, the MTT-assay in cell culture (Berridge 1993, Datki 2003, 2004). The assay reflects the activity of NAD(P)H-dependent oxidoreductase enzymes. Both the A β and tau protein in AD brain can form abnormal fibrillary structures associated with poor solubility in aqueous solution (Duyckaerts 2009).

Recently, the interest of AD researchers has turned to the iA β . It is now well accepted that two pools of A β exist in the brain: eA β and iA β , and there is a dynamic relationship between them

(LaFerla 2007). The “iA β hypothesis” of LaFerla (2007) assumes that iA β accumulation is the early, causative event in AD development: iA β is the cytotoxic substance and eA β deposition (in later stage of AD) is rather the result of cell death and destruction. iA β seems to initiate neuronal dysfunction. The formation and presence of iA β is very well documented in the intracellular deposits of the brain-parenchyma (Christensen 2009). A β also accumulates in choroid plexus epithelial cells and intracerebrovascular walls, where it induces blood-brain barrier (BBB) disruption (Spuch 2012).

4.5.2. The prionoid character of A β

oA β shows a prionoid character. Nath et al (2012) demonstrate direct evidence of the transmission of soluble oligomeric A β via connections between neuronal cells. Their finding of direct cell-to-cell A β transfer sheds light on the manner in which AD may be propagated via neuroanatomical connections. Polymorphism of fA β leads to different toxicity in amyloid diseases and may be the basis for prion strains, but the structural origin for fibril polymorphism is still elusive (Agopian 2012). The connections between prion diseases and other aggregation proteinopathies took an unexpected turn when it was suggested that A β triggers a toxic pathway that is mediated by cellular prion protein (Aguzzi 2009). Stöhr et al (2012) provide incontrovertible evidence that A β aggregates are prions and the formation of “A β -prions” very probably does not require additional proteins or cofactors.

It is believed that A β deposited in the brain originates from the brain tissue itself, however, A β is generated in both brain and peripheral tissues. Bu et al. showed in 2017 that blood-derived A β can enter the brain, form the A β -related pathologies and induce functional deficits of neurons. Using a model of parabiosis (binding together the blood circulation between APP^{swe}/PS1^{dE9} transgenic AD mice and their wild-type littermates), they observed that the human A β (originated from transgenic AD model mice) entered the circulation and accumulated in the brains of wild-type mice, and formed cerebral amyloid angiopathy and A β plaques after a 12-month period of parabiosis. More importantly, hippocampal CA1 long-term potentiation was also markedly impaired in parabiotic wild-type mice (Bu 2017).

4.5.3. Tau-based neurofibrillary tangles in the Braak stages

Many adverse responses to A β , such as cytotoxicity, microtubule loss, impaired memory and learning and neuritic degeneration are greatly amplified by tau expression (Nussbaum 2013). The extent of neurofibrillary changes correlates with the severity of dementia in AD, probably prior to the limbic area, subcortical nuclei such as the dorsal raphe nucleus and locus coeruleus develop

neurofibrillary changes much earlier, because they are sometimes detectable under 30 years of age in subclinical phases (Uematsu 2018). Clinical data show that the distribution of tangles formed by the tau is better correlated with cognitive decline than the plaques formed by A β accumulation (Braak and Braak 1991, Nath 2012). In pathological conditions, like in AD, first abnormal phosphorylation of tau protein decreases its tubulin binding capacity leading to microtubule disorganization. In the second step pTau self-polymerizes and aggregates into the form of NFTs (Kolarova 2012). In AD, the normal role of tau protein (keeping the cytoskeleton well organized for the axonal process) is missing because pTau loses its capacity to bind to microtubules. This abnormal behaviour is promoted by conformational changes and misfoldings that leads to aberrant pTau aggregation into fibrillary structures inside the neurons of demented individuals (Kolarova 2012). The neurofibrillary lesions are found in cell bodies and apical dendrites as NFTs, in distal dendrites as neuropil threads and in the abnormal neurites that are associated with neuritic plaques (Götz 2011). The typical brain-regional occurrence and progression of tau pathology correlates temporally and spatially well with neuronal and cognitive dysfunction, with the added weight of the correlation to cerebrospinal fluid-levels of pTau (Crespo-Biel 2012). Neurofibrillary changes are immunoreactive mainly toward the hyperphosphorylated form of tau protein: exon 9–12 of the tau gene, each containing imperfect repeat, encode a microtubule-binding domain, and inclusion or exclusion of exon 10 via alternative splicing generates isoforms with four repeats (4R tau) or three repeats (3R tau), respectively (Uematsu, 2018). Interestingly, regional extent of each isoform is differently regulated; for example, 3R tau-positive lesions are abundant in the areas in which tau deposition begins early, such as parahippocampal area and subiculum, while 4R tau-positive lesions are dominant in the areas in which tau deposition begins later, such as CA4 (Uematsu, 2018).

4.5.4. Central role of ER in protein homeostasis and the role of chaperone proteins

The endoplasmic reticulum (ER) is the major site for protein folding and trafficking in the cell and is central for many cellular functions. Under physiological conditions, ER is a central subcellular compartment for protein quality control in the secretory pathway that prevents protein misfolding and aggregation. Proteins synthesized in the ER are properly folded with the assistance of ER chaperones. When the amount of unfolded proteins exceed the folding capacity of the ER, human cells activate a defense mechanism called the ER stress response, which induces expression of ER chaperones and ER-assisted protein degradation (ERAD) components. These substances transiently attenuate protein synthesis to decrease the burden of ER.

It has been revealed that three independent response pathways separately regulate induction of expression of chaperones, ERAD components, and translational attenuation. Protein misfolding in the ER initiates the intracellular signaling network called unfolded protein response (UPR) for reestablish homeostasis in energy-starved neurons (Roussel 2013, Li 2014). ER dysfunction is involved in the initiation of neurodegenerative diseases. In general, a malfunction of ER stress response caused by aging, genetic mutations or environmental factors can result in “conformational diseases” (Yoshida 2007) and ER dysfunction might work as an important part in causing AD (Li 2014). Alterations in the UPR network are involved in cognitive impairment and memory loss (Duran-Aniotz 2014) and intracellular accumulation of “toxic turn A β ” is associated with ER stress in AD (Soejima 2013). iA β oligomers directly interact with ER, and thus mobilize Ca²⁺ and cause disruption of ER- Ca²⁺ homeostasis which is characteristic in AD (Honarnejad 2013, Jensen 2013, Popugaeva 2013). If cells fail in stress compensation, the UPR may shift adaptive programs toward apoptosis to eliminate damaged neurons (Endres 2013, Pereira 2013). Subcompartments of ER are in physical contact with mitochondria via mitochondria-associated ER-membranes (MAMs). A β elevates the expression of MAM-associated proteins, and thus increases ER-mitochondrial contacts in HC neurons (Hedskog 2013). A β exposure increases the Ca²⁺ shuttling from ER to mitochondria and disturbs the ER-mitochondrial Ca²⁺ cycle decreasing energy-metabolism pathways. ER-mitochondria contacts and cross-talk may play important role in AD pathology (Hedskog 2013).

4.6. Drug targets for treatment AD: a new era in drug research

The drugs currently used to treat AD (cholinesterase inhibitors, *N*-methyl D-aspartate (NMDA) receptor agonist, antipsychotic drugs) have limited therapeutic value. Potentially disease-modifying therapeutic approaches targeted A β and tau protein (Reitz 2012), however, most of them failed in clinical phases.

The failure of anti-A β antibody therapies targeting eA β in 2012-2017 does not mean that the amyloid hypothesis is incorrect, but the real culprit might be the intracellular A β . Various biomarkers show that *amyloid pathology correlates with progression at earlier stages of the disease*. The simplest therapeutic strategy is to rescue synaptic deterioration and dysfunction which is a result of the overactivation of the innate immune system by high A β levels both within the neuron and in the extracellular environment. A new strategy, a “triple therapy” is needed for removing both the intracellular A β (iA β) and extracellular A β (eA β) (Rosenblum 2014) as well as targeting the synthesis of A β peptides from APP (Rhinn 2013) and regulating protein folding in ER and ER-stress response.

Drug development approaches have been performed to date primarily against eA β and amyloid plaques than the attention has been placed on formation of iA β (LaFerla 2007) and ER-dysfunction. A β -related synapse damage and memory impairment correlate with intracellular levels of A β but not with plaque burden (Tampellini 2010). Senile plaques may originate from iA β as a result of its secretion into extracellular space or its release after neuronal death (Gouras 2000). An AD drug should prevent iA β -formation from APP or inhibit the formation of toxic A β structures. Simultaneously, a good AD drug should also neutralize the toxic eA β oligomers in the interstitial space. Clinical trials have largely been aimed at removing insoluble eA β in senile plaques and have not targeted the soluble, extremely neurotoxic iA β oligomers. Trafficking and APP processing (that is the formation of A β) in the cell should be also targeted (Rosenblum 2014). Last but not least, AD is spreading from neuron to neuron along the anatomical pathways in a prion-like fashion (the two prionoids participating in the propagation of AD are very probably pTau and A β). During the years of AD-progression a “quadruple therapy” is needed in the treatment: in the first phase A β -synthesis inhibitors, in the following phases A β removing and inhibiting agents should be used, averting ER stress and protein misfolding as well as regulation of the ER-mitochondria Ca²⁺-cycle, and in the last phases the prionoid propagation should also be prevented (e.g. by inhibiting exosomal propagation of prionoids). Although specific receptors of “supertoxic A β oligomers” might exist (Kim 2013), their validation as drug targets is very difficult.

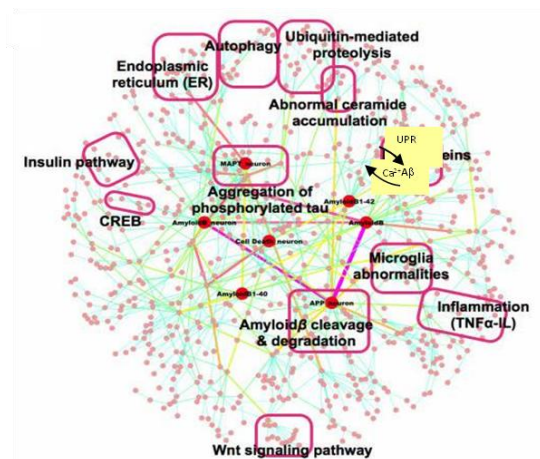


Fig. 6. The complex pathway system of formation and interaction of iA β , eA β (fA β), pTau in AD and cell-to-cell transmission possibilities (Mizuno 2012).

A β in monomeric form might have important neurotrophic activity, and the presence of iA β is common in normal brain (Blair 2014). However, it is widely accepted that A β oligomers have no physiological functions, all of their effects found to date have been negative. Misfolded, A β oligomer is a *pathological ligand*. As a consequence, the best way is to prevent intracellular synthesis of misfolded A β and interactions with cytoplasmic membrane proteins and subcellular

organelles. Fig. 6. shows the simplified pathway network of AD and the possible drug targets according to Mizuno et al.

4.6.1. Heat shock protein coinducers as putative AD drugs

Molecular chaperones, like heat shock protein70 (HSP70) has been shown to play important role in the cytotoxicity of both A β and tau (Evans 2010). For example, HSP72 blocks the early stages of A β aggregation *in vitro* at substoichiometric level (Evans 2010) and HSP70 has been shown to alter processing of the APP (Kumar 2007), also, this chaperone protects against A β -induced cytotoxicity via inhibiting caspase-9 and accelerating the elimination of A β (Veereshwarayya 2006). In addition to the effects on A β , HSP70 also binds tau at two sites within its tubulin-binding repeats, which is the same region required for tau self-association (Sarkar 2008). This finding suggests that HSP70 might compete with aggregation and toxicity and, consistent with this model, overexpression of HSP70 reduces aggregated tau in mouse models (Petrucci 2004).

HSP70 and co-chaperones form complex networks that are crucial to the folding of nascent polypeptides, unfolding and refolding misfolded proteins, transduction of cellular signals and the regulation of the cell cycle, proliferation and apoptosis (Jolly 2000, De Los Rios 2006). Activation of certain HSPs such as HSP70 that may have function as molecular chaperone could be also one of the most physiological methods of several possibilities for regulating the malfunction of ER stress response and decrease the formation of misfolded proteins.

Considering the central role of ER and molecular chaperones in AD and other conformational diseases, we started in our laboratory the development of novel therapeutic strategies based on ER stress regulation and molecular chaperon induction.

Our research team in cooperation with another group found a novel group of compounds (substituted 1,4-dihydropyridines, DHPs Fig. 7, (Kasza 2016).) that proved to be HSP co-inducers. These compounds can selectively modulate HSP activity, they act by regulating an existing stress response and have little or no effect in non-stressed (healthy) systems. These coinducer compounds do not affect HSP production, but can modulate HSP induction in combination with other mild stresses that are present in different disease states. These compounds might be useful also for neuroprotection in AD, simply by stabilizing the native structure of A β -oligomers (oA β 1-42) and preventing misfolding and formation of toxic oA β .

One of our aims was to investigate the neuroprotective effect of our newest chaperon protein coinducer LA1011 in a transgenic mouse model of AD.

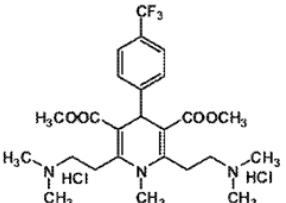
Code	Structure	Chemical Name
LA1011		Dimethyl 4-(4-trifluoromethylphenyl)-2,6-bis-(2-dimethylaminoethyl)-1-methyl-1,4-dihydropyridine-3,5-dicarboxylate dihydrochloride

Fig. 7. The chemical structure of 1,4-dihydropyridine derivatives with HSP coinducer activity.

4.7. Modeling Alzheimer's disease

In dementia research, animal models have become indispensable tools. They not only model aspects of the human condition, but also simulate processes that occur in humans and hence provide insight into how disease is initiated and propagated (Götz 2009). To elucidate the molecular basis of pathological processes in AD, several mouse models of AD have been developed (Sasaguri 2017, Esquerda-Canals 2017, Jankowsky 2017). Most of these models exhibit transgenic expression of one or more mutations in key proteins (APP, PS1, PS2) found in FAD (Dodart 2005, Kishimoto 2017). Creating animal models that can recapitulate characteristic features of AD is of great importance in increasing understanding of disease pathogenesis and developing new therapies (Dodart 2005). A β - and tau-pathology in sporadic and familial AD-cases are morphologically similar, rationalizing the use of mouse models with genetically engineered FAD mutations for understanding sporadic AD (SAD). However, the extent to which these models actually reproduce SAD remains unknown (Sasaguri 2017).

A great variety of transgenic mouse models of AD has been developed during the last decade for studying the pathophysiological processes of the disease (Fülöp 2004, Duyckaerts 2009, Götz 2009, Zussy 2013). Also a transgenic rat model was introduced (Glabe 2006). The most frequently used rodent models (Puzzo 2015, Kumar 2016, Salari 2016) have been widely reviewed recently. There is a big challenge to develop relevant animal models for AD owing to translation problems across species: therapies that work in rodents often do not translate to humans (De Felice 2016).

The transgenic mouse and knockout models analyze certain aspects of AD pathology, allowing exploration of unknown territories and revealing new pathogenic possibilities (Orta-Salazar, 2016). Summaries of the most prominent mouse models of AD have been published very recently (Cavanaugh 2014, Onos 2016, Esquerda-Canals 2017). However, tg-models have had limited success in translation of mouse experimental results into the clinics. The most obvious divergence of transgenic animal models from human AD is the artificial nature of the transgenic technology.

Table II shows the main characteristics of the most frequently used tg mouse models of AD.

Table II. Selected examples and the main characteristic of some frequently used tg mouse models of AD

Mouse model	Transgene	Mutation (promoter)	Pathology	Age of onset of pathology	Behavioural deficit (age of onset)	References
1. PDAPP Human APP		APPIndiana (human PDGFb)	Plaques Neuronal loss	6-9 mo	Learning/memory (13-15 mo)	(Games 1995)
2. Tg2576 Human APP		APPSwe (hamster PrP)	Plaques	ca. 8mo	Learning/memory (9-10 mo)	(Hsiao 1996)
3. APP23 Human APP		APPSwe (mouse Thy 1.2)	Plaques Neuronal loss	6 mo 14-18 mo	Learning/memory (3 mo)	(Calhoun 1999)
4. TgCRND8 Human APP (J20)		APPSwe+Indiana (hamster PrP)	Plaques	3 mo	Learning/memory (3 mo)	(Chishti 2001)
5. APP/PS1 Human APP PS1		APPSwe+PS1dE9 (mouse PrP)	Plaques	6 mo	Learning/memory (8 mo)	(Jankowsky 2001)
6. CVN-AD Human APP		APPSweDI/NOS2-/-	Plaques, pTau;	~ 5-6 mo	Learning/memory neuronalloss	(Colton 2008)
7. 3xTg-AD Human APP, PS1, tau		APPSwe+PS1M146V +TauP301L	Plaques, Neurofibrillary pathology	6 mo 12 mo	Learning/memory	(Oddo 2003)
8. 5XFAD Tg6799		huAPP ₆₉₅ (Swe/Flo/Lon); hu PSEN1 (M146/L/L286 V) (mouse Thy 1.2)	Plaques Gliosis, Neuronal loss	1.5-2 mo	5-6 mo	(Oakley 2006)
9. TauPS2APP Human APP, PS2, tau		Swe+PS1M146V +TauP301L (mouse Thy 1.2)	Plaques, Neurofibrillary pathology (with tangles)	3 mo 4-6 mo	None	(Grueninger 2010)
10.Tg4510 Human tau		TauP301L (CAMKII) (teto)	Plaques,Neurofibrillary pathology (with tangles), neurodegeneration	2.5 mo	Learning/memory (2.5 mo)	(Santacruz 2005)
11.JNPL3 Human tau		TauP301L (mouse PrP)	Plaques, Neurofibrillary pathology (with tangles), neurodegeneration	3 mo	Motoric (4.5 mo)	(Lewis 2001)
12.TauP301S Human tau		TauP301S (mouse Thy 1.2)	Plaques, Neurofibrillary pathology (with tangles), neurodegeneration	<5 mo	Motoric (4.5 mo)	(Allen 2002)

Rodents do not develop AD. The normal in vivo concentration of A β might be in picomolar range, contrary to that in human AD brains that has nanomolar A β levels. In addition, rodent A β differs from human A β by 3 AA substitutions (R5G, Y10F and H13R) and these changes also may prevent amyloid aggregation. As a consequence, the introduction of at least one of the main human AD genes (APP, PS1, PS2 and ApoE) is mandatory to model the pathology in rodents (Esquerda-Canalas 2017). The ideal transgenic model should mimic multiple aspects of the disease including its etiology and a time-dependent progression of the pathology, which involves similar structures and cells, alike in human pathology. Very recently, the Alzforum Research Models has offered 139 transgenic mouse models for studying AD (www.alzforum.org/res/com/tra).

Mice that overexpress the human mutant APP show learning deficits (Chen 2000) and are indeed valuable models for studying AD pathogenesis. However, it has been argued that the pathological sequences observed in these animals are different from those in human AD brain and the cost of the transgene technology limits their applicability (Sipos 2010), so nontransgenic animals are also suitable for studying the pathogenesises of A β and tau pathology (Oikawa 2010). Direct

administration of A β into the rodent brain has another advantage beyond the cost effectivity: the method may be used in young animals, the administered A β may cause rapid behaviour changes and thus it does not require long (4-6 month) experimental process. The soluble oA β observed in AD patients contain A β in its most predominant sequences: A β 1–40 or A β 1–42 (Zussy 2013). Most A β infusion models have been developed the assumption that brain A β deposition is a requisite to inducing behavioural impairments. Indeed, methodologies differ by the type of peptide infused (A β 1-40, A β 1-42, or shorter fragments), peptide concentration, duration of infusion (single versus chronic treatment), site of infusion (intracerebroventricular, icv versus intracerebral), and type of preparation infused (fresh versus “aged” A β preparation). Acute or chronic injections of A β or other exogenous chemicals in rodents allowed the creation of animal models showing several characteristics of AD. Minipumps that allow A β infusion over a 2-week period might not be appropriate, as the conformation of A β found in the minipump may vary considerably from day1 to day 14 at a constant temperature of 37°C.

Many of reports (O’Hare 1999, Sipos 2007, Takeda 2009, Balducci 2010) strongly support a disruptive action of soluble species of A β on behaviour, suggesting that acute brain A β infusion may be sufficient to induce learning and memory impairments (Dodart 2005). These less expensive animal models have been administering A β peptides intrahippocampally (Christensen 2007, Bagheri 2011, He 2011), intranasally (Sipos 2010), icv (Townsend 2006, Takeda 2009, Balducci 2010, Bozso 2010, Zussy 2011, Kim 2016) or by microinjections into the entorhinal cortex (Sipos 2007). It was found that the oA β 1-42peptide administered into the rodent brain enters the neurons from the interstitial space into the rodent brain. The most difficult problem of the use of oA β 1-42 microinjections is the structural heterogeneity of oligomeric samples, they may have different conformation, aggregation size and solubility. This heterogeneity causes severe problems in reproduction of in vivo experiments.

In our laboratory we tried to elaborate a novel, robust AD animal model using icv microinjections of oligomeric A β 1-42 into rat brain, it was the main aim of my thesis. For reproducible results the oA β 1-42 samples should be well characterized.

AD is a very complex and multifactorial disease, thus it is not easy to find a reliable *in vivo* model for translation the experimental results of drug candidates from animals to humans. However, as A β peptides play central role in starting AD, animal models using A β administration or A β overproduction (causing ER malfunction and disturbance of the ER-mitochondrial Ca²⁺-cycle in the rodent brain) could mimic the early phase of AD.

4.8. Aims

According to the recent studies, there is a need for a simple, cost-effective, reliable and repeatable animal model in which the characteristic features of AD are developing after injection of a wellcharacterized A β form into the brain. Our first aim was to find and validate a good rat model for studying the early phase of AD. We used icv injections of oligomeric A β 1-42.

Improvement of icv oA β 1-42 administration as a model of early AD had the following experimental steps:

1. Detect fluorescent 7-amino-4-methylcoumarin-3-acetic acid (AMCA) labeled oA β 1-42 after icv administration in the HC area.
2. Find the toxic form of the controlled “in situ” prepared oA β 1-42.
3. Estimate behavioural performance after administering the oA β 1-42icv injection.
4. Detect mophological changes - neuronal dysfunction and tau-pathology - with histological methods in the hippocampal area.
5. Examine degeneration of synapses by measuring the decrease of the number of dendritic spines in the cornu ammonis 1 (CA1) region.
6. Validate the model with an additional experiment according to the results using the toxic form of oA β 1-42.

Simultaneously with these experiments, we measured with our hevavioural and pharmacological methods the neuroprotective effect of LA1011 in a transgenic mouse model (APPxPS1) of AD.

5. MATERIALS AND METHODS

5.1. Preparation of used chemical compounds

5.1.1. Preparation of different A β 1-42 oligomeric assemblies

The oligomeric A β 1-42 peptide was synthesized in the following way: the A β peptide precursor iso-A β 1-42 was synthesized by Fmoc-chemistry and transformed at neutral pH to A β 1-42 by O \rightarrow N acyl migration in a short period of time, resulting in a water soluble oligomeric mixture of A β 1-42 oligomers as previously described (Bozso 2010). The aggregation grade of these oligomers thus formed could be standardized. In these studies, the soluble oA β 1-42 peptide samples were freshly prepared by incubating the oA β 1-42 peptide on 37°C in PBS at pH 7.4 for different time courses (24 h, 120 h, 168 h) at the concentrations of 25, 50, 75 and 200 μ M, respectively. It was subsequently diluted to the final concentration of 10 μ M. The amount of oA β 1-42 injected at the concentration of 10 μ M equaled 50 pmol or 225 ng of A β peptides.

The fluorescent labeled A β peptide (AMCA-A β) was synthesized in our research group (Fülöp 2001).

5.1.2. Atomic force microscopy studies (AFM) of oA β 1-42 assemblies

10 μ l of peptide solution were pipetted onto freshly cleaved mica (Muscovite mica, V-1 quality, Electron Microscopy Sciences, Washington DC, USA). After 2 min the samples were washed twice with 10 μ l of distilled water and then dried with nitrogen gas. The AFM images were obtained using tapping mode on a NT-MDT SOLVER Scanning Probe Microscope under ambient conditions. AFM tips type PPP-NVHAuD-10 manufactured by NANOSENSORS were applied with a nominal radius of curvature of 2 nm and 15 μ m length. The non-contact silicon cantilevers having typical force constant of 42 N/m and resonance frequency of 278.8 kHz. Further information of the tip: material n⁺-silicon, resistivity 0.01-0.02 Ohm cm, thickness 4.0 ± 1 μ m, length: 125 ± 10 μ m, width 30 ± 7.5 μ m.

5.2. Experimental animals and housing

After arrival, the animals were housed under constant temperature and lighting conditions (23°C, 12:12 h light/dark cycle, lights on at 07:00 h). The rodents had free access to food and water throughout the experiment. After arrival the animals were gently handled by daily measuring. Experiments were performed in accordance with the Hungarian Health Committee and the European Communities Council Directive of 24. November 1986 (86/609/EEC). Formal approvals

to conduct the experiments have been obtained from the Animal Experimentation Committees of the University of Szeged and of the Biological Research Center, and from the local authorities (XVI./03835/001/2006).

5.2.1. Wild-type rats

Adult male Charles River-Harlan rats (Domaszék, Hungary) were the subjects of the experiments, weighing 250–300 g before surgery.

5.2.2. Transgenic and wild-type mice

B6C3-Tg (APP^{swe}/PS1^{dE9})85Dbo/Mmjax mice (APPxPS1) were purchased from The Jackson Laboratory (Bar Harbor, ME, USA) and maintained on the C57BL/6 genetic background (tg). The mice were kept in individual ventilated cages (Acéllabor Ltd., Hungary).

5.3. Treatments

5.3.1. Experiments with rats

5.3.1.1. Surgery and icv administration of oA β 1-42

Before surgery, rats were deeply anesthetized by injecting ketamine (10.0 mg/100 g) and xylazine (0.8 mg/100 g) mixture, and were placed in a stereotaxic apparatus. A midline incision of the scalp was made, and the skull was carefully cleared from the skin and the muscles. After that two holes were drilled above the target regions. Every solution was injected icv with a Hamilton syringe bilaterally, into each hemisphere. 7.5 μ l solution was injected per site (1.5 μ l/min). The coordinates were from Bregma: AP: -1,0; ML: \pm 1,5; DV:-4,5 (Paxinos, 1982). The animals were treated after the surgery with antibiotics and analgesic.

5.3.1.2. Fluorescent microscopy for the pilot study

For fluorescent microscopy study, rats (n=2) received fibrillar form (fA β) and in the other experiment rats (n=4) received oligomeric form and of AMCA (7-Amino-4-methylcoumarin-3-acetic acid)-labeled A β 1-42 at a single dose in dilution of AMCA-A β 1-42: A β 1-42 2:7 ratio (concentrations: AMCA-A β 1-42 16.7 μ M; A β 1-42= 58.3 μ M in total of 75 μ M final peptide concentration). fA β was administered bilaterally (10-10 μ l per site), and oA β unilaterally into the right cerebroventricle (7.5 μ l pro animal). 60 minutes after fA β 1-42, and 5 or 60 minutes after oA β 1-42 administration the rats were transcardially perfused (100 ml PBS, pH = 7.4). The brains were removed and cut to 30 μ m thick sagittal sections. Sections were placed on glass slides, air dried, and mounted in Gel Mount (Biomed, USA). Fluorescent signal was examined in the

sections by a Nikon Eclipse TE2000 fluorescent microscope (Nikon, Japan) and photographed by a Spot RT digital camera (Diagnostic Instruments, USA).

5.3.1.3. *Studies of two different icv administered oA β 1-42*

Subjects were divided into three groups: the control group (n=12) was injected with hydrocarbonate buffered saline (HCBS) solution, the other two groups were injected with 24 h aggregated oA β 1-42 (n=12) and a 168 h aggregated oA β 1-42 (n=12).

5.3.1.4. *Systematic studies for finding the most toxic form among six different oA β 1-42 samples*

Table III. The six A β -treated groups.

Groups of A β -treated animals	Aggregation time (h)	Concentration (μ M) of A β
A (n=11)	24	25
B (n=11)	24	75
C (n=11)	24	200
D (n=12)	168	25
E (n=12)	168	75
F (n=12)	168	200

oA β samples were prepared in combination of three different oA β 1-42 concentrations (25, 75 and 200 μ M) with two different aggregation times (24 h and 168 h). The experiments were divided into two divisions: oA β samples of 24 h and 168 h, respectively (altogether six groups, n=12/group): the control groups (n=11 in the 24 h and n=12 in the 168 h experiments) in both studies were treated with HCBS. For the statistical analysis the mean of data of the two control groups were evaluated (n=23). Table III. summarizes the characteristics of A β -treated groups (A-F) to simplify further orientation.

5.3.1.5. *Validation of the toxic form of the A β 1-42oligomers with MWM task*

To validate the toxic oligomeric form of oA β 1-42, we used two of experimental groups: the rats were injected with 120 h aggregated oA β 1-42 in 50 μ M concentration (n=10) in conclusion recommended range and the control group was treated with HCBS (n=10).

5.3.2. Experiment with mice

5.3.2.1. *Experiment with drug candidate LA1011 in APP/PS1 tg line*

In these experiments we worked with APP/PS1 male transgenic (tg) mice and their wild type (wt) littermates. Animals were treated for six months by daily intraperitoneal (ip) administration of the

drug candidate LA1011 in 3 mg/kg, starting at age of 3 months of mice. Physiological saline was used as a vehicle solution. After the treatment, mice were tested in MWM at age of 9 months (n=8/group).

5.4. Behavioural testing

Developed in the 1980s by R. Morris, the Morris water maze (MWM) has become one of the most commonly used tasks to measure spatial learning for rodents. The test relies on distal cues to navigate from start locations around the perimeter of an open swimming arena to locate a submerged escape platform rodents (Morris 1982, Tomiyama 2010, Senechal 2008, Sipos 2007, Vorhees 2006, Kopniczky 2006, Steckler 2001, Chen 2000).

Rodents were trained in an open-field water maze (diameter: 180 cm for rats, 130 cm for mice, height: 60 cm), filled with water ($23\pm 1^{\circ}\text{C}$) that was made opaque by adding milk. The pool was divided into four virtual quadrants, the invisible platform (diameter: 10cm) was submerged in the middle of one of the four quadrants (that was a standard position) 2 cm for rats or 0.5 cm for mice below the water surface. Around the pool there was a black curtain with extramaze cues.

The experiment was a 5-day test. Four different starting points were used, the animals swam every day two times and were placed into the water facing the wall of the pool. The animals were given 90s to find the platform and 15s to stay on it. Animals that did not find the platform were gently guided and placed on it. The data were calculated automatically by a video tracking system. The means of the data from first trials were used for statistics.

5.5. Histology

After the Morris water maze test the animals were deeply anesthetized and transcardially perfused with 150 ml (rats) or 10 ml (mice) 4°C phosphate-buffered saline solution (PBS), followed by 250 ml (for rats) or 30 ml (for mice) of 4°C paraformaldehyde solution (4% in phosphate buffer, pH 7.4). The brains were removed and postfixed for 24 h in the same fixative (4°C), and subsequently cryoprotected in 30% sucrose solution for 72 h (4°C). Brains were cut on a cryostat to 30 μm hippocampal coronal sections, and the slices were collected and stored at 4°C in PBS for free floating histochemistry.

5.5.1. Cresyl-violet (Nissl) staining

The cresyl violet staining is used for neuronal tissue, the stain binds to the acidic components of the neuronal cytoplasm, showing the number of viable neurons. Slides (n=4, 2 slice/animal) were stained into the filtered 1% cresyl violet solution for 5 minutes and dehydrated subsequently in

50% 70%, 95%, and twice in 100 % ethanol for 1 minute each. Slides were finally placed in xylene for another 10 minutes and coverslipped.

5.5.2. TAU- and A β -immunohistology

To visualize the presence of neurofibrillary tangles, we used human PHF-tau Mab (clone AT100) primary antibody at 1:800 dilution in PBS (pH 7.4) for immunostaining (n=4, 4 slice/animal).

For the studies of A β 1-42 immunohistochemistry in mice, rabbit anti-beta 1-42 amyloid primary antibody (WO-2; Genetics Company) at 1:800 dilution was employed. The second antibody this time was goat anti-rabbit A β in 1:200 dilution.

The methodological steps for the immunohistological techniques were the same. After quenching of endogenous peroxidase activity and a blocking step, the sections were incubated overnight at 4°C with the primary antibody in the presence of 20% goat serum and Triton X-100 0.2%. On the following day the sections were washed in PBS and incubated 1 hour at room temperature with the second biotinylated goat anti-mouse antibody (Vector Laboratories, Burlingame, CA, USA, 1:400). The next step was an 1 hour incubation with avidin-biotin complex (Vectastain Elit ABC Kit, Vector Laboratories, Burlingame, CA, USA; 1:400) and detection with nickel-enhanced 3,3'-diaminobenzidine. After immunostaining and washing, all sections were mounted on gelatin-coated slides, air-dried, dehydrated and coverslipped with DPX mountant for histology (Fluka BioChemika, Buchs, Switzerland). Digital photographs were taken by a digital slide scanner (Mirax Midi, Carl Zeiss, Hungary), for the analysis we used the Histoquant program (3DHistech, Hungary).

5.6. Quantification of dendritic spine density using Golgi-Cox impregnation

The FD Rapid GolgiStain™ Kit (FD NeuroTechnologies, Consulting & Services, Inc., USA) was used (n=3 animal per group, 2-2 slides and 3-3 neurons per slide for rats and n=3 animal per group, 1 slide per animal and 2 neurons per slide for mice) for measuring changes of dendritic spine density in hippocampal CA1 area.

Experimental animals were deeply anesthetized before the brain was removed from the skull. The brains have to be removed as quickly as possible and have to be handled carefully to avoid damage or pressing of the tissue. The tissue was immersed in the impregnation solution (A+B solution) and stored at room temperature for 2 weeks in the dark. The brains were transferred into another solution (C) and stored at 4 °C in the dark for at least 48 hours. 100 μ m coronal sections were cut with microtome (Zeiss Microm HM 650V). Sections were mounted on gelatin coated glass slides.

After the staining procedure and dehydration, the slides were covered with DPX (VWR international).

The clear Golgi sections were studied by inverse light microscope, using oil-immersion objectives. The spine density of the proximal apical dendrite area was analyzed (100-200 μm from soma). One segment (100 μm in length) from a second-third-order dendrite protruding from its parent apical dendrite was chosen in each examined neuron for spine density quantification, as described by Nagy (2011). The dendrites were selected under a 100 \times oil immersion lens and the images (600 \times) of these apical dendrites were captured through a CCD camera (1,600 x 1,200 pixel) connected to a light microscope (Olympus Vanox-T AH-2) and a computer. Serial images were made from each dendrite in the whole of the analyzed segment. The captured multiple photomicrographs from one dendrite were then stacked into one file. To stack the images Image- Pro-Plus image analysis software (IPP; Media Cybernetics, Silver Spring, MD) was used. The whole process of measurement of the spine density was performed by two independent experimenters to blind the analysis.

5.7. Ex vivo electrophysiological studies

5.7.1. Stimulation protocols

Using standard procedures, 350 μm thick transverse acute hippocampal slices were prepared from the brain using a McIlwain tissue chopper (Campden Instruments, Loughborough, UK). Slices were incubated in carbogenated standard ACSF (pH 7.4) at ambient temperature for at least 60 min that contained the followings in mM: NaCl, 130; KCl, 3.5; CaCl_2 , 2; MgCl_2 , 2; NaH_2PO_4 , 0.96; NaHCO_3 , 24; D-glucose, 10. Individual slices were transferred to a 3D-MEA chip with 60 tip-shaped electrodes (40 μm in diameter and 50 – 70 μm in height, spaced by 200 μm , impedance at 1 kHz: 250 - 450 k Ω , noise level: 15 - 20 μV ; purchased from Ayanda Biosystems, S.A., Lausanne, Switzerland). The surrounding solution was removed quickly and the slice was immobilized by a grid. The slice was continuously perfused with carbogenated standard artificial *cerebrospinal fluid* (ACSF) (1.5 ml/min at 34 $^{\circ}\text{C}$) during the whole recording session. Data were recorded by a standard, commercially available MEA (multi-electrode array) setup (Multi Channel Systems MCS GmbH, Reutlingen, Germany).

The Schaffer-collateral was stimulated by injecting a biphasic current waveform ($\pm 100 \mu\text{s}$) through one selected electrode at 0.033 Hz, while the rest of them could be used as recording electrodes. The positioning of the stimulating electrodes and that of the regions in the slices, compared to each other, were constantly synchronized during the various investigations. The peak-to-peak amplitudes of field excitatory postsynaptic potentials (fEPSPs) at the stratum radiatum of CA1 were analyzed.

After a 30 min incubation period, the threshold and the maximum of stimulation intensity for evoke responses was determined. For evoking responses, 30 % of the maximal stimulation intensity was used. When stable evoked fEPSPs were detected (for at least 20 min) LTP was induced, using a theta-burst stimulation (TBS) protocol applied at the maximum stimulation intensity. TBS comprised of 15 trains administered at 5 Hz, the individual trains contained 4 pulses separated by 10 ms. LTP was followed for an hour.

For the statistical analysis of *ex vivo* recordings, the peak-to-peak amplitude of evoked fEPSPs recorded from the proximal part of stratum radiatum was calculated. The level of LTP was determined comparing the average of fEPSP amplitudes recorded in the last five min of the experiment to the baseline recording.

5.7.2. Multi-electrode array recordings

Electrophysiological measurements followed the Morris water maze task, in which different icv injected oA β 1-42 was tested. TBS induced LTP recordings were performed using a MEA setup.

After establishing a stable baseline, LTP was elicited by applying a theta-burst stimulation protocol and followed for an hour. The average of the peak-to-peak amplitudes of fEPSPs before the LTP induction was taken as 100%. The slices obtained from HCBS-injected animals showed robust potentiation after TBS ($230 \pm 24\%$; $n = 15$ channels from 5 slices). There were two more groups of icv injected animals treated with 24 h and 168 h oA β 1-42 aggregates. The 24 h oA β 1-42 assemblies caused a minor impairment in LTP ($184 \pm 7\%$; $n = 26$ channels from 6 slices) while the 168 h amyloid aggregates led to a major disruption of potentiation ($145 \pm 11\%$; $n = 21$ channels from 6 slices).

5.8. Statistical analysis

Statistical analysis of the Morris water maze experiment was performed using SPSS software and Python's Lifelines library (Davidson-Pilon 2016), Github repository. The latency time to attain the platform (with 90 seconds limit) was measured in order to decide which of the four groups has the highest learning rate. The longer the latency time to the platform is, the less the rats capable to learn. "Survival curves" using Cox Proportional Hazard model were fitted, where the days and the treatments were selected as covariates. The comparison of treatment groups was performed using log-rank tests (Jahn-Eimermacher 2011).

In cases of three or more treatment groups in histological analysis, dendritic spine density measurements and LTP analyses one-way ANOVA followed by Fisher's LSD post hoc test was used when appropriate. When the data did not meet the homogeneity of variances assumption, we

used the Games Howell post hoc test and Hochberg's GT2 post hoc test for unequal group sizes with a large n . When the assumptions of one-way ANOVA were not met, we used the nonparametric independent-samples Kruskal-Wallis test followed by Mann-Whitney U test.

Statistical significance was determined by parametric analysis of repeated measures of ANOVA for MWM. One-sample Student's t-test for dendritic spine density in validation experiment we used two treatment groups. All of statistical analyses were performed using SPSS software Differences with a p-value of less than 0.05, 0.01 or 0.001 were considered significant unless indicated otherwise.

6. RESULTS

6.1. Application of an AD model using icv microinjections of oA β 1-42 in rat

Our main aim was to find a novel, robust and relatively cheap animal model of AD. Thus we have studied the effect of well characterized oligomeric A β 1-42 administered icv into rat brain.

6.1.1. Pilot experiment with icv administration of AMCA-labeled A β 1-42 samples

Before the icv administration experiments, we wanted to see whether the A β 1-42 could penetrate across the cerebroventricular wall. We have shown that the diffusion of the fA β 1-42 is stopped by the ventricular wall, thus, an icv injection would be useless (Fig. 8). Therefore our first aim was to demonstrate that oligomeric form of A β 1-42 can reach the HC region after icv injection. Using an unilateral injection of AMCA-labeled oligomeric A β 1-42 into the right lateral ventricle, we have found that the oA β 1-42 appear in the brain parenchyma: we could detect a few of fluorescent signs in the HC area as early as 5 minutes after injection (Fig. 9A,B). The number of signs, namely of oA β 1-42, was evidently higher around the HC area 60 minutes after the injection (Fig. 9C), proving that the AMCA-labeled oA β 1-42 penetrates across the ependyma, or penetrates into the brain by the glymphatic flow (Iliff 2012).

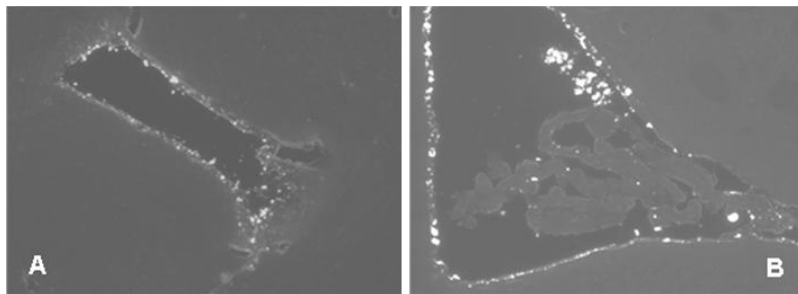


Fig. 8. icv administered fibrillar A β 1-42 does not enter the ependyma and remains in the ventricles. Representative examples of brain sections after icv injected AMCA-labelled A β 1-42fibrils. **A,B**: signs in ventricles from 2 different slides (1h after injection). Animals were injected bilaterally with 10-10 μ l solution of AMCA fA β 1-42, the surgical procedure was the same as described in Materials and Methods.

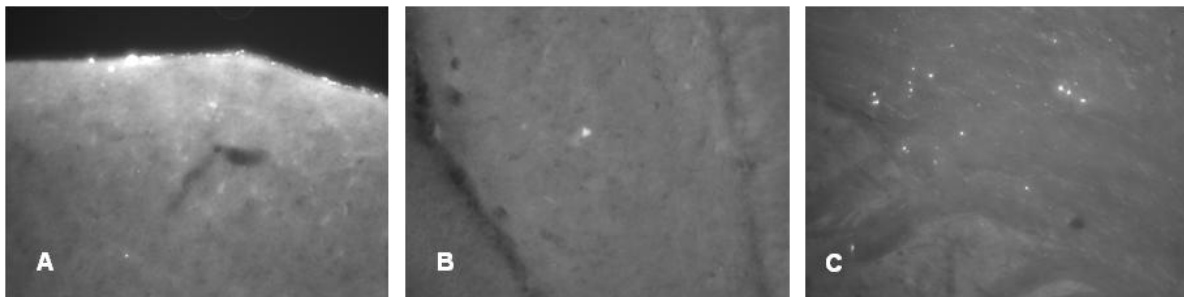


Fig. 9. Oligomeric A β 1-42 enters the brain parenchyma. Representative examples of brain sections after icv injected AMCA-labelled A β 1-42oligomers. **A**: diffusion from the ventricle (5 min after injection) **B**: sign in hippocampus (5 min after injection). **C**: signs in brainparenchyma (60 min after injection). Animals were injected unilaterally with 7.5 μ l solution, the surgical procedure was the same as described.

6.1.2. Studies on the neurotoxic effect of two different, icv administered oA β 1-42 aggregates

We demonstrated that oA β 1-42 can reach the HC area after icv administration. The effect of different oA β 1-42 (24 h and 168 h aggregation time in 25 μ M peptide concentration) was then studied. We analyzed the neuron viability with cresyl violet staining, tau level with tau-immunochemistry, and finally the change of dendritic spine number was also measured. Our aim was to study the neurotoxic effects of the oA β 1-42 in the HC.

In the experiment, three groups of rats were used: the 24 h and 168 h aggregated oA β 1-42 treated groups in the same concentration (25 μ M) as well as HCBS-treated control. Abbreviation used for oA β assemblies: 24 h/25 μ M and 168 h/25 μ M.

6.1.2.1. Histology

After icv administration of oA β 1-42 rats, significant difference exists between groups in number of neurons. Significantly more viable neurons were counted in the HCBS treated group than in the 168 h/25 μ M group ($p = 0.001$, Fig. 10A). The 24 h/25 μ M assembly did not cause significant decrease. Tau- immunohistochemistry resulted also neurotoxic effect in the oA β 1-42 treated groups, significantly more abnormally accumulated TNFs could be detected in both oA β 1-42 treated groups (24 h/25 μ M and 168 h/25 μ M) compared with the vehicle (HCBS) group (HCBS vs 24 h/25 μ M $p = 0.042$; HCBS vs 168 h/25 μ M oA β 1-42 $p = 0.007$, Fig. 10B).

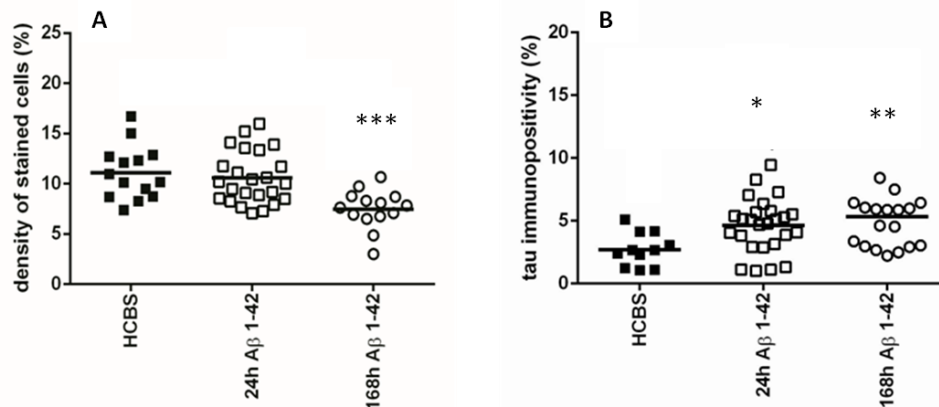


Fig. 10: Hippocampal slices after hydrocarbonated saline buffer (HCBS), 24 h aggregated and 168 h aggregated oA β 1-42 treatment (24 h/25 μ M and 168 h/25 μ M). **A:** Cresyl violet staining: significant difference in the number of stained cells were observed between HCBS vs. 168 h oA β 1-42 treated group ($n = 4$, 2 slices/animal; n refers to the number of animals per group). **B:** Tau-immunostaining: significant difference in the number of tau-immunopositive cells were observed between HCBS vs. 24 h oA β 1-42 treated group and HCBS vs. 168 h oA β 1-42 treated group ($n = 4$, 4 slices/animal; n refers to the number of animals per group). Each dot represents the counted raw data, while horizontal bars indicate mean values. Statistical significance was determined by one-way ANOVA, followed by Hochberg's GT2 post hoc test. Differences with a p -value of less than 0.05 (*), 0.01 (**) and 0.001 (***) were considered significant.

Representative examples of coronal HC sections (Fig. 11) show the staining of neurons after 25 μ M oA β 1-42 administration (A: control group, B: 24 h aggregation, C: 168 h aggregation assembly), and the abnormal aggregated NFTs (D: control group, E: 24 h aggregation, F: 168 h aggregation sample).

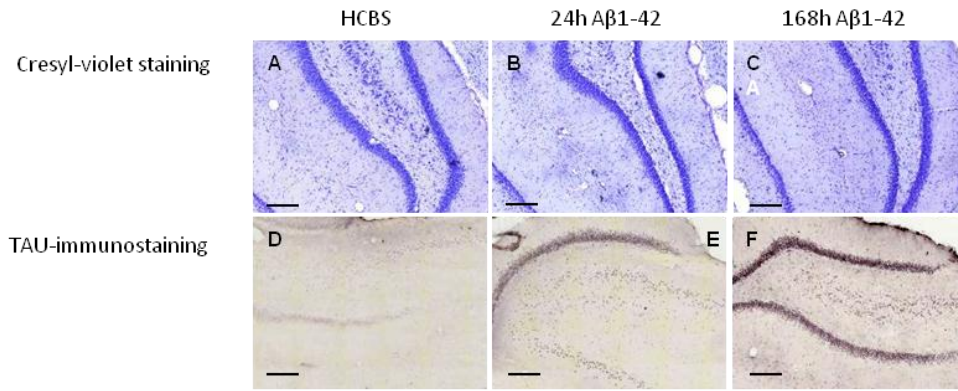


Fig. 11. Representative coronal examples of hippocampal sections stained with cresyl-violet staining (first row) to show the presence of neuron number (first row) and with tau-antibody to show the presence of abnormally aggregated NFTs (second row). **A,D**: control group, **B,E**: 24 h aggregated 25 μ M amyloid treated group, **C,F**: 168 h aggregated 25 μ M amyloid treated group. Scale bar: 200 μ m.

6.1.2.2. Studying the change of dendritic spine density using Golgi-Cox impregnation

The same three groups of animals (24 h/25 μ M; 168 h/25 μ M oA β 1-42 and HCBS-treated control) were used as in the former experiments. We found significant difference in spine density compared the 168 h aggregated oA β 1-42 treated and the control groups: the 168 h/25 μ M oA β 1-42 injected group had significant less dendritic spines than the HCBS-treated control group ($p=0.048$, Fig. 12). There was no significant difference in the 24 h aggregated oA β 1-42 group compared with the controls. Representative photomicrographs demonstrate the difference between groups (Fig. 12C, D, E).

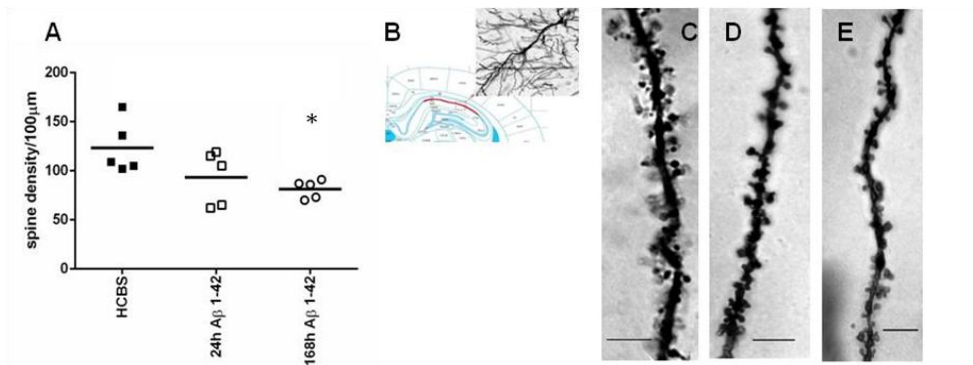


Fig. 12. Representative examples of hippocampal sections stained with Golgi-Cox method to show the presence of the prevailing changes in spine density after treatment with 24 h or 168 h aggregated oA β 1-42 (24 h/25 μ M and 168 h/25 μ M). **A**: Apical dendritic spine density. Each dot represents the counted raw data, while horizontal bars indicate mean values. Significant difference in spine densities was observed between after hydrocarbonated saline buffer (HCBS) and 168 h aggregated oA β 1-42 treated groups ($n=2$, 2-2 slices per group and 3-3 neurons per slice; n refers to the number of animals per group). Statistical significance was determined by one-way ANOVA, followed by Games Howell post hoc test. Differences with a p -value <0.05 were considered significant. **B**: 20x magnification of a CA1 subfield pyramidal neuron. **C**: control (HCBS) group **D**: 24 h aggregated 25 μ M oA β 1-42 treated group **E**: 168 h aggregated 25 μ M oA β 1-42 treated group. Scale bar: 10 μ m.

6.1.2.3. Electrophysiological studies

Ex vivo electrophysiological recordings with multi-electrode array (MEA) were performed in acute hippocampal slices in artificial cerebrospinal fluid (ACSF). After establishing a stable baseline, LTP was elicited by applying a theta-burst stimulation (TBS) protocol and followed for an hour.

The average of the peak-to-peak amplitudes of fEPSPs before the LTP induction was taken as 100% (Fig. 13). The slices obtained from HCBS-injected animals showed robust potentiation after TBS ($230 \pm 24\%$; $n = 5$ slices). The two groups of icv injected animals treated with 24 h/25 μM and 168 h/25 μM oA β 1-42 aggregates showed impairment of LTP. The 24 h oA β 1-42 assemblies caused only a minor impairment ($184 \pm 7\%$; $n = 6$ slices) while the 168 h amyloid aggregates led to a major disruption of potentiation ($145 \pm 11\%$; $n = 6$ slices, Fig. 13A,B).

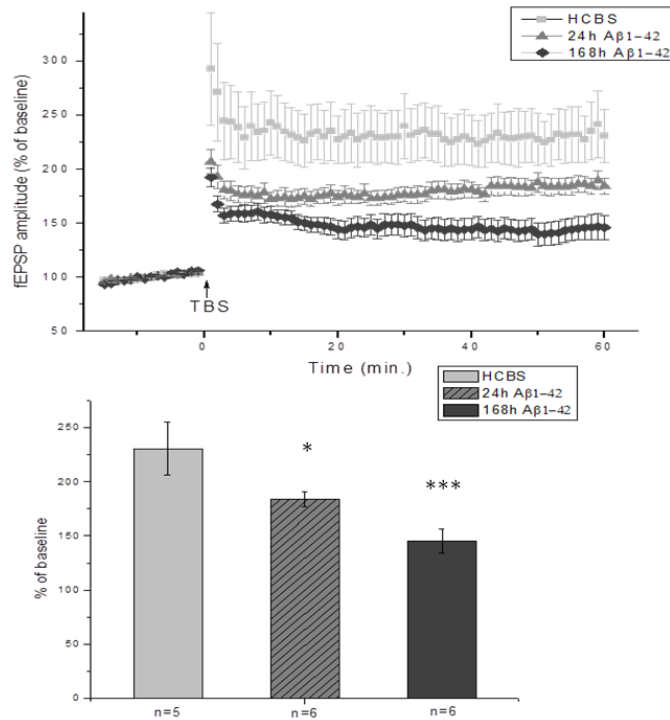


Fig. 13. The amplitude of fEPSPs normalized to preLTP control. The fEPSPs were recorded from the proximal stratum radiatum of CA1. The LTP of the 168 h oA β 1-42 treated animals showed robust impairment compared to after hydrocarbonated saline buffer (HCBS) treated ones, while decrease was smaller in the group of 24 h oA β 1-42 injected rats. Statistical significance was determined by one-way ANOVA, followed by Fisher's LSD post hoc test. The histogram shows the level of LTP between 55 and 60 min post-TBS for each group. Error bars represent mean \pm SEM. * $p \leq 0.05$ and *** $p \leq 0.001$.

6.1.3. Systematic studies for finding the most toxic form of the A β 1-42 oligomers

The influence of both the peptide concentration and the aggregation time on the toxicity of oA β 1-42 assemblies were studied in these experiments. Altogether the effect of 6 different oA β 1-42 assemblies was studied in the biological experiments (see Table III).

6.1.3.1. AFM studies of the concentration and the aggregation time of A β 1-42 oligomers

As the morphological characterization of a mixed oligomer preparation oA β 1-42 is crucial for the better understanding of the biological effects exerted by the different types of oligomers, we conducted in vitro aggregation studies, in which different concentrations of oA β 1-42 were incubated in physiologic buffers for an elongated period of time. Morphology and size of the aggregates were studied by atomic force microscopy (AFM) in tapping mode. The representative

images show that under the applied conditions, mainly spherical oligomers were formed after 24 hours, the size of which did not depend considerably from the peptide concentration (Fig. 14A-C) as average heights of the aggregates after 24 h of aggregation were as follows: in a 25 μ M solution (A) 6.5 nm, in 75 μ M (B) 5.4 nm, in 200 μ M (C) 10.3 nm.

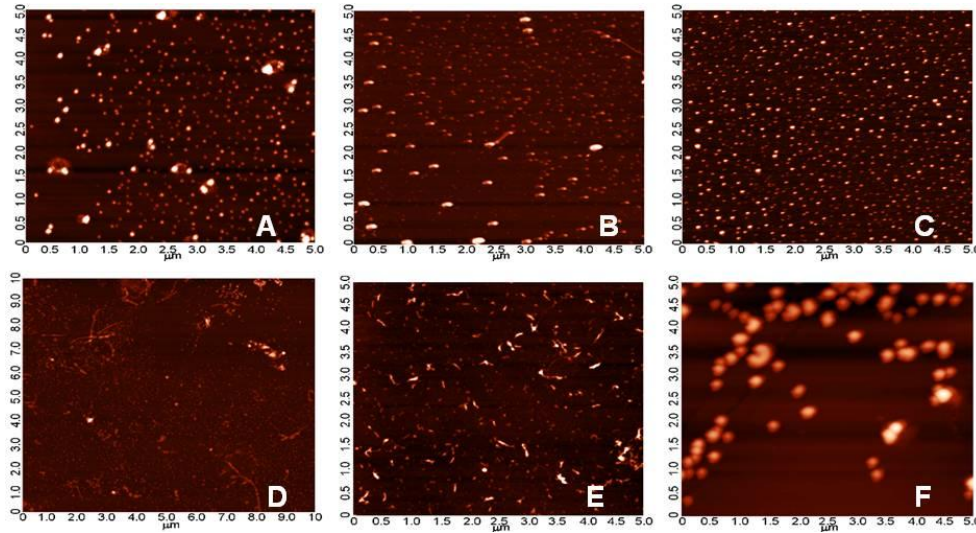


Fig. 14. Morphology of oA β 1-42 oligomers observed on a mica surface in AFM experiments. Average heights of the aggregates after 24 h of aggregation were as follows: in a 25 μ M solution (A) 6.5 nm, in 75 μ M (B) 5.4 nm, in 200 μ M (C) 10.3 nm. After 168 h the following average heights were detected: in 25 μ M (D) 8.2 nm, in 75 μ M (E) 8.0 nm, in 200 μ M (F) 21.5 nm. An elongated incubation resulted in the formation of protofibrillar aggregates besides the spherical ones, as it could be observed in images D-E.

After 168 h, besides the spherical oligomers, protofibrillar aggregates appeared at smaller concentrations (25 μ M and 75 μ M), while in the extremely high 200 μ M concentration we could experience the massive formation of large round aggregates, presumably due to the strong steric hindrance between the monomers in the overcrowded aggregation environment. The detected average heights were in 25 μ M (D) 8.2 nm, in 75 μ M (E) 8.0 nm, and in 200 μ M (F) 21.5 nm. Biological effectiveness of these different aggregates was further studied in consecutive biological experiments.

6.1.3.2. *Spatial navigation in Morris water maze*

The Morris water maze (MWM) task was used to assess spatial learning and memory. MWM is one of the most commonly used experimental models for rodents to measure spatial learning and memory (Morris 1984). The total time spent in arena from first trials (time spent with searching the platform) was the most informative data. The results are represented in Fig. 15A.

Compared to day one of testing, in the lower aggregation grade (24 h aggregation) the 75 μ M oA β -42 treated *Group B* ($p=0.003$), and 200 μ M oA β 1-42 treated *Group C* ($p=0.001$) rats were more likely to find the platform on day four ($p<0.001$) and five ($p<0.001$) than the HCBS treated group, however, on day two ($p=0.959$) and three ($p=0.06$) the change was not significant. The

probability to reach the platform was determined using the Cox Proportional Hazard model (Fig. 15A).

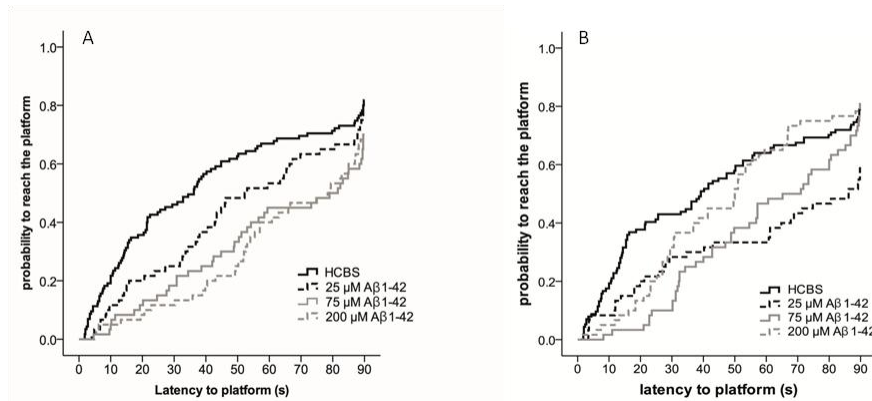


Fig. 15. Effect of different aggregation concentrations (25, 75 and 200 μ M) of synthetic oA β 1-42 on Morris water maze performance. **A:** 24 h aggregation grade. **B:** 168 h aggregation grade. We compared the the treatment groups groups using log-rank tests. The fitted survival curves using the Cox Proportional Hazard model represents the probability that animals find the platform during a trial, capped at 90 s. (n=12/group, except HCBS group, where n=23).

Compared to day one of testing, the rats in the 168 h/25 μ M oA β 1-42 treated *Group D* ($p=0.001$) found the platform more likely on day two ($p=0.002$), three ($p<0.001$), four ($p<0.001$) and five ($p<0.001$). The probability to reach the platform was determined using the Cox Proportional Hazard model (Fig. 15B).

6.1.3.3. Histology

Histochemical studies in the hippocampal region confirmed our behavioural results. Although, no significant difference was found between groups in the number of viable neurons after administration of 24 h aggregated oA β 1-42, there was a tendency which suggested that the increasing aggregation concentration of oA β 1-42 samples resulted in decreasing number of viable neurons in the examined area (Fig.16A).

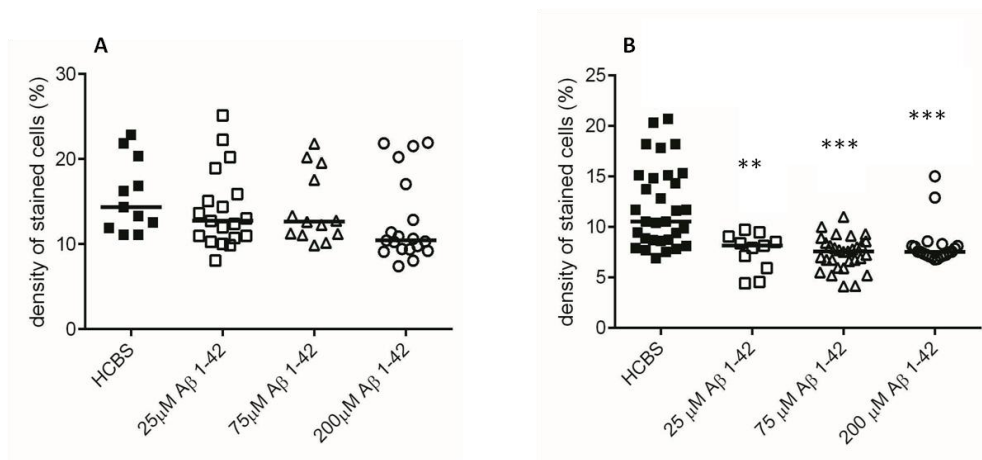


Fig. 16. Cresyl violet staining of hippocampal slices after treatment with different aggregation concentrations (25, 75 and 200 μ M) of oA β 1-42 at **A:** 24 h aggregation grade. **B:** 168 h aggregated grade. Each dot represents the counted raw data, while horizontal bars indicate median values (n= 4, 2 slices/animal; n refers to the number of animals per group). Statistical significance was determined by nonparametric independent-samples Kruskal-Wallis test followed by Mann-Whitney U post test. Differences with a p-value of less than 0.01 (**) and 0.001 (***) were considered significant.

Significant difference appears between the 168 h aggregation time groups: significant loss of viable neurons was found in the hippocampal area in each oA β 1-42 treated groups (*D, E and F*) compared to the control HCBS group (HCBS vs 25 μ M $p=0.01$; HCBS vs 75 μ M $p<0.001$; HCBS vs 200 μ M $p<0.001$; Fig.16B).

Monitoring the presence of abnormally accumulated TNFs and comparing to the control group, significantly higher number of tau immunopositive cells were observed in the 24 h/200 μ M treated (*Group C*, $p=0.015$, Fig.17A), the 168 h/25 μ M treated (*Group D*, $p<0.001$, Fig.17B) and the 168 h/75 μ M (*Group E*, $p<0.001$, Fig.17B) treated groups.

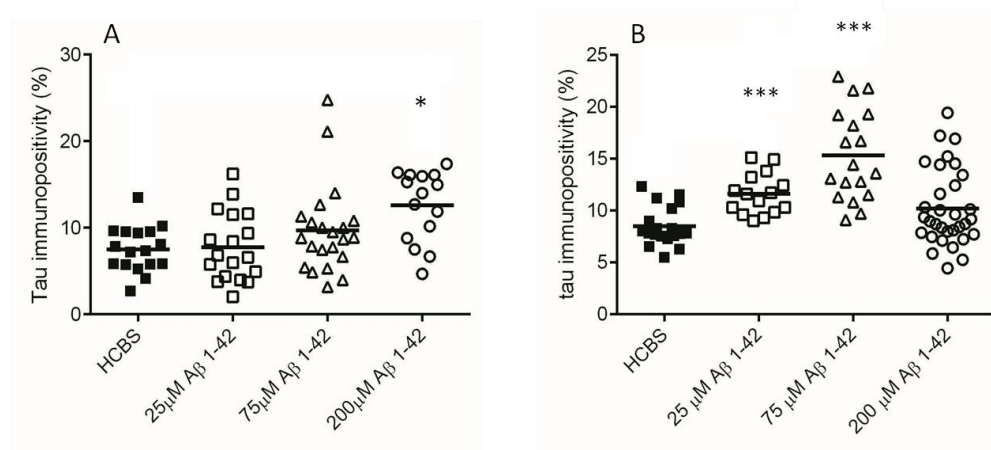


Fig. 17. Tau-immunostaining of hippocampal slices after treatment with oA β assemblies using increasing aggregation concentrations (25, 75 and 200 μ M) of oA β 1-42 treatment. **A:** 24 h aggregation grade. Statistical significance was determined by one-way ANOVA, followed by Hochberg's GT2 post hoc test. **B:** 168 h aggregation time. Statistical significance was determined one-way ANOVA, followed by Games-Howell post hoc test. Each dot represents the counted raw data, while horizontal bars indicate mean values, $n=4$, 4 slices/animal (n refers to the number of animals per group). Differences with a p -value of less than 0.05 (*) and 0.001 (***) were considered significant.

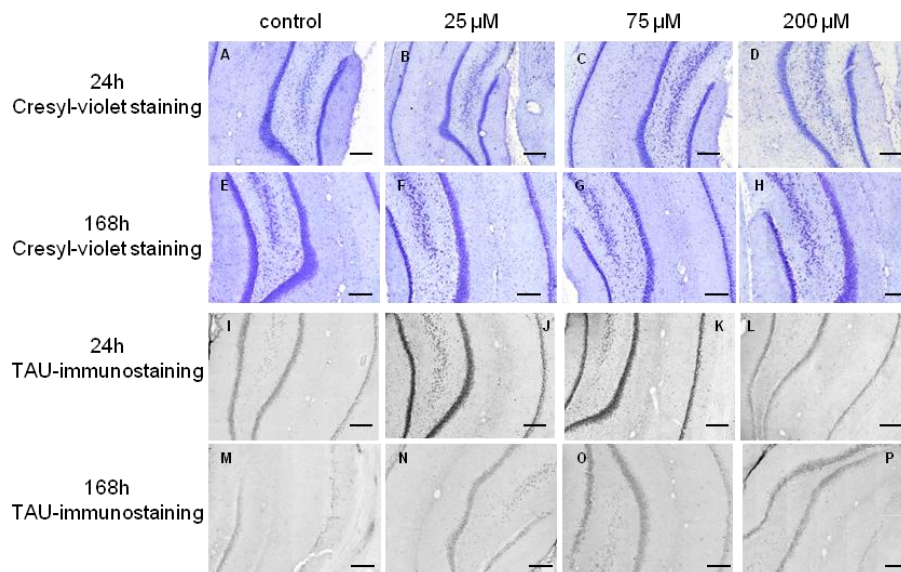


Fig. 18. Representative coronal examples of hippocampal sections with 24 h (first and third lines) and 168 h (second and fourth lines) aggregation grade groups showing the presence of neurons with cresyl-violet staining (upper rows) and with TAU-antibody to show the presence of abnormal aggregated NFTs (downer rows). A,E,I,M: control group; B,F,J,N: 25 μ M concentration; C,G,K,O: 75 μ M concentration; D,H,L,P: 200 μ M concentration. Scale bar: 200 μ m.

Representative examples of coronal HC sections show neurons after 25, 75 and 200 μM oA β 1-42 administration with 24 h aggregation time (Fig. 18A-D) and 168 h aggregation time (Fig. 18E-H) besides control group using cresyl violet staining. The abnormal aggregated NFTs are demonstrated in Fig. 18 (I-L) with 24 h aggregation and Fig. 18 (M-P) with 168 h aggregation time.

6.1.3.4. *Ex vivo electrophysiological recordings with multi-electrode array (MEA)*

The electrophysiological studies in the hippocampal region confirm our behavioural and immunohistochemical results. Slices were prepared from rats that had received icv administration of 24 h/25 μM (Group A), 24 h/75 μM (Group B) and 24 h/200 μM oA β 1-42 (Group C) oA β 1-42. oA β 1-42 samples with Groups A and B caused reduced potentiation after LTP induction ($168\pm 8\%$ and $185\pm 10\%$, $n=6$ and 10 ; respectively) compared to HCBS treated group ($233\pm 26\%$, $n=5$, Fig. 16), but the greatest reduction of LTP level caused the 24 h/200 μM oA β peptide (Group C) ($136\pm 3\%$, $n=8$, Fig. 19A).

The effect of the 168 h aggregates also showed concentration dependence (Fig. 19B). Similarly to the 24 h aggregation experiments, the effects of 25 μM (Group D) and 75 μM (Group E) peptide assemblies do not differ from each other, as they similarly reduced LTP level ($145\pm 11\%$; $n=6$ and $145\pm 4\%$; $n=12$, respectively). In contrast, the 168 h/200 μM (Group F) caused oA β aggregates much smaller reduction of LTP ($182\pm 9\%$; $n=5$ compared to HCBS group $232.5\pm 26\%$; $n=5$, 19B).

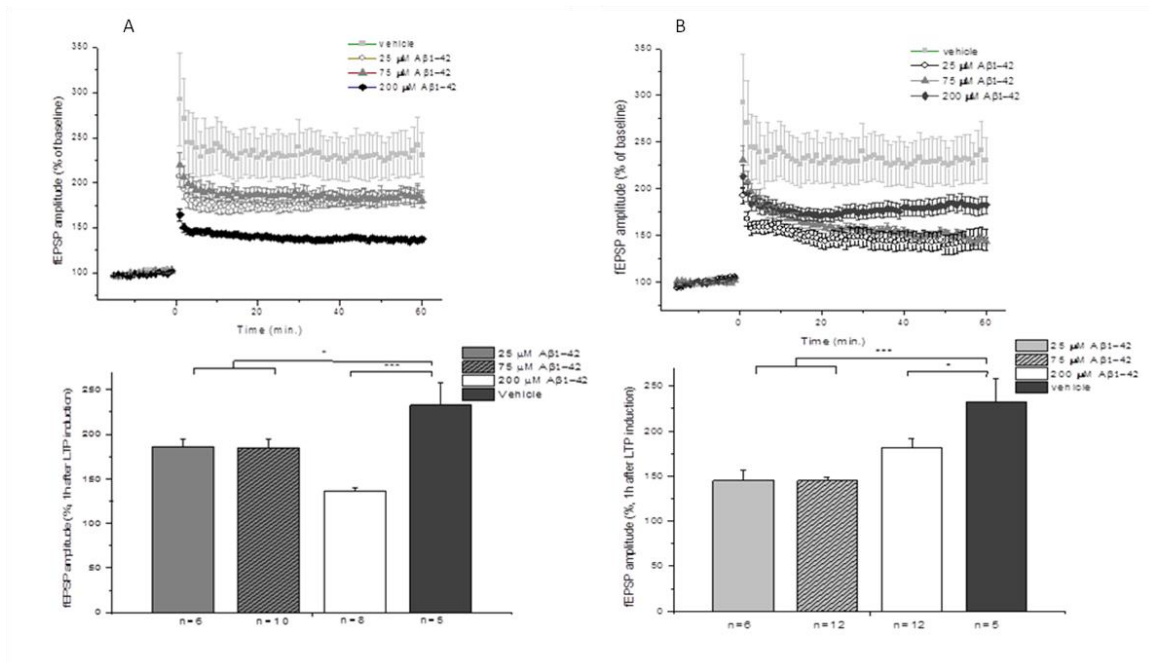


Fig. 19. LTP impairment depends on the aggregation concentration. The effect of 75 μM , 25 μM and 200 μM oA β samples on LTP in HC slices. **A:** 24 h aggregation grade. **B:** 168 h aggregation grade. Statistical significance was determined by one-way ANOVA, followed by Fisher's LSD post hoc test. The histogram shows the level of fEPSP potentiation between 55 and 60 min post-TBS. Error bars represent mean \pm SEM. * $p \leq 0.05$ and *** $p \leq 0.001$.

6.1.4. Validation of the most toxic form of the A β 1-42 oligomers

To validate the results of the icv injected oA β 1-42 experiments, namely that the oligomeric size has to be in range 8-10 nm to have toxic effect, we made a study with 120 h aggregation time and 50 μ M concentrated oA β 1-42. Aggregation was tested by AFM, average particle diameter was 8.5 nm.

6.1.4.1. *Spatial navigation in Morris water maze*

Mean of time spent in first trials in the arena resulted that oA β 1-42 in this concentration and aggregation grade (50 μ M, 120 h) disturb the spatial memory. There was a significant difference between groups ($F_{1,20}=1.713$, $p=0.001$), the HCBS injected animals spent significant less time with finding the platform compared with the oA β 1-42 treated group (Fig. 20).

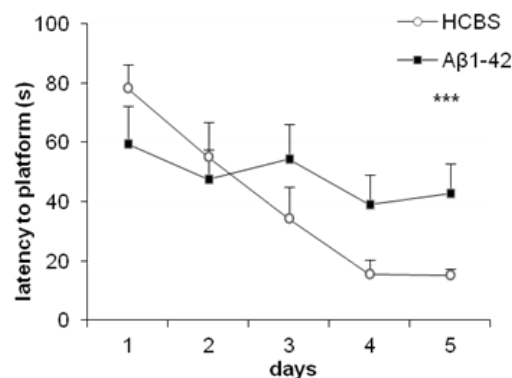


Fig 20. Mean time spent in first trials (\pm S.E.M.) in the arena. Statistical significance was determined by parametric analysis of repeated measured of ANOVA. Asterisks shows the difference compared with the control group. Differences with a p-value of less than 0.001 (***) were considered significant.

6.1.4.2. *Studying the change of dendritic spine density using Golgi-Cox impregnation*

Counting dendritic spines resulted significant difference in spine density compared the groups, the 120 h aggregated 50 μ M concentrated oA β 1-42 injected group had significant less dendritic spines compared with the control group ($t=9.092$, $p=0.001$, Fig. 21A). Representative photomicrographs show the effect of the 120 h, 50 μ M oA β 1-42 oligomers on spine number (21C,D).

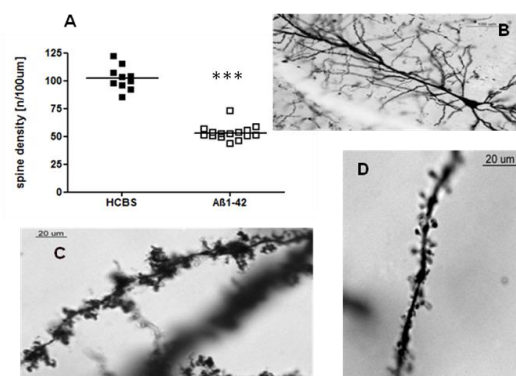


Fig. 21. **A:** Apical dendritic spine density analysis revealed that the amyloid treatment induced significant reduction in spine density compared with the control group. Statistical significance was determined by one-sample Student's t-test. Differences with a p-value of less than 0.001 (***) were considered significant. Representative examples of HC sections stained with Golgi-Cox staining to show the presence the prevailing changes in spine density. **B:** 20x magnification of a CA1 subfield pyramidal neuron **C:** HCBS treated group **D:** 120 h 50 μ M oA β 1-42 treated group.

6.2. Experiment with LA1011 drug candidate on APP/PS1 transgenic mice

6.2.1. Experiment with LA1011 treatment on APP/PS1 mice

The neuroprotective effect of the HSP coinducer LA1011 was studied in A β overproducing APPxPS1 tg mice both with behavioural and histological methods.

6.2.1.1. *Spatial navigation in Morris water maze*

After 6 months daily ip treatment of mice with either LA1011 (3 mg/kg) or saline, the MWM test was applied. The animals were placed into the water facing the sidewalls of the pool at different starting positions across trials, and the swim time to find the platform (escape latency) was followed with a tracking system. The animals learned to swim to the correct location with decreasing escape latencies across days. Pairwise comparison of daily performances was made using the log-rank test and included all mice. Compared to day one of testing, mice were more likely to find the platform on day two ($p=1.65e-5$), day three ($p=5.24e-6$), day four ($p=1.88e-11$) and day five ($p=4.55e-12$). The probability to reach the platform was determined using the Cox Proportional Hazard model. Significant differences were found between wt+saline vs. wt+LA1011 ($p=0.047$), wt+saline vs. tg+saline ($p=0.036$) and tg+saline vs. tg+LA1011 ($p=0.001$) groups. Importantly, mice in the tg+saline group required significantly more time to find the platform compared to the wt+saline group; however, the 6 months daily ip LA1011 treatment tg mice showed a significantly improved learning ability (tg+saline vs. tg+LA1011 $p=0.001$). Interestingly, we found LA1011 improved the memory potency (precognitive) of mice as wt+LA1011 treated mice required less time to complete the task compared with controls (wt+saline) ($p=0.047$).

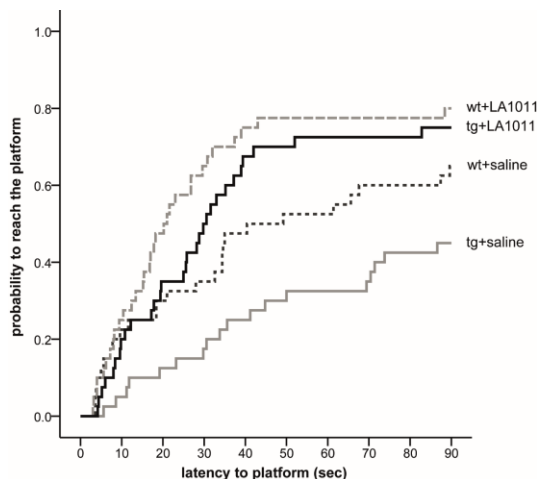


Figure 22. Effect of LA1011 treatment on Morris water maze performance. We compared the the treatment groups groups using log-rank tests. The fitted survival curves using the Cox Proportional Hazard model represents the probability that animals find the platform during a trial, capped at 90 s (n=8/group).

6.2.1.2. Histology

Brain sections (prepared as described in “Materials and Methods”) were stained with cresyl violet, which stain Nissl substance in the cytoplasm of neurons in paraformaldehyde or formalin-fixed tissue. Digital images were analyzed by HistoQuant program. The difference in the number of neurons was significant between the groups (Fig. 23A; Fig. 24A-D). Significantly fewer neurons were observed in the tg+saline group compared with the wt group (tg+saline vs. wt+saline group, $p=0.002$). Cresyl-violet staining confirmed that LA1011 was neuroprotective in the transgenic AD mouse model. Treating tg mice with LA1011 for 6 months significantly prevented the loss of neurons in this group (tg+saline vs. tg+LA1011, $p=0.041$, 23A).

Tau-pathology studies used immunohistochemistry to detect tau in PHF, a major component of the neurofibrillary tangles (NFTs) involved in the pathology of AD that are not present in normal biopsies (Nagy 2011). Digital images were analyzed by HistoQuant program. There were significant differences in the number of abnormally accumulated NFTs in the HC between the groups ($p=0.001$, Fig. 23B; Fig. 24E-H). There were more NFTs in the HC slices of the tg+saline group compared with the wt+saline group ($p=0.001$). Most importantly, the administration of HSP co-inducer LA1011 decreased the number of NFTs in tg mice HC to the level found in the HC of wt mice ($p=0.001$) (Fig. 23B).

Long-term memory is mediated in part by the growth of new dendritic spines (or the enlargement of pre-existing spines) to reinforce a particular neural pathway. According to the literature, APPxPS1 mice undergo spine loss already by the age of 4 months (Smith 2009). One of the best neurohistological methods to observe detailed morphology of neurons is Golgi staining.

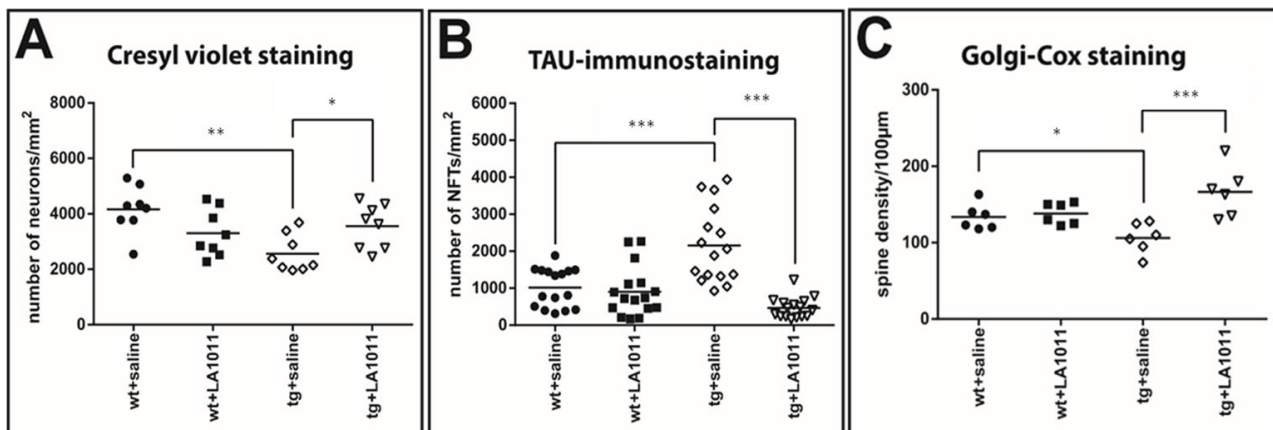


Figure 23. Cresyl-violet staining, TAU-immunostaining, and Golgi-Cox staining of hippocampal slices of wt and tg animals after 6 months treatment. (A) Number of counted neurons/mm²; n=4, 2 slices/animal, (B) number of counted neurofibrillary tangles/mm²; n=4, 4 slices/animal and (C) measured spine density/100 µm; n=3, 2 slices/animal. Each dot represents the counted raw data, while horizontal bars indicate mean values. Statistical significance was determined by one-way ANOVA, followed by Fisher's LSD post hoc test. Differences with a p-value of less than 0.05 (*), 0.01 (**) and 0.001 (***) were considered significant; n refers to the number of animals.

The Golgi-Cox protocol can be used to study the experimental effects of different pharmacological manipulations on the spatial distribution of neurons, dendrite density, spine number and morphology. After the Golgi-Cox staining of the HC CA1 area, digital images were used to count dendritic spines. The tg+saline group had fewer dendritic spines compared with the wt+saline group ($p=0.045$). The 6 month LA1011 treatment of transgenic animals resulted in a considerably greater number of spines in the HC slices (tg+saline vs. tg+LA1011; $p=0.001$, Fig. 23C).

The treatment did not affect the spine number of wt animals. This could be explained by the molecule's "HSP co-modulating activity" namely it acts like "smart molecules" by selective interactions with only those cells, which are under acute or chronic stress.

A β peptide initiates inflammation in the HC of the human brain in AD. A β is chemically "sticky" and gradually builds up into plaques (Duyckaerts 2009), which can be identified by immunohistochemistry using anti-A β antibody. We observed amyloid plaque-like structures in tg mice (Fig 24I-L). The representative examples of sections show a notable amount of plaque formation in the HC of transgenic saline treated animals compared to that of wt samples. Administering LA1011 to tg mice decreased plaque formation (Fig. 24K, L). There were no signs of amyloid plaques in sections from wt animals (Fig. 24I, J).

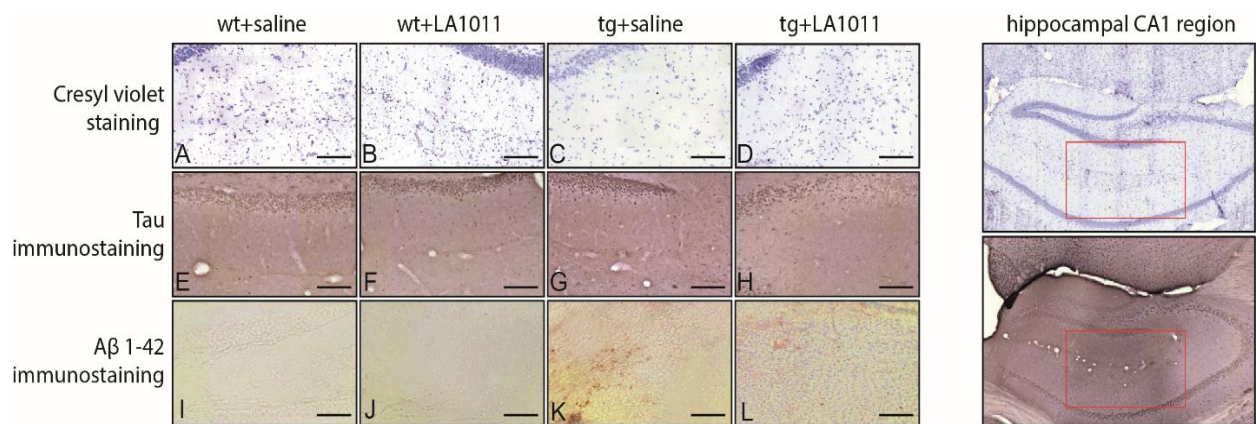


Fig. 24. Representative coronal examples of hippocampal sections showing the presence of neurons with cresyl-violet staining (A-D), the presence of abnormal aggregated NFTs using TAU-antibody (E-H) and the presence of amyloid plaque-like structures (I-L). A, E, I: wt+saline group B, F, J: wt+LA1011 group C, G, K: tg+saline group D, H, L: tg+LA1011 group. Scale bars: 100 μ m (A-H) and 25 μ m (I-L).

7. DISCUSSION

Alzheimer's disease (AD) is a very complex and multifactorial disorder. By now a large part of the pathomechanism of the disease is known, although the complete etiology of AD is not perfectly understood. One of the well proven characters of AD is that (similar to other neurodegenerative diseases) it is a protein misfolding disorder. Very probably the endoplasmic reticulum (ER) dysfunction, mitochondrial stress and the unfolded protein response (UPR) play pivotal role in the initiation of the disease (Pereira 2013, Hedskog 2013). These processes may start by the formation and accumulation of toxic A β aggregates. oA β is toxic for the ER and the mitochondria and starts the malfunction of synapses. These are the most probable pathomechanisms of AD. As a consequence, transgenic animals overexpressing A β could serve as good models for studying AD. Nontransgenic animal models (e.g. A β brain infusion models) are also available (Oikawa 2010), although they have not yet been standardized. The most difficult problem of the standardization has been the heterogeneity of the oA β 1-42 samples possessing different peptide conformation, aggregation size and solubility.

The main aim of the present work was a systematic study of the neurotoxic effects of icv administered oA β assemblies in rat brain. The present study explored the effects of different samples of oligomeric A β 1-42 aggregates on neuron viability, formation of NFTs, dendritic spine density, influence on synaptic plasticity and the change of spatial behaviour in nontransgenic rats. In addition our aim was to develop an icv administration protocol allowing an injection without direct technical damage and microglial inflammatory response in the target area caused by Hamilton syringe that we saw in our earlier study (Zhu 2016).

The role of amyloid plaques and oligomeric A β in the pathomechanism of AD has been debated for a long time. Depositions of extracellular A β and the surrounding oA β are considered as trigger signals for changing homeostatic to disease-associated microglia and to induce dendritic spine loss and synaptic dysfunction in AD. A β assemblies are synaptotoxic and dendritic spine loss is strongly correlated with cognitive impairment in AD. A β has been shown to target synapses (Wei 2010, Lacor 2004). Experiments demonstrated that synapse dysfunction was triggered by A β (Lacor 2007). Bilateral intrahippocampal (ihc) injections of fibrillar A β resulted in reduction of neuronal density, increased the intensity of glial fibrillary acidic protein and caused behaviour performance deficits (He 2011, Chacon 2004). Our former experiments also demonstrated that synthetic fA β after ihc administration simultaneously decreased spatial learning ability in MWM and reduced dendritic spine density in the rat hippocampus CA1 region (Borbény 2014). As fA β is a non-diffusible form and act only locally, in these experiments, very probably the diffusible

oligomeric A β assemblies (that surround fA β) affect the neurons and synapses (Sandberg 2010). It is widely accepted that accumulation of soluble toxic A β at the synapse may be on the critical path to neurodegeneration (Fonseca 2014). A β dependent disruption of neural cell adhesion molecules in AD HC may contribute to synapse loss (Kopniczky 2006). The synaptic changes in AD is recently reviewed (Avraamides 2008).

In the present work at first we studied the penetration of icv administered AMCA-labeled A β 1-42 into the brain parenchyma (Fig. 8 and 9). These experiments demonstrated that AMCA labeled fA β 1-42 remains in the ventricles after injection, but AMCA-oA β 1-42 penetrated across the ependyma or entered the brain parenchyma by the glymphatic flow. In this experiment we studied also the effect of two different oA β 1-42 aggregates using 25 μ M concentration and two different aggregation times, 24 and 168 h in HC slices. (The abbreviation of the samples: 24 h/25 μ M and 168 h/25 μ M, respectively). The results of the first series of experiments demonstrated that the aggregation time of oA β 1-42 plays a crucial role in the formation of toxic assemblies. 168 h aggregation time in 25 μ M concentration resulted in the formation of toxic assemblies, while the 24 h samples gave less toxic aggregates (Fig. 10,12,13).

In the second series of experiments we systematically studied the influence of both the peptide concentration and the aggregation time on the formation of neurotoxic aggregates.

AFM studies of the different oA β 1-42 samples demonstrated big differences in size of the samples (Fig. 14, Table III). The mean of the particle diameter was in the range of 6.5 and 21.5 nm. Besides the obvious differences in size, an altered morphology of the aggregates could also be observed, as protofibrils were formed together with the spherical oligomers in lower (25 and 75 μ M) concentrations after 168 h. We assume that size and different conformations resulting in altered morphology together are responsible for the enhanced toxicity. These oA β 1-42 assemblies were used in behavioural (learning and memory), histological and electrophysiological studies.

Our first aim was to examine whether these oA β s impair memory functions (especially the spatial memory) in rats and find optimal conditions to form toxic oligomers. We measured the effect of icv administered oA β samples in MWM, a hippocampal learning and memory test, in which the animals have to learn the location of the hidden platform (Morris 1984). Because the medial temporal lobe, including HC, appear to play a central role for establishment in long-term memory (Lavenex 2000) we determined the mean of the first swimings. The second trial every day was a potentiation for the animals to learn the exercise easier. The results demonstrated that finding of the hidden platform took longer time for the A β treated animals. After latency times of 5 days, oA β 1-42-treated animals exhibited significant differences compared with the control group. This finding is in accord with the hypothesis that icv injection of A β 1-42 oligomers impair the spatial memory.

The highest significance (greatest difference in latency time) compared with the control animals was exhibited by the *group C* (24 h/200 μ M), where the particle size was 10 nm and by the *group D* (168 h/25 μ M), where the particle size exceeds 8 nm. (Fig. 14 and 15).

Histological studies partly confirm the results of behavioural experiments. Although the 24 h aggregates do not significantly decrease the number of viable neurons, there is a clear tendency for neuronal loss (Fig. 16A). The 168 h samples cause significant decrease of viable neurons compared to the control (Fig. 16B; significances: in the 168 h/25 μ M group: $p=0.011$; in 168 h/75 μ M $p<0.001$; in 168 h/200 μ M $p<0.001$). Measurement of the abnormally accumulated NFTs in the HC slices gave interesting results (Fig. 17A): with lower aggregation grade only the 24 h/200 μ M oA β 1-42 (*Group C*) assembly caused significant NFT accumulation. 168 h aggregation time resulted in the formation of toxic assemblies in 25 and 75 μ M concentrations, but the 168 h/200 μ M sample did not cause change in the NFT level (Fig. 17B). These results are in a good correlation with the size and morphology of oA β assemblies (Table III, Fig. 14). Representative examples show the coronal HC sections, applied for neuron viability and NFT-accumulation measurements (Fig. 18).

Electrophysiological studies also support the results of the behavioural experiments. Only the 24 h/200 μ M oA β 1-42 (*Group C*) sample caused a great reduction in LTP, although the samples with lower aggregation concentrations also showed a clear tendency for decreasing LTP (Fig. 19A). Finally, the concentration-dependence in the 168 h groups was similar to the 24 h groups: the 25 and 75 μ M oA β 1-42 samples caused robust and significant reduction, the LTP reduction is much smaller in the 200 μ M group (Fig. 19B). These results also correlate well with the size and viability of the oA β assemblies.

The connection between amyloid aggregation, cellular toxicity and the biochemistry of neurodegeneration has been a challenge, the molecular details are more or less unknown. Determining the biophysical properties and conformational variety of a single species of amyloid peptides/proteins represents a high experimental challenge. The main problem is the heterogeneous nature and the nanoscale dimensions of the amyloid assemblies. Circular dichroism and infrared spectroscopy are bulk techniques and cannot characterize the inner properties of aggregates at the single species level (Ruggeri 2016). Lack of suitable methods prevents the profound study of the correlation between the biophysical properties and toxicity of individual amyloid species.

In our studies we found a simple correlation between the aggregate size and the morphology and toxicity of oA β 1-42. On the one hand there was an optimal size of oA β 1-42 assemblies (between 8 to 10 nm height) that caused elevated toxicity (24 h/200 μ M, 168 h/25 μ M and 168 h/75 μ M aggregates). On the other hand, too small and too big aggregates (24 h/25 μ M, 24 h/75 μ M, 168

h/200 μM) were less toxic or nontoxic (Figs 15-19). Although the peptide conformation within the oA β 1-42 samples has been unknown, we suppose that the toxic samples have not only similar particle size, but also structural similarity. To be sure, we tried the conformation in 50 μM concentration and 120 h aggregation grade, with 8.5 nm size to prove our findings. The test oligomeric form was also neurotoxic and we found impairment in the spatial memory and loss in dendritic spines (Fig. 20 and 21).

Our current study demonstrates that icv administration of oA β assemblies or A β protofibrils of defined size and structure into rats decreases cell viability and dendritic spine density, increases NFT formation, disturbs synaptic plasticity and impairs the learning and spatial behaviour of the animals. Our results could improve the “icv-administered A β ” rat model using well-characterized A β 1-42 oligomers.

During this work, our second aim was to find new drug candidates for treating AD possibly in early stage. Molecular chaperones and the ubiquitin-proteasome system represent the most important defensive mechanisms against misfolded proteins in AD (Sulistio 2015). Each protein aggregation disease can be characterized by a different set of HSPs that can rescue specific types of aggregation (Kakkar 2014). Some of these HSPs have demonstrated effectiveness *in vivo*, in mouse models of protein-aggregation diseases. HSP70 and HSP90 promote tau solubility and tau binding to microtubules, reduce insoluble tau, and reduce tau hyperphosphorylation in a transgenic mouse model of AD (Dou 2003).

We accepted the ER stress-UPR hypothesis and tried to find novel compounds that save the ER by inducing heat shock proteins and supporting the protein folding native structures. Our collaborators, F. Fülöp and co-workers prepared a series of 1,4-dihydropyridine derivatives. We chose the compound LA1011 as chaperon protein coinducer and a putative neuroprotective agent for *in vivo* experiments, and detect besides a neuroprotective effect a slight procognitive action.

It is known that unregulated HSP induction might cause the excessive overexpression of HSPs leading to instability of the stress response and unwanted side effects (Lamech 2015). However, in our experiments, LA1011 increases HSP expression only under stressed conditions, and thus the therapeutic use of DHPs in this study is novel and perhaps optimal strategy for the treatment of AD and other neurodegenerative diseases. The compound LA1011 proved to be a very interesting neuroprotective agent that will be used in further drug development studies. by the small Hungarian firm LipidArt.

8. SUMMARY

New scientific results of our studies summarized in the thesis:

1. We demonstrated that fluorescently labelled oligomeric form of oA β 1-42 penetrates into the brain parenchyma after icv administration.
2. We optimized the aggregation time and concentration for preparation of toxic oA β 1-42. The experiments demonstrated that the medium size (8-10 nm) aggregates contain the most toxic forms of oA β 1-42.
3. A novel rat model was introduced using icv administration of the freshly prepared oA β 1-42 aggregates as neurotoxic agents. The suitability of the model was demonstrated by behaviour experiments (MWM), histology studies: cell viability, Tau immunostaining and counting dendritic spine density, and LTP measurements.
4. It was demonstrated that the HSP coinducer LA1011, a 1,4-dihidropyridine derivate showed neuroprotective effect on an AD tg mouse model (APPxPS1 mice). LA1011 also showed a slight procognitive action in mice.

9. ACKNOWLEDGMENTS

I would like to express my gratitude to my supervisor and mentor, Prof. Dr. Botond Penke for his scientific guidance, encouragement and support throughout my PhD studies.

I thank Dr. Livia Fülöp, Dr. Zolt Bozsó, Klára Csete for the oA β 1-42 samples and AFM studies, and Dr. Viktor Szegedi, Dr. Gábor Juhász for the LTP measurements. I thank Anita Kurunczi for the studies on AMCA labeled A β samples.

I am thankful to Dr. Szűcs Mária for her professional in correcting my dissertation.

I am grateful to Dr. László Siklós for his support and suggestions in my work.

I thank Dr. Zsuzsa Penke-Verdier, Emőke Borbély, Zsuzsanna Frank, János Horváth and Eszter Sipos for their inspiring help in the studies.

I thank the members of the Research Group of Neurodegenerative Diseases and the Department of Medical Chemistry of the University of Szeged for their help and friendship.

Finally, I am especially thankful to my husband, my parents and all of my family and friends for their love and untiring support during my studies.

This research was supported by the FP-7 201159 (Memoload) and TÁMOP-4.2.2-11/1/KONV-2012-0052.

10. REFERENCES

1. Abner EL, Kryscio RJ, Schmitt FA, Santacruz KS, Jicha GA, Lin Y, Neltner JM, Smith CD, Van Eldik LJ, Nelson PT: **“End-stage” neurofibrillary tangle pathology in preclinical Alzheimer's disease: fact or fiction?** *J Alzheimers Dis.* 2011, **25**: 445-53.
2. Agopian A, Guo Z: **Structural origin of polymorphism for Alzheimer's amyloid- β fibrils.** *Biochem J.* 2012, **447**: 43-50.
3. Aguzzi A and Rajendran L: **The transcellular spread of cytosolic amyloids, prions, and prionoids.** *Neuron* 2009, **64**: 783-790.
4. Aisen PS: **Alzheimer's disease therapeutic research: the path forward.** *Alzheimers Res Ther.* 2009, **1**: 2.
5. Alberdi E, Wyssenbach A, Alberdi M, Sánchez-Gómez MV, Cavaliere F, Rodríguez JJ, Verkhratsky A, Matute C: **Ca(2+)-dependent endoplasmic reticulum stress correlates with astrogliosis in oligomeric amyloid β -treated astrocytes and in a model of Alzheimer's disease.** *Aging Cell.* 2013, **12**: 292-302.
6. Alkadhi KA: **Chronic stress and Alzheimer's disease-like pathogenesis in a rat model: prevention by nicotine.** *Curr Neuroparmacol.* 2010, **9**: 587-97.
7. Allen B, Ingram E, Takao M, Smith MJ, Jakes R, Virdee K, Yoshida H, Holzer M, Craxton M, Emson PC, Atzori C, Migheli A, Crowther RA, Ghetti B, Spillantini MG, Goedert M: **Abundant tau filaments and nonapoptotic neurodegeneration in transgenic mice expressing human P301S tau protein.** *J. Neurosci.* 2002, **22**: 9340-51.
8. Avraamides MN, Kelly JW: **Multiple systems of spatial memory and action.** *Cogn Process* 2008, **9**: 93-106.
9. Bagheri M, Joghataei MT, Mohseni S, Roghani M: **Genistein ameliorates learning and memory deficits in amyloid β (1–40) rat model of Alzheimer's disease.** *Neurobiol of Learn and Mem.* 2011, **95**: 270–276.
10. Balducci C, Beeg M, Stravalaci M, Bastone A, Scip A, Biasini E, Tapella L, Colombo L, Manzoni C, Borsello T, Chiesa R, Gobbi M, Salmona M, Forloni G: **Synthetic amyloid-beta oligomers impair long-term memory independently of cellular prion protein.** *Proc Natl Acad Sci. USA* 2010, **107**: 2295-300.
11. Baloyannis SJ: **Dendritic pathology in Alzheimer's disease.** *J. Neurol Sci.* 2009, **283**: 153-7.

12. Berridge MV: **Characterization of the cellular reduction of 3-(4,5-dimethylthiazol-2-yl)-2,5-diphenyltetrazolium bromide (MTT): subcellular localization, substrate dependence, and involvement of mitochondrial electron transport in MTT reduction.** *Arch Biochem Biophys.* 1993, **303**: 474-82.
13. Bishop GM, Robinson SR: **The amyloid hypothesis: let sleeping dogmas lie?** *Neurobiol Aging.* 2002, **23**: 1101-5.
14. Blair JA, Siedlak SL, Wolfram JA, Nunomura A, Castellani RJ, Ferreira ST, Klein WL, Wang Y, Casadesus G, Smith MA, Perry G, Zhu X, Lee HG: **Accumulation of Intraneuronal Amyloid- β is Common in Normal Brain.** *Curr Alzheimer Res.* 2014, in press
15. Borbély E, Horváth J, Furdan S, Bozsó Z, Penke B, Fülöp L: **Simultaneous changes of spatial memory and spine density after intrahippocampal administration of fibrillar A β 1-42 to the rat brain.** *BioMed Research International* 2014, in press
16. Bossers K, Wirz KT, Meerhoff GF, Essing AH, van Dongen JW, Houba P, Kruse CG, Verhaagen J, Swaab DF: **Concerted changes in transcripts in the prefrontal cortex precede neuropathology in Alzheimer's disease.** *Brain* 2010, **133**: 3699-723.
17. Bowen DM, Smith CB, White P, Davison AN: **Neurotransmitter-related enzymes and indices of hypoxia in senile dementia and other abiotrophies.** *Brain.* 1976, **99**: 459-96.
18. Bozsó Z, Penke B, Simon D, Laczkó I, Juhász G, Szegedi V, Kasza A, Soós K, Hetényi A, Wéber E, Tóháti H, Csete M, Zarándi M, Fülöp L: **Controlled in situ preparation of A beta(1-42) oligomers from the isopeptide "iso-A beta(1-42)", physicochemical and biological characterization.** *Peptides* 2010, **31**: 248-56.
19. Braak H and Braak E: **Neuropathological staging of Alzheimer-related changes.** *Acta Neuropathol.* 1991, **82**: 239-59.
20. Braak H, Braak E: **Staging of Alzheimer's disease-related neurofibrillary changes.** *Neurobiol Aging* 1995, **16**: 271-278.
21. Brännström K, Ohman A, Olofsson A: **A β peptide fibrillar architectures controlled by conformational constraints of the monomer.** *PLoS One* 2011, **6**: e25157.
22. Bu XL, Xiang Y, Jin WS, Wang J, Shen LL, Huang ZL, Zhang K, Liu YH, Zeng F, Liu JH, Sun HL, Zhuang ZQ, Chen SH, Yao XQ, Giunta B, Shan YC, Tan J, Chen XW, Dong ZF, Zhou HD, Zhou XF, Song W, Wang YJ: **Blood-derived amyloid- β protein induces Alzheimer's disease pathologies.** *Mol Psychiatry.* 2017, in press
23. Bush AI, Pettingel WH Jr, Paradis MD, Tanzi RE: **Modulation of A β adhesiveness and secretase site cleavage by zinc.** *J Biol Chem.* 1994, **269**: 12152-8.

24. Cakała M, Malik AR, Strosznajder JB: **Inhibitor of cyclooxygenase-2 protects against amyloid beta peptide-evoked memory impairment in mice.** *Pharmacol Rep.* 2007, **59**: 164-72.
25. Calhoun ME, Burgermeister P, Phinney AL, Stalder M, Tolnay M, Wiederhold KH, Abramowski D, Sturchler-Pierrat C, Sommer B, Staufenbiel M, Jucker M: **Neuronal overexpression of mutant amyloid precursor protein results in prominent deposition of cerebrovascular amyloid.** *Proc. Natl. Acad. Sci. USA.* 1999, **96**: 14088-14093.
26. Cavanaugh SE, Pippin JJ, Barnard ND: **Animal models of Alzheimer disease: Historical pitfalls and apath forward.** *ALTEX* 2014, **31**: 279–302.
27. Chen G, Chen KS, Knox J, Inglis J, Bernard A, Martin SJ, Justice A, McConlogue L, Games D, Freedman SB, Morris RG: **A learning deficit related to age and beta-amyloid plaques in a mouse model of Alzheimer's disease.** *Nature* 2000, **408**: 975-9.
28. Chishti MA¹, Yang DS, Janus C, Phinney AL, Horne P, Pearson J, Strome R, Zuker N, Loukides J, French J, Turner S, Lozza G, Grilli M, Kunicki S, Morissette C, Paquette J, Gervais F, Bergeron C, Fraser PE, Carlson GA, George-Hyslop PS, Westaway D: **Early-onset amyloid deposition and cognitive deficits in transgenic mice expressing a double mutant form of amyloid precursor protein 695.** *J. Biol. Chem.* 2001, **276**: 21562-21570.
29. Christensen DZ, Bayer TA and Wirths O: **Formic acid is essential for immunohistochemical detection of aggregated intraneuronal A β peptides in mouse models of Alzheimer's disease.** *Brain Res.* 2009, **1301**: 116-25.
30. Ciechanover A, Kwon YT: **Degradation of misfolded proteins in neurodegenerative diseases: therapeutic targets and strategies.** *Exp Mol Med.* 2015, **47**:e147.
31. Claeysen S, Cochet M, Donneger R, Dumuis A, Bockaert J, Giannoni P: **Alzheimer culprits: Cellular crossroads and interplay.** *Cell Signal.* 2012, **24**: 1831-40.
32. Cleary JP, Walsh DM, Hofmeister JJ, Shankar GM, Kuskowski MA, Selkoe DJ, Ashe KH: **Natural oligomers of the amyloid-beta protein specifically disrupt cognitive function.** *Nat Neurosci.* 2005, **8**: 79-84.
33. Clifford PM, Zarrabi S, Siu G, Kinsler KJ, Kosciuk MC, Venkataraman V, D'Andrea MR, Dinsmore S, Nagele RG: **Abeta peptides can enter the brain through a defective blood-brain barrier and bind selectively to neurons.** *Brain Res.* 2007, **1142**: 223-36.
34. Clippingdale AB, Wade JD, Barrow CJ: **The amyloid-beta peptide and its role in Alzheimer's disease.** *J Pept Sci.* 2001, **7**: 227-49.

35. Colton CA1, Wilcock DM, Wink DA, Davis J, Van Nostrand WE, Vitek MP: **The effects of NOS2 gene deletion on mice expressing mutated human AbetaPP.** *J. Alzheimers Dis.* 2008, **15**: 571-587.
36. Cooke SF and Bliss TV: **Plasticity in the human central nervous system.** *Brain* 2006, **129**: 1659-73.
37. Craddock TJA, Tuszynski JA, Chopra D, Casey N, Goldstein LE, Hameroff SR, Tanzi RE: **The Zinc Dyshomeostasis Hypothesis of Alzheimer's Disease.** *PLoS One.* 2012, **7**: e33552.
38. Crespo-Biel N, Theunis C, Van Leuven F: **Protein tau: prime cause of synaptic and neuronal degeneration in Alzheimer's disease.** *Int J Alzheimers Dis.* 2012, **2012**: 251426.
39. Datki Z, Juhász A, Gálfi M, Soós K, Papp R, Zádori D, Penke B: **Method for measuring neurotoxicity of aggregating polypeptides with the MTT assay on differentiated neuroblastoma cells.** *Brain Res Bull.* 2003, **62**: 223-9.
40. Datki Z, Papp R, Zádori D, Soós K, Fülöp L, Juhász A, Laskay G, Hetényi C, Mihalik E, Zarándi M, Penke B: **In vitro model of neurotoxicity of Abeta 1-42 and neuroprotection by a pentapeptide: irreversible events during the first hour.** *Neurobiol Dis.* 2004, **17**: 507-15.
41. De Felice FG, Munoz DP: **Opportunities and challenges in developing relevant animal models for Alzheimer's disease.** *Aging Res. Rev.* 2016, **26**: 112-114.
42. de la Torre JC, Stefano GB: **Evidence that Alzheimer's disease is a microvascular disorder: the role of constitutive nitric oxide.** *Brain Res Rev.* 2000, **34**: 119-36.
43. De Los Rios P, Ben-Zvi A, Slutsky O, Azem A, Goloubinoff P: **HSP70 chaperones accelerate protein translocation and the unfolding of stable protein aggregates by entropic pulling.** *Proc Natl Acad Sci USA.* 2006, **103**: 6166-71.
44. De Roo M, Klauser P, Muller D: **LTP promotes a selective long-term stabilization and clustering of dendritic spines.** *PLoS Biol.* 2008, **6**: 1850-60.
45. Dodart JC, May P: **Overview on rodent models of Alzheimer's disease.** *Curr Protoc Neurosci.* 2005, **9**: 9.22.
46. Doody RS: **Current treatments for Alzheimer's disease: cholinesterase inhibitors.** *J Clin Psychiatry.* 2003, **64**: 11-7.
47. Doran TM, Anderson EA, Latchney SE, Opanashuk LA, Nilsson BL: **Turn nucleation perturbs amyloid β self-assembly and cytotoxicity.** *J Mol Biol.* 2012, **421**: 315-28.

48. Dou F, Netzer WJ, Tanemura K, Li F, Hartl FU, Takashima A, Gouras GK, Greengard P, Xu HX: **Chaperones increase association of tau protein with microtubules.** *P Natl Acad Sci USA* 2003, **100**: 721-726.
49. Duran-Aniotz C, Martínez G, Hetz C: **Memory loss in Alzheimer's disease: are the alterations in the UPR network involved in the cognitive impairment?** *Front Aging Neurosci.* 2014, **30**: 6-8.
50. Duyckaerts C, Delatour B and Potier MC: **Classification and basic pathology of Alzheimer disease.** *Acta Neuropathol.* 2009, **118**: 5-36.
51. Endres K, Reinhardt S: **ER-stress in Alzheimer's disease: turning the scale?** *Am J Neurodegener Dis.* 2013, **2**: 247-65.
52. Engelhardt JJ, Tajti J, Appel SH: **Lymphocytic infiltrates in the spinal cord in amyotrophic lateral sclerosis.** *Arch Neurol-Chicago* 1993, **50**: 30-36.
53. Esquerda-Canals G, Montoliu-Gaya L, Guell-Bosch J, Villegas S: **Mouse models of Alzheimer's disease.** *J. Alzheimers Dis.* 2017, **57**: 1171–1183.
54. Esteban JA: **Living with the enemy: a physiological role for the beta-amyloid peptide.** *Trends Neurosci.* 2004, **27**: 1-3.
55. Evans CG, Chang L, Gestwicki JE: **Heat shock protein 70 (HSP70) as an emerging drug target.** *J Med Chem.* 2010, **53**: 4585-602.
56. Fernandez-Vizarra P, Lopez-Franco O, Mallavia B et al: **Immunoglobulin G Fc receptor deficiency prevents Alzheimer-like pathology and cognitive impairment in mice.** *Brain* 2012, **135**: 2826-37.
57. Fonseca, A.C.; Oliveira, C.R.; Pereira, C.F.; Cardoso, S.M. **Loss of proteostasis induced by amyloid beta peptide in brain endothelial cells.** *BBA-Mol Cell Res* 2014, **1843**: 1150-1161.
58. Földi I, Tóth AM, Szabó Z, Mózes E, Berkecz R, Datki ZL, Penke B, Janáky T: **Proteome-wide study of endoplasmic reticulum stress induced by thapsigargin in N2a neuroblastoma cells.** *Neurochem Int.* 2013, **62**: 58-69.
59. Frederickson CJ, Suh SW, Silva D, Frederickson CJ, Thompson RB: **Importance of zinc in the central nervous system: the zinc-containing neuron.** *J Nutr.* 2000, **130**: 1471-83.
60. Fullerton SM, Clark AG, Weiss KM, Nickerson DA, Taylor SL, Stengård JH, Salomaa V, Vartiainen E, Perola M, Boerwinkle E, Sing CF: **Apolipoprotein E variation at the sequence haplotype level: implications for the origin and maintenance of a major human polymorphism.** *Am J Hum Genet.* 2000, **67**: 881-900.
61. Fülöp L, Penke B, and Zarandi M: **Synthesis and fluorescent labeling of beta-amyloid peptides.** *J Pept Sci.* 2001, **7**: 397-401.

62. Fülöp L, Zarándi M, Datki Z, Soós K, Penke B: **Beta-amyloid-derived pentapeptide RIIGLa inhibits Abeta(1-42) aggregation and toxicity.** *Biochem Biophys Res Commun.* 2004, **324**: 64-9.
63. Games D, Adams D, Alessandrini R, Barbour R, Berthelette P, Blackwell C, Carr T, Clemens J, Donaldson T, Gillespie F, et al.: **Alzheimer-type neuropathology in transgenic mice overexpressing V717F beta-amyloid precursor protein.** *Nature.* 1995, **9**: 523-27.
64. Glabe CG: **Common mechanisms of amyloid oligomer pathogenesis in degenerative disease.** *Neurobiol of Aging* 2006, **27**: 570–575.
65. Goloubinoff P: **Mechanisms of protein homeostasis in health, aging and disease.** *Swiss Med Wkly.* 2016, **146**:w14306.
66. Gong CX, Grundke-Iqbal I, Iqbal K: **Targeting tau protein in Alzheimer's disease.** *Drugs Aging.* 2010, **27**: 351-65.
67. Gouras GK, Tsai J, Naslund J, Vincent B, Edgar M, Checler F, Greenfield JP, Haroutunian V, Buxbaum JD, Xu H, Greengard P, Relkin NR: **Intraneuronal Abeta42 accumulation in human brain.** *Am J Pathol.* 2000, **156**: 15-20.
68. Götz J, Eckert A, Matamalas M, Ittner LM, Liu X: **Modes of Aβ toxicity in Alzheimer's disease.** *Cell Mol Life Sci.* 2011, **68**: 3359-75.
69. Götz J, Probst A, Spillantini MG, Schäfer T, Jakes R, Bürki K, Goedert M: **Somatodendritic localization and hyperphosphorylation of tau protein in transgenic mice expressing the longest human brain tau isoform.** *Embo J.* 1995, **14**: 1304-1313.
70. Götz J, Schonrock N, Vissel B, Ittner LM: **Alzheimer's disease selective vulnerability and modeling in transgenic mice.** *J Alzheimers Dis.* 2009, **18**: 243-51.
71. Grimm MOW, Mett J, Grimm HS, Hartmann T: **APP function and lipids: a bidirectional link.** *Front. Mol. Neurosci.* 2017, **10**: art. 63.
72. Grueninger F., Bohrmann B., Czech C., Ballard T.M., Frey J.R., Weidensteiner C., von Kienlin M., Ozmen L: **Phosphorylation of Tau at S422 is enhanced by Aβ in TauPS2APP triple transgenic mice.** *Neurobiol Dis.* 2010, **37**: 294–306.
73. Hardy J, Allsop D: **Amyloid deposition as the central event in the aetiology of Alzheimer's disease.** *Trends Pharmacol Sci* 1991, **12**: 383-388.
74. Hardy J, Selkoe DJ: **The amyloid hypothesis of Alzheimer's disease: progress and problems on the road to therapeutics.** *Science* 2002, **297**: 353-356.
75. Hardy J: **The amyloid hypothesis for Alzheimer's disease: a critical reappraisal.** *J Neurochem* 2009, **110**: 1129-1134.

76. Harold D et al: **Genome-wide association study identifies variants at CLU and PICALM associated with Alzheimer's disease.** *Nat Genet.* 2009, **41**: 1088-93.
77. He FQ, Qiu BY, Zhang XH, Li TK, Xie Q, Cui DJ, Huang XL, Gan HT: **Tetrandrine attenuates spatial memory impairment and hippocampal neuroinflammation via inhibiting NF- κ B activation in a rat model of Alzheimer's disease induced by amyloid- β (1-42).** *Brain Res.* 2011, **1384**: 89-96.
78. Hedskog L, Pinho CM, Filadi R, Rönnbäck A, Hertwig L, Wiehager B, Larssen P, Gellhaar S, Sandebring A, Westerlund M, Graff C, Winblad B, Galter D, Behbahani H, Pizzo P, Glaser E, Ankarcrona M: **Modulation of the endoplasmic reticulum-mitochondria interface in Alzheimer's disease and related models.** *Proc Natl Acad Sci USA.* 2013, **110**: 7916-21.
79. Hefter D, Draguhn A: **APP as a protective factor in acute neuronal insults.** *Front. Mol. Neurosci.* 2017, **10**: art. 22.
80. Henkel JS, Engelhardt JI, Siklos L, Simpson EP, Kim SH, Pan T, Goodman JC, Siddique T, Beers DR, Appel SH: **The presence of immature and mature/activated dendritic cells, increased chemokine MCP-1, and activated microglia/macrophages in amyotrophic lateral sclerosis spinal cord tissue.** *Ann Neurol* 2004, **55**: 221-235.
81. Hetényi A, Fülöp L, Martinek TA, Wéber E, Soós K, Penke B: **Ligand-induced flocculation of neurotoxic fibrillar Abeta(1-42) by noncovalent crosslinking.** *Chembiochem.* 2008, **9**: 748-57.
82. Hetényi C, Körtvélyesi T, Penke B: **Mapping of possible binding sequences of two beta-sheet breaker peptides on beta amyloid peptide of Alzheimer's disease.** *Bioorg Med Chem.* 2002, **10**: 1587-93.
83. Hollingworth P et al: **ABCA7, MS4A4E, EPHA1, CD33 and CD2AP are associated with Alzheimer's disease.** *Nat Genet.* 2011, **43**: 429-35.
84. Honarnejad K, Daschner A and Herms J: **Development and Implementation of a High-Throughput Compound Screening Assay for Targeting Disrupted ER Calcium Homeostasis in Alzheimer's Disease.** *PLoS One.* 2013, **8**: e80645.
85. Hou Y, Song H, Croteau DL, Akbari M, Bohr VA: **Genome instability in Alzheimer disease.** *Mech. Aging Dev.* 2017, **161**: 83-94.
86. Hsiao K, Chapman P, Nilsen S, Eckman C, Harigaya Y, YOUNKIN S, Yang F, Cole G: **Correlative memory deficits, Abeta elevation, and amyloid plaques in transgenic mice.** *Science.* 1996, **274**: 99-102.

87. Hu NW, Smith IM, Walsh DM and Rowan MJ: **Soluble amyloid-beta peptides potentially disrupt hippocampal synaptic plasticity in the absence of cerebrovascular dysfunction in vivo.** *Brain* 2008, **131**: 2414-24.
88. Hung LW, Ciccotosto GD, Giannakis E, Tew DJ, Perez K, Masters CL, Cappai R, Wade JD, Barnham KJ: **Amyloid-beta peptide (Abeta) neurotoxicity is modulated by the rate of peptide aggregation: Abeta dimers and trimers correlate with neurotoxicity.** *J Neurosci.* 2008, **28**: 11950-8.
89. Ikonomovic MD, Klunk WE, Abrahamson EE, Mathis CA, Price JC, Tsopelas ND, Lopresti BJ, Ziolkowski S, Bi W, Paljug WR, Debnath ML, Hope CE, Isanski BA, Hamilton RL and DeKosky ST: **Post-mortem correlates of *in vivo* PiB-PET amyloid imaging in a typical case of Alzheimer's disease.** *Brain* 2008, **131**: 1630-45.
90. Iliff JJ1, Wang M, Liao Y, Plogg BA, Peng W, Gundersen GA, Benveniste H, Vates GE, Deane R, Goldman SA, Nagelhus EA, Nedergaard M. **A paravascular pathway facilitates CSF flow through the brain parenchyma and the clearance of interstitial solutes, including amyloid β .** *Sci Transl Med.* 4.
91. Iqbal K, Grundke-Iqbal I: **Pharmacological approaches of neurofibrillary degeneration.** *Curr Alzheimer Res.* 2005, **2**: 335-41.
92. Iqbal K, Liu F, Gong CX, Alonso Adel C, Grundke-Iqbal I: **Mechanisms of tau-induced neurodegeneration.** *Acta Neuropathol.* 2009, **118**: 53-69.
93. Ittner LM, Götz J: **Amyloid-beta and tau--a toxic pas de deux in Alzheimer's disease.** *Nat Rev Neurosci.* 2010, **12**: 65-72.
94. Jackson B, Cubela RB, Sakaguchi K, Johnston CI: **Characterization of angiotensin converting enzyme (ACE) in the testis and assessment of the *in vivo* effects of the ACE inhibitor perindopril.** *Endocrinology.* 1988, **123**: 50-5.
95. Jacobsen JS, Reinhart P and Pangalos MN: **Current concepts in therapeutic strategies targeting cognitive decline and disease modification in Alzheimer's disease.** *NeuroRx.* 2005, **2**: 612-26.
96. Jahn-Eimermacher A, Lasarzik I, Raber J: **Statistical analysis of latency outcomes in behavioural experiments.** *Behav Brain Res.* 2011, **221**: 271-5.
97. Jankowsky JL, Melnikova T, Fadale DJ, Xu GM, Slunt HH, Gonzales V, Younkin LH, Younkin SG, Borchelt DR, Savonenko AV: **Environmental Enrichment Mitigates Cognitive Deficits in a Mouse Model of Alzheimer's Disease.** *The Journal of Neuroscience* 2005, **25**: 5217-5224.

98. Jankowsky JL, Slunt HH, Ratovitski T, Jenkins NA, Copeland NG, Borchelt DR: **Co-expression of multiple transgenes in mouse CNS: a comparison of strategies.** *Biomol. Eng.* 2001, **17**: 157-65.
99. Jankowsky JL, Zheng H: **Practical considerations for choosing a mouse model of Alzheimer's disease.** *Mol. Neurodegener.* 2017, **12**: 89.
100. Jenkins T, Chai SY: **Dose response effect of the angiotensin converting enzyme inhibitor, perindopril, on spatial memory and anxiety-like behaviours in rats.** *Paper presented at Scottish Cardiovascular Forum* 2007, Belfast, Northern Ireland.
101. Jensen LE, Bultynck G, Luyten T, Amijee H, Bootman MD, Roderick HL: **Alzheimer's disease-associated peptide A β 42 mobilizes ER Ca(2+) via InsP3R-dependent and -independent mechanisms.** *Front Mol Neurosci.* 2013, **6**: 36.
102. Jolly C, Morimoto RI: **Role of the Heat Shock Response and Molecular Chaperones in Oncogenesis and Cell Death.** *J Natl. Cancer Inst* 2000, **92**: 1564–72.
103. Juhász G, Földi I, Penke B: **System biology of Alzheimer's disease. How diverse molecular changes results in memory impairment in AD.** *Neurochemistry International* 2011, **58**: 739-750.
104. Kakkar V, Meister-Broekema M, Minoia M, Carra S, Kampinga HH: **Barcoding heat shock proteins to human diseases: looking beyond the heat shock response.** *Dis Model Mech* 2014, **7**: 421-434.
105. Kam TI, Song S, Gwon Y et al: **Fc γ RIIb mediates amyloid- β neurotoxicity and memory impairment in Alzheimer's disease.** *J Clin. Invest.* 2013, **123**: 2791-2802.
106. Kasza Á, Hunya Á, Frank Z, Fülöp F, Török Z, Balogh G, Sántha M, Bálint Á, Bernáth S, Blundell KL, Prodromou C, Horváth I, Zeiler HJ, Hooper PL, Vigh L, Penke B: **Dihydropyridine Derivatives Modulate Heat Shock Responses and have a Neuroprotective Effect in a Transgenic Mouse Model of Alzheimer's Disease.** *J Alzheimers Dis.* 2016, **53**:557-71.
107. Kim HY, Lee DK, Chung BR, Kim HV, Kim Y: **Intracerebroventricular injection of amyloid- β peptides in normal mice to acutely induce Alzheimer-like cognitive deficits.** *JOVE-J. Vis. Exp.* 2016, **16**: doi: 10.3791/53308.
108. Kim T, Vidal GS, Djurisic M, William CM, Birnbaum ME, Garcia KC, Hyman BT, Shatz CJ: **Human LILRB2 is a β -amyloid receptor and its murine homolog PirB regulates synaptic plasticity in an Alzheimer's model.** *Science.* 2013, **341**: 1399-404.

109. Kishimoto Y, Fukumoto K, Nagai M, Mizuguchi A, Kobashi Y: **Early Contextual Fear Memory Deficits in a Double-Transgenic Amyloid- β Precursor Protein/Presenilin 2 Mouse Model of Alzheimer's Disease.** *Int J Alzheimers Dis.* 2017, **2017**:8584205.
110. Kolarova M, García-Sierra F, Bartos A, Ricny J, Ripova D: **Structure and Pathology of Tau Protein in Alzheimer Disease.** *Int J Alzheimers Dis.* 2012, **2012**: 731526.
111. Konzack S, Thies E, Marx A, Mandelkow EM, Mandelkow E: **Swimming against the tide: mobility of the microtubule-associated protein tau in neurons.** *J Neurosci.* 2007, **27**: 9916-9927.
112. Kopniczky Z, Dochnal R, Mácsai M, Pál A, Kiss G, Mihály A, Szabó G: **Alterations of behaviour and spatial learning after unilateral entorhinal ablation of rats.** *Life Sci.* 2006, **78**: 2683-8.
113. Korczyn AD: **The amyloid cascade hypothesis.** *Alzheimers Dement.* 2008, **4**: 176-8.
114. Kumar A, Aggarwal A, Singh A, Naidu PS: **Animal models in drug discovery of Alzheimer's disease: a mini review.** *EC Pharmacol. Toxicol.* 2016, **2**: 60-79.
115. Kumar P, Ambasta RK, Veereshwarayya V, Rosen KM, Kosik KS, Band H, Mestrlil R, Patterson C, Querfurth HW: **CHIP and HSPs interact with beta-APP in a proteasome-dependent manner and influence Abeta metabolism.** *Hum Mol Genet.* 2007, **16**: 848-64.
116. Lacor, P.N.; Buniel, M.C.; Chang, L.; Fernandez, S.J.; Gong, Y.S.; Viola, K.L.; Lambert, M.P.; Velasco, P.T.; Bigio, E.H.; Finch, C.E., *et al.* **Synaptic targeting by Alzheimer's-related amyloid beta oligomers.** *J Neurosci* 2004, **24**: 10191-10200.
117. Lacor, P.N.; Buniel, M.C.; Furlow, P.W.; Clemente, A.S.; Velasco, P.T.; Wood, M.; Viola, K.L.; Klein, W.L. **A beta oligomer-induced aberrations in synapse composition, shape, and density provide a molecular basis for loss of connectivity in Alzheimer's disease.** *J Neurosci* 2007, **27**: 796-807.
118. LaFerla FM, Green KN, Oddo S: **Intracellular amyloid-beta in Alzheimer's disease.** *Nat Rev Neurosci.* 2007, **8**: 499-509.
119. Lambert JC et al: **Genome-wide association study identifies variants at CLU and CR1 associated with Alzheimer's disease.** *Nat Genet.* 2009; **41**: 1094-9.
120. Lambert MP, Barlow AK, Chromy BA, Edwards C, Freed R, Liosatos M, Morgan TE, Rozovsky I, Trommer B, Viola KL, Wals P, Zhang C, Finch CE, Krafft GA, Klein WL: **Diffusible, nonfibrillar ligands derived from Abeta1-42 are potent central nervous system neurotoxins.** *Proc Natl Acad Sci. USA* 1998, **95**: 6448-53.
121. Lamech LT, Haynes CM. **The unpredictability of prolonged activation of stress response pathways.** *J Cell Biol* 2015, **209**: 781-787.

122. Lansbury PT and Lashuel HA: **A century-old debate on protein aggregation and neurodegeneration enters the clinic.** *Nature* 2006, **443**: 774-9.
123. Lavenex, P.; Amaral, D.G. Hippocampal-neocortical interaction: **A hierarchy of associativity.** *Hippocampus* 2000, **10**: 420-430.
124. Lesné S, Koh MT, Kotilinek L, Kaye R, Glabe CG, Yang A, Gallagher M, Ashe KH: **A specific amyloid-beta protein assembly in the brain impairs memory.** *Nature* 2006, **440**: 352-7.
125. Lewis J, Dickson DW, Lin WL, Chisholm L, Corral A, Jones G, Yen SH, Sahara N, Skipper L, Yager D, Eckman C, Hardy J, Hutton M, McGowan E: **Enhanced neurofibrillary degeneration in transgenic mice expressing mutant tau and APP.** *Science*. 2001, **293**: 1487-91.
126. Li JQ, Yu JT, Jiang T, Tan L: **Endoplasmic Reticulum Dysfunction in Alzheimer's Disease:** *Mol Neurobiol*. 2014: Epub ahead of print.
127. Liao D, Miller EC, Teravskis PJ: **Tau acts as a mediator for Alzheimer's disease-related synaptic deficits.** *Eur J Neurosci*. 2014, **39**: 1202-13.
128. Linkous DH, Flinn JM, Koh JY, Lanzirotti A, Bertsch PM, Jones BF, Giblin LJ, Frederickson CJ: Evidence That the ZNT3 Protein Controls the Total Amount of Elemental Zinc in **Synaptic Vesicles.** *J Histochem Cytochem*. 2008, **56**: 3–6.
129. Lorenzini CA, Baldi E, Bucherelli C, Sacchetti B and Tassoni G: **Role of dorsal hippocampus in acquisition, consolidation and retrieval of rat's passive avoidance response: a tetrodotoxin functional inactivation study.** *Brain Res*. 1996, **730**: 32-9.
130. Lovell MA, Robertson JD, Teesdale WJ, Campbell JL, Markesbery WR: **Copper, iron and zinc in Alzheimer's disease senile plaques.** *J Neurol Sci*. 1998, **158**: 47-52.
131. Mizuno S, Iijima R, Ogishima S, Kikuchi M, Matsuoka Y, Ghosh S, Miyamoto T, Miyashita A, Kuwano R, Tanaka H: **AlzPathway: a comprehensive map of signaling pathways of Alzheimer's disease.** *BMC Systems Biology* 2012, **6**: 52.
132. Monzón-Mayor M, Alvarez M, Arbelo-Galván J, Romero-Alemán M, Yanes C, Plaza ML, Rodríguez JR, Rodríguez JJ, Toledano A: **Long-term evolution of local, proximal and remote astrocyte responses after diverse nucleus basalis lesioning (an experimental Alzheimer model): GFAP immunocytochemical study.** *Brain Res*. 2000, **865**: 245-58.
133. Morris RG, Garrud P, Rawlins JN and O'Keefe J: **Place navigation impaired in rats with hippocampal lesions.** *Nature* 1982, **297**: 681-3.

134. Morris RG: **Synaptic plasticity and learning: selective impairment of learning rats and blockade of long-term potentiation in vivo by the N-methyl-D-aspartate receptor antagonist AP5.** *J Neurosci.* 1989, **9**: 3040-57.
135. Morris, R. **Developments of a water-maze procedure for studying spatial-learning in the rat.** *J Neurosci Methods* 1984, **11**: 47-60.
136. Mucke L: **Neuroscience: Alzheimer's disease.** *Nature* 2009, **461**: 895-7.
137. Müller UC, Deller T, Korte M: **Not just amyloid: physiological functions of the amyloid precursor protein family.** *Nat. Rev. Neurosci.* 2017, **18**: 281-298.
138. Nagy D, Kocsis K, Fuzik J: **Kainate postconditioning restores LTP in ischemic hippocampal CA1: onset-dependent second patophysiological stress.** *Neuropharmacology* 2011, **61**: 1026-32.
139. Naj AC et al: **Common variants at MS4A4/MS4A6E, CD2AP, CD33 and EPHA1 are associated with late-onset Alzheimer's disease.** *Nat. Genet.* 2011, **43**: 436-41.
140. Nath S, Agholme L, Kurudenkandy FR, Granseth B, Marcusson J, Hallbeck M: **Spreading of Neurodegenerative Pathology via Neuron-to-Neuron Transmission of β -Amyloid.** *J Neurosci.* 2012, **32**: 8767-77.
141. Nussbaum JM, Seward ME, Bloom GS: **Alzheimer disease: a tale of two prions.** *Prion.* 2013, **7**: 14-9.
142. Oakley H, Cole SL, Logan S, Maus E, Shao P, Craft J, Guillozet-Bongaarts A, Ohno M, Disterhoft J, Van Eldik L: **Intraneuronal β -amyloid aggregates, neurodegeneration, and neuron loss in transgenic mice with five familial Alzheimer's disease mutations: potential factors in amyloid plaque formation.** *J. Neurosci.* 2006, **26**: 10129-40.
143. Oddo S, Caccamo A, Shepherd JD, Murphy MP, Golde TE, Kaye R, Metherate R, Mattson MP, Akbari Y, LaFerla FM: **Triple-transgenic model of Alzheimer's disease with plaques and tangles: intracellular A β and synaptic dysfunction.** *Neuron.* 2003, **39**: 409-21.
144. O'Hare E, Weldon DT, Mantyh PW, Ghilardi JR, Finke MP, Kuskowski MA, Maggio JE, Shephard RA, Cleary J: **Delayed behavioural effects following intrahippocampal injection of aggregated A β (1-42).** *Brain Res.* 1999, **815**: 1-10.
145. Ohnishi: **Effects of brain-penetrating ACE inhibitors on Alzheimer disease progression.** *Neurology* 2004, **63**: 1324.
146. Oikawa N, Kimura N and Yanagisawa K: **Alzheimer-type tau pathology in advanced aged nonhuman primate brains harboring substantial amyloid deposition.** *Brain Res.* 2010, **1315**: 137-49.

147. Onos KD, Rizzo SJS, Howell GR, Sasnera M: **Toward more predictive genetic mouse models of Alzheimer's disease.** *Brain Res. Bull.* 2016, **122**:1–11.
148. Orehek AJ: **The micron stroke hypothesis of Alzheimer's disease and dementia.** *Medical Hypotheses* 2012, **78**: 562-570
149. Orta-Salazar E, Vargas-Rodríguez I, Castro-Chavira SA, Feria-Velasco AI, Díaz-Cintra S: **Alzheimer's disease: From animal models to the human syndrome.** In *Update on Dementia*; Moretti, D., Ed.; Intech: Rijeka, Croatia, 2016; ISBN 978-953-51-2654-6.
150. Paxinos G, Watson C: **The Rat Brain in Stereotaxic Coordinates.** *Academic Press, Sydney* 1982.
151. Penke B, Toth AM, Foldi I, Szucs M, Janaky T: **Intraneuronal β -amyloid and its interactions with proteins and subcellular organelles.** *Electrophoresis* 2012, **33**: 3608-3616.
152. Pereira CMF: **Crosstalk between Endoplasmic Reticulum Stress and Protein Misfolding in Neurodegenerative Diseases.** *ISRN Cell Biology* 2013, Article ID **256404**.
153. Petrucelli L, Dickson D, Kehoe K, Taylor J, Snyder H, Grover A, De Lucia M, McGowan E, Lewis J, Prihar G, Kim J, Dillmann WH, Browne SE, Hall A, Voellmy R, Tsuboi Y, Dawson TM, Woloizin B, Hardy J, Hutton M: **CHIP and HSP70 regulate tau ubiquitination, degradation and aggregation.** *Hum Mol Genet.* 2004, **13**: 703-14.
154. Popugaeva E, Bezprozvanny I: **Role of endoplasmic reticulum Ca^{2+} signaling in the pathogenesis of Alzheimer disease.** *Front Mol Neurosci.* 2013, **6**: 29.
155. Prince M, Comas-Herrera A, Knapp M, Guerchet M, Karagiannidou: **Improving healthcare for people living with dementia. Coverage, quality and costs now and in the future.** *Alzheimer's Disease International*, 2016, World Alzheimer's Report
156. Proctor CJ, Gray DA: **A unifying hypothesis for familial and sporadic Alzheimer's disease.** *Int J Alzheimers Dis.* 2012, **2012**: 978742.
157. Progress Collaborative Group: **Randomised trial of a perindopril-based blood-pressure-lowering regimen among 6105 individuals with previous stroke or transient ischaemic attack.** *The Lancet* 2001, **358**: 1033.
158. Puzzo D, Gulisano W, Palmeri A, Arancio O: **Rodent models for Alzheimer's disease drug discovery.** *Expert Opin. Drug Discov.* 2015, **10**: 703-11.
159. Reinvang I, Grambaite R, Espeseth T: **Executive dysfunction in MCI: subtype or early symptom.** *Int J Alzheimers Dis.* 2012, **2012**: 936272.
160. Reitz C: **Alzheimer's disease and the amyloid cascade hypothesis: a critical review.** *Int J Alzheimers Dis.* 2012, **2012**: 369808.

161. Reitz C, Tosto G, Mayeux R, Luchsinger JA: **Genetic variants in the Fat and Obesity Associated (FTO) gene and risk of Alzheimer's disease.** *PLoS One.* 2012, **7**: e50354.
162. Rezai-Zadeh K, Douglas Shytle R, Bai Y, Tian J, Hou H, Mori T, Zeng J, Obregon D, Town T, Tan J: **Flavonoid-mediated presenilin-1 phosphorylation reduces Alzheimer's disease beta-amyloid production.** *J Cell Mol Med.* 2009, **13**: 574-88.
163. Rhein V, Song X, Wiesner A, Ittner LM, Baysang G, Meier F, Ozmen L, Bluethmann H, Dröse S, Brandt U, Savaskan E, Czech C, Götz J, Eckert A: **Amyloid-beta and tau synergistically impair the oxidative phosphorylation system in triple transgenic Alzheimer's disease mice.** *Proc Natl Acad Sci. USA* 2009, **106**: 20057-62.
164. Rhinn H, Fujita R, Qiang L, Cheng R, Lee JH, Abeliovich A: **Integrative genomics identifies APOE ϵ 4 effectors in Alzheimer's disease.** *Nature* 2013, **500**: 45-50.
165. Rosenblum WI: **Why Alzheimer trials fail: removing soluble oligomeric beta amyloid is essential, inconsistent, and difficult.** *Neurobiol Aging* 2014, **35**: 969-74.
166. Roussel BD, Kruppa AJ, Miranda E, Crowther DC, Lomas DA, Marciniak SJ: **Endoplasmic reticulum dysfunction in neurological disease.** *Lancet Neurol.* 2013, **12**: 105-18.
167. Rowan MJ, Klyubin I, Wang Q, Hu NW, Anwyl R: **Synaptic memory mechanisms: Alzheimer's disease amyloid beta-peptide-induced dysfunction.** *Biochem Soc Trans.* 2007, **35**: 1219-23.
168. Ruggeri, F.S.; Habchi, J.; Cerreta, A.; Dietler, G. **Afm-based single molecule techniques: Unraveling the amyloid pathogenic species.** *Curr Pharm Des* 2016, **22**: 3950-3970.
169. Salari S, Bagheri M: **A review of animal models of Alzheimer's disease: a brief insight into pharmacologic and genetic models.** *Physiol. Pharmacol.* 2016, **20**: 5-11.
170. Sanabria-Castro A, Alvarado-Echeverría I, Monge-Bonilla C: **Molecular pathogenesis of Alzheimer's disease: an update.** *Ann. Neurosci.* 2017, **24**: 46-54.
171. Sandberg, A.; Luheshi, L.M.; Sollvander, S.; de Barros, T.P.; Macao, B.; Knowles, T.P.J.; Biverstal, H.; Lendel, C.; Ekholm-Petterson, F.; Dubnovitsky, A., *et al.* **Stabilization of neurotoxic Alzheimer amyloid-beta oligomers by protein engineering.** *Proc Natl Acad Sci USA* 2010, **107**: 15595-15600.
172. Santacruz K, Lewis J, Spire T, Paulson J, Kotilinek L, Ingelsson M, Guimaraes A, DeTure M, Ramsden M, McGowan E, Forster C, Yue M, Orne J, Janus C, Mariash A, Kuskowski M, Hyman B, Hutton M, Ashe KH: **Tau suppression in a neurodegenerative mouse model improves memory function.** *Science.* 2005, **309**: 476-81.

173. Sarkar M, Kuret J, Lee G.: **Two motifs within the tau microtubule-binding domain mediate its association with the hsc70 molecular chaperone.** *J Neurosci Res.* 2008, **86**: 2763-73.
174. Sasaguri H, Nilsson P, Hashimoto S, Nagata K, Saito T, De Strooper B, Hardy J, Vassar R, Winblad B, Saido TC: **APP mouse models for Alzheimer's disease preclinical studies.** *The EMBO Journal* 2017 **36**: 2473-2487
175. Senechal Y, Kelly PH and Dev KK: **Amyloid precursor protein knockout mice show age-dependent deficits in passive avoidance learning.** *Behav Brain Res.* 2008, **186**: 126-32.
176. Seshadri S et al: **Genome-wide analysis of genetic loci associated with Alzheimer's disease.** *Jama.* 2010, **303**: 1832-40.
177. Shankar GM, Li S, Mehta TH, Garcia-Munoz A, Shepardson NE, Smith I, Brett FM, Michael A. Farrell, Michael J. Rowan, Cynthia A. Lemere, Ciaran M. Regan, Walsh DM, Sabatini BL and Selkoe DJ: **Amyloid- β protein dimers isolated directly from Alzheimer's brains impair synaptic plasticity and memory.** *Nat Med.* 2008, **14**: 837–842.
178. Simon A, Frechilla D, del Río J: **Perspectivas sobre la hipótesis de la cascada del amiloide en la enfermedad de Alzheimer.** *Rev. Neurol.* 2010, **50**: 667-675.
179. Sipos E, Kurunczi A, Fehér A, Penke Z, Fülöp L, Kasza A, Horváth J, Horvát S, Veszélka S, Balogh G, Kürti L, Eros I, Szabó-Révész P, Párducz A, Penke B, Deli MA: **Intranasal delivery of human beta-amyloid peptide in rats: effective brain targeting.** *Cell Mol Neurobiol.* 2010, **30**: 405-13.
180. Sipos E, Kurunczi A, Kasza A, Horváth J, Felszeghy K, Laroche S, Toldi J, Párducz A, Penke B, Penke Z: **Beta-amyloid pathology in the entorhinal cortex of rats induces memory deficits: implications for Alzheimer's disease.** *Neuroscience* 2007, **147**: 28-36.
181. Smith DL, Pozueta J, Gong B, Arancio O, Shelanski M: **Reversal of long-term dendritic spine alterations in Alzheimer disease models.** *Proc Natl Acad Sci USA,* 2009, **106**: 16877-82.
182. Soejima N, Ohyagi Y, Nakamura N, Himeno E, Iinuma KM, Sakae N, Yamasaki R, Tabira T, Murakami K, Irie K, Kinoshita N, LaFerla FM, Kiyohara Y, Iwaki T, Kira J: **Intracellular accumulation of toxic turn amyloid- β is associated with endoplasmic reticulum stress in Alzheimer's disease.** *Curr Alzheimer Res.* 2013, **10**: 11-20.
183. Song F, Poljak A, Crawford J, Kochan NA, Wen W, Cameron B, Lux O, Brodaty H, Mather K, Smythe GA, Sachdev PS: **Plasma apolipoprotein levels are associated with cognitive status and decline in a community cohort of older individuals.** *PLoS One* 2012,**7**: e34078.

184. Spowart-Manning L, van der Staay FJ: **Spatial discrimination deficits by excitotoxic lesions in the Morris water escape task.** *Behav. Brain Res.* 2005, **156**: 269-76.
185. Spuch C, Ortolano S, Navarro C: **New insights in the amyloid-Beta interaction with mitochondria.** *J Aging Res.* 2012, **2012**: 324968.
186. Steckler T and Holsboer F: **Interaction between the cholinergic system and CRH in the modulation of spatial discrimination learning in mice.** *Brain Res* 2001, **906**(1-2):46-59.
187. Stöhr J, Watts JC, Mensinger ZL, Oehler A, Grillo SK, Dearmond SJ, Prusiner SB, Giles K: **Purified and synthetic Alzheimer's amyloid beta (A β) prions.** *Proc Natl Acad Sci. USA* 2012, **109**: 11025-30.
188. Strozyk D, Launer LJ, Adlard PA, Cherny RA, Tsatsanis A, Volitakis I, Blennow K, Petrovitch H, White LR, Bush AI: **Zinc and Copper Modulate Alzheimer A β Levels in Human Cerebrospinal Fluid,** *Neurobiol Aging.* 2009, **30**: 1069–1077.
189. Sulistio YA, Heese K. **The Ubiquitin-Proteasome System and Molecular Chaperone Deregulation in Alzheimer's Disease.** *Mol Neurobiol* 2015, 905-931.
190. Takashima A: **Amyloid-beta, tau, and dementia.** *J Alzheimers Dis.* 2009, **17**: 729-36.
191. Takeda S, Sato N, Niisato K, Takeuchi D, Kurinami H, Shinohara M, Rakugi H, Kano M, Morishita R: **Validation of Abeta1-40 administration into mouse cerebroventricles as an animal model for Alzheimer disease.** *Brain Res.* 2009, **1280**: 137-47.
192. Takeuchi A, Irizarry MC, Duff K, Saido TC, Ashe KH, Hasegawa M, DMA Mann, Hyman BT and Iwatsubo T: **Age-related amyloid β deposition in transgenic mice overexpressing both Alzheimer mutant presenilin 1 and amyloid β precursor protein Swedish mutant is not associated with global neuronal loss.** *Am J Pathol.* 2000, **157**: 331-9.
193. Tampellini D, Capetillo-Zarate E, Dumont M, Huang Z, Yu F, Lin MT, Gouras GK: **Effects of synaptic modulation on beta-amyloid, synaptophysin, and memory performance in Alzheimer's disease transgenic mice.** *J Neurosci.* 2010, **30**: 14299-304.
194. Tomiyama T, Matsuyama S, Iso H, Umeda T, Takuma H, Ohnishi K, Ishibashi K, Teraoka R, Sakama N, Yamashita T, Nishitsuji K, Ito K, Shimada H, Lambert MP, Klein WL, Mori H: **A mouse model of amyloid beta oligomers: their contribution to synaptic alteration, abnormal tau phosphorylation, glial activation, and neuronal loss in vivo.** *J Neurosci.* 2010, **30**: 4845-56.
195. Townsend M, Cleary JP, Mehta T, Hofmeister J, Lesne S, O'Hare E, Walsh DM, Selkoe DJ: **Orally available compound prevents deficits in memory caused by the Alzheimer Amyloid- β oligomers.** *Ann Neurol.* 2006, **60**: 668–676.


196. Trojanowski JQ, Lee VM: **Phosphorylation of paired helical filament tau in Alzheimer's disease neurofibrillary lesions: focusing on phosphatases.** *FASEB J.* 1995, **9**: 1570-6.
197. Uematsu M, Nakamura A, Ebashi M, Hirokawa K, Takahashi R, Uchihara T: **Brainstem tau pathology in Alzheimer's disease is characterized by increase of three repeat tau and independent of amyloid β .** *Acta Neuropathol Commun.* 2018, **6**:1.
198. van Groen T, Puurunen K, Mäki HM, Sivenius J, Jolkkonen J: **Transformation of diffuse beta-amyloid precursor protein and beta-amyloid deposits to plaques in the thalamus after transient occlusion of the middle cerebral artery in rats.** *Stroke.* 2005, **36**: 1551-6.
199. Veereshwarayya V, Kumar P, Rosen KM, Mestrlil R, Querfurth HW: **Differential effects of mitochondrial heat shock protein 60 and related molecular chaperones to prevent intracellular beta-amyloid-induced inhibition of complex IV and limit apoptosis.** *J Biol Chem.* 2006, **281**: 29468-78
200. Vorhees CV, Williams MT: **Morris water maze: procedures for assessing spatial and related forms of learning and memory.** *Nat Protoc.* 2006, **1**: 848-58.
201. Walsh DM, Klyubin I, Fadeeva JV, Cullen WK, Anwyl R, Wolfe MS, Rowan MJ, Selkoe DJ: **Naturally secreted oligomers of amyloid beta protein potently inhibit hippocampal long-term potentiation in vivo.** *Nature.* 2002, **416**: 535-9.
202. Wang H, Megill A, He K, Kirkwood A, Lee HK: **Consequences of inhibiting amyloid precursor protein processing enzymes on synaptic function and plasticity.** *Neural Plast.* 2012, **2012**: 272374.
203. Wang Z, Jackson RJ, Hong W, Taylor WM, Corbett GT, Moreno A, Liu W, Li S, Frosch MP, Slutsky I, Young-Pearse TL, Spires-Jones TL, Walsh DM: **Human brain derived A β bind to synapses and disrupt synaptic activity in a manner that requires APP.** *J. Neurosci.* 2017, **37**: 11947-11966.
204. Wei, W.; Nguyen, L.N.; Kessels, H.W.; Hagiwara, H.; Sisodia, S.; Malinow, R. **Amyloid beta from axons and dendrites reduces local spine number and plasticity.** *Nat Neurosci* 2010, **13**: 190-U171.
205. Whitehouse PJ, Price DL, Clark AW, Coyle JT, DeLong MR: **Alzheimer disease: evidence for selective loss of cholinergic neurons in the nucleus basalis.** *Ann Neurol.* 1981, **10**: 122-6.
206. Yerbury JJ, Ooi L, Dillin A, Saunders DN, Hatters DM, Beart PM, Cashman NR, Wilson MR, Ecroyd H: **Walking the tightrope: proteostasis and neurodegenerative disease.** *J Neurochem.* 2016, **137**:489-505.
207. Yoshida H: **ER stress and diseases.** *FEBS J.* 2007, **274**: 630-58.

208. Zhang W, Jiao B, Zhou M, Zhou T, Shen L: **Modeling Alzheimer's disease with induced pluripotent stem cells: current challenges and future concerns.** *Stem Cells Int.* 2016, **2016**, art. 7828049.
209. Zhu, D.; Yang, N.; Liu, Y.Y.; Zheng, J.; Ji, C.; Zuo, P.P. **M2 macrophage transplantation ameliorates cognitive dysfunction in amyloid-beta-treated rats through regulation of microglial polarization.** *J Alzheimers Dis* 2016, **52**: 483-495.
210. Zussy C, Brureau A, Delair B, Marchal S, Keller E, Ixart G, Naert G, Meunier J, Chevallier N, Maurice T, Givalois L: **Time-course and regional analyses of the physiopathological changes induced after cerebral injection of an amyloid- β fragment in rats.** *Am J Pathol.* 2011, **179**: 315-34.
211. Zussy C, Brureau A, Keller E, Marchal S, Blayo C, Delair B, Ixart G, Maurice T, Givalois L: **Alzheimer's disease related markers, cellular toxicity and behavioural deficits induced six weeks after oligomeric amyloid- β peptide injection in rats.** *PLoS One.* 2013, **8**: e53117.

11. APPENDIX**I**

Article

Studies for Improving a Rat Model of Alzheimer's Disease: Icv Administration of Well-Characterized β -Amyloid 1-42 Oligomers Induce Dysfunction in Spatial Memory

Ágnes Kasza ¹, Botond Penke ^{1,*}, Zsuzsanna Frank ¹, Zsolt Bozsó ¹, Viktor Szegedi ¹ , Ákos Hunya ², Klaudia Németh ¹, Gábor Kozma ³ and Livia Fülöp ¹

¹ Department of Medical Chemistry, University of Szeged, Dome square 8, Szeged H-6720, Hungary; kaszagi@gmail.com (Á.K.); frankzsu@gmail.com (Z.F.); bozso.zsolt@med.u-szeged.hu (Z.B.); szegv@yahoo.com (V.S.); klausz20@gmail.com (K.N.); fulop.livia@med.u-szeged.hu (L.F.)

² LipidArt Research and Development Ltd., Temesvári krt. 62, Szeged H-6726, Hungary; akos.hunya@lipidart.com

³ Department of Applied and Environmental Chemistry, University of Szeged, Rerrich Béla square 1, Szeged H-6720, Hungary; kozmag@chem.u-szeged.hu

* Correspondence: penke.botond@med.u-szeged.hu; Tel.: +36-62-545-135

Received: 9 October 2017; Accepted: 13 November 2017; Published: 18 November 2017

Abstract: During the past 15 years, several genetically altered mouse models of human Alzheimer's disease (AD) have been developed. These costly models have greatly facilitated the evaluation of novel therapeutic approaches. Injecting synthetic β -amyloid ($A\beta$) 1-42 species into different parts of the brain of non-transgenic rodents frequently provided unreliable results, owing to a lack of a genuine characterization of the administered $A\beta$ aggregates. Previously, we have published a new rat AD-model in which protofibrillar-fibrillar $A\beta$ 1-42 was administered into rat entorhinal cortex (Sipos 2007). In order to develop a more reliable model, we have injected well-characterized toxic soluble $A\beta$ 1-42 species (oligomers, protofibrils and fibrils) intracerebroventricularly (icv) into rat brain. Studies of the distribution of fluorescent-labeled $A\beta$ 1-42 in the brain showed that soluble $A\beta$ -species diffused into all parts of the rat brain. After seven days, the $A\beta$ -treated animals showed a significant decrease of spatial memory in Morris water maze test and impairment of synaptic plasticity (LTP) measured in acute hippocampal slices. The results of histological studies (decreased number of viable neurons, increased tau levels and decreased number of dendritic spines) also supported that icv administration of well-characterized toxic soluble $A\beta$ species into rat brain provides a reliable rat AD-model.

Keywords: amyloid beta; AD rat model; icv administration; hippocampus; spatial memory; Morris water maze; long-term potentiation; Golgi staining

1. Introduction

Alzheimer's disease (AD) is the most common form of dementia. AD is a neurodegenerative disease that begins with synaptic dysfunction, which results in the loss of dendritic spines and post-synaptic density, finally leading to the failure of neuronal networks [1]. The initial abnormal neuronal activity progressively triggers neuronal cell death [2] as a consequence of the disruption of many intracellular processes (e.g., protein folding and degradation, mitochondrial function, etc.) [3]. β -amyloid ($A\beta$) may play a crucial role in the initiation of AD.

AD demonstrates phenotypic (clinical, imaging and pathological) heterogeneity [4]. Plenty of hypotheses try to explain the etiopathology of the disease. Based on the time of onset, AD is classified

into two types [5]. Early-onset AD (EOAD) typically develops before the age of 65 years. The other form, late-onset AD (LOAD), develops in patients older than 65 years. The production and clearance of A β is regulated by a large group of genes. The genetic background of AD is widely reviewed [6–9]. For references, see also <http://www.molgen.ua.ac.be/admutations/>.

From the different AD theories, only the A β hypothesis has survived the conflicting results of AD research. The original hypothesis states that accumulation of A β in the brain is the primary event that drives AD pathogenesis [10,11]. The A β protein (a heterogeneous mixture of peptides of 39–43 AA) is derived from the proteolytic cleavage of amyloid precursor protein (APP) by β - and γ -secretases. A β accumulates in the brain mainly as extracellular plaques, but accumulation of intracellular A β also occurs in the early stage of AD [12,13].

According to Walsh, soluble oligomers and protofibrils initiate AD pathomechanism [14]. Other results emphasize the important role of A β oligomers, protofibrils and fibrils in A β toxicity [15]. Recently, the formation of soluble toxic oligomers is considered to be a key event in AD pathogenesis. Increasing evidence indicates that the low-molecular weight oligomeric pre-fibrillar aggregates are the most highly cytotoxic species [16]. The precise molecular mechanisms of AD are still not fully understood despite 30 years of very intensive research. It is clear that LOAD is a multifactorial disease with a complex genetic background.

The familial type EOAD has simple genetics: one of the three main AD proteins (the amyloid precursor protein (APP), presenilin-1 and -2 (PSEN1 and PSEN2)) have mutations. Protein dyshomeostasis and amyloid formation are central events of both forms of AD, neuroinflammation and vascular dysfunction may play crucial roles in the onset of LOAD.

There is no “natural” animal model of the disease due to a poor understanding of AD and the complexity of the human brain [17]. Pharmacological and genetic AD- models and different animal species (primates, dogs, rodents, etc.) have been used in AD experiments during the 25 last years [18,19]. Genetically modified (transgenic, knock-in and knock-out) animal AD models provide a powerful approach to understand AD pathogenesis and study the disease [20]. These models allow investigation of the early stages of the disorder. There are several *Caenorhabditis elegans* [21,22] and *Drosophila melanogaster* [23,24] models of AD [20], which are widely used in screening experiments. A great variety of first- and second-generation transgenic mouse models of AD have been developed during the last 20 years for studying the pathophysiological processes of the disease, as reviewed in [25–31]. The transgenic mouse and knockout models analyze certain aspects of AD pathology, allowing exploration of unknown territories and revealing new pathogenic possibilities [32]. Summaries of the most prominent mouse models of AD have been published very recently [31,33,34]. Transgenic rat models were also introduced [35,36], possessing the key histopathological features of human AD (amyloid plaques, neurofibrillary tangles) without widespread cell loss. However, they have had limited success in translation of these findings into the clinics. The most obvious divergence of transgenic animal models from human AD is the artificial nature of transgenic technology. Rodents do not develop AD. The normal in vivo concentration of A β might be in picomolar range, contrary to that in human AD brains that has nanomolar A β levels. In addition, rodent A β differs from human A β by 3 AA substitutions (R5G, Y10F and H13R) and these changes also might prevent amyloid aggregation. As a consequence, the introduction of at least one of the main human AD genes (APP, PS1, PS2 and ApoE) is mandatory to model the pathology in rodents [33]. The ideal transgenic model should mimic multiple aspects of the disease including its etiology and a time-dependent progression of the pathology, which involves similar structures and cells, alike in human pathology.

Other less expensive, pharmacological animal models have also been introduced during the last 20 years. AD is considered to be a synaptic failure [37] and A β oligomers induce synaptic dysfunction [38,39], thus A β peptides have been used in model experiments. Synthetic A β -oligomers impaired long-term memory after icv injection into mice [40–44]. (A β peptides after icv injections reach brain cells by CSF (cerebrospinal fluid) influx via the perivascular and glymphatic pathways [45]). Rats offer numerous advantages over mice for developing AD models. Rats are closer to humans than

mice [46]. Larger body and brain size facilitates in vivo electrophysiology, neurosurgical procedures and neuroimaging. The resurgence of interest in the rat as the animal model of AD led to the use of different types of rat models [19]. A β peptides were also administered intrahippocampally into rat brains [47–50]. Intracerebroventricular injection of A β 1–42 to rats and mice were used to model AD [51,52]. Intranasal delivery or microinjecting A β oligomers into the entorhinal cortex was also applied in rats [53,54]. Two recent articles have compared the different pharmacological and genetic models of AD used in drug discovery [55,56].

The crucial problem of the application of A β in rat models is the heterogeneity of the peptide samples [57]. A β exists in vitro and in vivo as a continuum of different oligomeric states, none of which are particularly stable. All forms of A β -derived oligomers are potentially neurotoxic. During the fibril formation, several coexisting species are formed, giving rise to a highly heterogeneous mixture. The most difficult problem of the use of A β 1–42 microinjections is the structural heterogeneity of oligomeric samples. This heterogeneity may cause severe problems in the evaluation of the results of A β -injection animal models and reproduction of in vivo experiments.

In our laboratory, we have tried to work out a novel, robust AD rat model, using icv administration of oligomeric A β 1–42. The aim of the present study was to develop a reliable and cheap method by administering well-characterized A β peptides into the brain of wild-type rats. Atomic force microscopy was used for the characterization of A β oligomers. We have used histochemical methods to track the distribution of fluorescently labeled A β and characterize various neurodegenerative markers (number of viable neurons and dendritic spines, levels of tau). We also show that oligomeric A β -treated rats exhibit impaired synaptic plasticity (decreased LTP level) and cognitive disturbances (memory and learning behavior changes).

2. Results

2.1. Pilot Experiment with Icv Administration of AMCA-Labeled A β 1–42 Oligomers

Before the icv administration experiments, we wanted to see whether A β 1–42 oligomers could penetrate across the cerebroventricular wall. We have shown that the diffusion of the fibrillar form of A β 1–42 is stopped by the ventricular wall, thus, an icv injection would be useless (Figure 1). Therefore our first aim was to demonstrate that oligomeric form of A β 1–42 can reach the hippocampal (HC) region after icv injection. Using an unilateral injection of AMCA-labeled oligomeric A β 1–42 (oA β 1–42) into the right lateral ventricle, we have found that the A β 1–42 oligomers appear in the brain parenchyma: we could detect a few of fluorescent signs in the HC area as early as 5 min after injection (Figure 2A,B). The number of signs, namely of A β 1–42 oligomers, was evidently higher around the HC area 60 min after the injection (Figure 2C), proving that the AMCA-labeled A β 1–42 penetrates across the ependyma, or penetrates into the brain by the glymphatic flow [58].

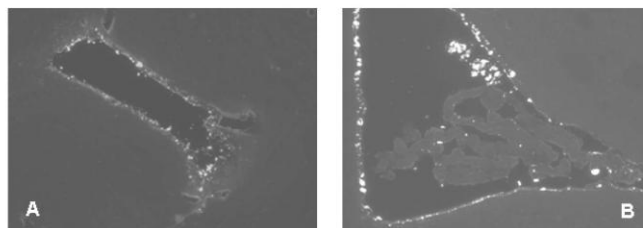


Figure 1. In this figure, icv administered fibrillar A β 1–42 does not penetrate the ependyma and remains in the ventricles. Two representative examples of brain sections (A,B) after icv injected AMCA-labelled A β 1–42 fibrils show the presence of the peptide in the ventricles at 1h after injection. Animals were injected bilaterally with 10–10 μ L solution of AMCA fA β 1–42, and the surgical procedure was the same as described in Materials and Methods.

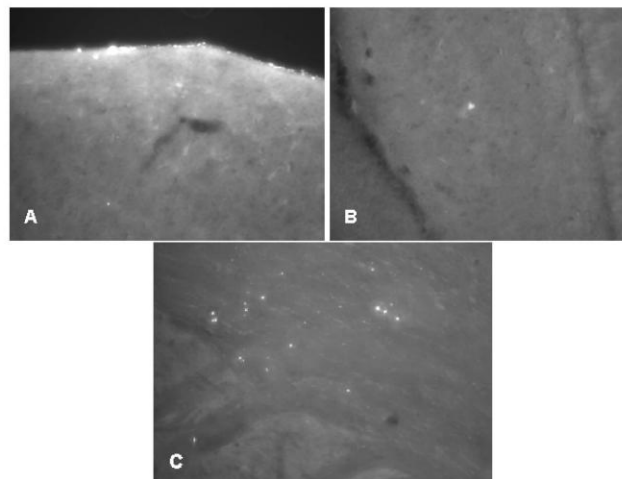


Figure 2. Oligomeric A β 1-42 enters the brain parenchyma. Representative examples of brain sections after icv injected AMCA-labelled A β 1-42 oligomers. (A): diffusion from the vehicle (5 min after injection) (B): signal in hippocampus (5 min after injection); (C): signals in brain parenchyma (60 min after injection). Animals were injected unilaterally with 7.5 μ L solution, the surgical procedure was the same as described in Materials and Methods.

2.2. Studies on the Neurotoxic Effect of Two Different, Icv Administered A β 1-42 Aggregates into Rat Brains

We demonstrated that A β 1-42 oligomers can reach the HC area after icv administration. The effect of different A β 1-42 oligomers (24 h and 168 h aggregation time in 25 μ M peptide concentration) was then studied. We analyzed the neuron viability with cresyl violet staining, tau level with tau-immunochemistry and the change of dendritic spine number was also measured. Our aim was to study if the A β 1-42 oligomers show neurotoxic effects in the HC.

In the experiment, three groups of rats were used: the 24 h and 168 h aggregated A β 1-42 treated groups in the same concentration (25 μ M) as well as HCBS-treated control. Abbreviation used for oA β -assemblies were: 24 h/25 μ M and 168 h/25 μ M.

2.2.1. Histology

After icv administration of oA β 1-42 rats, significant differences exist between groups in the number of neurons. Significantly more viable neurons were counted in the HCBS treated group than in the 168 h/25 μ M group ($p = 0.001$, $n = 4$ for each group, two slices/animal, Figure 3). (The 24 h/25 μ M assembly did not cause a significant decrease.). Tau-immunochemistry showed neurotoxic effect in the A β 1-42 treated groups, significantly more abnormally accumulated TNFs could be detected in both A β 1-42 treated groups (24 h/25 μ M and 168 h/25 μ M) compared with the vehicle (HCBS) group (HCBS vs. 24 h/25 μ M $p = 0.042$; HCBS vs. 168 h/25 μ M oA β 1-42 $p = 0.007$, $n = 4$ for each group, four slices/animal, Figure 4).

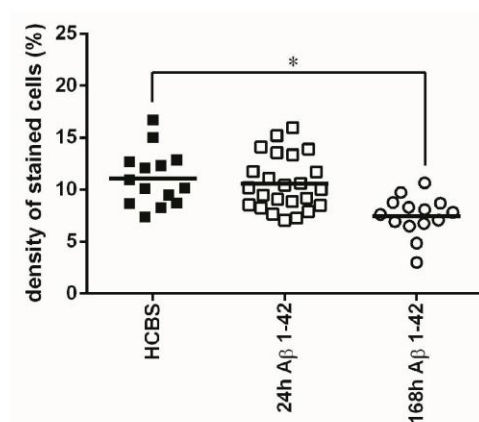


Figure 3. Cresyl violet staining of hippocampal slices after HCBS, 24 h aggregated and 168 h aggregated A β 1-42 treatment (24 h/25 μ M and 168 h/25 μ M). Each dot represents the counted raw data, while horizontal bars indicate mean values. Significant difference in staining density were observed when compared HCBS vs. 168 h aggregated A β 1-42 group ($p = 0.001$, $n = 4$, 2 slices/animal; n refers to the number of animals per group). Statistical significance was determined by one-way ANOVA, followed by Hochberg's GT2 post hoc test. * Differences with a p -value < 0.05 were considered significant.

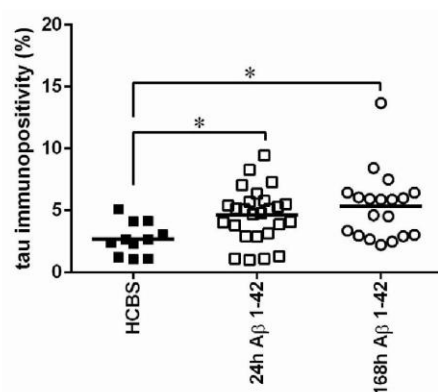


Figure 4. Tau-immunostaining of hippocampal slices after HCBS, 24 h aggregated and 168 h aggregated A β 1-42 treatment (24 h/25 μ M and 168 h/25 μ M). Each dot represents the counted raw data, while horizontal bars indicate mean values. Significant difference in the number of tau-immunopositive cells were observed between HCBS vs. 24 h A β 1-42 treated group and HCBS vs. 168 h A β 1-42 treated group, ($p = 0.042$ and $p = 0.007$ respectively. $n = 4$, 4 slices/animal; n refers to the number of animals per group). Statistical significance was determined by one-way ANOVA, followed by Hochberg's GT2 post hoc test. * Differences with a p -value < 0.05 were considered significant.

Representative examples of coronal HC sections (Figure 5) show the staining of neurons after 25 μ M A β 1-42 administration (A: control group, B: 24 h aggregation, C: 168 h aggregation assembly), and the abnormal aggregated NFTs (D: control group, E: 24 h aggregation, F: 168 h aggregation sample).

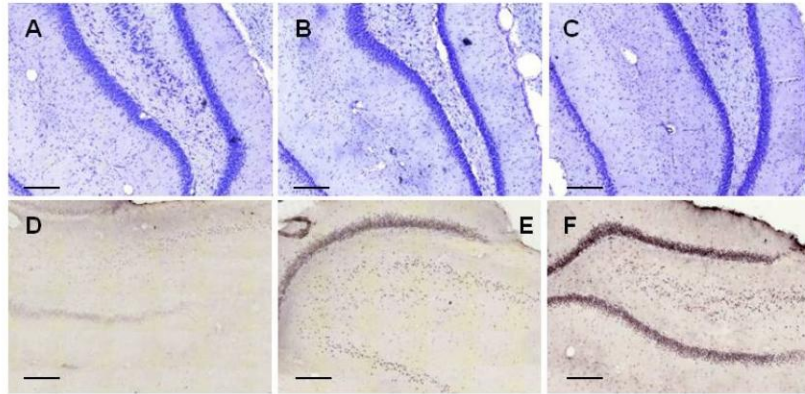


Figure 5. Representative coronal examples of hippocampal sections stained with cresyl-violet (first row) to show the presence of neuron number (first row) and with tau-antibody to show the presence of abnormally aggregated NFTs (second row). (A,D): control group; (B,E): 24 h aggregated 25 μ M amyloid treated group; (C,F): 168 h aggregated 25 μ M amyloid treated group. Scale bar: 200 μ m.

2.2.2. Studying the Change of Dendritic Spine Density Using Golgi-Cox Impregnation

The same three groups of animals (24 h/25 μ M; 168 h/25 μ M oA β 1-42 and HCBS-treated control) were used as in the former experiments. We found significant differences in spine density comparing the 168 h aggregated A β 1-42 treated to the control group. The 168 h/25 μ M oA β 1-42 injected group had significantly less dendritic spines than the HCBS-treated control group ($p = 0.048$, Figure 6). There was no significant difference in the 24 h aggregated A β 1-42 group compared with the controls. Representative photomicrographs demonstrated the difference between groups (Figure 6C–E, $n = 2$, 2–2 slices/group and 3–3 neurons per slice).

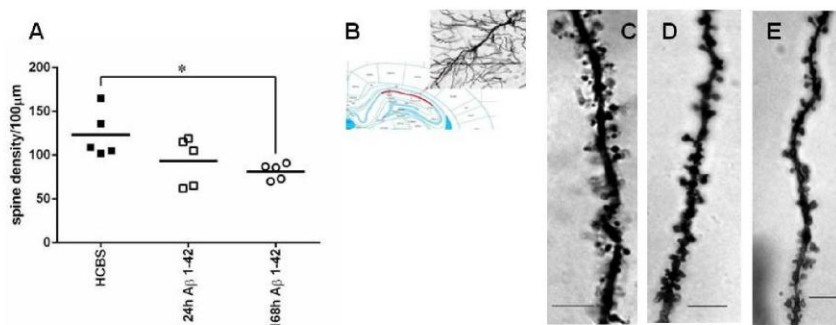


Figure 6. Representative examples of hippocampal sections stained with Golgi-Cox method to show the presence of the prevailing changes in spine density after treatment with 24 h or 168 h aggregated A β 1-42 (24 h/25 μ M and 168 h/25 μ M). (A): apical dendritic spine density. Each dot represents the counted raw data, while horizontal bars indicate mean values. Significant difference in spine densities was observed between HCBS and 168 h aggregated oA β 1-42 treated groups ($p = 0.048$, $n = 2$, 2–2 slices per group and 3–3 neurons per slice; n refers to the number of animals per group). Statistical significance was determined by one-way ANOVA, followed by a Games Howell post hoc test. * Differences with a p -value < 0.05 were considered significant; (B): 20 \times magnification of a CA1 subfield pyramidal neuron; (C): control (HCBS) group; (D): 24 h aggregated 25 μ M A β 1-42 treated group; (E): 168 h aggregated 25 μ M A β 1-42 treated group. Scale bar: 10 μ m.

2.2.3. Electrophysiological Studies

Ex vivo electrophysiological recordings with multi-electrode array (MEA) were performed in acute hippocampal slices in artificial cerebrospinal fluid (ACSF). After establishing a stable baseline, LTP was elicited by applying a theta-burst stimulation (TBS) protocol and followed for an hour. The average of the peak-to-peak amplitudes of fEPSPs before the LTP induction was taken as 100% (Figure 7). The slices obtained from HCBS-injected animals showed robust potentiation after TBS ($230 \pm 24\%$; $n = 5$ slices). The two groups of icv injected animals treated with 24 h/25 μ M and 168 h/25 μ M oA β 1-42 aggregates showed impairment of LTP. The 24 h A β 1-42 assemblies caused only a minor impairment ($184 \pm 7\%$; $n = 6$ slices), while the 168 h amyloid aggregates led to a major disruption of potentiation ($145 \pm 11\%$; $n = 6$ slices, Figure 7).

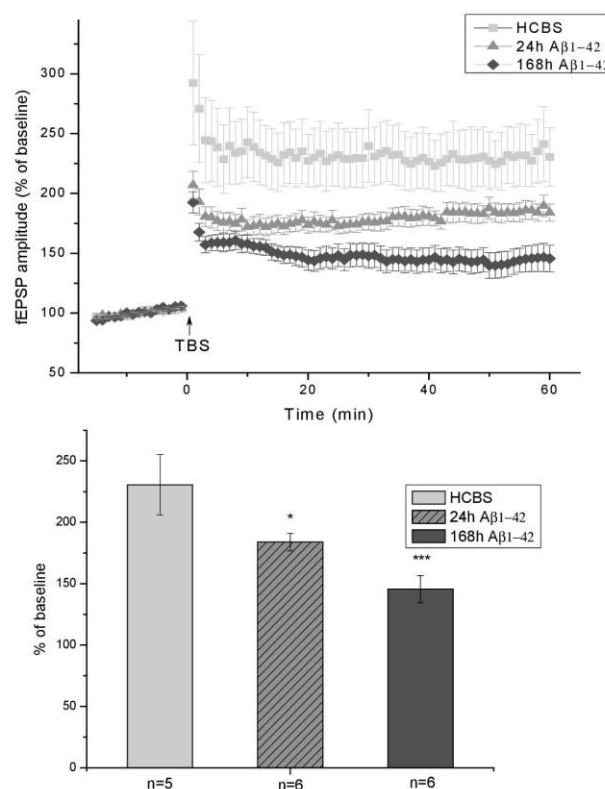


Figure 7. Shows the amplitude of fEPSPs normalized to pre-LTP control. The fEPSPs were recorded from the proximal stratum radiatum of CA1. The LTP of the 168 h oA β 1-42 treated animals showed robust impairment compared to HCBS treated ones, while the decrease was smaller in the group of 24 h oA β 1-42 injected rats. The histogram shows the level of LTP between 55 and 60 min post-TBS for each group. Error bars represent mean \pm SEM. * $p \leq 0.05$ and *** $p \leq 0.001$.

2.3. Systematic Studies for Finding the Most Toxic form of the A β 1-42 Oligomers

The influence of both the peptide concentration and the aggregation time on the toxicity of oA β 1-42 assemblies were studied in these experiments. Altogether, the effect of six different A β 1-42 assemblies were studied in the biological experiments (see Table 1).

Table 1. Variation of aggregation time and concentration for systematic studies of the effect on toxic A β 1-42 aggregates used in biological experiments.

Groups of A β -Treated Animals	Aggregation Time (Hour)	Concentration (μ M) of A β during Aggregation
A ($n = 11$), 24 h/25 μ M	24	25
B ($n = 11$), 24 h/75 μ M	24	75
C ($n = 11$), 24 h/200 μ M	24	200
D ($n = 12$), 168 h/25 μ M	168	25
E ($n = 12$), 168 h/75 μ M	168	75
F ($n = 12$), 168 h/200 μ M	168	200

The control groups ($n = 11$ and $n = 12$, respectively) got icv HCBS solution.

2.3.1. AFM Studies of the Effect of the Concentration and the Aggregation Time on the Size of A β 1-42 Oligomers

As the morphological characterization of a mixed oligomer preparation of A β 1-42 is crucial for the better understanding of the biological effects exerted by the different types of oligomers, we conducted in vitro aggregation studies, in which different concentrations of A β 1-42 were incubated in physiologic buffers for an elongated period of time. Morphology and size of the aggregates were studied by atomic force microscopy (AFM) in tapping mode. The representative images showed that, under the applied conditions, mainly spherical oligomers were formed after 24 h, the size of which did not depend considerably from the peptide concentration (Figure 8A–C) as average heights of the aggregates after 24 h of aggregation were as follows: (A) 6.5 nm in a 25 μ M solution; (B) 6.5 nm in 75 μ M; (C) 10.3 nm in 200 μ M. After 168 h, besides the spherical oligomers, protofibrillar aggregates appeared at smaller concentrations (25 μ M and 75 μ M), while, in the extremely high 200 μ M concentration, we could experience the massive formation of large round aggregates, presumably due to the strong steric hindrance between the monomers in the overcrowded aggregation environment. The detected average heights were (D) 8.2 nm in 25 μ M, (E) 8.0 nm in 75 μ M, and (F) 21.5 nm in 200 μ M, respectively. Biological effectiveness of these different aggregates was further studied in consecutive biological experiments.

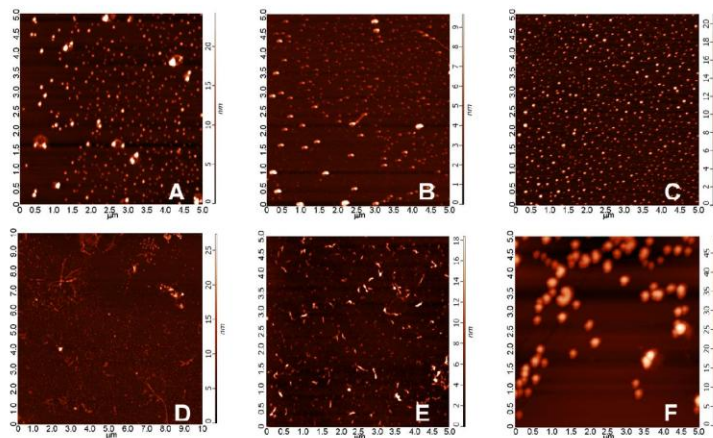


Figure 8. Morphology of A β 1-42 oligomers observed on a mica surface in AFM experiments. Average heights of the aggregates after 24 h of aggregation were as follows: (A) 6.5 nm in a 25 μ M solution; (B) 5.4 nm in 75 μ M; (C) 10.3 nm in 200 μ M. After 168 h, the following average heights were detected (D) 8.2 nm: in 25 μ M; (E) 8.0 nm in 75 μ M; (F) 21.5 nm in 200 μ M. An elongated incubation resulted in the formation of protofibrillar aggregates besides the spherical ones, as it could be observed in images (D,E).

2.3.2. Spatial Navigation in Morris Water Maze

The Morris water maze (MWM) task was used to assess spatial learning and memory. MWM is one of the most commonly used experimental models for rodents to measure spatial learning and memory [59–64]. The total time spent in arena from first trials (time spent with searching the platform) was the most informative data. The results are represented in Figures 9 and 10.

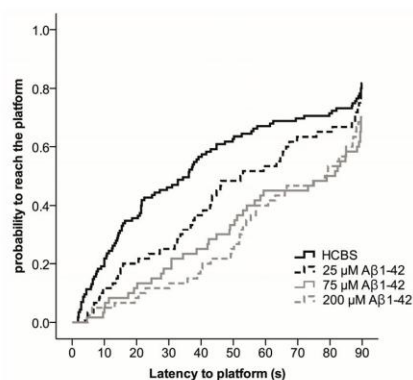


Figure 9. Effect of different aggregation concentrations (25, 75 and 200 μM) of synthetic A β 1-42 (24 h aggregation time) on Morris water maze performance. The fitted survival curves using the Cox Proportional Hazard model represents the probability that animals find the platform during a trial, capped at 90 s. We compared HCBS vs. 25 μM oA β 1-42 ($p = 0.219$), HCBS vs. 75 μM oA β 1-42 ($p = 0.003$), and HCBS vs. 200 μM oA β 1-42 ($p = 0.001$) treatment groups using log-rank tests ($n = 12/\text{group}$, except the HCBS group, where $n = 23$).

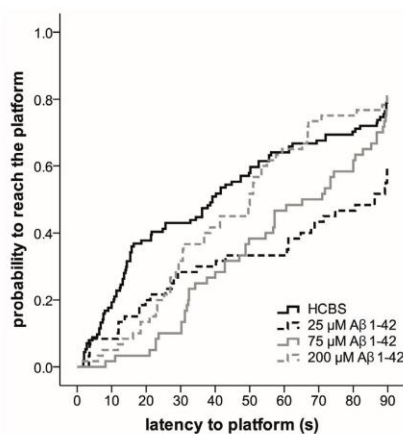


Figure 10. Effect of different aggregation concentrations (25, 75 and 200 μM) of synthetic A β 1-42 (168 h time) on Morris water maze performance. The fitted survival curves using the Cox Proportional Hazard model represents the probability that animals find the platform during a trial, capped at 90 s. We compared HCBS versus 25 μM oA β 1-42 ($p = 0.001$), HCBS vs. 75 μM oA β 1-42 ($p = 0.053$), and HCBS versus 200 μM oA β 1-42 ($p = 0.534$) treatment groups using log-rank tests ($n = 12/\text{group}$, except HCBS group, where $n = 23$).

Compared to day one of testing, in the lower aggregation grade (24 h aggregation), the 75 μM A β 1-42 treated *Group B* ($p = 0.003$) and 200 μM A β 1-42 treated *Group C* ($p = 0.001$) rats were more likely to find the platform on day four ($p < 0.001$) and five ($p < 0.001$) than the HCBS treated group; however, the change was not significant on day two ($p = 0.959$) and three ($p = 0.06$). The probability to reach the platform was determined using the Cox Proportional Hazard model (Figure 9).

Compared to day one of testing, the rats in the 168 h/25 μM oA β 1-42 treated *Group D* ($p = 0.001$) found the platform more likely on day two ($p = 0.002$), three ($p < 0.001$), four ($p \leq 0.001$) and five ($p < 0.001$). The probability to reach the platform was determined using the Cox Proportional Hazard model (Figure 10).

2.3.3. Histology

Histochemical studies in the hippocampal region confirmed our behavioral results. Although no significant difference was found between the treatment groups in the number of viable neurons after administration of 24 h aggregated oA β 1-42 oligomers, there was a tendency that suggested that the increasing aggregation concentration of A β 1-42 samples resulted in decreasing number of viable neurons in the examined area ($n = 4$; 2 slices/animal, Figure 11). Significant difference appeared between the 168 h aggregation time groups: significant loss of viable neurons was found in the hippocampal area between all oA β 1-42 treated groups (*D–F*) compared to the control HCBS group (HCBS vs. 25 μM $p = 0.011$; HCBS vs. 75 μM $p < 0.001$; HCBS vs. 200 μM $p < 0.001$; $n = 4$, 2 slices/animals, Figure 12).

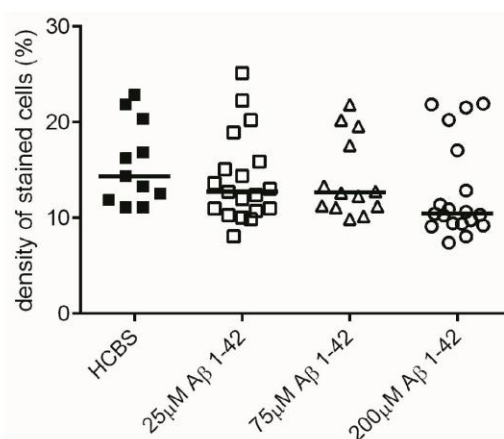


Figure 11. Cresyl violet staining (of hippocampal slices after treatment with different aggregation concentrations (25, 75 and 200 μM) of A β 1-42 at a 24 h aggregation time. Each dot represents the counted raw data, while horizontal bars indicate median values. No significant difference in staining density, only a clear tendency of decrease was observed among the treatment groups compared to the HCBS group at the 0.05 significance level, $n = 4$, 2 slices/animal; n refers to the number of animals per group. Statistical significance was determined by the nonparametric independent-samples Kruskal-Wallis test.

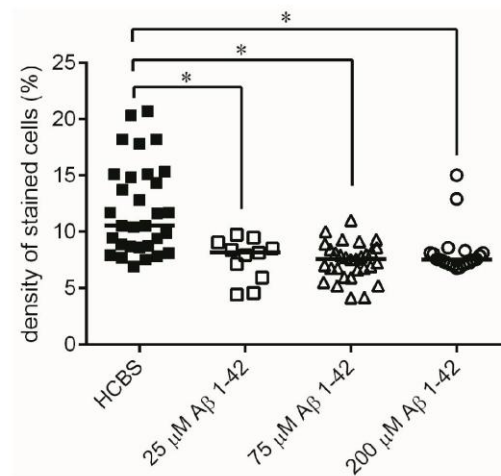


Figure 12. Cresyl violet staining of hippocampal slices after treatment with 168 h aggregated oAβ assemblies using increasing aggregation concentrations (25, 75 and 200 μM) of synthetic Aβ1-42. Each dot represents the counted raw data, while horizontal bars indicate median values. Significant differences in the staining density were observed between HCBS and the 25 μM Aβ1-42 treated group ($p = 0.011$), HCBS and the 75 μM Aβ1-42 treated group ($p < 0.001$), as well as between HCBS and the 200 μM Aβ1-42 treated group ($p < 0.001$), $n = 4$, 2 slices/animal; n refers to the number of animals per group. Statistical significance was determined by a nonparametric independent-samples Kruskal–Wallis test. * Differences with a p -value < 0.05 were considered significant.

Monitoring the presence of abnormally accumulated TNFs and comparing to the control group, significantly higher number of tau-immunopositive cells were observed in the 24 h/200 μM treated Group C ($p = 0.015$, $n = 4$, 4 slices/animal, Figure 13), the 168 h/25 μM treated Group D ($p < 0.001$, Figure 14) and the 168 h/75 μM Group E, ($p < 0.001$, $n = 4$, 4 slices/animal, Figure 14) treated groups.

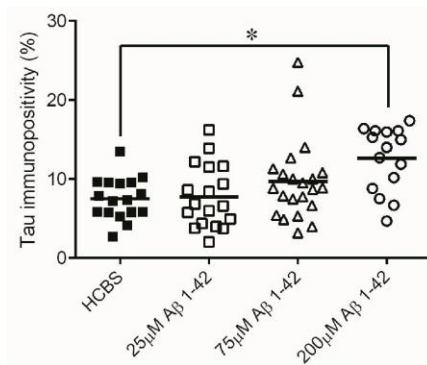


Figure 13. Tau-immunostaining of hippocampal slices after treatment with 24 h aggregated oAβ assemblies using increasing aggregation concentrations (25, 75 and 200 μM) of Aβ1-42 treatment. Each dot represents the counted raw data, while horizontal bars indicate mean values. Significant difference in the number of tau-immunopositive cells were observed only between the HCBS and the 200 μM Aβ1-42 treated group ($p = 0.015$, $n = 4$, 4 slices/animal; n refers to the number of animals per group) Statistical significance was determined by one-way ANOVA, followed by Hochberg's GT2 post hoc test. * Differences with a p -value < 0.05 were considered significant.

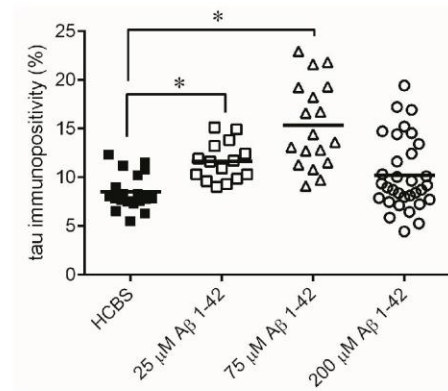


Figure 14. Tau-immunostaining of hippocampal slices after treatment of 168 h aggregated A β assemblies using increasing aggregation concentrations (25, 75 and 200 μ M) of synthetic A β 1-42. Each dot represents the counted raw data, while horizontal bars indicate mean values. Increasing number of tau immunopositive cells were observed comparing the HCBS and the 25 μ M oA β 1-42 treated ($p < 0.001$), as well as the HCBS and the 75 μ M oA β 1-42 treated groups ($p < 0.001$). There is no significant difference between HCBS and 200 μ M oA β 1-42 treated groups ($p = 0.284$), $n = 4$, 4 slices/animal; n refers to the number of animals per group. Statistical significance was determined by one-way ANOVA, followed by a Games–Howell post hoc test. * Differences with a p -value < 0.05 were considered significant.

Representative examples of coronal HC sections show neurons after 25, 75 and 200 μ M oA β 1-42 administration with 24 h aggregation time (Figure 15A–D) using cresyl violet staining. The abnormal aggregated NFTs are demonstrated in Figure 15E–H).

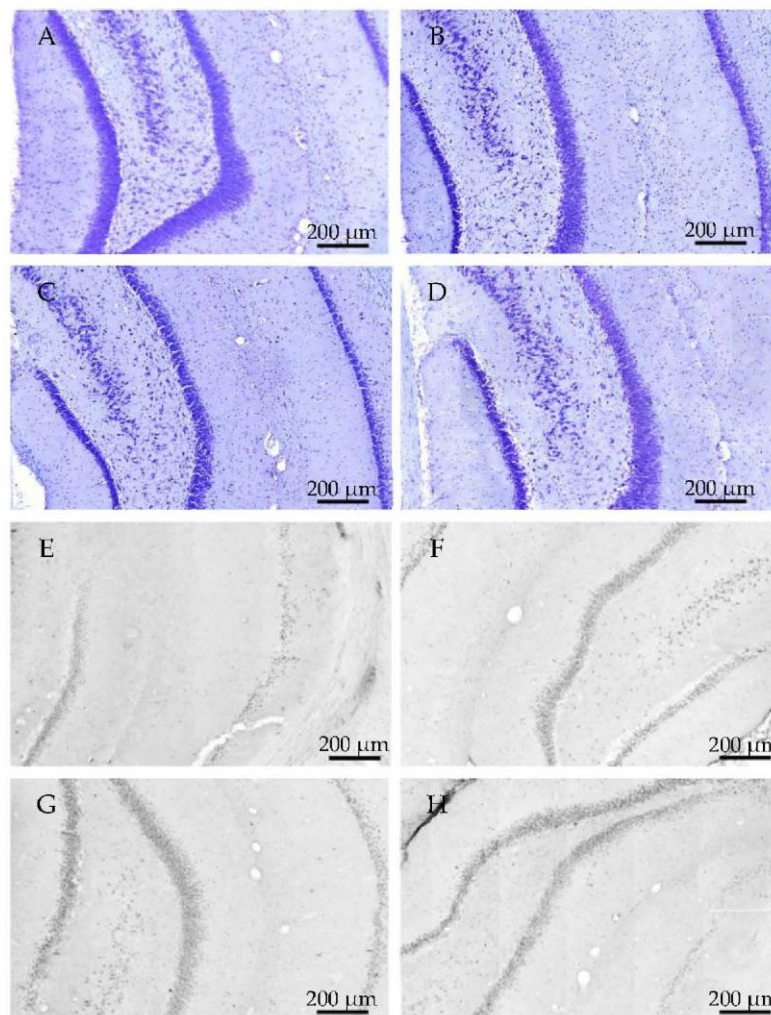


Figure 15. Representative examples of hippocampal sections in 24 h aggregation groups, using cresyl-violet staining, show the change of viable neuron number (A–D). Immunohistochemistry with tau-antibody shows the presence of abnormally aggregated NFTs (E–H). (A,E): control group; (B,F): 25 μ M concentration; (C–G): 75 μ M concentration; (D–H): 200 μ M concentration.

Representative examples of coronal HC sections show the presence of neurons after 25, 75 and 200 μ M oAβ1-42 administration with 168 h aggregation time (A–D), using cresyl violet staining. The abnormally aggregated NFTs are shown in Figure 16.

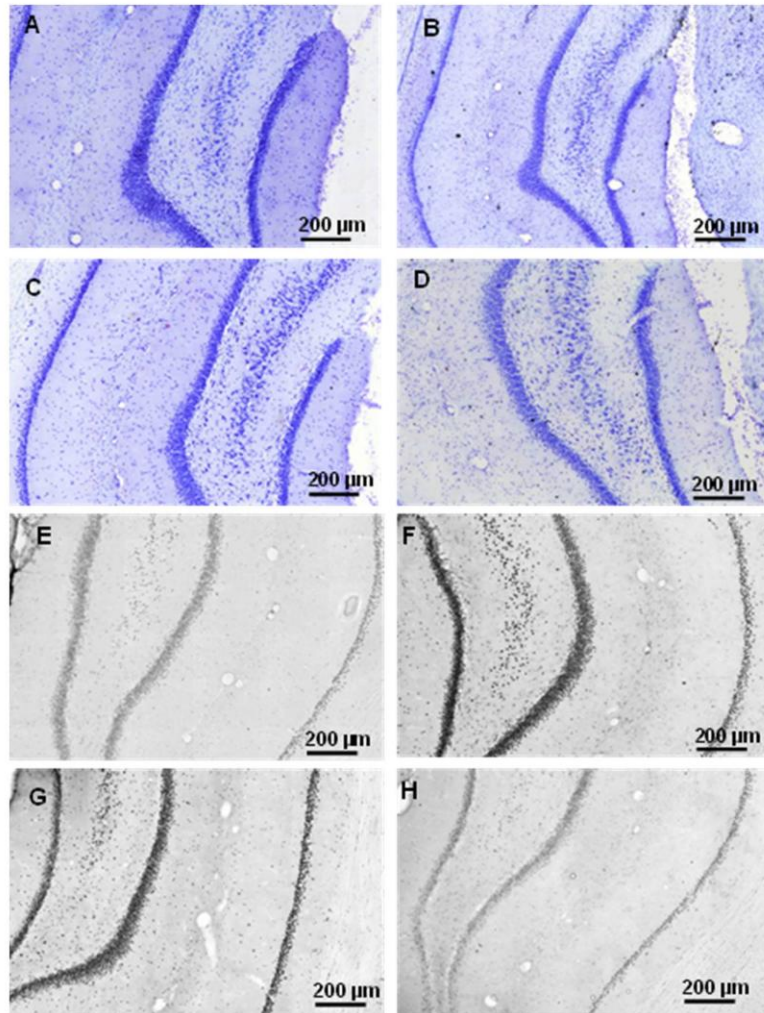


Figure 16. Representative examples of hippocampal sections in 168 h aggregation time groups using cresyl-violet staining to show the decrease of viable neuron number (A–D). Immunohistochemistry with tau-antibodies shows the increase of abnormally aggregated NFTs (E–H). (A,E): control group; (B,F): 25 μ M concentration; (C–G): 75 μ M concentration; (D–H): 200 μ M concentration.

2.3.4. Ex Vivo Electrophysiological Recordings with Multi-Electrode Array (MEA)

The electrophysiological studies in the hippocampal region confirm our behavioral and immunohistochemical results. Slices were prepared from rats that had received icv administration of 24 h/25 μ M (Group A) and 24 h/75 μ M oA β 1–42 (Group B). Both oA β 1–42 samples caused reduced potentiation after LTP induction ($168 \pm 8\%$ and $185 \pm 10\%$, $n = 6$ and 10 , respectively) compared to the HCBS treated group ($233 \pm 26\%$, $n = 5$, Figure 17). The 24 h/200 μ M oA β peptide (Group C) caused the greatest reduction of LTP level ($136 \pm 3\%$, $n = 8$, Figure 17).

24 h aggregation

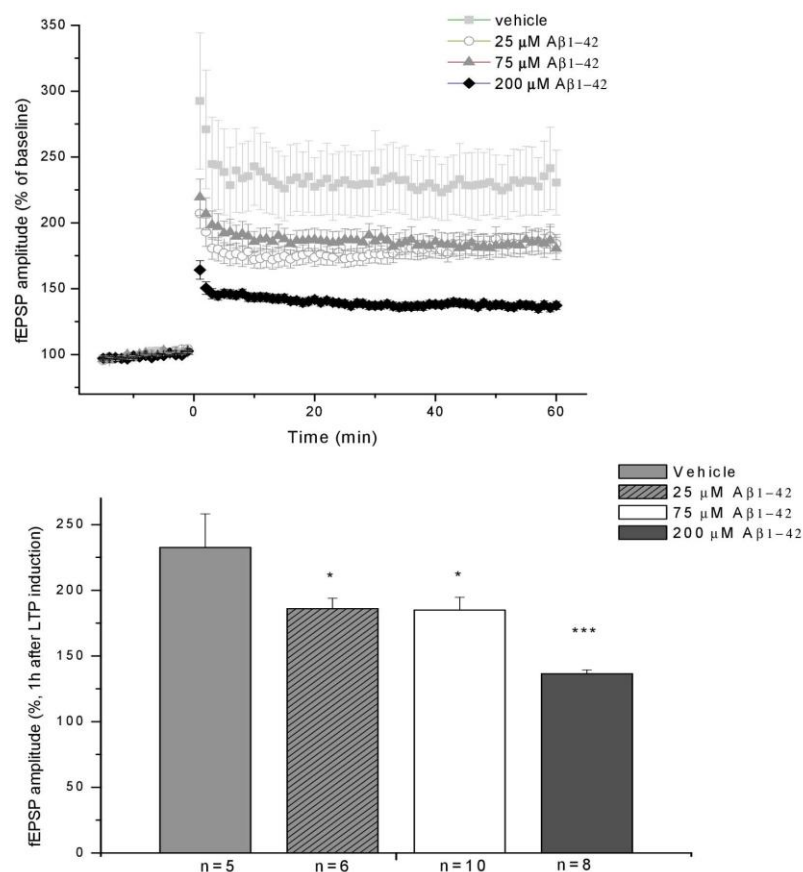


Figure 17. LTP impairment depends on the aggregation concentration. The effect of 24 h/75 μM, 24 h/25 μM and 24 h/200 μM oAβ samples on LTP in HC slices. The histogram shows the level of fEPSP potentiation between 55 and 60 min post-TBS. Error bars represent mean ± SEM. * $p \leq 0.05$ and *** $p \leq 0.001$.

The effect of the 168 h aggregates also showed concentration dependence (Figure 18). Similarly to the 24 h aggregation experiments, the effects of 25 μM (Group D) and 75 μM (Group E) peptide assemblies did not differ from each other, as they similarly reduced LTP level ($145 \pm 11\%$; $n = 6$ and $145 \pm 4\%$; $n = 12$, respectively). In contrast, the 168 h/200 μM (Group F) oAβ aggregates caused much smaller reduction of LTP ($182 \pm 9\%$; $n = 5$ compared to HCBS group $232.5 \pm 26\%$; $n = 5$).

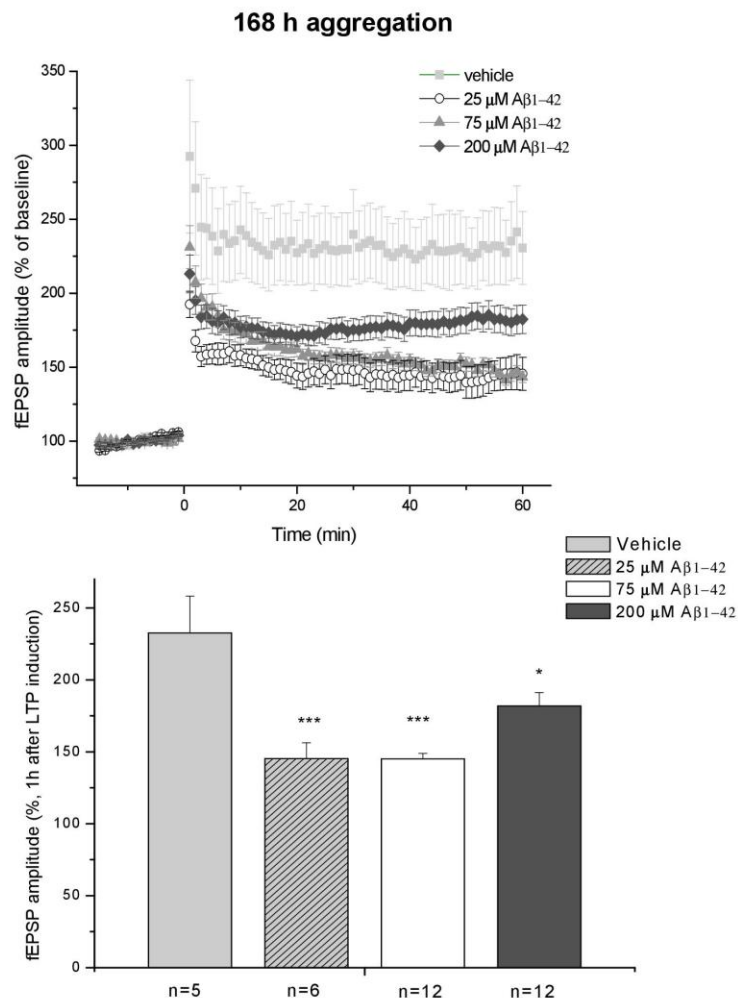


Figure 18. LTP impairment depends on the aggregation concentration of A β 1-42. The effect of 168/25 μ M, 168 h/75 μ M and 168/200 μ M oA β 1-42 samples in acute HC slices. The histogram shows the level of fEPSP potentiation between 55 and 60 min post-TBS. Error bars represent \pm SEM. * $p \leq 0.05$ and *** $p \leq 0.001$.

3. Discussion

The main aim of the present work was a systematic study of the neurotoxic effects of icv administered oA β assemblies in rat brain. Our principal aims were:

- (1) Preparation of toxic A β 1-42 oligomers from a precursor peptide (iso-A β 1-42) and standardization of the method of the synthesis and characterization of oA β 1-42 assemblies.
- (2) Measurement of the effect of different oA β 1-42 samples on neuron viability, NFT-formation, dendritic spine density, synaptic plasticity and spatial behavior in nontransgenic rats.
- (3) Development of a novel rat model of AD using icv administration of well-characterized oA β 1-42 samples.

The role of amyloid plaques and oligomeric A β in AD etiopathology has been debated for a long time. Depositions of extracellular A β and the surrounding oA β are considered as trigger signals to induce dendritic spine loss and synaptic dysfunction in AD. A β assemblies are synaptotoxic, and dendritic spine loss is strongly correlated with cognitive impairment in AD. A β has been shown to target synapses [65,66]. Experiments demonstrated that synapse dysfunction was triggered by A β oligomers [67]. Bilateral intrahippocampal (ihc) injections of fibrillar A β reduced neuronal density, increased the intensity of glial fibrillary acidic protein and caused behavior performance deficits [49,68]. Our former experiments also demonstrated that synthetic fA β after ihc administration simultaneously decreased spatial learning ability in MWM and reduced dendritic spine density in the rat hippocampus CA1 region [69]. As fA β is a non-diffusible form and act only locally, the diffusible oligomeric A β assemblies (that surround fA β) very probably affect the neurons and synapses in these experiments [70]. It is widely accepted that accumulation of soluble toxic A β at the synapse may be on the critical path to neurodegeneration [71]. A β -dependent disruption of neural cell adhesion molecules in AD hippocampus may contribute to synapse loss [72,73].

In our former studies, we found that the aggregation grade of the oligomeric A β 1-42 samples plays a crucial role in the toxicity [53,54]. We demonstrated that the aggregation grade can be standardized using controlled in situ preparation of A β 1-42 oligomers from the A β -precursor isoform (iso-A β 1-42), and oA β 1-42 assemblies can be physicochemically characterized [74]. This method was used in the present work for preparation of different oA β 1-42 assemblies in two series of experiments. Different aggregation times (24 h and 168 h) and peptide concentrations (25 μ M, 75 μ M, 200 μ M) were used, and the AFM method was applied for characterization of oA β assemblies.

In the first experiment, one peptide concentration (25 μ M) and two different aggregation times (24 h and 168 h), in the second experiment three peptide concentrations (25 μ M, 75 μ M and 200 μ M) and two different aggregation times (24 h and 168 h) were used. (The samples of the oA β 1-42 were signed as 24 h/25 μ M, 168 h/25 μ M, 24 h/75 μ M, 168 h/75 μ M, 24 h/200 μ M, 168 h/200 μ M.). The morphology of some of the oA β 1-42 assemblies is shown in Figure 8.

A pilot study (Figures 1 and 2) demonstrated that AMCA-labeled fibrillar A β 1-42 remained in the ventricles after injection, but AMCA-oA β 1-42 penetrated across the ependyma or entered the brain parenchyma by the glymphatic flow.

The results of the first experiments are shown in Figures 3–7. There was a considerable difference between the effects of the two oA β 1-42 samples: the 168 h/25 μ M sample showed significant change in neuronal viability ($p = 0.001$, Figure 3), increase in NFT-level ($p = 0.007$, Figures 4 and 5), decrease of dendritic spine density (Figure 6, $p = 0.048$) and robust impairment of LTP (Figure 7, $p < 0.001$). The effects of 24 h/25 μ M sample were not significant in the viability test (Figures 3 and 5B), as well as in dendritic spine density measurement (Figure 6A). These results demonstrated that the aggregation time of A β 1-42 plays a crucial role in the formation of toxic assemblies. In addition, 168 h aggregation time in 25 μ M concentration resulted in the formation of toxic assemblies, while the 24 h samples gave less toxic aggregates.

In the second series of experiments, the effect of six different oA β 1-42 samples were systematically studied. AFM studies of these oA β 1-42 samples demonstrated big differences in the size of the assemblies (Figure 8). The mean of the particle diameter was in the range of 6.5 and 21.5 nm. Besides the obvious differences in size, an altered morphology of the aggregates could also be observed, as protofibrils were formed together with the spherical oligomers in lower (25 and 75 μ M) concentrations after 168 h. These oA β 1-42 assemblies were used in behavioral (learning and memory), histological and electrophysiological studies.

In this series of experiments, we examined whether these A β oligomers impair memory functions in rats, especially the spatial memory. We measured the effect of icv administered oA β samples in MWM, a hippocampal learning and memory test, in which the animals have to learn the location of the hidden platform [60]. As HC appears to play a central role for establishment in long-term memory [75],

we determined the mean of the first swimming session. The second trial every day was a potentiation for the animals to learn the exercise easier.

Finding of the hidden platform took a longer time for the A β -treated animals. After latency times of five days, A β 1-42-treated animals exhibited significant differences compared to the control group. This finding is in accordance with the hypothesis that icv injection of iso-A β 1-42 derived oligomers impair the spatial memory. The highest significance (greatest difference in latency times) compared with the control animals was exhibited by the *group C* (24 h/200 μ M), where the particle size was 10 nm (Figures 8 and 9), the *group D* (25 μ M and 168 h), where the particle size exceeds 8 nm (Figures 8 and 10).

Histological studies partly confirmed the results of behavioral experiments. Although the 24 h aggregates did not significantly decrease the number of viable neurons, there was a clear tendency for neuronal loss (Figure 11). The 168 h samples cause a significant decrease of viable neurons compared to the control (Figure 12).

Measurement of the abnormally accumulated NFTs in the HC slices gave interesting results (Figure 13): only the 24 h/200 μ M oA β 1-42 assembly caused significant NFT accumulation. Aggregation time of 168 h in 25 and 75 μ M concentrations resulted in the formation of toxic assemblies, but the 168 h/200 μ M sample did not cause a change in the NFT level (Figure 14). These results were in good correlation with the size and mobility of oA β assemblies (Figure 8). Representative examples showed the coronal HC sections, applied for neuron viability and NFT-accumulation measurements (Figures 15 and 16).

Electrophysiological studies also supported the results of the behavioral experiments. Only the 24 h/200 μ M oA β 1-42 sample caused a great reduction in LTP, although the samples with lower aggregation concentrations also showed a clear tendency for decreasing LTP (Figure 17). Finally, the concentration dependence in the 168 h groups was similar to the 24 h groups: the 25 and 75 μ M oA β 1-42 samples caused robust and significant reduction, while the LTP reduction was much smaller in the 200 μ M group (Figure 18). These results also correlate well with the size and viability of the oA β assemblies.

Summarizing our studies, we found a simple correlation between the aggregation size and the mobility and toxicity of oA β 1-42. There was an optimal size of oA β 1-42 assemblies (between 8 to 10 nm height) that caused elevated toxicity (24 h/200 μ M, 168 h/25 μ M and 168 h/75 μ M aggregates, (Figures 9, 10, 12–14, 17 and 18). Too small and too big aggregates (24 h/25 μ M, 24 h/75 μ M, 168 h/200 μ M) were less toxic or nontoxic (Figures 9, 11, 13, 14, 17 and 18). We assume that the size and different conformations, resulting in altered morphology, together are responsible for the enhanced toxicity. In addition, the peptide conformation within the oA β 1-42 samples is unknown, and we suppose that the toxic samples not only have similar particle size, but also structural similarity, containing oligomeric and protofibrillar A β 1-42 species.

The connection between amyloid aggregation, cellular toxicity and the biochemistry of neurodegeneration has been a challenge, and the molecular details are more or less unknown. Determining the biophysical properties and conformational variety of a single species of amyloid peptides/proteins represents a high experimental challenge. The main problem is the heterogeneous nature and the nanoscale dimensions of the amyloid assemblies. Circular dichroism and infrared spectroscopy are bulk techniques and cannot characterize the inner properties of the aggregates at the single species level [57].

Taken together, the suitability of a new rat model was demonstrated. Our aim was to work out a novel, robust AD rat model using icv administration of well characterized oligomeric A β 1-42. Such kind of model has several advantages compared to the existing mice and rat models:

- (1) Mice are typically more variable in their behavior than rats; thus, we were able to use fewer animals for getting significant results in rats than in mice in MWM and other behavior experiments.

- (2) Rats are physiologically, genetically and morphologically closer to humans than mice [46]. Their larger body and brain size facilitate neurosurgical procedures, neuroimaging and in vivo electrophysiology.
- (3) Our research group also successfully used intranasal delivery of human A β 1-42 for rat brain targeting, but intranasal administration is complicated and very time-consuming.
- (4) The recent method is a short-term model: it is possible to get pathology and behavior changes within two weeks after the icv administration into rats.
- (5) Several laboratories have used short human A β fragments (e.g., A β 25–35) in rat experiments; however, these kinds of short A β peptides are not natural metabolites of A β degradation, only aggregation-prone synthetic products.
- (6) Other laboratories (e.g., [49]) used a rat model of AD injecting fibrillary A β 1-42 into the rat brain. In this model, the injected fibrillar A β aggregates form a deposit in the brain and a long time is necessary for destabilization and disintegration of the assemblies to diffusible toxic A β -oligomers. The use of icv administration of toxic oA β 1-42 samples is advantageous, and the optimal size of the A β 1-42 assemblies is 8 to 10 nm height.

Our current study demonstrated that icv administration of oA β assemblies or A β protofibrils of definite size and structure into rats decreased cell viability and dendritic spine density, increased NFT formation, disturbed synaptic plasticity and impaired the learning and spatial behavior of the animals. Our results improve the “icv-administered A β ” rat model using well-characterized A β 1-42 oligomers.

4. Materials and Methods

4.1. Preparation of A β 1-42 Peptide Samples and Different Oligomeric Assemblies

4.1.1. Preparation of Different A β 1-42 Oligomeric Assemblies

The oligomeric A β 1-42 peptide was synthesized in the following way: the A β peptide precursor iso-A β 1-42 was synthesized by Fmoc-chemistry and transformed at neutral pH to A β 1-42 by O \rightarrow N acyl migration in a short period of time, resulting in a water soluble oligomeric mixture of A β 1-42 oligomers as previously described [74]. Synthetic iso-A β peptide was pre-treated with HFIP in order to facilitate its oligomerization, and to standardize its aggregation. The aggregation grade of these oligomers thus formed was standardized. In these studies, the soluble A β 1-42 oligomeric peptide samples were freshly prepared by incubating the oligomeric A β 1-42 peptide on 37 °C in PBS at pH 7.4 for different time courses (24 h and 168 h) at the concentrations of 25, 75 and 200 μ M, respectively. Samples were sonicated in normal bath sonicator for 5 min. Before use, each sample was subsequently diluted to the final concentration of 10 μ M, and 15 μ L ($2 \times 7.5 \mu$ L) of these solutions were injected into rat brain hemispheres (see Surgery). The amount of A β 1-42 injected at the concentration of 10 μ M in each case equaled 50 pmol or 225 ng of A β peptides.

The fluorescent labeled A β peptide (AMCA-A β) was synthesized also in our research group [76].

4.1.2. Atomic Force Microscopy Studies (AFM) of A β 1-42 Assemblies

For the experiment, 10 μ L of peptide solution were pipetted onto freshly cleaved mica (Muscovite mica, V-1 quality, Electron Microscopy Sciences, Washington, DC, USA). After 2 min, the samples were washed twice with 10 μ L of distilled water and then dried with nitrogen gas. The AFM images were obtained using tapping mode on a NT-MDT Solver Scanning Probe Microscope (NT-MDT Spectrum Instruments, Moscow, Russia) under ambient conditions. AFM tips type PPP-NVHAuD-10 manufactured by NANOSENSORS (Neuchâtel, Switzerland) were applied with a nominal radius of curvature of 2 nm and 15 μ m length. The non-contact silicon cantilevers having typical force constant of 42 N/m and resonance frequency of 278.8 kHz. Further information of the tip: material n⁺-silicon, resistivity 0.01–0.02 Ω cm, thickness $4.0 \pm 1 \mu$ m, length: $125 \pm 10 \mu$ m, width $30 \pm 7.5 \mu$ m.

4.1.3. Fluorescent Microscopy

For fluorescent microscopy study, rats ($n = 2$) received fibrillar form, and, in the other experiment, rats ($n = 4$) received oligomeric form and of AMCA (7-Amino-4-methylcoumarin-3-acetic acid)-labeled A β 1-42 as a single dose in dilution of AMCA-A β 1-42:A β 1-42 2:7 ratio (concentrations: AMCA-A β 1-42 16.7 μ M; A β 1-42 = 58.3 μ M in total of 75 μ M final peptide concentration). fA β was administered bilaterally (10–10 μ L per site), and oA β unilaterally into the right cerebroventricle (7.5 μ L pro animal). 60 min after fA β 1-42, and 5 or 60 min after oA β 1-42 administration the rats were transcardially perfused (100 mL PBS, pH = 7.4). The brains were removed and cut to 30 μ m thick sagittal sections. Sections were placed on glass slides, air dried, and mounted in Gel Mount (Biomed, San Diego, CA, USA). Fluorescent signal was examined in the sections by a Nikon Eclipse TE2000 fluorescent microscope (Nikon, Tokyo, Japan) and photographed by a Spot RT digital camera (Diagnostic Instruments, Sterling Heights, MI, USA).

4.2. Treatment Groups

4.2.1. Studies on Two Different A β 1-42 Oligomers (24 h and 168 h Aggregation Time, Concentration 25 μ M)

Subjects were divided into three groups: the control group ($n = 12$) was injected with hydrocarbonate buffered saline (HCBS) solution, the other two groups were injected with 24 h aggregated A β 1-42 ($n = 12$) and a 168 h aggregated A β 1-42 ($n = 12$).

4.2.2. Systematic Studies for Finding the Most Toxic Form among Six Different A β 1-42 Oligomers

oA β samples were prepared in combination of three different A β 1-42 aggregation concentrations (25, 75 and 200 μ M) with two different aggregation times (24 h and 168 h). The experiments were divided into two divisions: oA β samples of 24 h and 168 h, respectively (altogether six groups):

- A/ A β 1-42, 24 h aggregation time, $c = 25$ μ M; mean particle diameter 6.5 nm,
- B/ A β 1-42, 24 h aggregation time, $c = 75$ μ M; mean particle diameter 6.5 nm,
- C/ A β 1-42, 24 h aggregation time, $c = 200$ μ M; mean particle diameter 10.3 nm,
- D/ A β 1-42, 168 h aggregation time, $c = 25$ μ M; mean particle diameter 8.2 nm,
- E/ A β 1-42, 168 h aggregation time, $c = 75$ μ M; mean particle diameter 8.0 nm,
- F/ A β 1-42, 168 h aggregation time, $c = 200$ μ M; mean particle diameter 21.5 nm.

The control groups ($n = 11$ in the 24 h and $n = 12$ in the 168 h experiments) in both studies were treated with HCBS. For the statistical analysis, the mean of data of the two control groups were evaluated ($n = 23$). Table 1 summarizes the characteristics of A β -treated groups (A–F) to simplify further orientation.

4.2.3. Surgery and Icv Administration of oA β 1-42

Before surgery, rats were deeply anesthetized by e.g., injection of ketamine (10.0 mg/100 g) and xylazine (0.8 mg/100 g) mixture, and were placed in a stereotaxic apparatus. A midline incision of the scalp was made, and the skull was carefully cleared from the skin and the muscles. After that two holes were drilled above the target regions. Every solution was injected icv with Hamilton syringe bilaterally, into each hemisphere. Furthermore, a 7.5 μ L solution was injected per site (1.5 μ L/min). The coordinates were from bregma: AP: -1.0 ; ML: ± 1.5 ; DV: -4.5 . [77]. The animals were treated after the surgery with antibiotics and analgesic.

4.3. Spatial Navigation of Rats in a Morris Water Maze (MWM)

4.3.1. Experimental Animals and Housing

Adult male Charles River-Harlan rats (Domaszék, Hungary) were the subjects of the experiments, weighing 250–300 g before surgery. After arrival, the animals were housed under constant temperature and lighting conditions (23 °C, 12:12 h light/dark cycle, lights on at 7:00). The rodents had free access to food and water throughout the experiment. After arrival, the animals were gently handled by daily measuring. Experiments were performed in accordance with the Hungarian Health Committee and the European Communities Council Directive of 24. November 1986 (86/609/EEC). Formal approvals to conduct the experiments have been obtained from the Animal Experimentation Committees of the University of Szeged and of the Biological Research Center, and from the local authorities (XVI/03835/001/2006).

4.3.2. Morris-Water Maze Experiments

Animals were trained in open-field water maze (diameter: 180 cm) filled with water (23 ± 1 °C) that was made opaque with milk. The pool was divided into four virtual quadrants, and the invisible platform (diameter: 10 cm) was submerged in the middle of one of the four quadrants. Around the pool, there was a black curtain. The animals were allowed to swim for 5 days, twice a day and launched from four different starting points. They were placed into the water facing the wall of the pool and were given 90 s to find the platform and 15 s to stay on it. Animals that did not find the platform were gently guided and placed on it. The escape latency data were calculated automatically by a video tracking system (EthoVision 2002, Noldus Information Technology, Wageningen, The Netherlands). The means of the data (+SEM) from the first swimming sessions were used for statistics.

4.4. Histology

After the Morris water maze test, the animals were deeply anesthetized and transcardially perfused with 150 mL 4 °C phosphate-buffered saline solution (PBS), followed by 250 mL 4 °C paraformaldehyde solution (4% in phosphate buffer, pH 7.4). The brains were removed and postfixed for 24 h in the same fixative (4 °C), and subsequently cryoprotected in 30% sucrose solution for 72 h (4 °C). Brains were cut on a cryostat to 30 µm hippocampal coronal sections, and the slices were collected and stored at 4 °C in PBS for free floating histochemistry.

4.4.1. Cresyl Violet (Nissl) Staining

The cresyl violet staining is used for neuronal tissue, the stain binds to the acidic components of the neuronal cytoplasm, showing the number of viable neurons. Slides were stained into the filtered 1% cresyl violet solution for 5 min and dehydrated subsequently in 50%, 70%, 95%, and twice in 100% ethanol for 1 min each. Slides were finally placed in xylene for another 10 min and coverslipped.

4.4.2. Tau-Immunohistology

To visualize the presence of neurofibrillary tangles, we used human PHF-tau Mab (clone AT100) primer antibody at 1:800 dilution in PBS (pH 7.4) for immunostaining.

After quenching of endogenous peroxidase activity and a blocking step, the sections were incubated overnight at 4 °C with the primary antibody in the presence of 20% goat serum and Triton X-100 0.2%. On the following day, the sections were washed in PBS and incubated 1 h at room temperature with the second biotinylated goat anti-rat antibody (Vector Laboratories, Burlingame, CA, USA, 1:400). The next step was a 1-hour incubation with avidine-biotin complex (Vectastain Elit ABC Kit, Vector Laboratories, Burlingame, CA, USA; 1:400) and detection with nickel-enhanced 3,3'-diaminobenzidine. After immunostaining and washing, all sections were mounted on gelatin-coated slides, air-dried, dehydrated and coverslipped with DPX, a synthetic

resin mounting media for histology (Fluka BioChemika, Buchs, Switzerland). Digital photographs were taken by a digital slide scanner (Mirax Midi, Carl Zeiss, Hungary); for the analysis, we used the Histoquant program (3DHistech, Budapest, Hungary).

4.5. Quantification of Dendritic Spine Density Using Golgi Impregnation

The FD Rapid GolgiStain™ Kit (FD NeuroTechnologies, Consulting & Services, Inc., San Diego, CA, USA) was used ($n = 6$, 2–2 slices per group and 3–3 neurons per slice) for measuring changes of dendritic spine density in the hippocampal CA1 area.

Experimental animals were deeply anesthetized before the brain was removed from the skull. The brains were removed as quickly as possible and handled carefully to avoid damage or pressing of the tissue. The tissue was immersed in the impregnation solution (A + B solution) and stored at room temperature for 2 weeks in the dark. The brains were transferred into another solution (C) and stored at 4 °C in the dark for at least 48 h. In addition, 100 µm coronal sections were cut with microtome (Zeiss Microm HM 650 V, Carl Zeiss AG, Oberkochen, Germany). Sections were mounted on gelatin coated glass slides. After the staining procedure and dehydration, the slides were covered with DPX (VWR international).

The Golgi sections were studied by inverse light microscope, using oil-immersion objectives. The spine density of the proximal apical dendrite area was analyzed (100–200 µm from soma). One segment (100 µm in length) from a second-third-order dendrite protruding from its parent apical dendrite was chosen in each examined neuron for spine density quantification, as described by [78]. The dendrites were selected under a 100× oil immersion lens and the images (600×) of these apical dendrites were captured through a CCD camera (1600 × 1200 pixel) connected to a light microscope (Olympus Vanox-T AH-2, Olympus Optical CO, LTD., Tokyo, Japan) and a computer. Serial images were made from each dendrite in the whole of the analyzed segment. The captured multiple photomicrographs from one dendrite were then stacked into one file. To stack the images, the Image-Pro-Plus image analysis software (IPP; Media Cybernetics, Silver Springs, MD, USA) was used. Measurement of the spine density was performed by two independent experimenters to blind the analysis.

4.6. Ex Vivo Electrophysiological Studies

4.6.1. Stimulation Protocols

Using standard procedures, 350 µm thick transverse acute hippocampal slices were prepared from the brain using a McIlwain tissue chopper (Campden Instruments, Loughborough, UK). Slices were incubated in carbogenated standard artificial cerebrospinal fluid (ACSF; pH 7.4) at ambient temperature for at least 60 min that contained the followings in mM: NaCl, 130; KCl, 3.5; CaCl₂, 2; MgCl₂, 2; NaH₂PO₄, 0.96; NaHCO₃, 24; D-glucose, 10. Individual slices were transferred to a 3D-MEA chip with 60 tip-shaped electrodes (40 µm in diameter and 50–70 µm in height, spaced by 200 µm, impedance at 1 kHz: 250–450 kΩ, noise level: 15–20 µV; purchased from Ayanda Biosystems, S.A., Lausanne, Switzerland). The surrounding solution was removed quickly and the slice was immobilized by a grid. The slice was continuously perfused with carbogenated standard ACSF (1.5 mL/min at 34 °C) during the whole recording session. Data were recorded by a standard, commercially available MEA (multi-electrode array) setup (Multi Channel Systems MCS GmbH, Reutlingen, Germany).

The Schaffer-collateral was stimulated by injecting a biphasic current waveform (± 100 µs) through one selected electrode at 0.033 Hz, while the rest of them could be used as recording electrodes. The positioning of the stimulating electrodes and that of the regions in the slices, compared to each other, were constantly synchronized during the various investigations. The peak-to-peak amplitudes of field excitatory postsynaptic potentials (fEPSPs) at the stratum radiatum of CA1 were analyzed. After a 30 min incubation period, the threshold and the maximum of stimulation intensity for evoke responses was determined. For evoking responses, 30% of the maximal stimulation intensity was used.

When stable evoked fEPSPs were detected (for at least 20 min) LTP was induced, using a theta-burst stimulation (TBS) protocol applied at the maximum stimulation intensity. TBS comprised of 15 trains administered at 5 Hz, the individual trains contained 4 pulses separated by 10 ms. LTP was followed for an hour.

For the statistical analysis of ex vivo recordings, the peak-to-peak amplitude of evoked fEPSPs recorded from the proximal part of stratum radiatum was calculated. The level of LTP was determined comparing the average of fEPSP amplitudes recorded in the last 5 min of the experiment to the baseline recording.

4.6.2. Multi-Electrode Array (MEA) Recordings

Electrophysiological measurements followed the Morris water maze task, in which different icv injected A β 1-42 was tested. TBS induced LTP recordings were performed using a multi-electrode array (MEA) setup.

After establishing a stable baseline, LTP was elicited by applying a theta-burst stimulation protocol and followed for an hour. The average of the peak-to-peak amplitudes of fEPSPs before the LTP induction was taken as 100%. The slices obtained from HCBS-injected animals showed robust potentiation after TBS ($230 \pm 24\%$; $n = 15$ channels from 5 slices). There were two more groups of icv injected animals treated with 24 h and 168 h A β 1-42 aggregates. The 24 h A β 1-42 assemblies caused a minor impairment in LTP ($184 \pm 7\%$; $n = 26$ channels from 6 slices), while the 168 h amyloid aggregates led to a major disruption of potentiation ($145 \pm 11\%$; $n = 21$ channels from 6 slices).

4.7. Statistical Analysis

Statistical analysis of MEA recordings: all data were expressed as the mean \pm SEM. Statistical significance was determined by parametric analysis of one-way ANOVA followed by Fisher's LSD post hoc test for LTP using the statistical software OriginPro 8 package (Origin Lab, Northampton, MA, USA). Differences with a p -value of less than 0.05 (*), 0.01 (**) and 0.001 (***) were considered significant. Statistical analysis of the Morris water maze experiment (Figures 9 and 10) was performed using SPSS software and Python's Lifelines library (Davidson-Pilon, C., Lifelines, 2016), Github repository. The latency time to attain the platform (with 90 s limit) was measured in order to decide which of the four groups has the highest learning rate. The longer the latency time to the platform is, the less the rats' capability to learn. "Survival curves" using the Cox Proportional Hazard model were fitted, where the days and the treatments were selected as covariates. The comparison of treatment groups was performed using log-rank tests.

One-way ANOVA followed by Fisher's LSD post hoc test was used for histological analysis, for dendritic spine density measurements and for LTP analysis using SPSS statistical software. Differences with a p -value of less than 0.05 were considered significant unless indicated otherwise.

Acknowledgments: We are very grateful for László Siklós for the measurements of dendritic spine density. The authors express their thanks to Anita Kurunczi and Eszter Sipos for the studies on AMCA labeled A β fibrils. This work was supported by the EC Health Program "Memoload" (FP-7 project n° 201.159) and the Hungarian NKFIH research grant GINOP-2.3.2-15-2016-00060.

Author Contributions: Ágnes Kasza was responsible for the study plan, icv administration, MWM performance, and Golgi-Cox procedure; Botond Penke took care of the study plan and writing the manuscript; Zsuzsanna Frank was responsible for icv administration, histology and the Golgi-Cox procedure; Zsolt Bozsó handled amyloid synthesis; Viktor Szegedi took care of the study plan and LTP measurements; Ákos Hunya was responsible for MWM and histology statistics, and graphics; Klaudia Németh took care of icv administration; Gábor Kozma handled AFM studies; and Livia Fülöp was responsible for the study plan, amyloid synthesis, and AFM studies.

Conflicts of Interest: The authors declare no conflict of interest.

Abbreviations

ACSF	Artificial cerebrospinal fluid
AD	Alzheimer's disease
AFM	Atomic force microscopy
AMCA	7 Amino-4-methylcoumarin-3-acetic acid
ANOVA	Analysis of variance
ApoE	Apolipoprotein E
APP	Amyloid precursor protein
A β	Beta-amyloid
CA	Cornu Ammonis
EOAD	Early-onset AD
ER	Endoplasmic reticulum
fA β	Fibrillar form of A β
fEPSP	Field excitatory postsynaptic potential
HC	Hippocampus
HCBS	Hydrocarbonate buffered saline
icv	Intracerebroventricular
LOAD	Late-onset AD
LTP	Long term potentiation
MEA	Multi-electrode array
MWM	Morris water maze
NFTs	Neurofibrillary tangles
oA β	Oligomeric form of A β
PBS	Phosphate-buffered saline solution
PCA-AD	Posterior cortical atrophy variant of AD
PSEN1, 2	Presenilin-1 and 2
r-AD	Rapidly progressive form of AD
t-AD	Typical prolonged-duration form of AD
TBS	Theta-burst stimulation

References

- Halliday, M.; Mallucci, G.R. Targeting the unfolded protein response in neurodegeneration: A new approach to therapy. *Neuropharmacology* **2014**, *7*, 169–174. [[CrossRef](#)] [[PubMed](#)]
- Bredesen, D.E.; Rao, R.V.; Mehlen, P. Cell death in the nervous system. *Nature* **2006**, *443*, 796–802. [[CrossRef](#)] [[PubMed](#)]
- Rubinsztein, D.C. The roles of intracellular protein-degradation pathways in neurodegeneration. *Nature* **2006**, *443*, 780–786. [[CrossRef](#)] [[PubMed](#)]
- Lam, B.; Masellis, M.; Freedman, M.; Stuss, D.T.; Black, S.E. Clinical, imaging, and pathological heterogeneity of the Alzheimer's disease syndrome. *Alzheimers Res. Ther.* **2013**, *5*, 1–14. [[CrossRef](#)] [[PubMed](#)]
- Blennow, K.; de Leon, M.J.; Zetterberg, H. Alzheimer's disease. *Lancet* **2006**, *368*, 387–403. [[CrossRef](#)]
- Tanzi, R.E. The genetics of Alzheimer disease. *Cold Spring Harb. Perspect. Med.* **2012**, *2*. [[CrossRef](#)] [[PubMed](#)]
- Piaceri, I.; Nacmias, B.; Sorbi, S. Genetics of familial and sporadic Alzheimer's disease. *Front. Biosci. (Elite Ed.)* **2013**, *5*, 167–177. [[CrossRef](#)] [[PubMed](#)]
- Bettens, K.; Sleegers, K.; Van Broeckhoven, C. Genetic insights in Alzheimer's disease. *Lancet Neurol.* **2013**, *12*, 92–104. [[CrossRef](#)]
- Giri, M.; Zhang, M.; Lu, Y. Genes associated with Alzheimer's disease: An overview and current status. *Clin. Interv. Aging* **2016**, *11*, 665–681. [[CrossRef](#)] [[PubMed](#)]
- Hardy, J. The amyloid hypothesis for Alzheimer's disease: A critical reappraisal. *J. Neurochem.* **2009**, *110*, 1129–1134. [[CrossRef](#)] [[PubMed](#)]
- Hardy, J.; Allsop, D. Amyloid deposition as the central event in the etiology of Alzheimer's Disease. *Trends Pharmacol. Sci.* **1991**, *12*, 383–388. [[CrossRef](#)]

12. Cavallucci, V.; D'Amelio, M.; Cecconi, F. Abeta toxicity in Alzheimer's disease. *Mol. Neurobiol.* **2012**, *45*, 366–378. [[CrossRef](#)] [[PubMed](#)]
13. Sakono, M.; Zako, T. Amyloid oligomers: Formation and toxicity of A-beta oligomers. *FEBS J.* **2010**, *277*, 1348–1358. [[CrossRef](#)] [[PubMed](#)]
14. Walsh, D.M.; Klyubin, I.; Fadeeva, J.V.; Cullen, W.K.; Anwyl, R.; Wolfe, M.S.; Rowan, M.J.; Selkoe, D.J. Naturally secreted oligomers of amyloid beta protein potently inhibit hippocampal long-term potentiation in vivo. *Nature* **2002**, *416*, 535–539. [[CrossRef](#)] [[PubMed](#)]
15. Upadhaya, A.R.; Capetillo-Zarate, E.; Kosterin, I.; Abramowski, D.; Kumar, S.; Yamaguchi, H.; Walter, J.; Fandrich, M.; Staufenbiel, M.; Thal, D.R. Dispersible amyloid beta-protein oligomers, protofibrils, and fibrils represent diffusible but not soluble aggregates: Their role in neurodegeneration in amyloid precursor protein (APP) transgenic mice. *Neurobiol. Aging* **2012**, *33*, 2641–2660. [[CrossRef](#)] [[PubMed](#)]
16. Hayden, E.Y.; Teplow, D.B. Amyloid beta-protein oligomers and Alzheimer's disease. *Alzheimers Res. Ther.* **2013**, *5*, 60–70. [[CrossRef](#)] [[PubMed](#)]
17. De Felice, F.G.; Munoz, D.P. Opportunities and challenges in developing relevant animal models for Alzheimer's disease. *Ageing Res. Rev.* **2016**, *26*, 112–114. [[CrossRef](#)] [[PubMed](#)]
18. Casadesus, G. *Ebook: Handbook of Animal Models in Alzheimer's Disease*, 1st ed.; IOS Press: Amsterdam, The Netherlands, 2011; pp. 1–352, ISBN 978-1-60750-733-8.
19. Lecanu, L.; Papadopoulos, V. Modeling Alzheimer's disease with non-transgenic rat models. *Alzheimers Res. Ther.* **2013**, *5*. [[CrossRef](#)]
20. Sasaguri, H.; Nilsson, P.; Hashimoto, S.; Nagata, K.; Saito, T.; De Strooper, B.; Hardy, J.; Vassar, R.; Winblad, B.; Saido, T.C. App mouse models for Alzheimer's disease preclinical studies. *EMBO J.* **2017**, *36*, 2473–2487. [[CrossRef](#)] [[PubMed](#)]
21. Link, C.D. Expression of human beta-amyloid peptide in transgenic caenorhabditis-elegans. *Proc. Natl. Acad. Sci. USA* **1995**, *92*, 9368–9372. [[CrossRef](#)] [[PubMed](#)]
22. Link, C.D. C-elegans models of age-associated neurodegenerative diseases: Lessons from transgenic worm models of Alzheimer's disease. *Exp. Gerontol.* **2006**, *41*, 1007–1013. [[CrossRef](#)] [[PubMed](#)]
23. Bouleau, S.; Tricoire, H. Drosophila models of Alzheimer's disease: Advances, limits, and perspectives. *J. Alzheimers Dis.* **2015**, *45*, 1015–1038. [[PubMed](#)]
24. Crowther, D.C.; Kinghorn, K.J.; Miranda, E.; Page, R.; Curry, J.A.; Duthie, F.A.I.; Gubb, D.C.; Lomas, D.A. Intraneuronal a beta, non-amyloid aggregates and neurodegeneration in a Drosophila model of Alzheimer's disease. *Neuroscience* **2005**, *132*, 123–135. [[CrossRef](#)] [[PubMed](#)]
25. Dodart, J.C.; May, P. Overview on rodent models of Alzheimer's disease. *Curr. Protoc. Neurosci.* **2005**. [[CrossRef](#)]
26. Gotz, J.; Schonrock, N.; Vissel, B.; Ittner, L.M. Alzheimer's disease selective vulnerability and modeling in transgenic mice. *J. Alzheimers Dis.* **2009**, *18*, 243–251. [[CrossRef](#)] [[PubMed](#)]
27. Puzzo, D.; Lee, L.; Palmeri, A.; Calabrese, G.; Arancio, O. Behavioral assays with mouse models of Alzheimer's disease: Practical considerations and guidelines. *Biochem. Pharmacol.* **2014**, *88*, 450–467. [[CrossRef](#)] [[PubMed](#)]
28. Webster, S.J.; Bachstetter, A.D.; Nelson, P.T.; Schmitt, F.A.; Van Eldik, L.J. Using mice to model Alzheimer's dementia: An overview of the clinical disease and the preclinical behavioral changes in 10 mouse models. *Front. Genet.* **2014**, *5*, 88. [[CrossRef](#)] [[PubMed](#)]
29. Klohs, J.; Rudin, M.; Shimshek, D.R.; Beckmann, N. Imaging of cerebrovascular pathology in animal models of Alzheimer's disease. *Front. Aging Neurosci.* **2014**, *6*, 32. [[CrossRef](#)] [[PubMed](#)]
30. Lindholm, J.S.O.; Castren, E. Mice with altered BDNF signaling as models for mood disorders and antidepressant effects. *Front. Behav. Neurosci.* **2014**, *8*, 143. [[CrossRef](#)] [[PubMed](#)]
31. Onos, K.D.; Rizzo, S.J.S.; Howell, G.R.; Sasner, M. Toward more predictive genetic mouse models of Alzheimer's disease. *Brain Res. Bull.* **2016**, *122*, 1–11. [[CrossRef](#)] [[PubMed](#)]
32. Orta-Salazar, E.; Vargas-Rodríguez, I.; Castro-Chavira, S.A.; Feria-Velasco, A.I.; Díaz-Cintra, S. Alzheimer's disease: From animal models to the human syndrome. In *Update on Dementia*; Moretti, D., Ed.; Intech: Rijeka, Croatia, 2016; ISBN 978-953-51-2654-6.
33. Esquerda-Canals, G.; Montoliu-Gaya, L.; Guell-Bosch, J.; Villegas, S. Mouse models of Alzheimer's disease. *J. Alzheimers Dis.* **2017**, *57*, 1171–1183. [[CrossRef](#)] [[PubMed](#)]

34. Cavanaugh, S.E.; Pippin, J.J.; Barnard, N.D. Animal models of Alzheimer disease: Historical pitfalls and a path forward. *ALTEX* **2014**, *31*, 279–302. [[CrossRef](#)] [[PubMed](#)]
35. Filipcik, P.; Zilka, N.; Bugos, O.; Kucerak, J.; Koson, P.; Novak, P.; Novak, M. First transgenic rat model developing progressive cortical neurofibrillary tangles. *Neurobiol. Aging* **2012**, *33*, 1448–1456. [[CrossRef](#)] [[PubMed](#)]
36. Cohen, R.M.; Rezaei-Zadeh, K.; Weitz, T.M.; Rentsendorj, A.; Gate, D.; Spivak, I.; Bholat, Y.; Vasilevko, V.; Glabe, C.G.; Breunig, J.J.; et al. A transgenic Alzheimer rat with plaques, tau pathology, behavioral impairment, oligomeric abeta, and frank neuronal loss. *J. Neurosci.* **2013**, *33*, 6245–6256. [[CrossRef](#)] [[PubMed](#)]
37. Selkoe, D.J. Alzheimer's disease is a synaptic failure. *Science* **2002**, *298*, 789–791. [[CrossRef](#)] [[PubMed](#)]
38. Selkoe, D.J. Soluble oligomers of the amyloid beta-protein impair synaptic plasticity and behavior. *Behav. Brain Res.* **2008**, *192*, 106–113. [[CrossRef](#)] [[PubMed](#)]
39. Shankar, G.M.; Walsh, D.M. Alzheimer's disease: Synaptic dysfunction and A-beta. *Mol. Neurodegener.* **2009**, *4*, 48. [[CrossRef](#)] [[PubMed](#)]
40. Balducci, C.; Beeg, M.; Stravalaci, M.; Bastone, A.; Scip, A.; Biasini, E.; Tapella, L.; Colombo, L.; Manzoni, C.; Borsello, T.; et al. Synthetic amyloid-beta oligomers impair long-term memory independently of cellular prion protein. *Proc. Natl. Acad. Sci. USA* **2010**, *107*, 2295–2300. [[CrossRef](#)] [[PubMed](#)]
41. Takeda, S.; Sato, N.; Niisato, K.; Takeuchi, D.; Kurinami, H.; Shinohara, M.; Rakugi, H.; Kano, M.; Morishita, R. Validation of a beta 1–40 administration into mouse cerebroventricles as an animal model for Alzheimer disease. *Brain Res.* **2009**, *1280*, 137–147. [[CrossRef](#)] [[PubMed](#)]
42. Townsend, M.; Cleary, J.P.; Mehta, T.; Hofmeister, J.; Lesne, S.; O'Hare, E.; Walsh, D.M.; Selkoe, D.J. Orally available compound prevents deficits in memory caused by the Alzheimer amyloid-beta oligomers. *Ann. Neurol.* **2006**, *60*, 668–676. [[CrossRef](#)] [[PubMed](#)]
43. Zussy, C.; Brureau, A.; Delair, B.; Marchal, S.; Keller, E.; Ixart, G.; Naert, G.; Meunier, J.; Chevallier, N.; Maurice, T.; et al. Time-course and regional analyses of the physiopathological changes induced after cerebral injection of an amyloid beta fragment in rats. *Am. J. Pathol.* **2011**, *179*, 315–334. [[CrossRef](#)] [[PubMed](#)]
44. Kim, H.Y.; Lee, D.K.; Chung, B.R.; Kim, H.V.; Kim, Y. Intracerebroventricular injection of amyloid-beta peptides in normal mice to acutely induce Alzheimer-like cognitive deficits. *J. Vis. Exp.* **2016**. [[CrossRef](#)]
45. Tarasoff-Conway, J.M.; Carare, R.O.; Osorio, R.S.; Glodzik, L.; Butler, T.; Fieremans, E.; Axel, L.; Rusinek, H.; Nicholson, C.; Zlokovic, B.V.; et al. Clearance systems in the brain-implications for Alzheimer disease. *Nat. Rev. Neurol.* **2015**, *11*, 457–470. [[CrossRef](#)] [[PubMed](#)]
46. Jacob, H.J.; Kwitek, A.E. Rat genetics: Attaching physiology and pharmacology to the genome. *Nat. Rev. Genet.* **2002**, *3*, 33–42. [[CrossRef](#)] [[PubMed](#)]
47. Bagheri, M.; Joghataei, M.T.; Mohseni, S.; Roghani, M. Genistein ameliorates learning and memory deficits in amyloid beta(1–40) rat model of Alzheimer's disease. *Neurobiol. Learn. Mem.* **2011**, *95*, 270–276. [[CrossRef](#)] [[PubMed](#)]
48. Christensen, D.Z.; Bayer, T.A.; Wirths, O. Formic acid is essential for immunohistochemical detection of aggregated intraneuronal a beta peptides in mouse models of Alzheimer's disease. *Brain Res.* **2009**, *1301*, 116–125. [[CrossRef](#)] [[PubMed](#)]
49. He, F.Q.; Qiu, B.Y.; Zhang, X.H.; Li, T.K.; Xie, Q.; Cui, D.J.; Huang, X.L.; Gan, H.T. Tetrandrine attenuates spatial memory impairment and hippocampal neuroinflammation via inhibiting NF-kappaB activation in a rat model of Alzheimer's disease induced by amyloid-beta(1–42). *Brain Res.* **2011**, *1384*, 89–96. [[CrossRef](#)] [[PubMed](#)]
50. O'Hare, E.; Weldon, D.T.; Mantyh, P.W.; Ghilardi, J.R.; Finke, M.P.; Kuskowski, M.A.; Maggio, J.E.; Shephard, R.A.; Cleary, J. Delayed behavioral effects following intrahippocampal injection of aggregated a beta(1–42). *Brain Res.* **1999**, *815*, 1–10. [[CrossRef](#)]
51. Hong, S.; Beja-Glasser, V.F.; Nfonoyim, B.M.; Frouin, A.; Li, S.M.; Ramakrishnan, S.; Merry, K.M.; Shi, Q.Q.; Rosenthal, A.; Barres, B.A.; et al. Complement and microglia mediate early synapse loss in Alzheimer mouse models. *Science* **2016**, *352*, 712–716. [[CrossRef](#)] [[PubMed](#)]
52. Zhu, D.; Yang, N.; Liu, Y.Y.; Zheng, J.; Ji, C.; Zuo, P.P. M2 macrophage transplantation ameliorates cognitive dysfunction in amyloid-beta-treated rats through regulation of microglial polarization. *J. Alzheimers Dis.* **2016**, *52*, 483–495. [[CrossRef](#)] [[PubMed](#)]

53. Sipos, E.; Kurunczi, A.; Andras, F.; Penke, Z.; Fulop, L.; Kasza, A.; Janos, H.; Sandor, H.; Veszelka, S.; Balogh, G.; et al. Intranasal delivery of human beta-amyloid peptide in rats: Effective brain targeting. *Cell. Mol. Neurobiol.* **2010**, *30*, 405–413. [[CrossRef](#)] [[PubMed](#)]
54. Sipos, E.; Kurunczi, A.; Kasza, A.; Horvath, J.; Felszeghy, K.; Laroche, S.; Toldi, J.; Parducz, A.; Penke, B.; Penke, Z. Beta-amyloid pathology in the entorhinal cortex of rats induces memory deficits: Implications for Alzheimer's disease. *Neuroscience* **2007**, *147*, 28–36. [[CrossRef](#)] [[PubMed](#)]
55. Kumar, A.; Aggarwal, A.; Singh, A.; Naidu, P.S. Animal models in drug discovery of Alzheimer's disease: A mini review. *EC Pharmacol. Toxicol.* **2016**, *2*, 60–79.
56. Salari, S.; Bagheri, M. A review of animal models of Alzheimer's disease: A brief insight into pharmacologic and genetic models. *Physiol. Pharmacol.* **2016**, *20*, 5–11.
57. Ruggeri, F.S.; Habchi, J.; Cerreta, A.; Dietler, G. AFM-based single molecule techniques: Unraveling the amyloid pathogenic species. *Curr. Pharm. Des.* **2016**, *22*, 3950–3970. [[CrossRef](#)] [[PubMed](#)]
58. Iliff, J.J.; Wang, M.H.; Liao, Y.H.; Plogg, B.A.; Peng, W.G.; Gundersen, G.A.; Benveniste, H.; Vates, G.E.; Deane, R.; Goldman, S.A.; et al. A paravascular pathway facilitates csf flow through the brain parenchyma and the clearance of interstitial solutes, including amyloid beta. *Sci. Transl. Med.* **2012**, *4*, 147ra111. [[CrossRef](#)] [[PubMed](#)]
59. Mendez-Lopez, M.; Mendez, M.; Sampedro-Piquero, P.; Arias, J.L. Spatial learning-related changes in metabolic activity of limbic structures at different posttask delays. *J. Neurosci. Res.* **2013**, *91*, 151–159. [[CrossRef](#)] [[PubMed](#)]
60. Morris, R. Developments of a water-maze procedure for studying spatial-learning in the rat. *J. Neurosci. Methods* **1984**, *11*, 47–60. [[CrossRef](#)]
61. Morris, R.G.M.; Anderson, E.; Lynch, G.S.; Baudry, M. Selective impairment of learning and blockade of long-term potentiation by an N-methyl-D-aspartate receptor antagonist, AP5. *Nature* **1986**, *319*, 774–776. [[CrossRef](#)] [[PubMed](#)]
62. Morris, R.G.M.; Garrud, P.; Rawlins, J.N.P.; Okeefe, J. Place navigation impaired in rats with hippocampal-lesions. *Nature* **1982**, *297*, 681–683. [[CrossRef](#)] [[PubMed](#)]
63. Vorhees, C.V.; Williams, M.T. Morris water maze: Procedures for assessing spatial and related forms of learning and memory. *Nat. Protoc.* **2006**, *1*, 848–858. [[CrossRef](#)] [[PubMed](#)]
64. Qiang, W.; Yau, W.M.; Lu, J.X.; Collinge, J.; Tycko, R. Structural variation in amyloid-beta fibrils from Alzheimer's disease clinical subtypes. *Nature* **2017**, *541*, 217–221. [[CrossRef](#)] [[PubMed](#)]
65. Wei, W.; Nguyen, L.N.; Kessels, H.W.; Hagiwara, H.; Sisodia, S.; Malinow, R. Amyloid beta from axons and dendrites reduces local spine number and plasticity. *Nat. Neurosci.* **2010**, *13*, 190–196. [[CrossRef](#)] [[PubMed](#)]
66. Lacor, P.N.; Buniel, M.C.; Chang, L.; Fernandez, S.J.; Gong, Y.S.; Viola, K.L.; Lambert, M.P.; Velasco, P.T.; Bigio, E.H.; Finch, C.E.; et al. Synaptic targeting by Alzheimer's-related amyloid beta oligomers. *J. Neurosci.* **2004**, *24*, 10191–10200. [[CrossRef](#)] [[PubMed](#)]
67. Lacor, P.N.; Buniel, M.C.; Furlow, P.W.; Clemente, A.S.; Velasco, P.T.; Wood, M.; Viola, K.L.; Klein, W.L. A beta oligomer-induced aberrations in synapse composition, shape, and density provide a molecular basis for loss of connectivity in Alzheimer's disease. *J. Neurosci.* **2007**, *27*, 796–807. [[CrossRef](#)] [[PubMed](#)]
68. Chacon, M.A.; Barria, M.I.; Soto, C.; Inestrosa, N.C. Beta-sheet breaker peptide prevents a beta-induced spatial memory impairments with partial reduction of amyloid deposits. *Mol. Psychiatry* **2004**, *9*, 953–961. [[CrossRef](#)] [[PubMed](#)]
69. Borbely, E.; Horvath, J.; Furdan, S.; Bozso, Z.; Penke, B.; Fulop, L. Simultaneous changes of spatial memory and spine density after intrahippocampal administration of fibrillar A β (1–42) to the rat brain. *Biomed. Res. Int.* **2014**, *2014*, 345305. [[CrossRef](#)] [[PubMed](#)]
70. Sandberg, A.; Luheshi, L.M.; Sollvander, S.; de Barros, T.P.; Macao, B.; Knowles, T.P.J.; Biverstal, H.; Lendel, C.; Ekholm-Pettersson, F.; Dubnovitsky, A.; et al. Stabilization of neurotoxic Alzheimer amyloid-beta oligomers by protein engineering. *Proc. Natl. Acad. Sci. USA* **2010**, *107*, 15595–15600. [[CrossRef](#)] [[PubMed](#)]
71. Fonseca, A.C.; Oliveira, C.R.; Pereira, C.F.; Cardoso, S.M. Loss of proteostasis induced by amyloid beta peptide in brain endothelial cells. *Biochim. Biophys. Acta* **2014**, *1843*, 1150–1161. [[CrossRef](#)] [[PubMed](#)]
72. Kopniczky, Z.; Dochnal, R.; Macsai, M.; Pal, A.; Kiss, G.; Mihaly, A.; Szabo, G. Alterations of behavior and spatial learning after unilateral entorhinal ablation of rats. *Life Sci.* **2006**, *78*, 2683–2688. [[CrossRef](#)] [[PubMed](#)]
73. Avraamides, M.N.; Kelly, J.W. Multiple systems of spatial memory and action. *Cogn. Process.* **2008**, *9*, 93–106. [[CrossRef](#)] [[PubMed](#)]

74. Bozso, Z.; Penke, B.; Simon, D.; Laczko, I.; Juhasz, G.; Szegedi, V.; Kasza, A.; Soos, K.; Hetenyi, A.; Weber, E.; et al. Controlled in situ preparation of a beta(1–42) oligomers from the isopeptide “iso-a beta(1–42)”, physicochemical and biological characterization. *Peptides* **2010**, *31*, 248–256. [[CrossRef](#)] [[PubMed](#)]
75. Lavenex, P.; Amaral, D.G. Hippocampal-neocortical interaction: A hierarchy of associativity. *Hippocampus* **2000**, *10*, 420–430. [[CrossRef](#)]
76. Fulop, L.; Penke, B.; Zarandi, M. Synthesis and fluorescent labeling of beta-amyloid peptides. *J. Pept. Sci.* **2001**, *7*, 397–401. [[CrossRef](#)] [[PubMed](#)]
77. Paxinos, G.; Watson, C. *The Rat Brain in Stereotaxic Coordinates*, 6th ed.; Academic Press: London, UK; Sydney, Australia, 2006; pp. 1–456, ISBN 0080475159.
78. Nagy, D.; Kocsis, K.; Fuzik, J.; Marosi, M.; Kis, Z.; Teichberg, V.I.; Toldi, J.; Farkas, T. Kainate postconditioning restores LTP in ischemic hippocampal ca1: Onset-dependent second pathophysiological stress. *Neuropharmacology* **2011**, *61*, 1026–1032. [[CrossRef](#)] [[PubMed](#)]

Sample Availability: Samples of the compounds iso-A β (1–42) and A β (1–42) are available from the authors.



© 2017 by the authors. Licensee MDPI, Basel, Switzerland. This article is an open access article distributed under the terms and conditions of the Creative Commons Attribution (CC BY) license (<http://creativecommons.org/licenses/by/4.0/>).

II

Dihydropyridine Derivatives Modulate Heat Shock Responses and have a Neuroprotective Effect in a Transgenic Mouse Model of Alzheimer's Disease

Ágnes Kasza^{a,1}, Ákos Hunya^{b,1}, Zsuzsa Frank^a, Ferenc Fülöp^c, Zsolt Török^{b,d}, Gábor Balogh^d, Miklós Sántha^d, Árpád Bálint^d, Sándor Bernáth^e, Katie L.I.M. Blundell^f, Chrisostomos Prodromou^f, Ibolya Horváth^d, Hans-Joachim Zeiler^g, Philip L. Hooper^h, László Vigh^{d,*} and Botond Penke^{a,*}

^aDepartment of Medical Chemistry, University of Szeged, Szeged, Hungary

^bLipidArt Research and Development Ltd., Szeged, Hungary

^cDepartment of Pharmaceutical Chemistry, University of Szeged, Szeged, Hungary

^dBiological Research Center of HAS, Institute of Biochemistry, Szeged, Hungary

^eFontaMed Consulting Ltd., Telki, Hungary

^fGenome Damage and Stability Centre, University of Sussex, Falmer, Brighton, UK

^gCreative Therapeutics GmbH, Wuppertal, Nordrhein-Westfalen, Germany

^hDivision of Endocrinology, Metabolism and Diabetes, Department of Medicine, University of Colorado Medical School, Anschutz Medical Campus, Aurora, CO, USA

Handling Associate Editor: Jose Abisambra

Accepted 8 April 2016

Abstract. Heat shock proteins (Hsps) have chaperone activity and play a pivotal role in the homeostasis of proteins by preventing misfolding, by clearing aggregated and damaged proteins from cells, and by maintaining proteins in an active state. Alzheimer's disease (AD) is thought to be caused by amyloid- β peptide that triggers tau hyperphosphorylation, which is neurotoxic. Although proteostasis capacity declines with age and facilitates the manifestation of neurodegenerative diseases such as AD, the upregulation of chaperones improves prognosis. Our research goal is to identify potent Hsp co-inducers that enhance protein homeostasis for the treatment of AD, especially 1,4-dihydropyridine derivatives optimized for their ability to modulate cellular stress responses. Based on favorable toxicological data and Hsp co-inducing activity, LA1011 was selected for the *in vivo* analysis of its neuroprotective effect in the APPxPS1 mouse model of AD. Here, we report that 6 months of LA1011 administration effectively improved the spatial learning and memory functions in wild type mice and eliminated neurodegeneration in double mutant mice. Furthermore, Hsp co-inducer therapy preserves the number of neurons, increases dendritic spine density, and reduces tau pathology and amyloid plaque formation in transgenic AD mice. In conclusion, the Hsp co-inducer LA1011 is neuroprotective and therefore is a potential pharmaceutical candidate for the therapy of neurodegenerative diseases, particularly AD.

Keywords: Alzheimer's disease, dihydropyridines, heat-shock proteins, Hsp co-induction, neuroprotection

¹These authors contributed equally to this work.

*Correspondence to: Botond Penke, H-6726 Szeged, Dom ter 8, Hungary. Tel.: +36 62 545 135; Fax: +36 62 545 971; E-mail: penke.botond@med.u-szeged.hu and László Vigh, H-6726 Szeged, Temesvári krt. 63-65, Hungary. Tel.: +36 62 599 632; Fax: +36 62 433 506; E-mail: vigh@brc.hu.

penke.botond@med.u-szeged.hu and László Vigh, H-6726 Szeged, Temesvári krt. 63-65, Hungary. Tel.: +36 62 599 632; Fax: +36 62 433 506; E-mail: vigh@brc.hu.

INTRODUCTION

Protein quality control requires constant surveillance to prevent proteins misfolding, aggregating and their subsequent loss of function. Maintenance of proteome integrity and protein homeostasis (proteostasis) critically depends on a complex network of heat shock proteins (Hsps) that act as molecular chaperones [1]. Small Hsps, together with other members of the chaperone network such as the Hsp70 protein family, help maintain normal protein homeostasis that is essential for cellular function [2]. However, Hsps decline with age [3, 4] and this correlates with a loss in the capacity of cells to maintain protein homeostasis. It is therefore not surprising that the prevalence of neurodegenerative diseases (NDDs) such as Alzheimer's disease (AD) and Parkinson's disease increases with age [2, 5]. Hsps play a role in extending longevity in animal models, but it is unclear whether this is true in humans [6].

Despite great diversity in the primary amino-acid sequence of proteins, the oligomers of different misfolded amyloidogenic proteins (hyperphosphorylated tau, amyloid- β , α -synuclein) elicit toxicity by common mechanisms [7]. This toxicity involves membrane perturbations, calcium dysregulation, the accumulation of reactive oxygen species, endoplasmic reticulum (ER)-stress, impairment of the ubiquitin-proteasome system, and the activation of apoptotic signaling pathways [8–11]. Indeed, it is hypothesized that the initiation of NDDs is a result of ER-stress, damaged mitochondria, and loss of Ca^{2+} - and protein homeostasis [12–16]. Additionally, ER-stress caused by ER Ca^{2+} -depletion, hypoxia, and/or hypoglycemia, initiates the unfolded protein response (UPR) [17] and prolongs UPR activation thus triggering apoptotic pathways that result in cell death [18]. Furthermore, mitochondrial energy production failure and the mitochondria-associated ER membrane may play key roles in the generation of amyloid proteins and the initiation of NDDs [19, 20].

Maintenance of protein homeostasis by the modulation of protein processing and folding systems by chaperone induction are key therapeutic targets of drug discovery for AD treatment [21]. The induction of Hsps also offers a potential strategy for the treatment of other neurodegenerative disorders [22, 23]. Small Hsps (such as Hsp27) bind to improperly folded, partially denatured proteins, preventing their aggregation and promoting cell survival. Recovery is further enhanced when sHsp-

bound proteins are transferred to ATP-dependent chaperones like Hsp70, which facilitates refolding [24] or transfer to protein degradation machinery. It was reported that Hsp27, Hsp70, proteasomes, and autophagosomes form a complex network that maintains protein homeostasis [25, 26]. Hsp27 and Hsp70 are usually co-expressed in response to stress stimuli [27]. Sequestration of misfolded proteins into chaperone-enriched aggregates is a protective strategy that slows the decline of proteostasis during aging of the nematode *Caenorhabditis elegans* [28]. Because Hsp27 and 70 have a central role in protein homeostasis, their induction may prevent and disassemble toxic protein aggregates, which might represent a novel target for the treatment of NDDs [2, 29–37].

Regulation of intracellular Ca^{2+} levels contributes to neuronal defense against protein misfolding. Thus, Ca^{2+} channel blockers (CCBs) may be putative drugs for the prevention and treatment of NDDs such as AD [38–40]. The family of 1,4-dihydropyridines (DHPs) represents one of the most important groups of CCBs. DHPs were originally identified as calcium antagonists (nifedipine) and are widely used to treat hypertension and heart failure [41]. Substitution of the CCB molecular nucleus with variety of groups is the most commonly tested scaffold among L-type CCBs. These CCB variations result in a plethora of diverse activities at receptors, channels, transporters, and metabolizing enzymes [42]. In particular, DHPs interact with ion channels and G-protein coupled receptors [43]. CCBs have also been used in dementia therapy and nilvadipine is well tolerated by AD patients and is a promising candidate for AD treatment [38, 44, 45].

Clinical data suggest that the underlying therapeutic mechanism in AD is independent of the anti-hypertensive action of the CCB. Longitudinal studies of elderly people with AD support the use of CCBs as potential disease progression therapy. An ongoing advanced clinical trial (CT number 02017340) for the treatment of AD with nilvadipine is due to close in 2017 [39]. Clinical evidence from epidemiological studies, including a cohort of 3,000 people over 74 years of age, supports the efficacy of DHP CCBs in reducing or delaying the development of AD [44]. The recent Systolic Hypertension in Europe randomized control trial reported a 55% reduction in the incidence of dementia in people taking nitrendipine over a 5-year follow-up period [46].

The neuroprotective mechanism of CCBs is poorly understood. In the presence of CCBs, amyloid- β ($A\beta$) production, aggregation, and neurotoxicity is decreased, improving neuronal function both *in vitro* and *in vivo* [38, 40]. BAY w 9798 is a DHP structurally related to the Ca-antagonist nifedipine with anti-inflammatory and anti-oxidative properties but with no calcium antagonistic effects [47]. Because lipophilic compounds DHPs bind to the membrane lipid bilayer, they potentially act indirectly as allo-network drugs via the propagation of changes in cellular networks. In fact, lipid bilayer partitioning of DHPs occurs prior to the drug binding to receptors [48, 49]. Changes in the lipid phase of membranes alter cell signaling [50, 51], which is also associated with a variety of diseases including NDDs. Modulation of the cell membrane composition and structure as a molecular base for drug discovery and new disease treatment was recently reviewed and the term “membrane lipid therapy” was introduced [52].

Hsp co-inducer hydroxamic acid derivatives can normalize the dysregulated expression of Hsps in pathological conditions and interact with membranes, resulting in specific alterations in the membrane nanostructure [53–55]. We searched for novel substances that do not directly exert stress on cells, but have long-term effects on cellular stress responses and viability (co-inducing activity). Such Hsp co-inducer compounds potentiate the response to a pre-existing stress without exhibiting effects in non-stressed environments. These compounds provide a higher degree of selectivity affecting only the diseased/damaged tissue compared with non-specific stressors. They also augment normal physiologic stress response systems rather than just blocking or activating a single enzyme that likely leads to a compensatory feedback loop, counteracting its long-term benefits.

The aim of this study was to investigate the beneficial effect of Hsp co-inducers in a mouse model of AD. A family of novel co-inducer compounds was synthesized [56] from which three were selected for further investigations (LA1011, LA1030, and LA1044). The co-inducing effect of Hsp27, Hsp40, and Hsp70 was verified. The neuroprotective effect of the optimized compound LA1011 was demonstrated in the APPxPS1 AD transgenic mouse model using a spatial navigation test. Histology studies of mouse brain slices were performed to investigate neuronal viability, changes in dendritic spine density and

the presence of $A\beta$ and tau-pathology-characteristic abnormalities in AD [57].

MATERIALS AND METHODS

Preparation and optimization of 1,4-dihydropyridines

BAY w 9798 [58] was selected as a starting compound in our study [56]. During optimization using standard dihydropyridine synthetic protocols, the substituents at positions 1, 2, 4, and 6 were modified systematically, resulting in LA1030, a more lipophilic compound with improved activity. To augment the oral bioavailability of the compounds, one or two cationic centers were introduced to substituents at positions 2 and 6. LA1011 and LA1044 were the most active compounds. The compounds were synthesized using conventional techniques from commercially available starting materials [59–63] (Fig. 1). Compounds were characterized by melting point and ^1H -NMR data (recorded on a DRX 400 MHz Bruker spectrometer).

Synthesis of LA1011

Dihydropyridine (1 mmol), 5 mmol dimethylamine-hydrochloride, 5 mmol paraformaldehyde, and 1 ml acetic acid were mixed and heated at 95°C for 5 h. The mixture was evaporated, dissolved in water and extracted with ether. After separation, the aqueous phase was neutralized with NaHCO_3 and extracted with ethyl acetate. The organic phase was dried and evaporated, and the residue was purified by column chromatography on silica with a mixture of hexane/ethyl acetate. The pure fractions were collected, transferred to hydrochloride or to other salts, and recrystallized from methanol diethyl ether. The melting point (Mp) was $273\text{--}276^\circ\text{C}$. ^1H NMR data: D_2O , 400 MHz, δ : 7.51 (d, $J = 8.3$ Hz, 2 H, ArH), 7.28 (d, $J = 8.6$ Hz, 2 H, ArH), 5.07 (s, 1 H, CH), 3.67 (s, 6 H, COOCH_3), 3.14–3.59 (m, 11 H, $-\text{CH}_2-$, $-\text{CH}_3$), 2.87 (s, 12 H, $-\text{CH}_3$).

Synthesis of LA1030

A mixture of 0.05 mol p-trifluoromethyl benzaldehyde, 0.1 mol methyl 3-oxovalerate, and 0.05 mol methylamine hydrochloride was refluxed in 25 ml pyridine for 5 h. The residue was dissolved in dichloromethane and washed with water after evaporation of the solvent. The organic phase was dried and evaporated. The residue was crystallized from

Code	Structure	Chemical Name
BAY w 9798		Dimethyl 1,2,6-trimethyl-4-(4-methylphenyl)-1,4-dihydropyridine-3,5-dicarboxylate
LA1011		Dimethyl 4-(4-trifluoromethylphenyl)-2,6-bis-(2-dimethylaminoethyl)-1-methyl-1,4-dihydropyridine-3,5-dicarboxylate dihydrochloride
LA1030		Dimethyl 2,6-diethyl-1-methyl-4-(trifluoromethylphenyl)-1,4-dihydropyridine-3,5-dicarboxylate
LA1044		Dimethyl 2-(1,2,3,4-tetrahydro-1H-isoquinolin-2-ylmethyl)-1,6-dimethyl-4-(4-trifluoromethylphenyl)-1,4-dihydropyridine-3,5-dicarboxylate hydrochloride

Fig. 1. Chemical structure of the synthesized 1,4-dihydropyridine derivatives.

methanol. The Mp was 133–138°C; ¹HNMR data: CDCl₃, 400 MHz, δ : 7.39 (d, J = 8.6 Hz, 2 H, ArH), 7.21 (d, J = 8.6 Hz, 2 H, ArH), 5.08 (s, 1 H, CH), 3.67 (s, 6 H, COOCH₃), 3.14 (s, 3 H, N-CH₃), 2.99–3.11 (m, 2 H, -CH₂-), 2.71–2.84 (m, 2 H, -CH₂-), 1.06–1.12 (m, 6 H, CH₃).

Synthesis of LA1044

Compound LA1044 was transformed to the 2-bromomethyl derivative in pyridine with pyridiniumbromoperbromide [62]. One mmol of this product was dissolved in 10 ml acetonitrile and 2 eq. of K₂CO₃ and 1.1 eq. of 1,2,3,4-tetrahydroisoquinoline was then added. The mixture was stirred until the reaction was complete, then filtered and evaporated, and the residue was purified by chromatography. The Mp was 175–177°C; ¹HNMR data: CDCl₃,

400 MHz, δ : 7.47 (d, J = 8.2 Hz, 2 H, ArH), 7.29 (d, J = 8.2 Hz, 2 H, ArH), 7.06–7.16 (m, 3 H, ArH), 6.91–6.97 (m, 1 H, ArH), 5.22 (s, 1 H, CH), 4.20 (d, J = 14.2 Hz, 1 H, C-CH₂-N), 3.80 (d, J = 14.2 Hz, 1 H, C-CH₂-N), 3.73 (s, 3 H, COOCH₃), 3.72 (s, 3 H, COOCH₃), 3.58–3.69 (m, 2 H, CH₂), 3.35 (s, 3 H, N-CH₃), 2.67–2.85 (m, 4 H, CH₂), 2.48 (s, 3 H, CH₃).

Measurement of Hsp co-inducing activity

The effect of drug candidates on the stress response was tested with the SH-SY5Y (ATCC® CRL-2266™) human neuroblastoma cell line stably transfected with a plasmid containing the Hsp70 promoter fused to yellow fluorescent protein (YFP) (pEYFP-N1, Clontech), a kind gift of Lea Sistonen (Åbo Akademi University, Turku, Finland) (SH-SY5Y-pHsp70-YFP). Cells were maintained in

a logarithmic-phase of growth on 100 mm dishes (Orange Scientific, Braine-l'Alleud, Belgium) in DMEM-F12 (1:1) medium (Life Technologies, NY, USA) supplemented with 10% heat-inactivated fetal bovine serum (Life Technologies). Cultures were maintained at 37°C in a humidified atmosphere incubator with 5% CO₂. When cells reached 80% confluence, they were harvested in Trypsin/EDTA Solution (Lonza, Basel, Switzerland) and were plated at a density of 5×10^5 cells/6-cm culture dishes (Orange Scientific). After 24 h, cells were pre-incubated either with or without LA1011 (5 µM) or LA1044 (40 µM) for 30 min. Following pre-incubation, plates were divided into two groups: The control group was maintained at 37°C for 17 h and the other was heat-shocked at 42°C for 1 h and then placed back at 37°C for a 16 h recovery period (HS group). After recovery the expression of YFP, which is directly correlated to the activity of its Hsp70 promoter, was followed by measuring the fluorescence intensity of the cells with a BD Accuri C6 flow cytometer (Becton, Dickinson and Company, NJ, USA) [64].

Western blot analysis

SH-SY5Y cells were grown and treated with the drug candidates and heat exactly as described above. Following the recovery, cells were extracted in RIPA (radioimmunoprecipitation assay) buffer. Cell lysates were constantly agitated at 4°C for 2 h then centrifuged at $12,000 \times g$ for 1 min and supernatants were saved. After determining the protein concentration (BCA assay kit, Thermo Scientific, Rockford, IL, USA), 20 µg of total protein was separated by sodium dodecyl sulfate polyacrylamide gel electrophoresis under reducing conditions according to the method of Laemmli [65]. Proteins were blotted onto polyvinylidene difluoride membranes (Immobilon-P; Millipore, MA, USA). The blot was incubated overnight at 4°C in the presence of α-Hsp27 (ADI-SPA-803), α-Hsp70 (ADI-SPA-810), α-Hsp60 (ADI-SPA-806), α-Hsp90 (ADI-SPA-830) (Enzo Life Sciences, NY, USA), and α-Hsp40 (C-20:sc-1800, Santa Cruz Biotechnology, Santa Cruz, CA, USA), antibodies diluted 1:1000 in phosphate-buffered saline solution (PBS). After overnight incubation, the membrane was washed three times in PBS–0.05% Tween and incubated for 1 h in peroxidase-conjugated anti-mouse, anti-rabbit or anti-goat IgG antibody (Sigma-Aldrich, St. Louis, MO, USA) diluted 1:50,000 in PBS con-

taining 3% non-fat dry milk powder. The immune complexes were detected using enhanced chemiluminescence (ECL) (Amersham, Little Chalfont, Buckinghamshire, UK) according to the supplier's instructions and analyzed using AlphaEase FC software (Alpha Innotech, San Leandro, Canada). Immunoreactive bands were normalized to the density α-GAPDH (1:20,000) (G9545; Sigma-Aldrich) from the same sample.

Cytotoxicity assays

In vitro test: SH-SY5Y cells were homogenously distributed on 96-well plates in 5×10^3 cells/well density and incubated at 37°C. Then, 24 h later, cells were treated with LA1011, LA1030 or LA1044 at a 100 nM–200 µM concentration range for 24 h. The viability of the cells was measured using alamarBlue[®] assay kit (Life Technologies) according to the supplier's instructions. The *in vivo* acute toxicity of drugs selected for animal experiments were assayed in 2-month-old BALB/c mice ($n=10$) by injecting the compound in PBS solution intraperitoneally (ip) at a 300 mg/kg dose.

Measurement of neuroprotection

Animals and treatments

B6C3-Tg (APP^{swe}/PS1^{dE9})85Dbo/Mmjax mice (APPxPS1) were purchased from The Jackson Laboratory (Bar Harbor, ME, USA) and maintained on the C57BL/6 genetic background (tg). The mice were kept in individual ventilated cages (Acéllabor Ltd., Hungary) on a 12/12 h dark/light cycle (lights on from 7 a.m. to 7 p.m.) with food and water available *ad libitum* and were treated ip with 3 mg/kg LA1011 once a day for 6 months. Four groups (8 animals/group) of 3 months old male mice were used: 1) wild type (C57BL/6) mice (wt) treated with saline; 2) wt treated with LA1011; 3) tg treated with saline; and 4) tg treated with LA1011.

Animal care followed the Communities Council Directive of 22 September 2010 (2010/63/EU on the protection of animals used for scientific purposes). Formal approval to conduct the experiments described was obtained from the Animal Experimentation Committee of the University of Szeged.

Behavioral test

The Morris water maze (MWM) is one of the most commonly used experimental rodent models to measure spatial learning and memory [66–73].

Animals were trained in an open-field water maze (diameter: 130 cm) filled with water ($23 \pm 1^\circ\text{C}$) made opaque with milk. The pool was divided into four virtual quadrants and the invisible platform (diameter: 10 cm) was submerged in the middle of one of the four quadrants. Around the pool there was a black curtain. The animals swam twice a day for 5 consecutive days, and were launched from four different starting points. They were placed into the water facing the wall of the pool and were given 90 s to find the platform and 15 s to stay on it. Animals that did not find the platform were gently guided and placed on it. The escape latency data were calculated automatically by a video tracking system (EthoVision 2002, Noldus Information Technology, Netherlands).

Histology studies

After the MWM test, the mice were deeply anesthetized and transcardially perfused with 10 ml of 4°C PBS, followed by 30 ml of 4°C paraformaldehyde solution (4% in phosphate buffer, pH 7.4). Mouse brains were removed and post-fixed for 24 h in the same fixative (4°C), and subsequently placed in a 30% sucrose solution for 72 h at 4°C . Hippocampal coronal sections were cut to 30 μm on a cryostat, and the slices were collected and stored at 4°C in PBS for free floating histochemistry.

Cresyl violet (Nissl) staining

Cresyl violet readily binds to the acidic components of RNA-rich ribosomes, as well as the nuclei and nucleoli of nerve cells and is used to determine neuron density. Slices ($n=4$, 2 slice/animal) were mounted on slides and stained in filtered 1% cresyl violet solution for 5 min and dehydrated subsequently in 50% 70%, 95%, and twice in 100% ethanol for 1 min each. Slides were finally placed in xylene for another 10 min and coverslipped. Digital images were captured by a digital slide scanner (Mirax Midi, Carl Zeiss, Hungary), and analysis was performed using the Histoquant program (3DHitech, Hungary).

Tau immunohistochemistry

After quenching of endogenous peroxidase activity and non-specific blocking, the sections ($n=4$, 4 slices/animals) were incubated overnight at 4°C with paired helical filament (PHF)-tau monoclonal antibody (clone AT100, Pierce Biotechnology, USA) at a 1:800 dilution in PBS (pH 7.4) in the presence of 20% goat serum and 0.2% Triton X-100. On the following day, the sections were washed

in PBS and incubated for 1 h at room temperature with biotinylated goat anti-mouse antibody (1:400) followed by 1 h incubation with avidin-biotin complex (Vectastain Elite ABC Kit, Vector Laboratories, Burlingame, CA, USA; 1:400). After washing, sections were incubated in peroxidase substrate solution (nickel-enhanced 3,3'-diaminobenzidine) until the desired stain intensity developed. Following rinsing in tap water, sections were mounted on gelatin-coated slides, air-dried, dehydrated, and coverslipped with DPX mountant for histology (Fluka BioChemika, Buchs, Switzerland). Digital images were captured by a digital slide scanner (Mirax Midi), and analysis was performed using the Histoquant program (3DHitech).

Quantification of dendritic spine density using Golgi impregnation

The FD Rapid GolgiStain™ Kit (FD NeuroTech-nologies, Consulting & Services, Inc., Columbia, MD, USA) was used ($n=3$, 1 slice per animal and 2 neurons per slice) to measure dendritic spine density in the hippocampal CA1 area. Experimental animals were deeply anesthetized before brains were removed as quickly as possible and then carefully handled to avoid damage or pressing of the tissue. The tissue was immersed in an impregnation solution (A + B solution) and stored at room temperature for 2 weeks in the dark. The brains were transferred into another solution (C) and stored at 4°C in the dark for at least 48 h. Then, 100- μm thick coronal sections were cut with a microtome (Zeiss Microm HM 650 V). Sections were mounted on gelatin coated glass slides. After the staining and dehydration procedure, the slides were covered with DPX (VWR International, Radnor, PA, USA).

Golgi sections were studied by inverse light microscopy using oil-immersion objectives. The spine density of the proximal apical dendrite area was analyzed (100–200 μm from soma). One segment (100 μm in length) from a second-third-order dendrite protruding from its parent apical dendrite was chosen in each examined neuron for spine density quantification, as described by Nagy et al. [74]. The dendrites were selected under a $100\times$ oil immersion lens and the images ($600\times$) of these apical dendrites were captured through a CCD camera ($1,600 \times 1,200$ pixel) connected to a light microscope (Olympus Vanox-T AH-2) and a computer. Serial images were captured from each dendrite in the analyzed segment. The captured multiple photomicrographs from one dendrite were then stacked into one file. To stack

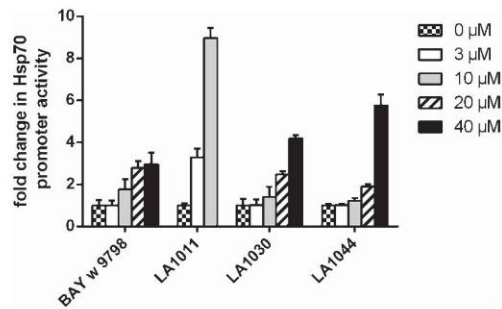


Fig. 2. The Hsp70 co-inducer effect of various LA drug candidates was screened by using a promoter-probing assay. Bars representing co-induction were calculated by the following formula: Fold change = $[(F_x(42) - F_0(37)) / (F_0(42) - F_0(37))]$, where “F” represents the fluorescent intensity of cells incubated in the absence “0” or presence of drug candidates of concentration “x” at 37°C or 42°C for 1 h. The missing bars for LA1011 (20 and 40 μM) indicate that the drug was toxic at these concentrations. Data are means \pm SD.

the images Image-Pro-Plus image analysis software (IPP; Media Cybernetics, Silver Spring, MD, USA) was used. Measurement of the spine density was performed by two independent experimenters to blind the analysis.

Statistical analysis

For statistical evaluation of western blots (Fig. 3), one-way ANOVA with *post hoc* Games-Howell test was used, which was performed by R 3.1.1 for Windows software. Data represent the mean \pm standard deviation (SD) ($n=6$) (Figs. 2 and 3). A $p < 0.05$ value was considered statistically significant. Statistical analysis of the Morris water maze experiment (Fig. 4) was performed using SPSS software and Python’s Lifelines library (Davidson-Pilon, C., Lifelines, 2016), Github repository. The latency time to attain the platform (with a 90-s limit) was measured to determine which of the four groups had the highest learning rate. The longer the latency time to the platform is, the lower the learning capacity of the mice. “Survival curves” using the Cox Proportional Hazard model [75] were fitted, and the days and the treatments were selected as covariates. The comparison of treatment groups was performed using log-rank tests.

One-way ANOVA followed by Fisher’s LSD *post hoc* test was used for histological analysis and for dendritic spine density measurements (Fig. 5) using SPSS statistical software. Differences with a p -value of less than 0.05 were considered significant unless indicated otherwise.

RESULTS

Hsp co-inducing activity of LA1011, LA1030, and LA1044

We used SH-SY5Y human neuroblastoma cells stably expressing YFP under the control of an Hsp70 promoter to select the non-toxic concentrations of active Hsp co-inducing compounds (data not shown). In addition to the original lead compound (BAY w 9798), we investigated the effects of three novel drug candidates (LA1011, LA1030, and LA1044) on Hsp70 promoter activity (Fig. 2).

The drug candidates were added to SH-SY5Y-pHsp70-YFP cells at the four indicated concentrations 30 min prior to heat treatment (42°C, 1 h), which was followed by a 16 h recovery period at 37°C. After recovery, the expression of YFP was determined by flow cytometry. At 37°C none of the compounds had a significant effect on Hsp70 promoter activity (data not shown); however, at an elevated temperature (42°C) pronounced expression of YFP was observed (2–3 fold increase in intensity), which was further increased by administering the LA compounds, thus indicating the co-induction property of these drug candidates (Fig. 2). From these highly active “hit” molecules we chose water soluble LA1011 and water insoluble LA1044 for further *in vitro* and *in vivo* investigations.

The Hsp co-inducing effect of LA1011 and LA1044 on different Hsp-classes in SH-SY5Y cells was studied by western blot. Representative immunoblots (Fig. 3) demonstrate that heat shock induced Hsp27, Hsp40, and Hsp70 proteins; however, the level of Hsp60 and Hsp90 remained unchanged (Supplementary Figure 1). The administration of LA1011 (5 μM) and LA1044 (40 μM) further increased the level of Hsp27, Hsp40, and Hsp70. Importantly, in the absence of heat shock (cellular stress), these compounds did not alter the level of any Hsps measured. Results summarized in Fig. 3 demonstrate the unique Hsp co-inducer properties of LA1011 and LA1044, as they act only during stress. Inhibition of the ATPase activity of Hsp90 by naturally identified antibiotics and synthetic molecules is well-documented [76, 77] and is a known mechanism for the upregulation of the heat shock response. We therefore tested the ability of LA1011 to modulate the ATPase activity of yeast Hsp90. We found that LA1011 did not modify the ATPase activity of yeast Hsp90 at concentrations of 5 and 10 μM (Supplementary Figure 2).

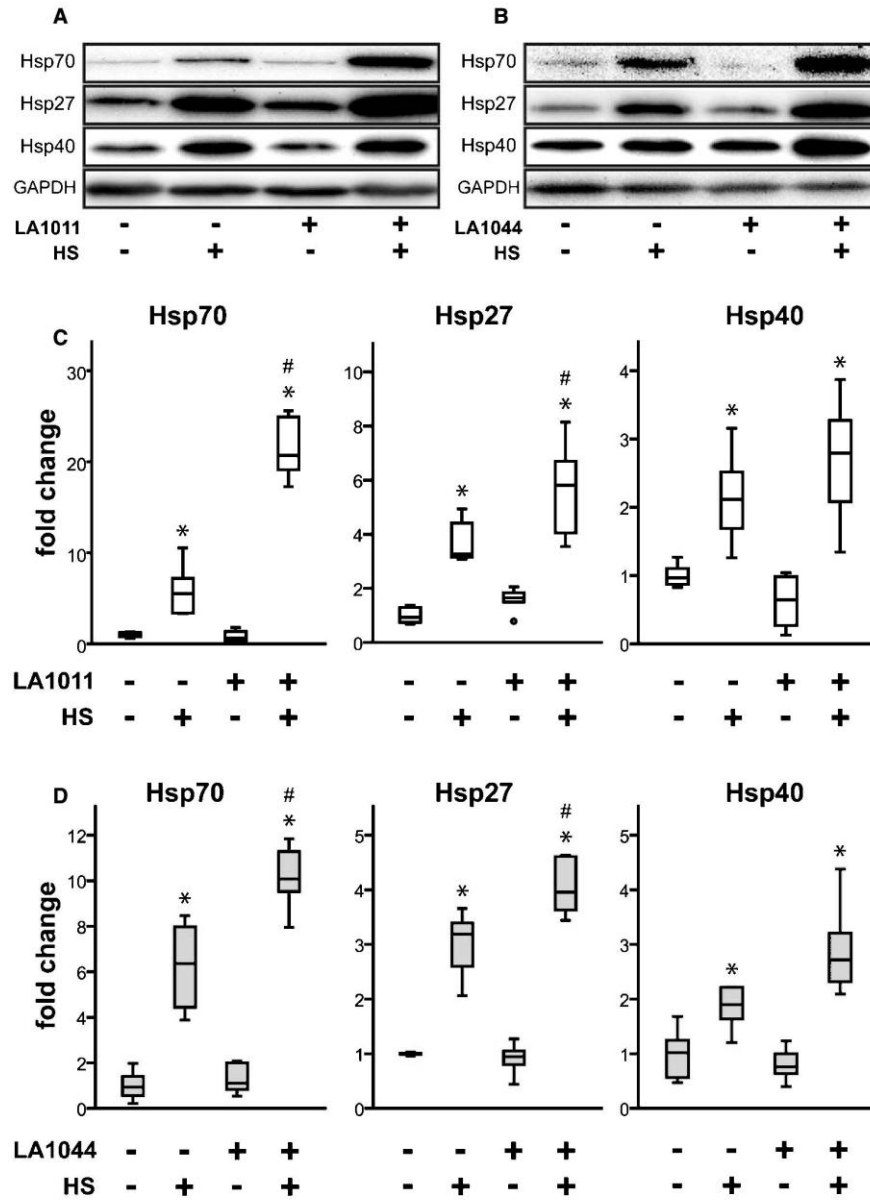


Fig. 3. Effect of heat and LA1011 or LA1044 treatment on Hsp70, Hsp27 and Hsp40 levels in SH-SY5Y human neuroblastoma cell line measured by western blotting (A, B) and quantitative densitometric analysis (C, D). Cells were untreated or treated with LA1011 (5 μ M) or LA1044 (40 μ M) at 37°C or 42°C. Box plots represent quantitative data normalized to GAPDH. All data represent the mean \pm SD ($n=6$) and $p<0.05$ was considered statistically significant. HS = heat shock at 42°C, 1 h. * $p<0.05$, when data are compared to LA compound (-), HS (-) sample. # $p<0.05$, when data are compared to LA compound (-), HS (+) sample. One way ANOVA followed by a Tukey *post hoc* test was used for statistical comparisons.

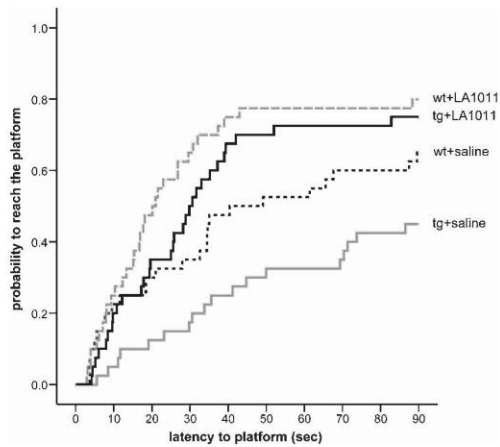


Fig. 4. Effect of LA1011 treatment on Morris water maze performance. The fitted survival curves using the Cox Proportional Hazard model represents the probability that animals find the platform during a trial, capped at 90 s. The effect of day has been modeled in. We compared wt+saline versus wt+LA1011 ($p=0.047$), wt+saline versus tg+saline ($p=0.036$), and tg+saline versus tg+LA1011 ($p=0.001$) treatment groups using log-rank tests ($n=8/\text{group}$).

In vivo neuroprotective effect of LA1011

After the acute toxicity test (at 300 mg/kg) was negative, the neuroprotective effect of the Hsp co-inducer LA1011 was studied in tg mice using behavioral and histological methods. The applied chronic dosage of 3 mg/kg for the *in vivo* experiments was selected based on the *in vitro* results.

Spatial navigation in MWM

After 6 months daily ip treatment of mice with either LA1011 (3 mg/kg) or saline, the MWM test

was applied. The animals were placed into the water facing the sidewalls of the pool at different starting positions across trials, and the swim time to find the platform (escape latency) was followed with a tracking system. The animals learned to swim to the correct location with decreasing escape latencies across days (Supplementary Figure 3). Pairwise comparison of daily performances was made using the log-rank test and included all mice. Compared to day one of testing, mice were more likely to find the platform on day two ($p=1.65\text{e-}5$), day three ($p=5.24\text{e-}6$), day four ($p=1.88\text{e-}11$), and day five ($p=4.55\text{e-}12$). The probability to reach the platform was determined using the Cox Proportional Hazard model (Fig. 4). Significant differences were found between wt+saline versus wt+LA1011 ($p=0.047$), wt+saline versus tg+saline ($p=0.036$), and tg+saline versus tg+LA1011 ($p=0.001$) treatment groups. Importantly, mice in the tg+saline group required significantly more time to find the platform compared to the wt+saline group; however, the 6 months daily ip LA1011 treatment tg mice showed a significantly improved learning ability (tg+saline versus tg+LA1011 $p=0.001$). Interestingly, we found LA1011 improved the memory potency (procognitive) of mice as wt+LA1011 treated mice required less time to complete the task compared with controls (wt+saline) ($p=0.047$).

Histology

The animals were treated as described in “Animals and treatments”. Brain sections (prepared as described in “Materials and Methods”) were stained with cresyl violet, which stain Nissl substance in the cytoplasm of neurons in paraformaldehyde or

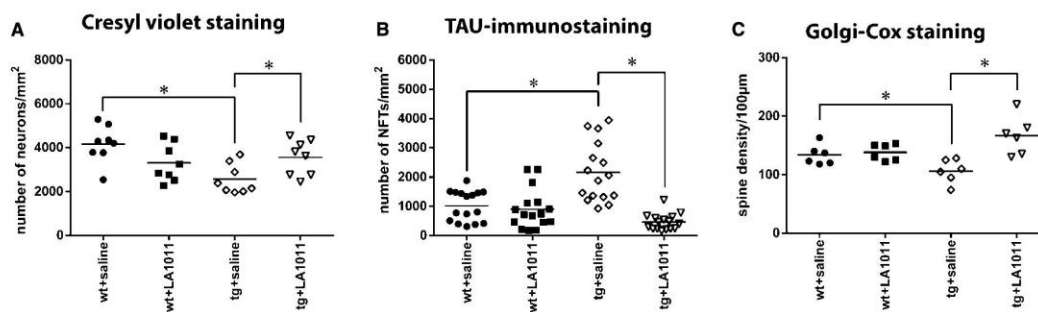


Fig. 5. Cresyl-violet staining, tau-immunostaining, and Golgi-Cox staining of hippocampal slices of wt and tg animals after 6 months treatment. (A) Number of counted neurons/mm²; $n=4$, 2 slices/animal, (B) number of counted neurofibrillary tangles/mm²; $n=4$, 4 slices/animal and (C) measured spine density/100 µm; $n=3$, 2 slices/animal. Each dot represents the counted raw data, while horizontal bars indicate mean values. Statistical significance was determined by one-way ANOVA, followed by Fisher's LSD *post hoc* test. Differences with a p -value <0.05 were considered significant; n refers to the number of animals.

formalin-fixed tissue. Digital images were analyzed by HistoQuant program. The difference in the number of neurons was significant between the groups (Fig. 5A–D). Significantly fewer neurons were observed in the tg+saline group compared with the wt group (tg+saline versus wt+saline group, $p=0.002$). Cresyl-violet staining confirmed that LA1011 was neuroprotective in the transgenic AD mouse model. Treating mice with LA1011 for 6 months significantly prevented the loss of neurons in this group (tg+saline versus tg+LA1011, $p=0.041$).

Tau-pathology studies used immunohistochemistry to detect tau in PHF, a major component of the neurofibrillary tangles (NFTs) involved in the pathology of AD that are not present in normal biopsies [78]. Digital images were analyzed by HistoQuant program. There were significant differences in the number of abnormally accumulated NFTs in the hippocampus (HC) between the groups ($p=0.001$) (Fig. 5B; Supplementary Figure 4E–H). There were more NFTs in the HC slices of the tg+saline group compared with the wt+saline group ($p=0.001$). Most importantly, the administration of Hsp co-inducer LA1011 decreased the number of NFTs in tg mice HC to the level found in the HC of wt mice ($p=0.001$) (Fig. 5B).

Long-term memory is mediated in part by the growth of new dendritic spines (or the enlargement of pre-existing spines) to reinforce a particular neural pathway. According to the literature, APPxPS1 mice undergo spine loss already by the age of 4 months [79]. One of the best neurohistological methods to observe detailed morphology of neurons is Golgi staining. The Golgi-Cox protocol can be used to study the experimental effects of different pharmacological manipulations on the spatial distribution of neurons, dendrite density, spine number, and morphology. After the Golgi-Cox staining of the HC CA1 area, digital images were used to count dendritic spines. The tg+saline group had fewer dendritic spines compared with the wt+saline group ($p=0.045$). The 6-month LA1011 treatment of transgenic animals resulted in a considerably greater number of spines in the HC slices (tg+saline versus tg+LA1011; $p=0.001$). The treatment did not affect the spine number of wt animals. This could be explained by the molecule's "HSP co-modulating activity" namely it acts like "smart molecules" by selective interactions with only those cells, which are under acute or chronic stress.

A β peptide initiates inflammation in the HC of the human brain in AD. A β is chemically "sticky"

and gradually builds up into plaques [57], which can be identified by immunohistochemistry using anti-A β antibody. We observed amyloid plaque-like structures in tg mice (Supplementary Figure 4I–L). The representative examples of sections show a nos amount of plaque formation in the HC of transgenic saline treated animals compared to that of wt samples. Administering LA1011 to tg mice decreased plaque formation (Supplementary Figure 4K, L). There were no signs of amyloid plaques in sections from wt animals (Supplementary Figure 4I, J).

DISCUSSION

At present, there are few drugs that improve the memory deficits associated with normal aging and none that prevent cognitive decline in chronic neurodegenerative conditions such as AD. Except for rare cases of familial AD, the cause of AD is not known, but disease is highly correlated with aging, a process involving a wide variety of physiological changes. Therefore, it is likely that cells in the aging brain are compromised not from a single cause but from the convergence of multiple insults. Unfortunately, drug candidates for AD have all failed in clinical trials, perhaps because one target is not sufficient or because the targets are also critical for normal brain function. Molecular chaperones have central roles in each of the arms of cellular proteostasis (synthesis, folding, disaggregation, and degradation of proteins); therefore, the approach described in this study, the administration of Hsp co-inducer 1,4 DHPs, might have therapeutic benefits for NDDs including AD.

The most important finding of this study is that the novel Hsp co-inducer is broadly neuroprotective and has the ability to enhance memory in normal animals as well as to prevent memory deficits in AD transgenic mice. The neurotrophic and memory-enhancing activities of LA1011 might be associated with an increase in the levels of Hsp70, Hsp40, and Hsp25.

The Hsp co-inducer effect of the novel 1,4-DHP compounds LA1011 and LA1044 was demonstrated *in vitro* by a promoter probing assay (Fig. 2), and by western blot in a SH-SY5Y human neuroblastoma cell line (Fig. 3). The inhibition of the ATPase activity of Hsp90 is a known mechanism for the upregulation of the heat shock response. We therefore tested the ability of LA1011 to modulate the ATPase activity of yeast Hsp90 and found that LA1011 did not modify

the ATPase activity of yeast Hsp90 at concentrations of 5 and 10 μ M (Supplementary Figure 2).

The observed Hsp modulating activity of the compounds was separable from the Ca^{2+} channel antagonist effect responsible for the antihypertensive activity of many known 1,4-DHPs. For the known Ca^{2+} channel antagonist nilvadipine, the EC_{50} for Hsp-modulation and for Ca^{2+} channel inhibition is equal [56, 80]. The EC_{50} for the novel compounds described in this study was above 10; thus, the separation of a potential antihypertensive effect allows the selected compounds to be used to treat pathophysiological conditions mediated by Hsps, including NDDs, without the risk of hypotension. The best co-inducer, LA1011 was selected for *in vivo* experiments in the tg mouse model of AD and proved to be neuroprotective. LA1011 prevented neuron loss in the HC of tg mice (Fig. 5A), decreased NFT accumulation (Fig. 5B), and saved dendritic spine numbers (Fig. 5C). In the MWM task, both wt groups showed a progressive decrease in latency to reach the platform, a measure of spatial learning. Tg animals, however, showed significantly higher latencies compared to all other experimental groups suggestive of delayed learning. In line with the histological results, 6 months treatment with LA1011 significantly restored the spatial learning capability of tg mice ($p=0.001$) and further improved the memory of wt animals (Fig. 4). These results can be explained in the context of our knowledge of the pathogenetic mechanisms of AD. Furthermore, maintenance of protein homeostasis by chaperone induction predicts the induction of a beneficial effect of LA1011 on brain function and morphology.

AD is a complex, multifactorial syndrome with a number of leading mechanisms, including astrocyte hyperactivity (reactive astrogliosis), neuroinflammation, mitochondrial dysfunction, and the accumulation of misfolded proteins ($\text{A}\beta$, NFT, α -synuclein) in the brain [57]. A net loss of dendritic spines is observed in AD and cases of intellectual disability. Because dendritic spines are plastic structures whose lifespan is influenced by input activity [81], spine dynamics may play an important role in the maintenance of memory over a lifetime.

The original $\text{A}\beta$ hypothesis of Hardy states that an imbalance exists between $\text{A}\beta$ production and clearance resulting in $\text{A}\beta$ accumulation [82, 83]. During the last 20 years, intensive research has targeted the biosynthesis of $\text{A}\beta$ (β - and γ -secretases), as well as the clearance of $\text{A}\beta$ and amyloid plaques from the brain [84]. However, these trials were unsuccessful

and no efficient drug treatment of AD exists currently, although a number of novel AD drug trials are in progress.

Recent data on the molecular basis of AD pathophysiology suggest a number of leading mechanisms [85]. Mitochondrial DNA mutations leading to oxidative stress-induced mitochondria dysfunction triggers a chain of cellular events leading to neurodegeneration and a “vicious circle” that ends in dementia [86, 87]. Molecular chaperones and the ubiquitin-proteasome system represent the most important defensive mechanisms against misfolded proteins in AD [88]. Each protein aggregation disease can be characterized by a different set of Hsps that can rescue specific types of aggregation [89]. Some of these Hsps have demonstrated effectiveness *in vivo*, in mouse models of protein-aggregation diseases. Hsp70 and Hsp90 promote tau solubility and tau binding to microtubules, reduce insoluble tau, and reduce tau hyperphosphorylation in a transgenic mouse model of AD [90]. In addition, therapeutic inducers of the Hsp70/Hsp110 system protected Hsp-deficient mice against traumatic brain injury [30] and the upregulation of Hsp by geldanamycin reduced brain injury in a mouse model of intracerebral hemorrhage [33]. A molecular chaperone, the human BRICHOS domain, can specifically inhibit the $\text{A}\beta$ -catalytic cycle ($\text{A}\beta_{1-42}$ fibrils effectively catalyze the formation of neurotoxic $\text{A}\beta$ -oligomers) and limit human $\text{A}\beta_{1-42}$ toxicity [91]. In addition, some molecular chaperones forcibly untangle protein aggregates (disaggregases) [92]. Omi/HtrA2, a mammalian chaperone, selectively binds and detoxifies oligomeric $\text{A}\beta$ by disaggregation [93]. Exogenous human Hsp70 had dramatic neuroprotective effects in olfactory bulbectomy mice and 5xFAD mouse models of neurodegeneration [29] based on its anti-apoptotic and anti-inflammatory effects. Consequently, small molecule activators of the heat shock response provide great therapeutic promise [94]. Ca^{2+} -dependent activation of heat shock factor 1 suppressed protein misfolding and reprogramming of protein homeostasis [95]. Arimoclomol, an Hsp co-inducer, may protect motor neurons by enhancing Hsp expression, thus directly affecting protein aggregation and clearance of misfolded assemblies via the proteasome-ubiquitin system [32]. Recent experiments have demonstrated the dual role of Hsp70 [96], which functions as a molecular chaperone for damaged proteins, as well as simultaneously stabilizing lysosomes, which can revert NDD-associated lysosomal pathology [96–98].

In summary, unregulated Hsp induction could cause the excessive overexpression of Hsps leading to instability of the stress response and unwanted side effects [99]. Because LA1011 and LA1044 increase Hsp expression only under stressed conditions, the therapeutic use of DHPs in this study is novel and perhaps an optimal strategy for the treatment of AD and other NDDs.

ACKNOWLEDGMENTS

We are grateful to László Siklós for the measurements of dendritic spine density and to Zsolt Datki and Mónika Mihók for animal treatment. This work was supported by the EC Health Program “Memoload” (FP-7 project N° 201.159), the Hungarian National Development Agency (TAMOP-4.1.1.C-13/1/KONV-2014-0001), the Hungarian Basic Research Fund (OTKA, NK100857, NN111006) and LipidArt Ltd. Chrisostomos Prodromou and Katie L.I.M. Blundell are supported by the Wellcome Trust, 095605/Z11/Z.

Authors’ disclosures available online (<http://j-alz.com/manuscript-disclosures/15-0860r2>).

SUPPLEMENTARY MATERIAL

The supplementary material is available in the electronic version of this article: <http://dx.doi.org/10.3233/JAD-150860>.

REFERENCES

- [1] Kim YE, Hipp MS, Bracher A, Hayer-Hartl M, Hartl FU (2013) Molecular chaperone functions in protein folding and proteostasis. *Annu Rev Biochem* **82**, 323-355.
- [2] Toth ME, Santha M, Penke B, Vigh L (2015) How to stabilize both the proteins and the membranes: Diverse effects of sHsps in neuroprotection. In *The Big Book on Small Heat Shock Proteins, Heat Shock Proteins 8*, Tanguay RM, Hightower LE, eds. Springer, Cham, pp. 527-562.
- [3] Calderwood SK, Murshid A, Prince T (2009) The shock of aging: Molecular chaperones and the heat shock response in longevity and aging—a mini-review. *Gerontology* **55**, 550-558.
- [4] Kayani AC, Morton JP, McArdle A (2008) The exercise-induced stress response in skeletal muscle: Failure during aging. *Appl Physiol Nutr Metab* **33**, 1033-1041.
- [5] Valastyan JS, Lindquist S (2014) Mechanisms of protein-folding diseases at a glance. *Dis Model Mech* **7**, 9-14.
- [6] Murshid A, Eguchi T, Calderwood SK (2013) Stress proteins in aging and life span. *Int J Hyperther* **29**, 442-447.
- [7] Bemporad F, Chiti F (2012) Protein misfolded oligomers: Experimental approaches, mechanism of formation, and structure-toxicity relationships. *Chem Biol* **19**, 315-327.
- [8] Resenberger UK, Harmeier A, Woerner AC, Goodman JL, Muller V, Krishnan R, Vabulas RM, Kretzschmar HA, Lindquist S, Hartl FU, Multhaup G, Winklhofer KF, Tatzelt J (2011) The cellular prion protein mediates neurotoxic signalling of beta-sheet-rich conformers independent of prion replication. *EMBO J* **30**, 2057-2070.
- [9] Bucciantini M, Giannoni E, Chiti F, Baroni F, Formigli L, Zurdo JS, Taddei N, Ramponi G, Dobson CM, Stefani M (2002) Inherent toxicity of aggregates implies a common mechanism for protein misfolding diseases. *Nature* **416**, 507-511.
- [10] Demuro A, Mina E, Kaye R, Milton SC, Parker I, Glabe CG (2005) Calcium dysregulation and membrane disruption as a ubiquitous neurotoxic mechanism of soluble amyloid oligomers. *J Biol Chem* **280**, 17294-17300.
- [11] Bence NF, Sampat RM, Kopito RR (2001) Impairment of the ubiquitin-proteasome system by protein aggregation. *Science* **292**, 1552-1555.
- [12] Endres K, Reinhardt S (2013) ER-stress in Alzheimer's disease: Turning the scale? *Am J Neurodegener Dis* **2**, 247-265.
- [13] Hetz C, Mollereau B (2014) Disturbance of endoplasmic reticulum proteostasis in neurodegenerative diseases. *Nat Rev Neurosci* **15**, 233-249.
- [14] Li JQ, Yu JT, Jiang T, Tan L (2015) Endoplasmic reticulum dysfunction in Alzheimer's disease. *Mol Neurobiol* **51**, 383-395.
- [15] Li SH, Yang L, Selzer ME, Hu Y (2013) Neuronal endoplasmic reticulum stress in axon injury and neurodegeneration. *Ann Neurol* **74**, 768-777.
- [16] Tadic V, Prell T, Lautenschlaeger J, Grosskreutz J (2014) The ER mitochondria calcium cycle and ER stress response as therapeutic targets in amyotrophic lateral sclerosis. *Front Cell Neurosci* **8**, 147.
- [17] Hetz C, Chevet E, Harding HP (2013) Targeting the unfolded protein response in disease. *Nat Rev Drug Discov* **12**, 703-719.
- [18] Placido AI, Pereira CMF, Duarte AI, Candeias E, Correia SC, Santos RX, Carvalho C, Cardoso S, Oliveira CR, Moreira PI (2014) The role of endoplasmic reticulum in amyloid precursor protein processing and trafficking: Implications for Alzheimer's disease. *Biochim Biophys Acta* **1842**, 1444-1453.
- [19] Schon EA, Area-Gomez E (2013) Mitochondria-associated ER membranes in Alzheimer disease. *Mol Cell Neurosci* **55**, 26-36.
- [20] Schreiner B, Hedskog L, Wiehager B, Ankarcrona M (2015) Amyloid-beta peptides are generated in mitochondria-associated endoplasmic reticulum membranes. *J Alzheimers Dis* **43**, 369-374.
- [21] Alavez S, Vantipalli MC, Zucker DJS, Klang IM, Lithgow GJ (2011) Amyloid-binding compounds maintain protein homeostasis during ageing and extend lifespan. *Nature* **472**, 226-229.
- [22] Nagai Y, Fujikake N, Popiel HA, Wada K (2010) Induction of molecular chaperones as a therapeutic strategy for the polyglutamine diseases. *Curr Pharm Biotechnol* **11**, 188-197.
- [23] Klettner A (2004) The induction of heat shock proteins as a potential strategy to treat neurodegenerative disorders. *Drug News Perspect* **17**, 299-306.
- [24] Hartl FU, Bracher A, Hayer-Hartl M (2011) Molecular chaperones in protein folding and proteostasis. *Nature* **475**, 324-332.

- [25] Ehrnsperger M, Graber S, Gaestel M, Buchner J (1997) Binding of non-native protein to Hsp25 during heat shock creates a reservoir of folding intermediates for reactivation. *EMBO J* **16**, 221-229.
- [26] Mymrikov EV, Seit-Nebi AS, Gusev NB (2011) Large potentials of small heat shock proteins. *Physiol Rev* **91**, 1123-1159.
- [27] Finka A, Mattoo RUH, Goloubinoff P (2011) Meta-analysis of heat- and chemically upregulated chaperone genes in plant and human cells. *Cell Stress Chaperones* **16**, 15-31.
- [28] Walther DM, Kasturi P, Zheng M, Pinkert S, Vecchi G, Ciryam P, Morimoto RI, Dobson CM, Vendruscolo M, Mann M, Hartl FU (2015) Widespread proteome remodeling and aggregation in aging *C. elegans*. *Cell* **161**, 919-932.
- [29] Bobkova NV, Garbuz DG, Nesterova I, Medvinskaya N, Samokhin A, Alexandrova I, Yashin V, Karpov V, Kukharsky MS, Ninkina NN, Smimov AA, Nudler E, Evgen'ev M (2014) Therapeutic effect of exogenous Hsp70 in mouse models of Alzheimer's disease. *J Alzheimers Dis* **38**, 425-435.
- [30] Eroglu B, Kimbler DE, Pang JF, Choi J, Moskopidhis D, Yanasak N, Dhandapani KM, Mivechi NF (2014) Therapeutic inducers of the HSP70/HSP110 protect mice against traumatic brain injury. *J Neurochem* **130**, 626-641.
- [31] Franklin TB, Krueger-Naug AM, Clarke DB, Arrigo AP, Currie RW (2005) The role of heat shock proteins Hsp70 and Hsp27 in cellular protection of the central nervous system. *Int J Hyperther* **21**, 379-392.
- [32] Kalmar B, Lu CH, Greensmith L (2014) The role of heat shock proteins in amyotrophic lateral sclerosis: The therapeutic potential of Arimoclomol. *Pharmacol Therapeut* **141**, 40-54.
- [33] Hoshino T, Murao N, Namba T, Takehara M, Adachi H, Katsuno M, Sobue G, Matsushima T, Suzuki T, Mizushima T (2011) Suppression of Alzheimer's disease-related phenotypes by expression of heat shock protein 70 in mice. *J Neurosci* **31**, 5225-5234.
- [34] Wang H, Tan MS, Lu RC, Yu JT, Tan L (2014) Heat shock proteins at the crossroads between cancer and Alzheimer's disease. *Biomed Res Int* **2014**, 239164.
- [35] Morimoto RI (2008) Proteotoxic stress and inducible chaperone networks in neurodegenerative disease and aging. *Genes Dev* **22**, 1427-1438.
- [36] Soti C, Csermely P (2002) Chaperones and aging: Role in neurodegeneration and in other civilizational diseases. *Neurochem Int* **41**, 383-389.
- [37] Toth ME, Szegedi V, Varga E, Juhasz G, Horvath J, Borbely E, Csibran B, Alfoldi R, Lenart N, Penke B, Santha M (2013) Overexpression of Hsp27 ameliorates symptoms of Alzheimer's disease in APP/PS1 mice. *Cell Stress Chaperones* **18**, 759-771.
- [38] Iwasaki K, Egashira N, Takagaki Y, Yoshimitsu Y, Hatip-Al-Khatib I, Mishima K, Fujiwara M (2007) Nilvadipine prevents the impairment of spatial memory induced by cerebral ischemia combined with beta-amyloid in rats. *Biol Pharm Bull* **30**, 698-701.
- [39] Broadstock M, Ballard C, Corbett A (2014) Latest treatment options for Alzheimer's disease, Parkinson's disease dementia and dementia with Lewy bodies. *Expert Opin Pharmacother* **15**, 1797-1810.
- [40] Corbett A, Ballard C (2013) Is a potential Alzheimer's therapy already in use for other conditions? Can medications for hypertension, diabetes and acne help with the symptoms? *Expert Opin Investig Drugs* **22**, 941-943.
- [41] Cattaruzza M, Wachter R, Wagner AH, Hecker M (2000) Modulation by dihydropyridine-type calcium channel antagonists of cytokine-inducible gene expression in vascular smooth muscle cells. *Br J Pharmacol* **129**, 1155-1162.
- [42] Carosati E, Ioan P, Micucci M, Broccatelli F, Cruciani G, Zhorov BS, Chiarini A, Budriesi R (2012) 1,4-dihydropyridine scaffold in medicinal chemistry, the story so far and perspectives (part 2): Action in other targets and antitargets. *Curr Med Chem* **19**, 4306-4323.
- [43] Ioan P, Carosati E, Micucci M, Cruciani G, Broccatelli F, Zhorov BS, Chiarini A, Budriesi R (2011) 1,4-dihydropyridine scaffold in medicinal chemistry, the story so far and perspectives (part 1): Action in ion channels and GPCRs. *Curr Med Chem* **18**, 4901-4922.
- [44] Kennelly S, Abdullah L, Kenny RA, Mathura V, Luis CA, Mouzon B, Crawford F, Mullan M, Lawlor B (2012) Apolipoprotein E genotype-specific short-term cognitive benefits of treatment with the antihypertensive nilvadipine in Alzheimer's patients—an open-label trial. *Int J Geriatr Psychiatry* **27**, 415-422.
- [45] Kennelly SP, Abdullah L, Paris D, Parish J, Mathura V, Mullan M, Crawford F, Lawlor BA, Kenny RA (2011) Demonstration of safety in Alzheimer's patients for intervention with an anti-hypertensive drug Nilvadipine: Results from a 6-week open label study. *Int J Geriatr Psychiatry* **26**, 1038-1045.
- [46] Forette F, Seux ML, Staessen JA, Thijs L, Babarskiene MR, Babeanu S, Bossini A, Fagard R, Gil-Extremiera B, Laks T, Kopalava Z, Sarti C, Tuomilehto J, Vanhanen H, Webster J, Yodfat Y, Birkenhäger WH, Systolic Hypertension in Europe Investigators (2002) The prevention of dementia with antihypertensive treatment. *Arch Intern Med* **162**, 2046-2052.
- [47] Matsui T, Yamagishi S, Nakamura K, Inoue H (2007) Bay w 9798, a dihydropyridine structurally related to nifedipine with no calcium channel-blocking properties, inhibits tumour necrosis factor- α -induced vascular cell adhesion molecule-1 expression in endothelial cells by suppressing reactive oxygen species generation. *J Int Med Res* **35**, 886-891.
- [48] Herbert LG, Vanterve YMH, Rhodes DG (1989) Interaction of 1,4 dihydropyridine calcium-channel antagonists with biological-membranes - lipid bilayer partitioning could occur before drug-binding to receptors. *J Mol Cell Cardiol* **21**, 187-201.
- [49] Mason RP, Chester DW (1989) Diffusional dynamics of an active rhodamine-labeled 1,4-dihydropyridine in sarcolemmal lipid multibilayers. *Biophys J* **56**, 1193-1201.
- [50] Balogh G, Peter M, Glatz A, Gombos I, Torok Z, Horvath I, Harwood JL, Vigh L (2013) Key role of lipids in heat stress management. *FEBS Lett* **587**, 1970-1980.
- [51] Torok Z, Crul T, Maresca B, Schutz GJ, Viana F, Dindia L, Piotto S, Brameshuber M, Balogh G, Peeter M, Porta A, Trapani A, Gombos I, Glatz A, Gungor B, Peksel B, Vigh L, Csoboz B, Horvath I, Vijayan MM, Hooper PL, Harwood JL, Vigh L (2014) Plasma membranes as heat stress sensors: From lipid-controlled molecular switches to therapeutic applications. *Biochim Biophys Acta* **1838**, 1594-1618.
- [52] Escriba PV, Busquets X, Inokuchi JL, Balogh G, Torok Z, Horvath I, Harwood JL, Vigh L (2015) Membrane lipid therapy: Modulation of the cell membrane composition and structure as a molecular base for drug discovery and new disease treatment. *Prog Lipid Res* **59**, 38-53.

- [53] Torok Z, Tsvetkova NM, Balogh G, Horvath I, Nagy E, Penzes Z, Hargitai J, Bensaude O, Csermely P, Crowe JH, Maresca B, Vigh L (2003) Heat shock protein coinducers with no effect on protein denaturation specifically modulate the membrane lipid phase. *Proc Natl Acad Sci U S A* **100**, 3131-3136.
- [54] Gombos I, Crul T, Piotto S, Gungor B, Torok Z, Balogh G, Peter M, Slotte JP, Campana F, Pilbat AM, Hunya A, Toth N, Literati-Nagy Z, Vigh L, Glatz A, Brameshuber M, Schutz GJ, Hevener A, Febbraio MA, Horvath I, Vigh L (2011) Membrane-lipid therapy in operation: The HSP co-inducer BGP-15 activates stress signal transduction pathways by remodeling plasma membrane rafts. *PLoS One* **6**, e28818.
- [55] Vigh L, Literati PN, Horvath I, Torok Z, Balogh G, Glatz A, Kovacs E, Boros I, Ferdinandy P, Farkas B, Jaszits L, Jednakovits A, Koranyi L, Maresca B (1997) Bimoclomol: A nontoxic, hydroxylamine derivative with stress protein-inducing activity and cytoprotective effects. *Nat Med* **3**, 1150-1154.
- [56] Fulop F, Vigh L, Torok Z, Penke B, Horvath I, Balogh G, Bernath S, Hunya Á (2013) 1,4 dihydropyridine derivatives with HSP modulating activity. PCT. *Int Appl*, WO2013076516 A1.
- [57] Duyckaerts C, Delatour B, Potier MC (2009) Classification and basic pathology of Alzheimer disease. *Acta Neuropathol* **118**, 5-36.
- [58] Behner O, Wollweber H, Rosen B, Zaiss S, Goldmann S (1991) Use of N-alkylated 1,4-dihydropyridine carboxylic acid esters as drugs, new compounds and process for their preparation. *European Patent*, EP 0451654 A2, B1.
- [59] Aritomi J, Ueda S, Nishimura H (1980) Mannich reaction of dihydropyridine derivatives. 1. Reactions with secondary-amines. *Chem Pharm Bull* **28**, 3163-3171.
- [60] Dekamin MG, Ilkhanizadeh S, Latifidoost Z, Daemi H, Karimi Z, Barikani M (2014) Alginic acid: A highly efficient renewable and heterogeneous biopolymeric catalyst for one-pot synthesis of the Hantzsch 1,4-dihydropyridines. *RSC Adv* **4**, 56658-56664.
- [61] Desai B, Dallinger D, Kappe CO (2006) Microwave-assisted solution phase synthesis of dihydropyrimidine C5 amides and esters. *Tetrahedron* **62**, 4651-4664.
- [62] Ebiike H, Maruyama K, Ozawa Y, Yamazaki Y, Achiwa K (1997) Asymmetric synthesis of (R)-nilvadipine and (S)-NB 818 via regioselective bromination of chiral 1,4-dihydropyridines as a key step and enzymatic resolution of racemic 2-hydroxymethyl-1,4-dihydropyridine derivatives. *Chem Pharm Bull* **45**, 869-876.
- [63] Hantzsch A (1881) Condensationsprodukte aus aldehydammoniak und ketonartigen verbindungen. *Chem Ber* **14**, 1637-1638.
- [64] Wysocka A, Krawczyk Z (2000) Green fluorescent protein as a marker for monitoring activity of stress-inducible hsp70 rat gene promoter. *Mol Cell Biochem* **215**, 153-156.
- [65] Laemmli UK (1970) Cleavage of structural proteins during the assembly of the head of bacteriophage T4. *Nature* **227**, 680-685.
- [66] Morris RGM, Garrud P, Rawlins JNP, Okeefe J (1982) Place navigation impaired in rats with hippocampal lesions. *Nature* **297**, 681-683.
- [67] D'Hooge R, De Deyn PP (2001) Applications of the Morris water maze in the study of learning and memory. *Brain Res Rev* **36**, 60-90.
- [68] Mendez-Lopez M, Mendez M, Sampedro-Piquero P, Arias JL (2013) Spatial learning-related changes in metabolic activity of limbic structures at different posttask delays. *J Neurosci Res* **91**, 151-159.
- [69] Morris R (1984) Developments of a water-maze procedure for studying spatial-learning in the rat. *J Neurosci Methods* **11**, 47-60.
- [70] Morris RGM, Anderson E, Lynch GS, Baudry M (1986) Selective impairment of learning and blockade of long-term potentiation by an N-methyl-D-aspartate receptor antagonist, AP5. *Nature* **319**, 774-776.
- [71] Moser MB, Moser EI, Forrest E, Andersen P, Morris RGM (1995) Spatial-learning with a Minislab in the dorsal hippocampus. *Proc Natl Acad Sci U S A* **92**, 9697-9701.
- [72] Sipos E, Kurunczi A, Kasza A, Horvath I, Felszeghy K, Laroche S, Toldi J, Parducz A, Penke B, Penke Z (2007) beta-amyloid pathology in the entorhinal cortex of rats induces memory deficits: Implications for Alzheimer's disease. *Neuroscience* **147**, 28-36.
- [73] Vorhees CV, Williams MT (2006) Morris water maze: Procedures for assessing spatial and related forms of learning and memory. *Nat Protoc* **1**, 848-858.
- [74] Nagy D, Kocsis K, Fuzik J, Marosi M, Kis Z, Teichberg VI, Toldi J, Farkas T (2011) Kainate postconditioning restores LTP in ischemic hippocampal CA1: Onset-dependent second pathophysiological stress. *Neuropharmacology* **61**, 1026-1032.
- [75] Jahn-Eimermacher A, Lasarzik I, Raber J (2011) Statistical analysis of latency outcomes in behavioral experiments. *Behav Brain Res* **221**, 271-275.
- [76] Zhao H, Michaelis ML, Blagg BS (2012) Hsp90 modulation for the treatment of Alzheimer's disease. *Adv Pharmacol* **64**, 1-25.
- [77] Roe SM, Prodromou C, O'Brien R, Ladbury JE, Piper PW, Pearl LH (1999) Structural basis for inhibition of the Hsp90 molecular chaperone by the antitumor antibiotics radicicol and geldanamycin. *J Med Chem* **42**, 260-266.
- [78] Zheng-Fischhofer Q, Biernat J, Mandelkow EM, Illenberger S, Godemann R, Mandelkow E (1998) Phosphorylation of tau protein at Ser214 regulates the binding of tau to microtubules and is part of the epitope of the Alzheimer-tau specific antibody AT100. *Mol Biol Cell* **9**, 395a.
- [79] Smith DL, Pozueta J, Gong B, Arancio O, Shelanski M (2009) Reversal of long-term dendritic spine alterations in Alzheimer disease models. *Proc Natl Acad Sci U S A* **106**, 16877-16882.
- [80] Hoffmann A, Kraul H, Burkardt I (1997) Nilvadipine in hypertension - Experience in ambulatory treatment. *Int J Clin Pharmacol Ther* **35**, 195-203.
- [81] De Roo M, Klauser P, Muller D (2008) LTP promotes a selective long-term stabilization and clustering of dendritic spines. *PLoS Biol* **6**, 1850-1860.
- [82] Hardy J, Allsop D (1991) Amyloid deposition as the central event in the etiology of Alzheimer's disease. *Trends Pharmacol Sci* **12**, 383-388.
- [83] Hardy J (2009) The amyloid hypothesis for Alzheimer's disease: A critical reappraisal. *J Neurochem* **110**, 1129-1134.
- [84] Anand R, Gill KD, Mahdi AA (2014) Therapeutics of Alzheimer's disease: Past, present and future. *Neuropharmacology* **76**, 27-50.
- [85] van Dijk G, van Heijningen S, Reijne AC, Nyakas C, van der Zee EA, Eisel UL (2015) Integrative neurobiology of metabolic diseases, neuroinflammation, and neurodegeneration. *Front Neurosci* **9**, 173.

- [86] Cha MY, Kim DK, Mook-Jung I (2015) The role of mitochondrial DNA mutation on neurodegenerative diseases. *Exp Mol Med* **47**, e150.
- [87] Simoncini C, Orsucci D, Ienco EC, Siciliano G, Bonuccelli U, Mancuso M (2015) Alzheimer's pathogenesis and its link to the mitochondrion. *Oxid Med Cell Longev* **2015**, 803942.
- [88] Sulistio YA, Heese K (2016) The ubiquitin-proteasome system and molecular chaperone deregulation in Alzheimer's disease. *Mol Neurobiol* **53**, 905-931.
- [89] Kakkar V, Meister-Broekema M, Minoia M, Carra S, Kampinga HH (2014) Barcoding heat shock proteins to human diseases: Looking beyond the heat shock response. *Dis Model Mech* **7**, 421-434.
- [90] Dou F, Netzer WJ, Tanemura K, Li F, Hartl FU, Takashima A, Gouras GK, Greengard P, Xu HX (2003) Chaperones increase association of tau protein with microtubules. *Proc Natl Acad Sci U S A* **100**, 721-726.
- [91] Cohen SIA, Arosio P, Presto J, Kurudenkandy FR, Biverstal H, Dolfe L, Dunning C, Yang XT, Frohm B, Vendruscolo M, Johansson J, Dobson CM, Fisahn A, Knowles TPJ, Linse S (2015) A molecular chaperone breaks the catalytic cycle that generates toxic A beta oligomers. *Nat Struct Mol Biol* **22**, 207-213.
- [92] Doyle SM, Genest O, Wickner S (2013) Protein rescue from aggregates by powerful molecular chaperone machines. *Nat Rev Mol Cell Biol* **14**, 617-629.
- [93] Liu ML, Liu MJ, Shen YF, Ryu H, Kim HJ, Klupsch K, Downward J, Hong ST (2009) Omi is a mammalian heat-shock protein that selectively binds and detoxifies oligomeric amyloid-beta. *J Cell Sci* **122**, 1917-1926.
- [94] West JD, Wang YY, Morano KA (2012) Small molecule activators of the heat shock response: Chemical properties, molecular targets, and therapeutic promise. *Chem Res Toxicol* **25**, 2036-2053.
- [95] Silva MC, Amaral MD, Morimoto RI (2013) Neuronal reprogramming of protein homeostasis by calcium-dependent regulation of the heat shock response. *PLoS Genet* **9**, e1003711.
- [96] Yamashima T (2013) Reconsider Alzheimer's disease by the 'calpain-cathepsin hypothesis'-A perspective review. *Prog Neurobiol* **105**, 1-23.
- [97] Zhu H, Yoshimoto T, Yamashima T (2014) Heat shock protein 70.1 (Hsp70.1) affects neuronal cell fate by regulating lysosomal acid sphingomyelinase. *J Biol Chem* **289**, 27432-27443.
- [98] Horvath I, Vigh L (2010) Cell biology: Stability in times of stress. *Nature* **463**, 436-438.
- [99] Lamech LT, Haynes CM (2015) The unpredictability of prolonged activation of stress response pathways. *J Cell Biol* **209**, 781-787.
- [100] Prodromou C, Siligardi G, O'Brien R, Woolfson DN, Regan L, Panaretou B, Ladbury JE, Piper PW, Pearl LH (1999) Regulation of Hsp90 ATPase activity by tetratricopeptide repeat (TPR)-domain co-chaperones. *EMBO J* **18**, 754-762.

III



Controlled in situ preparation of A β (1–42) oligomers from the isopeptide “iso-A β (1–42)”, physicochemical and biological characterization

Zsolt Bozso^{a,*}, Botond Penke^{a,b,c}, Dóra Simon^a, Ilona Laczkó^d, Gábor Juhász^b, Viktor Szegedi^b, Ágnes Kasza^a, Katalin Soós^a, Anasztázia Hetényi^{a,e}, Edit Wéber^e, Hajnalka Tóháti^f, Mária Csete^f, Márta Zarándi^a, Livia Fülöp^a

^a Department of Medical Chemistry, University of Szeged, Szeged, Hungary

^b BAYGEN, Bay Zoltán Foundation for Applied Research, Szeged, Hungary

^c Supramolecular and Nanostructured Material Research Group of the Hungarian Academy of Sciences, Szeged, Hungary

^d Institute of Biophysics, Biological Research Center, Szeged, Hungary

^e Institute of Pharmaceutical Chemistry, University of Szeged, Szeged, Hungary

^f Department of Experimental Physics, University of Szeged, Szeged, Hungary

ARTICLE INFO

Article history:

Received 23 July 2009

Received in revised form 1 December 2009

Accepted 1 December 2009

Available online 6 December 2009

Keywords:

β -Amyloid

Oligomers

Aggregation

Alzheimer's disease

Isopeptide

ABSTRACT

β -Amyloid (A β) peptides play a crucial role in the pathology of the neurodegeneration in Alzheimer's disease (AD). Biological experiments (both in vitro and animal model studies of AD) require synthetic A β peptides of standard quality, aggregation grade, neurotoxicity and water solubility. The synthesis of A β peptides has been difficult, owing to their hydrophobic character, poor solubility and high tendency for aggregation. Recently an isopeptide precursor (iso-A β (1–42)) was synthesized by Fmoc-chemistry and transformed at neutral pH to A β (1–42) by O \rightarrow N acyl migration in a short period of time. We prepared the same precursor peptide using Boc-chemistry and studied the transformation to A β (1–42) by acyl migration. The peptide conformation and aggregation processes were studied by several methods (circular dichroism, atomic force and transmission electron microscopy, dynamic light scattering). The biological activity of the synthetic A β (1–42) was measured by ex vivo (long-term potentiation studies in rat hippocampal slices) and in vivo experiments (spatial learning of rats). It was proven that O \rightarrow N acyl migration of the precursor isopeptide results in a water soluble oligomeric mixture of neurotoxic A β (1–42). These oligomers are formed in situ just before the biological experiments and their aggregation grade could be standardized.

© 2009 Elsevier Inc. All rights reserved.

1. Introduction

Alzheimer disease (AD) is a progressive neurodegenerative disorder. The probability of the disease is exponentially increasing with age. The presence of amyloid deposits and neurofibrillary tangles are the main pathologic features of AD. The main components of the amyloid deposits are β -amyloid (A β) peptides. These peptides consist of 39–43 amino acids. The monomeric A β peptides are produced from a membrane protein, the amyloid precursor protein (APP) with the cleavage by β and γ secretases [23]. Initially these peptides are water soluble, then explore β -sheet conformation. This conformational transition induces aggregation producing A β -oligomers, protofibrils and fibrils, simultaneously the water solubility of these A β -species substantially decrease. A β -peptides are neurotoxic both in vivo and in

vitro [21,35]. The most toxic form of the A β peptide is the one that contains 42 residues.

For AD research it is crucial to prepare A β (1–42) peptide to study the aggregation process resulting in toxic A β -species and the in vitro effects of the peptide in neuronal cells and brain tissues as well as examine the progression of the disease in animal models.

It is well known that the synthesis of A β (1–42) is troublesome thus it is considered to be a ‘difficult sequence’ [4,33,38]. The difficulties arise from the hydrophobic nature of the peptide. The presence of high number of hydrophobic amino acids in the sequence and the high tendency of the peptide to adopt β -sheet conformation – both in solution and on the resin matrix – induces aggregation. The aggregation of the growing peptide chains on the solid support causes steric hindrance during the assembly of the molecule. Several methods were reported to overcome the synthetic problem associated with the aggregation of peptide chains on the resin, such as using different solvents [13,38], adding chaotropic salts [11], performing the synthesis at elevated temperature [34], building up the peptide in resins made from or grafted with

* Corresponding author.

E-mail address: zbozso@yahoo.com (Z. Bozso).

polyethylene glycol [15,22], incorporating pseudo-proline residues [36,37] and applying backbone protection [14,24]. Even if the synthesis is successful, it is difficult to dissolve the crude A β peptide for loading it into an HPLC column. The broad elution profile – as a result of aggregation – also makes the purification of the peptide troublesome.

Until recently the synthetic commercial A β (1–42) samples were not homogeneous as for aggregation grade and water solubility. As a consequence, the biological studies performed by these peptides were not always reproducible. The high sensitivity of peptide conformation to handling (solvents, temperature, pH, peptide concentration) might be the reason for different aggregation grade and solubility. Different procedures were worked out during the years [6,16] to obtain oligomers or fibrils from the altering product of the syntheses. Recent publications outline, that it is important to access oligomers of A β , since these are the most toxic form of the peptide [2,7].

Kiso and co-workers [28], Carpino et al. [5] and Mutter and co-workers [10] have independently described a method to ease the synthesis and purification of A β (1–42) by preparing a precursor of the peptide with low tendency for aggregation using N^{α} -Fmoc protected amino acids. The serine residue at position 26 was incorporated as Boc-Ser-OH followed by the acylation of its free hydroxyl side chain with the subsequent residue Gly²⁵. After cleavage of the peptide from the resin, the peptide chain contains an ester bond in its backbone ('isopeptide') and a free α -amino group at Ser²⁶. The incorporated ester bond decreases the propensity of the peptide to aggregate, thus the isopeptide (iso-A β (1–42)) has an enhanced water solubility. When the pH is raised to the physiological value, a fast $O \rightarrow N$ acyl-transfer reaction occurs resulting in A β (1–42). The $O \rightarrow N$ acyl-shift can occur both in vitro and in vivo, thus iso-A β (1–42) can be used as a good precursor for A β (1–42).

Some possible drawbacks of the Fmoc-synthesis such as incomplete deprotection of the growing peptide chain by the 20% piperidine in N,N -dimethylformamide (DMF) [9,18], potential hydrolysis of the ester bond and diketopiperazine formation [8,26] can be minimized if Boc-chemistry is applied for the synthesis of depsi-peptides [29].

Our aim was to prepare A β (1–42) with a simple and cheap method and characterize the A β -peptide assemblies with a series of microscopic, physicochemical and biological methods. Neurobiologists require well characterized, stable and water soluble A β (1–42) of standard quality for reproducible biological experiments. First we synthesized iso-A β (1–42) in solid phase using Boc-chemistry. The subsequent $O \rightarrow N$ acyl-shift at pH 7.4 produced oligomers and other A β species with different aggregation state, depending on the time of the assembly formation. Thus iso-A β (1–42) can be used as a good precursor for A β (1–42), as it was suggested by Sohma and Kiso [27] and recently by us [3]. In vitro and preliminary ex vivo biological experiments were presented by Kiso's [20] group and by us [3], respectively.

In order to follow the aggregation process, conformational and structural studies of the peptide were done by circular dichroism spectroscopy (CD), dynamic light scattering (DLS), transmission electron microscopy (TEM), nuclear magnetic resonance (NMR) and atomic force microscopy (AFM). The biological activity of the A β (1–42) formed from the precursor isopeptide was measured in different test systems (ex vivo electrophysiological studies in rat hippocampal slices and spatial learning of rats in Morris water maze).

2. Materials and methods

2.1. Materials

All N -terminally protected amino acids were purchased from Orpegen (Heidelberg, Germany) and GL Biochem (Shanghai, China).

N -(2-chlorobenzoyloxycarbonyloxy)succinimide (2-Cl-Z-OSu) and O -tert-butyl-L-serine (H-Ser(OtBu)-OH), N,N -dicyclohexylcarbodiimide (DCC), 1-hydroxybenzotriazole (HOBT), 1-hydroxy-7-azabenzotriazole (HOAt) were purchased from GL Biochem (Shanghai, China). Solvents and N,N -diisopropylethylamine (DIEA) were obtained from Sigma-Aldrich. High performance liquid chromatography (HPLC) grade trifluoroacetic acid (TFA) was ordered from Pierce.

2.2. Synthesis of 2-Cl-Z-Ser(OtBu)-OH

8.5 g (30 mmol) 2-Cl-Z-OSu in 60 mL DMF were added to 4 g (25 mmol) of H-Ser(OtBu)-OH dissolved in 10% Na₂CO₃ solution (60 mL, pH 9.5). The mixture was stirred on ice for 2 h, then the ice bath was removed and the reaction was continued at room temperature. The pH was maintained between 9 and 9.5 for 3 h, when the change of the pH ceased. Then the mixture was diluted with a three fold amount of water and extracted three times with diethyl-ether. The pH of the aqueous phase was adjusted to 2 with 6 M HCl and was extracted three times with ethyl acetate (EtOAc). EtOAc fractions were pooled, washed with brine solution and dried over MgSO₄. The purity of the product was checked by HPLC and thin layer chromatography (TLC; 20% t -butanol–acetic acid–water (4:1:1) in EtOAc, R_f = 0.79), the molecular weight (MW) was determined with mass spectrometry (MS).

2.3. Solid phase synthesis of iso-A β (1–42) with Boc-chemistry

The peptide was synthesized on a Boc-Ala-PAM resin. The loading of the resin was 0.7 mmol/g. The side chains of Asp and Glu were protected with cyclohexyl group. The N^{ϵ} of Lys was masked with 2-chlorobenzoyloxycarbonyl (2-Cl-Z) group. The side chains of Asn and Gln were unprotected. The guanidino group of the Arg was tosylated. The imidazol group of His was protected with benzyloxymethyl group. The aromatic OH of Tyr was masked with 2-bromobenzoyloxycarbonyl (2-Br-Z) group. The side chain of Ser was benzylated. Free hydroxyl groups of the resin were capped by reacting it with 0.25 M acetic acid anhydride in the presence of 0.25 M N -methyl-imidazol (NMI) in dichloromethane (DCM) for an hour. Following removal of the Boc group, 1 g of the resin was treated with a mixture of Boc-Ile-OH/DCC/HOAt (0.35 mmol each) in DCM/DMF (3:1) overnight. The unreacted amino groups of Ala⁴² were acetylated by reacting the peptide-resin with acetic acid/DCC/HOAt (3 mmol each, 1 h). The final loading of the resin was 0.32 mmol/g (determined with picric acid test). Peptide chain elongation were done by activating three fold excess of N^{α} -Boc protected amino acids with DCC/HOBT in DCM/DMF (1:1) and the peptide-resin was reacted with this mixture for 2 h. The couplings were monitored with qualitative ninhydrin test. If the result of the test had indicated, the coupling was repeated either using DCC/HOBT or DCC/HOAt activation. The α -amino protecting groups were removed by treating the resin with 50% TFA/DCM mixture twice (5 + 25 min). Neutralization was done with 5% DIEA/DCM (2 \times 1 min). Ser²⁶ was introduced into the peptide chain utilizing 2-Cl-Z-Ser(OtBu)-OH and the same conditions as detailed above. The side chain of this serine was deblocked and neutralized with the same method that was used in case of the α -amino groups. Acylation of the hydroxyl group of Ser²⁶ with Boc-Gly-OH was done by treating the peptide-resin with Boc-Gly-OH/DCC/NMI (10-fold excess) in DCM/DMF (3:1) for 2 \times 4 h. Then the possibly unreacted hydroxyl groups of Ser²⁶ were capped as those of the resin mentioned previously.

When the assembly of the isopeptide was completed, 3.0 g peptide-resin was obtained. The peptide was cleaved from the resin with a cleavage mixture containing HF (10 mL), anisole (0.2 mL), dimethyl sulfide (DMS; 0.8 mL) and dithiothreitol (DTT;

0.1 g) for 1 g of peptide-resin at 0 °C for 45 min. The peptide was precipitated and washed with diethyl-ether and dissolved in 50% acetic acid/water and lyophilized. 409 mg peptide was obtained from 1.0 g peptide-resin (85% yield).

2.4. Analytical and preparative HPLC

Analytical analysis was done on a Hewlett-Packard Agilent 1100 Series HPLC apparatus using a Luna C18 column (100 Å, 5 µm, 250 × 4.60 mm, Phenomenex) and the flow rate was 1.2 mL/min. Preparative chromatography was done on a Shimadzu HPLC apparatus equipped with a Jupiter C4 column (300 Å, 10 µm, 250 × 21.2 mm, Phenomenex) with a flow rate of 5 mL/min. 0.1% TFA in d.i. water and 80% acetonitrile (ACN), 0.1% TFA in d.i. water was used as eluent A and eluent B, respectively. 85 mg pure peptide were resulted from the purification of 200 mg crude peptide (42.5% yield).

2.5. Mass spectrometry

Mass spectrometry measurements were done on a FinniganMat TSQ 7000 mass spectrometer in ESI-MS mode.

2.6. Standard Aβ(1–42) sample preparation for microscopic and DLS measurements

To obtain an acidic solution of iso-Aβ(1–42), the peptide was dissolved in 0.1% (v/v) TFA solution, sonicated for 5 min and filtered through a syringe filter equipped with a 0.1 µm pore size PVDF membrane (Millex, Millipore Ireland, Carrigtwohill, Ireland). For a pH 7.4 solution, the peptide was dissolved prior in MilliQ ultrapure water to a concentration of 500 µM (2.5 mg/mL) and sonicated for 5 min. The solution was diluted in HBS (10 mM HEPES, 0.154 M NaCl, pH 7.4) to a final peptide concentration of 50 µM and filtered the same way as written above. The solution was incubated for the required time intervals at ambient temperature. In case of AFM study of the effect of long-term incubation on the aggregation of iso-Aβ(1–42), the peptide solution was seeded with pre-formed fibrils of Aβ(1–42) suspended in MilliQ water; the concentration of the fibrils reached 1 µM in the final volume of the sample.

2.7. Atomic force microscopy measurements

10 µL of peptide solution were pipetted onto freshly cleaved mica (Muscovite mica, V-1 quality, Electron Microscopy Sciences, Washington DC, USA). After 2 min the samples were washed twice 10 µL of distilled water and then dried with nitrogen gas.

The AFM images were obtained using tapping mode on a PSIA XE-100 SPM under ambient conditions. Tapping mode AFM tips (Type NSG01, NT-MDT, Moscow, Russia) were applied with a nominal radius of curvature of 10 nm, the non-contact silicon cantilevers having typical force constant of 5.5 N/m and resonant frequency of 150 kHz. The scan rate was 1 Hz and the resolution of the AFM scans was 512 × 512 pixels.

2.8. Dynamic light scattering measurements

All experiments were performed at 25 °C with a Malvern Zetasizer Nano ZS Instrument (Malvern Instruments Ltd., Worcestershire, UK) equipped with a He–Ne laser (633 nm) applying the non-invasive back scatter (NIBS[®]) technology. The translational diffusion coefficients were obtained from the measured autocorrelation functions using the regularization algorithm CONTIN built in the software package Dispersion Technology Software 4.0 (Malvern Instruments Ltd., Worcestershire, UK). Assuming the

scattering particles as hard spheres, their apparent hydrodynamic radius can be calculated from the diffusion parameters by using the Stokes–Einstein equation $R_h = k_B T / (6\pi\eta D_T)$, where k_B is the Boltzmann constant, T is the absolute temperature, η is the viscosity of the medium and D_T is the translational diffusion coefficient. Samples were prepared as given in the section of sample preparation. Correlation function and distribution of the apparent hydrodynamic radii (R_h) over the scattered intensity of the samples were monitored for the expected time intervals.

2.9. Transmission electron microscopy measurements

10 µL droplets of solutions were placed on 400 mesh carbon-coated copper grids (Electron Microscopy Sciences, Washington, PA), incubated for 2 min, fixed with 0.5% (v/v) glutaraldehyde solution, washed three times with d.i. water, and finally stained with 2% (w/v) uranyl acetate. Specimens were studied with a Philips CM 10 transmission electron microscope (FEI Company, Hillsboro, Oregon, USA) operating at 100 kV. Images were taken by a Megaview II Soft Imaging System at a magnification of ×64,000 and analyzed by an AnalySis[®] 3.2 software package (Soft Imaging System GmbH, Münster, Germany).

2.10. Circular dichroism spectroscopy

CD measurements were performed at 25 °C on a Jobin–Yvon Mark VI dichrograph using a quartz cell of 0.1 cm pathlength. All the spectra were the averages of four scans and the resolution was 0.2 nm. The iso-Aβ(1–42) was dissolved either in 5 mM phosphate buffer (pH 7.4) or 0.1% TFA (pH 2) at a concentration of 50 µM. The samples were sonicated for 5 min immediately after dissolution and prior to aging at room temperature. CD spectra were expressed as mean residue ellipticity $[\Theta]_{MR}$, in units of deg cm² dmol^{−1} using a mean residue weight of 110.

2.11. Nuclear magnetic resonance

All NMR spectra were recorded on a Bruker AV600 spectrometer that was equipped with a 2.5 mm triple-resonance capillary probe at 285 K. The iso-Aβ(1–42) was dissolved in water at a concentration of 0.31 mg/120 µL and pH 2.1, 3.0 or 4.7. The ¹H NMR spectroscopy measurements were performed with a WATERGATE solvent suppression scheme. The spectra were recorded with identical conditions (same experimental setup, the same spectrometer and the same probe) after dissolution and a week later. For the relaxation delay, 2 s was used; the delay for binomial water suppression was 150 ms; the number of scans was 256. The NOESY measurements were carried out with a WATERGATE solvent suppression scheme. For the NOESY mixing time 610 ms were used; the number of scans was 64. The TOCSY measurements were carried out with homonuclear Hartman–Hahn transfer with the MLEV17 sequence, with an 80 ms mixing time; the number of scans was 32. For all the 2D spectra, 2024 time domain points and 512 increments were applied. The processing was carried out by using a cosine-bell window function, with single zero filling and automatic baseline correction.

2.12. Pretreatment of rat hippocampal slices with Aβ(1–42) oligomers in artificial cerebrospinal fluid (ACSF)

Using standard procedures, 400 µm thick transverse hippocampal slices were prepared from the brain of 3 months old male Wistar rats using a McIlwain tissue chopper (Campden Instruments, Loughborough, UK). Slices were incubated in a custom-built incubation system in oxygenated standard artificial cerebrospinal fluid (ACSF, composition in mM: NaCl, 130; KCl, 3.5; CaCl₂, 2;

MgCl₂, 2; NaH₂PO₄, 0.96; NaHCO₃, 24; D-glucose, 10 and pH 7.4) at ambient temperature for at least 60 min. Individual slices were transferred to a 3D-MEA (multielectrode array) chip with 60 tip-shaped and 60-μm-high electrodes spaced by 200 μm (Ayuda Biosystems, S.A., Lausanne, Switzerland). The surrounding ACSF solution was removed quickly and the slice was immobilized by a grid. Iso-Aβ(1–42) was dissolved in ACSF at pH 7.4 (1 μM final concentration) and let to transform to Aβ(1–42) and oligomerize in 10 min. The slice was incubated continuously with this solution and perfused with oxygenated ACSF (1.5 mL/min at 34 °C). Incubation was performed for 30 min on the chip before recording commenced. Data were recorded by a standard, commercially available MEA setup (Multi Channel Systems MCS GmbH, Reutlingen, Germany).

2.13. Ex vivo electrophysiological recordings: measurement of long-term potentiation (LTP)

The Schaffer-collateral was stimulated by injecting a biphasic current waveform (–100/+100 μs) through one selected electrode at 0.0166 Hz. Care was taken to choose the stimulating electrode in the same region from one slice to the other one. The peak-to-peak amplitudes of field excitatory postsynaptic potentials (fEPSPs) at the proximal part of stratum radiatum of CA1 were analyzed. After a 30 min incubation period, the threshold and the maximum of stimulation intensity of the evoked responses were determined. To evoke responses, 30% of the maximal stimulation intensity was used. Following a stable 15-min control sequence, LTP was induced using a theta-burst stimulation (TBS) protocol applied at the maximum stimulation intensity. TBS comprised four trains administered at 20 s intervals with 10 bursts given at 5 Hz per train and four pulses given at 100 Hz per burst. LTP was followed for 180 min.

2.14. Learning studies in rats in Morris water maze

A mixture of Aβ(1–42) oligomers was formed in hydrocarbonate buffered saline (HCBS, 20 mM NaHCO₃, 130 mM NaCl, purged with CO₂, pH 7.4) containing 50 μM Aβ(1–42) freshly prepared from iso-Aβ(1–42) at 20 °C for 120 h. Aggregation was tested by AFM (average particle diameter was 8.5 nm). This preparation, which contains mostly oligomers and a small amount of protofibrils, will be referred as “oligomeric mixture” later in this paper.

Adult male Wistar rats (age 8–9 weeks, weight 300–350 g) were operated and Morris water maze experiments were performed as published in [25] with some exception, detailed below. In the control (*n* = 10) and test group (*n* = 10) 15 μL hydrocarbonate buffered saline (HCBS) and 15 μL of Aβ(1–42) solution in HCBS (*c* = 50 μM) were administered intracerebroventricularly (icv). Administration was performed bilaterally with Hamilton syringe, 7.5 μL solution was injected in both sides. The coordinates were from Bregma: AP: –1.0; ML: ±1.5; DV 4.3. Rats were treated with antibiotics and analgesics after surgery.

Spatial learning and memory were assessed in Morris water maze on days 8–12 post-surgery. The maze consisted of a circular blue plastic (diameter: 180 cm, height: 60 cm) filled to a depth of 40 cm with water of 23 ± 1 °C. The water was rendered opaque with the addition of milk. The rats had to learn to find a transparent, hidden escape platform (diameter: 10 cm) in the quadrants on the basis of several constant spatial cues around the pool. The position of the platform was stable during the 5 days study. Daily two trials were conducted between 9:00 and 12:00. Rats were given a maximum of 90 s to find the platform and were then allowed to stay on it for 20 s. Animals that did not find the platform were gently guided and placed on it.

The data recorded by video-tracking were used to calculate the time to reach the platform, during learning. Data were evaluated using independent *T*-test.

3. Results

3.1. Boc-synthesis of iso-Aβ(1–42)

The synthesis of 2-Cl-Z-Ser(OtBu)-OH resulted an oil, which was pure enough to be used in a solid phase synthesis, as it was judged by TLC and HPLC, and it possessed the right molecular weight (MW: 329.7). HPLC chromatogram in Fig. 1A was obtained from the crude product of the synthesis of iso-Aβ(1–42). Peaks a and b have molecular weights of 4530.4 and 4514.2, respectively. (HPLC of the pure iso-Aβ(1–42) is in the Appendix A. Supplementary data).

3.2. Physicochemical characterization of iso-Aβ(1–42)

TEM (Fig. 2) measurements revealed that iso-Aβ(1–42) contains small aggregates even in a pH 2 solution, which are either round-shaped oligomers with an average width of 4–6 nm, or bunches of protofibrils with an average length of 20–30 nm, typical of this type of assembly.

The occurrence of the O→N acyl-shift at acidic pH was studied by NMR. The enhanced solubility of iso-Aβ(1–42) caused a satisfying signal dispersion at 285 K, which cannot be observed in case of the native Aβ(1–42) sequence. Based on the 1H, 2D TOCSY and NOESY spectra, signal assignments could be carried out for the residues 1–30 of the iso-Aβ(1–42). Conversion of the peptide was monitored at different pH values (pH 2.1, 3.0 and 4.7) for a week. During the observation period the isopeptide was stable at pH 2.1, but new peaks appeared in the spectra at pH 3.0. The signal assignment of the new peaks confirmed that these resonances can be attributed to the native Aβ(1–42) form. Thus, O→N acyl-shift starts even in the pH 3.0 solution: about 16% of the

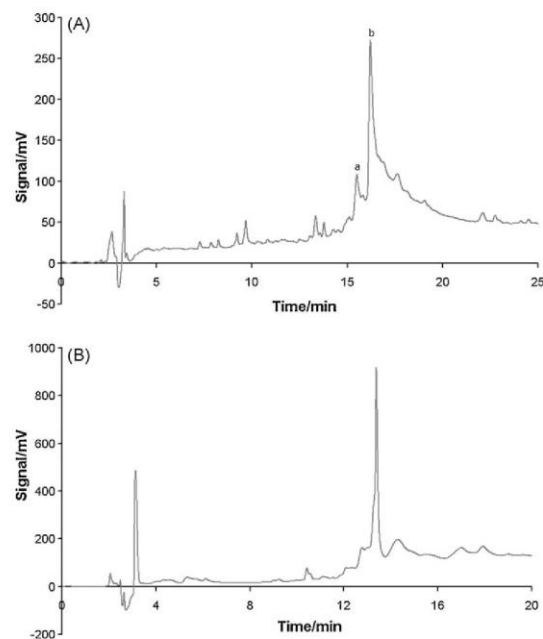


Fig. 1. (A) HPLC of crude iso-Aβ(1–42) synthesized by Boc-chemistry. Gradient: from 5% eluent B in eluent A to 80% eluent B in eluent A over 25 min. (a) [Met(O)]³⁵-iso-Aβ(1–42), (b) iso-Aβ(1–42). (B) HPLC of crude iso-Aβ(1–42) dissolved in HFIP. Gradient: from 20% eluent B in eluent A to 60% eluent B in eluent A over 25 min.

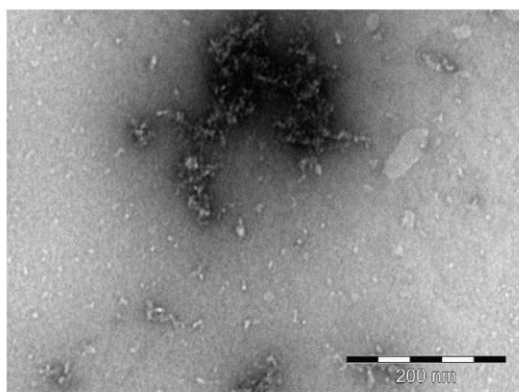


Fig. 2. TEM of iso-Aβ(1–42) dissolved in 0.1% TFA (pH 2.0, $c = 50 \mu\text{M}$).

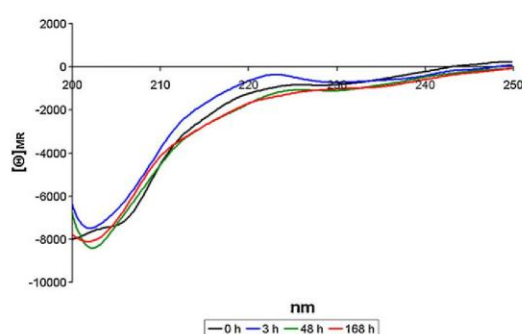


Fig. 3. CD of iso-Aβ(1–42) dissolved in 0.1% TFA (pH 2.0, $c = 50 \mu\text{M}$).

ester was converted to amide bond in a week. At pH 4.7, the acyl-transfer was instantaneous and some precipitation was observed in the NMR tube.

CD spectroscopy showed that the structure of this peptide is relatively stable in a pH 2.0 solution for a week and it explores mostly random coil conformation (Fig. 3).

3.3. Standard preparation of Aβ(1–42) samples formed by O–N acyl migration of iso-Aβ(1–42)

AFM study showed, that the average width of the particles was 1.8 and 3.4 nm, depending on that the sample was or was not dissolved in d.i. water prior the adjustment of the pH to 7.4, respectively (Fig. 4).

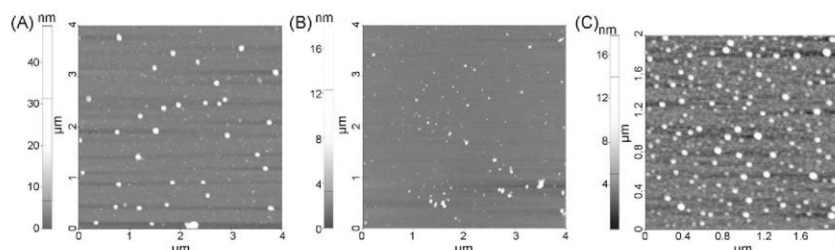


Fig. 4. AFM of Aβ(1–42) after O–N acyl migration of iso-Aβ(1–42) (A) dissolved in pH 7.4 PBS buffer, (B) first taken up into d.i. water followed by adjustment of the pH to 7.4 with PBS buffer and 1 h after 'standard sample preparation' (pH 7.4, $c = 50 \mu\text{M}$).

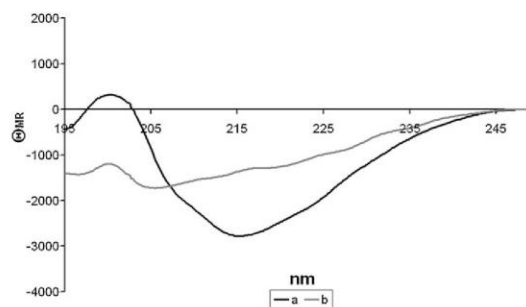


Fig. 5. CD spectra of Aβ(1–42) (a) dissolved in d.i. water, then the pH adjusted to 7.4; (b) first incubated in HFIP overnight, then HFIP is evaporated, followed by the same treatment as that of a ($c = 50 \mu\text{M}$).

CD spectroscopy (Fig. 5) confirmed that hexafluoro-2-propanol (HFIP) treatment prior the adjustment of the pH to 7.4 of the iso-Aβ(1–42) decreases the negative band intensity at 215 nm (characteristic for β-sheets) of the spectra.

AFM detected the presence of oligomers with regular shape and size (Fig. 4C, average width: 3.9 nm) if the sample was treated with HFIP overnight, and after evaporation of the HFIP the peptide was dissolved in d.i. water followed by the adjustment of pH to 7.4 ('standard sample preparation') and it was incubated in this solution for an hour.

3.4. Characterization of the aggregation process of Aβ(1–42): change of conformation and fibrillization

CD spectroscopy and DLS confirmed that both the β-sheet content of the peptide and the average hydrodynamical diameter of the particles were increasing with time if the iso-Aβ(1–42) was subjected to 'standard sample preparation' (Figs. 6 and 7).

AFM study in Fig. 8, shows the fibrillization of an Aβ(1–42) sample prepared from iso-Aβ(1–42). The isopeptide was dissolved in HBS to a concentration of $50 \mu\text{M}$, and seeded with a $100 \mu\text{M}$ fibrillar suspension of Aβ(1–42) in 1:50 volume ratio. By this method, formation of fibrillar structures (with an average width of 5–7 nm, which is typical for the mature amyloid fibrils) and large globule-like assemblies could be observed in 24 h of incubation time at ambient temperature.

3.5. Biological effect Aβ(1–42) oligomer mixtures: ex vivo and in vivo experiments

In an ex vivo electrophysiology experiment (Fig. 9) control slices exhibited a robust LTP recorded from the proximal part of the str. radiatum ($129 \pm 8\%$ 180 min after TBS, $n = 16$ electrodes from

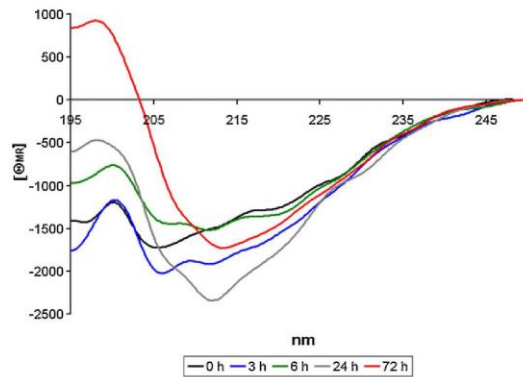


Fig. 6. Aggregation of the A β (1–42) peptide after 'standard sample preparation', monitored by CD spectroscopy (pH 7.4, $c = 50 \mu\text{M}$).

four slices). On the other hand, A β (1–42) treated slices showed a significantly reduced LTP ($105 \pm 4\%$ 180 min after TBS, $n = 15$ electrodes from four slices).

The results of the Morris water maze showed, that the performance of the control and A β (1–42) treated groups increased across trials. However, statistic analysis of experimental data (time needed to find the platform) revealed that learning was significantly slower in A β (1–42) treated rats compared to the control group (Fig. 10) at day 4 ($*P = 0.048$) and day 5 ($**P = 0.017$).

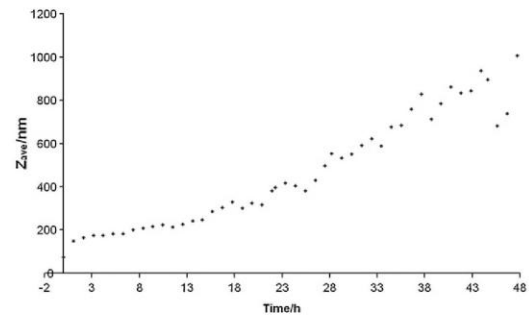


Fig. 7. Aggregation of the A β (1–42) peptide after 'standard sample preparation', monitored by DLS measurement (pH 7.4, $c = 50 \mu\text{M}$).

4. Discussion

4.1. Boc-synthesis of iso-A β (1–42)

The crucial part of devising a Boc strategy for the synthesis of iso-A β (1–42) was to determine what kind of protection should be used on the Ser²⁶. The side chain of this residue will be masked to avoid unwanted acylation during its activation. The protecting group should be easily removable after the incorporation of the building block. Thus, tBu group was selected for the protection of the side chain of Ser²⁶, since it is removable with 50% TFA/DCM mixture, routinely used in syntheses utilizing N^α -Boc protected

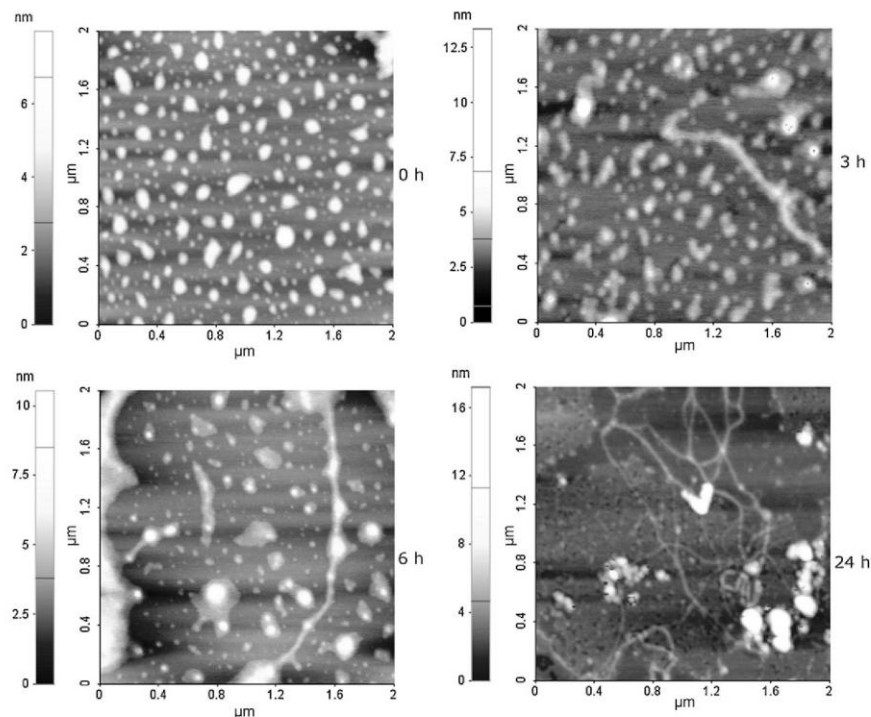


Fig. 8. Aggregation of the A β (1–42) peptide ($c = 50 \mu\text{M}$) after 'standard sample preparation' and seeding with A β (1–42) fibrils ($c = 1 \mu\text{M}$), studied by AFM (pH 7.4).

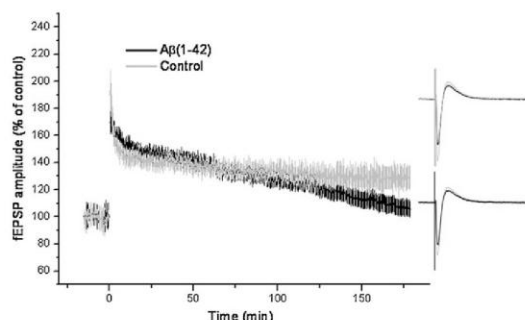


Fig. 9. The effect of A β (1–42) oligomer treatment on TBS induced LTP in hippocampal slices. Data are mean \pm SEM. Insets show representative superimposed fEPSPs recorded 1 min before (black) and 180 min after (gray) TBS.

amino acids. The protecting group of the α -amino group of the Ser²⁶ had to withstand repetitive TFA treatments and be removable during the cleavage of the peptide from the resin to make the precursor ready for the intramolecular $O \rightarrow N$ acyl-shift. Choosing the 2-Cl-Z group was plausible. 2-Cl-Z-Ser(OtBu)-OH was prepared from 2-Cl-Z-OSu and H-Ser(OtBu)-OH as it was detailed in Section 2.2 and later it was used for the incorporation of Ser²⁶.

The presence of A β (1–25) as a byproduct was reported by Sohma et al. [26] previously when certain resins were used for the synthesis of iso-A β (1–42). It was originated from the simultaneous acylation of the side chain of Ser²⁶ and the free hydroxyl groups of the resin during formation of the ester bond between the 25th and 26th residue [8]. To avoid side product formation unreacted free hydroxyl groups of the resin were acetylated. After acylation of the deprotected side chain of Ser²⁶ with Boc-Gly-OH using DCC/NMI activation, the free hydroxyl groups were capped.

The major peak of our crude peptide (Fig. 1A, peak b) in the HPLC has a molecular weight of 4514.2 which is in agreement with the molecular weight of iso-A β (1–42) (calc. MW: 4514.0). The molecular weight of peak b is by 16 mass unit higher than that of the desired product, thus it is [Met(O)]³⁵-iso-A β (1–42). This minor byproduct can be completely eliminated, if the 'low-high' cleavage procedure [30] is used, or if the crude peptide is treated with DMS/NH₄l in TFA for 30 min at 0 °C [12]. In our synthesis no hydrolysis

product or diketopiperazine formation was detected. It was observed that the main peak had a wide tailing. Fractions belonging to this part of the peak possessed no sign of any byproduct, only iso-A β (1–42), when analyzed by MS. If these fractions were sonicated in HFIP for 15 min after lyophilization, a sharp peak was obtained in the HPLC (peaks in Fig. 1B after 14 min are present in the HFIP, see Appendix A. Supplementary data). Thus the tailing can be due to some sort of aggregation of the iso-A β (1–42). If we compare Fig. 1B with chromatograms from the literature, where the peptide was synthesized with Fmoc-chemistry and injected into the HPLC in a disaggregating solvent (dimethyl sulfoxide; DMSO) [26,32], it can be concluded that the Boc-synthesis gave comparable results with them.

4.2. Physicochemical characterization of iso-A β (1–42)

The findings of other groups have outlined the improved water solubility and stability of the isopeptide that could be explained by its unique structure, lowering its propensity toward aggregation. However, TEM (Fig. 2) measurements showed that iso-A β (1–42) forms either round-shaped oligomers, or protofibrils. As no $O \rightarrow N$ acyl migration occurs at pH 2.0 (NMR studies) it seems to be very probable that iso-A β (1–42) still has some propensity to form small aggregates. Residues 17–20 and 30–35 play a crucial role in the aggregation of the native A β peptides and fragments containing these residues are either enhance aggregation of the full length peptide or themselves are prone to aggregate [19]. These regions are intact in the iso-A β (1–42), so the isopeptide can preserve some of their aggregation properties, despite of the structure disrupting effect of the ester bond between residues 25 and 26. Aggregation states of an amyloid peptide are greatly influenced by previous treatments. In our studies no chaotropic agents (e.g. DMSO or HFIP) were applied upon purification to destroy the pre-formed aggregates as it were in [26] and [32]. This can be the cause of the discrepancy between our results and Taniguchi et al.'s [31], who detected isopeptide monomers only with CD and size exclusion chromatography. Our preparation most likely also contains some monomers besides the oligomers, since monomers cannot be detected by AFM. CD spectra of the iso-A β (1–42) showed mostly random conformation for a week (Fig. 3). Nevertheless the isopeptide still has superior solubility properties and much lower tendency to aggregate than A β (1–42) has.

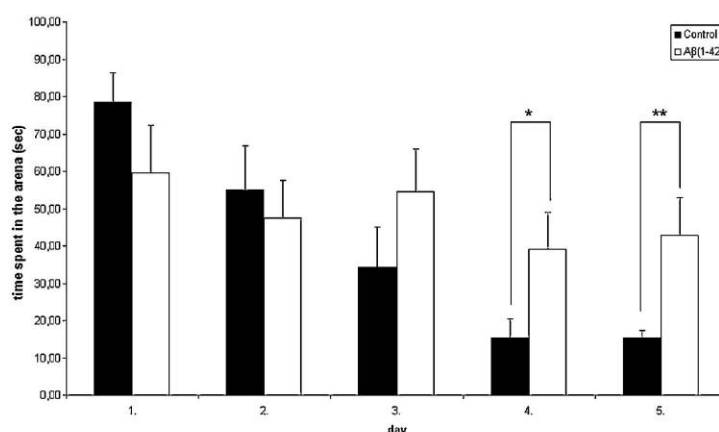


Fig. 10. The effect of A β (1–42) treatment (50 μ M, icv administration) on the learning of rats during 5 days (Morris water maze, time spent in the arena during the first swims, T-test: * P = 0.048; ** P = 0.017).

4.3. Standard preparation of A β (1–42) samples formed by O \rightarrow N acyl migration of iso-A β (1–42)

It was confirmed by AFM measurements that particles with smaller size could be obtained if the peptide was dissolved in d.i. water prior to the adjustment of the pH to 7.4 compared to the protocol, which applies only pure pH 7.4 buffer as dissolution media (Fig. 4). CD spectroscopy confirmed that HFIP treatment of the iso-A β (1–42) decreased the β -sheet content of the resulting A β (1–42) after adjustment of the pH to 7.4 (Fig. 5). Based on these findings, a 'standard sample preparation' protocol was worked out to obtain starting material which possesses reproducible aggregation properties for our future experiments. According to this, the peptide is first treated with HFIP overnight. Followed by the evaporation of the HFIP, the iso-A β (1–42) is dissolved in d.i. water, then the pH is changed to 7.4 with an appropriate buffer. In Fig. 4C AFM image taken 1 h after sample preparation followed by the standard preparation protocol shows the overwhelming presence of the small round oligomers of regular shape and size.

4.4. Characterization of the aggregation process of A β (1–42): change of conformation and fibrillization

Both CD spectroscopy and DLS (Figs. 6 and 7) showed growing β -sheet content and particle size of the A β (1–42) formed from iso-A β (1–42) upon incubation. Care must be taken with the interpretation of DLS results, since the increase of the diameters detected by DLS are always distorted by the large particles, as the observed scattering intensity is proportional to the sixth power of the hydrodynamical radius of the scattering particle (the bigger is the scattering particle, the more is its contribution to the scattering intensity). Thus, the increase of the average size in a given time interval is possibly smaller, than that measured by DLS. We observed this phenomenon, when attempted to follow the A β (1–42) aggregation by AFM, and found that though the formation of large aggregates could be detected upon incubation of the sample for an elongated time period, their occurrence compared to the small oligomers was reduced. Proper fibrillization could be achieved by seeding the sample with pre-formed fibrils of A β (1–42), as it is presented by a series of AFM measurements (Fig. 8).

4.5. Biological effect A β (1–42) oligomer mixtures *ex vivo* and *in vivo* experiments

The effect of the peptide on synaptic plasticity was studied in an *ex vivo* electrophysiology experiment. A β (1–42) has been repeatedly shown to impair long-term potentiation in hippocampal slices [1,17], thus we investigated LTP. The results in Fig. 9 indicate that A β (1–42) formed from the precursor isopeptide hinders the long-term potentiation, thus it decreases synaptic plasticity, a correlate of learning and memory.

Icv administered A β (1–42) oligomeric mixture (prepared from iso-A β (1–42) and aggregated for 120 h) caused memory deficit in rats (Morris water maze, Fig. 10). The difference of the treated and control group proved to be significant on the 4th and 5th days of the experiments. Icv administration into the 3rd ventricle has an advantage (compared to microinjection into the entorhinal cortex) that soluble A β (1–42) oligomers reach large areas of brain beside minimal brain injury.

5. Conclusion

Iso-A β (1–42) was successfully synthesized using a Boc strategy. The preparation of the 2-Cl-Z-Ser(OtBu)-OH building block (used to introduce Ser at the position of the ester bond formation)

is easy and convenient. The applied protecting groups have been widely used, well known and fulfill the stability requirements toward acidic treatments. A β assemblies with different aggregation grade – oligomers and (after prolonged incubation times and seeding) fibrillar structures – can be obtained from iso-A β (1–42). It was demonstrated that the isopeptide was a good precursor of A β (1–42) for both structural and biological studies. This isopeptide is water soluble, stable and the aggregation of the formed A β (1–42) can be well characterized, thus it can be useful to perform reproducible biological experiments. Moreover, by administering this isopeptide chronically into animals, the O \rightarrow N acyl-transfer could happen *in situ* and *in vivo*. This chronic administration of the A β -isopeptide may serve as a proper model system in order to study Alzheimer's disease from an early onset.

Acknowledgements

This work was supported by the following grants: OTKA NK 73672 from the Hungarian National Sciences Foundation; Memo-load FP-7 201159 and Lipididiet FP-7 211696 and the Teller Ede (Napbio) grant of NKTH. L.F. and A.H. acknowledges support from a János Bolyai Postdoctoral Fellowship.

The authors thank to Dr. Zoltán Kele for mass spectrometry and to Dr. Tamás Martinek for providing the NMR facility.

Appendix A. Supplementary data

Supplementary data associated with this article can be found, in the online version, at doi:10.1016/j.peptides.2009.12.001.

References

- [1] Barghorn S, Nimmrich V, Striebing A, Krantz C, Keller P, Janson B, et al. Globular amyloid β -peptide1–42 oligomer—a homogenous and stable neuro-pathological protein in Alzheimer's disease. *J Neurochem* 2005;95:834–47.
- [2] Bernstein SL, Dupuis NF, Lazo ND, Wyttenbach T, Condron MM, Bitan G, et al. Amyloid- β protein oligomerization and the importance of tetramers and dodecamers in the aetiology of Alzheimer's disease. *Nat Chem* 2009;1:326–31.
- [3] Bozsó Z, Penke B, Juhász G, Szegedi V, Laczkó I, Soós K, et al. The synthesis and structural study of iso-A β (1–42). In: Hilkka Lankinen, editor. *Peptides 2008, Proceedings of the thirtieth European peptide symposium*. Finland: The Finnish Peptide Society; 2008. p. 364–5.
- [4] Burdick D, Soreghan B, Know M, Kosmoski J, Knauer M, Henschen A, et al. Assembly and aggregation properties of synthetic Alzheimer's A4/b amyloid peptide analogs. *J Biol Chem* 1992;267:546–54.
- [5] Carpino LA, Krause E, Sferdean CD, Schümann M, Fabian H, Bienert M, et al. Synthesis of "Difficult" peptide sequences: application of a depsipeptide technique to the Jung-Redemann 10- and 26-mers and the amyloid peptide A β (1–42). *Tetrahedron Lett* 2004;45:7519–23.
- [6] Chromy BA, Nowak RJ, Lambert MP, Viola KL, Chang L, Velasco PT, et al. Self assembly of A β (1–42) into globular neurotoxins. *Biochemistry* 2003;42:12749–60.
- [7] Clemmer DE, Valentine SJ. Protein oligomers frozen in time. *Nat Chem* 2009;1:257–8.
- [8] Coin I, Dölling R, Krause E, Bienert M, Beyermann M, Sferdean CD, et al. Depsipeptide methodology for solid phase peptide synthesis: circumventing side reactions and development of an automated technique via depsipeptide units. *J Org Chem* 2006;71:6171–7.
- [9] Dettin M, Pegoraro S, Rovero P, Biciatto S, Bagno A, Di Bello C. SPSS of difficult sequences. *J Peptide Res* 1997;49:103–11.
- [10] Dos Santos S, Chandravarkar A, Mandal B, Mimna R, Murat K, Saucedo L, et al. Switch-peptides: controlling self-assembly of amyloid beta-derived peptides *in vitro* by consecutive triggering of acyl migrations. *J Am Chem Soc* 2005;127:11888–9.
- [11] Hendrix JC, Halverson KJ, Jarrett JT, Lansbury PT. A novel solvent system for solid-phase synthesis of protected peptides: the disaggregation of resin-bound antiparallel β -sheet. *J Org Chem* 1990;55:4517–8.
- [12] Huang H, Rabenstein DL. A cleavage cocktail for Met containing peptides. *J Pept Res* 1999;53:548–53.
- [13] Hyde C, Owen JD, Quibell M, Sheppard RC. Some 'difficult sequences' made easy. *Int J Peptide Protein Res* 1994;43:431–40.
- [14] Johnson T, Quibell M, Sheppard RC. N,O-bisFmoc derivatives of N-(2-hydroxy-4-methoxybenzyl)-amino acids: useful intermediates in peptide synthesis. *J Pept Sci* 1995;1:11–25.

- [15] Kates SA, Solé NA, Beyermann M, Barany G, Albericio F. Optimized preparation of deca(L-alanyl)-L-valinamide by 9-fluorenylmethyloxycarbonyl (Fmoc) solid-phase synthesis on polyethylene glycol-polystyrene (PEG-PS) graft supports, with 1,8-diazobicyclo[5.4.0]-undec-7-ene (DBU) deprotection. *Peptide Res* 1996;9:106–13.
- [16] Klein WL. A β toxicity in Alzheimer's disease: globular oligomers (ADDLs) as new vaccine and drug targets. *Neurochem Int* 2002;41:345–52.
- [17] Klyubin I, Betts V, Welzel AT, Blennow K, Zetterberg H, Wallin A, et al. Amyloid β protein dimer-containing human CSF disrupts synaptic plasticity: prevention by systemic passive immunization. *J Neurosci* 2008;28:4231–7.
- [18] Larsen BD, Holm A. Incomplete Fmoc deprotection in solid-phase synthesis of peptides. *Int J Peptide Protein Res* 1994;43:1–9.
- [19] Liu R, McAllister C, Lyubshenko Y, Sierks MR. Residues 17–20 and 30–35 of beta-amyloid play critical role in aggregation. *J Neurosci Res* 2004;75:162–71.
- [20] Matsuzaki K, Okada T, Tsukuda M, Ikeda K, Sohma Y, Chiyomori Y, et al. Design, synthesis, and biophysical properties of a helical A β 1–42 analog: inhibition of fibrillogenesis and cytotoxicity. *Biochem Biophys Res Commun* 2008;371:777–80.
- [21] Mattson MP, Cheng B, Davis B, Bryant K, Liederburg I, Rydel RE. β amyloid peptides destabilize calcium homeostasis and render human cortical neurons vulnerable to excitotoxicity. *J Neurosci* 1992;12:376–89.
- [22] Meldal M. PEGA: a flow stable polyethylene glycol dimethyl acrylamide copolymer for solid phase synthesis. *Tetrahedron Lett* 1992;33:3077–80.
- [23] Selkoe DJ. Physiological production of the β -amyloid protein and the mechanism of Alzheimer's disease. *Trends Neurosci* 1993;16:403–9.
- [24] Simmonds RC. Use of Hmb backbone-protecting group in the synthesis of difficult sequences. *Int J Peptide Protein Res* 1996;47:36–41.
- [25] Sipos E, Kurunczi A, Kasza A, Horváth J, Felszeghy K, Laroche S, et al. β -amyloid pathology in the entorhinal cortex of rats induces memory deficits: implications for Alzheimer's disease. *Neuroscience* 2007;147:28–36.
- [26] Sohma Y, Hayashi Y, Kimura M, Chiyomori Y, Taniguchi A, Sasaki M, et al. The 'O-acyl isopeptide method' for the synthesis of difficult sequence-containing peptides: application to the synthesis of Alzheimer's disease-related amyloid β peptide (A β)1–42. *J Peptide Sci* 2005;11:441–51.
- [27] Sohma Y, Kiso Y. "Click peptides"—chemical biology-oriented synthesis of Alzheimer disease-related amyloid β (A β) analogues based on the "O-acyl isopeptide method". *ChemBioChem* 2006;7:1549–57.
- [28] Sohma Y, Sasaki M, Hayashi Y, Kimura T, Kiso Y. Design and synthesis of a novel water-soluble A β 1–42 isopeptide: an efficient strategy for the preparation of Alzheimer's disease-related peptide, A β 1–42, via O-N intramolecular acyl migration reaction. *Tetrahedron Lett* 2004;45:5965–8.
- [29] Spengler J, Koksche B, Albericio F. Simple machine-assisted protocol for solid-phase synthesis of depsi-peptides. *Biopolymers* 2007;88:823–8.
- [30] Tam JP, Heath WF, Merrifield RB. SN2 deprotection of synthetic peptides with a low concentration of HF in dimethyl sulfide: evidence and application in peptide synthesis. *J Am Chem Soc* 1983;105:6442–55.
- [31] Taniguchi A, Sohma Y, Hirayama Y, Mukai H, Kimura T, Hayashi Y, et al. "Click-peptide": pH-triggered in situ production and aggregation of monomer A β 1–42. *ChemBioChem* 2009;10:710–5.
- [32] Taniguchi A, Yoshiya T, Abe N, Fukao F, Sohma Y, Kimura T, et al. 'O-Acyl isopeptide method' for peptide synthesis of A β 1–42 isopeptide using 'O-acyl isopeptide unit'. *J Peptide Sci* 2007;13:868–74.
- [33] Tickler AK, Clippingdale B, Wade JD. Amyloid- β as a "Difficult Sequence" in Solid Phase Peptide Synthesis. *Protein Pept Lett* 2004;11:377–84.
- [34] Varanda LM, Miranda MTM. Solid-phase peptide synthesis at elevated temperatures: a search for an optimized synthesis condition of unsulfated cholecystokinin-12. *J Peptide Res* 1997;50:102–8.
- [35] Waite J, Cole GM, Frautsky SA, Connor DJ, Thal LJ. Solvent effect on beta protein toxicity in vivo. *Neurobiol Aging* 1992;13:595–9.
- [36] Wöhr T, Mutter M. Pseudo-prolines in peptide synthesis: direct insertion of serine and threonine derived oxazolidines in dipeptides. *Tetrahedron Lett* 1995;36:3847–8.
- [37] Wöhr T, Wahl F, Nefzi A, Rohwedder B, Sato T, Sun X, et al. Pseudo-prolines as a solubilizing, structure-disrupting protection technique in peptide synthesis. *J Am Chem Soc* 1996;118:9218–27.
- [38] Zarándi M, Soós K, Fülöp L, Bozsó Zs, Datki Zs, Tóth GK, et al. Synthesis of A β (1–42) and its derivatives with improved efficiency. *J Pept Sci* 2007;13:94–9.